RADIOMIC TEXTURE ANALYSIS TO ASSESS POST-RADIATION T2 MRI CHANGES IN NON-TUMORAL BRAIN REGIONS OF PAEDIATRIC PATIENTS WITH PRIMARY BRAIN TUMOURS

By

Priyanka Umesh Sakhavalkar

A Dissertation

Submitted To

The University of Liverpool

In Partial Fulfilment of The Requirements
For The Degree Of

Doctor Of Philosophy

7th May 2022

DECLARATION

I hereby certify that this dissertation constitutes my product, that where the language of others is set forth, quotation marks so indicate. That appropriate credit is given where I have used the language, ideas, expressions, or writings of another.

I declare that the dissertation describes original work that has not been presented for the award of any other institution's degree.

Signed,

Priyanka Umesh Sakhavalkar

“This dissertation contains material that is confidential and/or commercially sensitive. It is included here to understand that this will not be revealed to any person not involved in the assessment process”.

ABSTRACT

1. Background: Many paediatric survivors treated for brain tumours suffer from life-changing, long-term neurological and cognitive disabilities. Magnetic Resonance Imaging (MRI) scans often show signal changes in the treated part of the brain. Changes can also be present in the non-tumoral brain following radiation. It is impossible to predict which patients will manifest these MRI tissue changes after treatment. The routine qualitative radiological analysis is subjective and suffers from the inherent limitations of the human eye. An objective quantitative assessment may be a more robust method of assessing these tissue changes. We hypothesised that quantitative MRI texture features could be used as surrogates of these underlying structural tissue changes following radiation therapy. This thesis developed an objective method to quantitatively assess complex radiation-induced brain changes by facilitating higher-order characterisation.

2. Objectives: This exploratory study aimed to understand I. the effects of dose and time on textural features in non-tumoral brain regions; II. compare the textural feature values between proton and photon therapy at the same dose levels and assess if there was any difference, and III. compare textural feature values in patients with and without 21 months and 5-year T2 qualitative signal change and determine if radiomic texture analysis could predict these changes earlier in paediatric medulloblastoma.

3. Methods: This retrospective longitudinal study explored the MRI data of 51 paediatric brain tumour patients (Brainstem 4, Cerebellar 19, Hemispheric cerebral 7 and Supratentorial midline 10 tumours) treated with radiotherapy (30 Photon and 21 protons). The Median RT treatment dose was 28.52Gy (0-60Gy). T2 MRI scans were bias-corrected and registered with the post-surgical baseline MRI before the start of radiotherapy. Regions of interest (ROIs) were drawn at eleven different non-tumoral brain regions on each follow-up MRI up to 2 years following radiotherapy. Textural features were extracted and analysed.
    I. For the first aim, radiation dose was calculated in each of these 11 ROIs, and texture features were extracted using pyradiomics. Data were analysed using machine learning and statistical analysis. A general linear multivariate model was used to understands

the effects on primary texture features over 12 months by radiation dose, time, and the effect of dose*time together at each ROI separately.

II. For the second aim, sixteen primary texture features were compared with the Mann Whitney U test between proton and photon therapy across the whole brain and in each ROI separately at the same dose levels (between 0-60 Gy).

III. For the third aim, nine paediatric patients (total of 78 scans) with medulloblastoma (radiation dose 50-70 Gy) were selected. 21months and 5-year follow-up MRIs were qualitatively analysed based on the presence or absence of progressive T2 signal change (PSC) in the cerebellar white matter. Textural features were extracted from the right and left cerebellar ROIs. Values were compared with the Mann Whitney U test. Receiver operator characteristic curve (ROC) and area under curve (AUC) analysis was carried out to assess the diagnostic ability of each textural feature.

4. Results:

1.1 Multivariate analysis showed a significant effects ($p < 0.001$) of radiation dose and longitudinal primary texture features in all 11 ROIs. The study shows that dose level in groups has a statistically significant effect on Texture features @10percentile, @90percentile, contrast, Correlation, Energy, Entropy, Maximum, Mean, Mean Absolute Deviation, Median, Minimum, Range, Total Energy, and Uniformity. Time has a statistically significant effect on Texture features at 10percentile, 90percentile, Correlation, Energy, Entropy, Maximum, Mean, Mean Absolute Deviation, Median, Minimum, Range, Total Energy, and Uniformity.

It is also seen that the interaction effect of dose levels in groups with time has a statistically significant effect on Texture features Correlation, Energy, and Total Energy.

1.2 A key contribution of this thesis is to provide evidence of a significant difference in texture feature value between proton and photon therapy at the same dose level.

- A. Whole-brain: When all 11 ROIs were analysed together in 50 patients, the mean of longitudinal textural feature values showed significant differences ($p<0.005$) between both therapies at each dose level. Several observations (N) were different at each dose group in each therapy due to differences in dose distribution. At dose group A (0-10.55Gy;N=Ph144,Pr 609) & C (20.56-30.55Gy; N=Ph172, Pr26) means of 15 longitudinal feature value showed significant difference; at B(10.56- 20.55Gy;

Ph58, Pr83) & E (40.56-50.55Gy;N=Ph108, Pr42), a significant difference was shown by mean of 1 feature, at dose D (30.56-40.55Gy; N=Ph196, Pr27) mean of 3 feature values showed difference and 11 features mean values showed significant difference at dose F(50.56-60.55Gy; N=Ph514, Pr128).

- B. In each ROI: When a similar ROI was selected and compared, a significant difference ($p<0.005$) was seen in some mean feature values. Individual features showing significant differences vary as per dose group. For E.g. The Mean of total energy at dose E at pons showed a significant difference.

1.3 At 21 months seven patients qualitatively showed T2 hyperintensity, and two did not. At five years, six patients qualitatively showed T2 hyperintensity while three did not. On radiomic analysis significant difference ($p<0.05$) was shown by all 16 primary textural features (contrast, energy, entropy, kurtosis, maximum, mean, mean absolute deviation, median, minimum, range, skewness, total energy, uniformity, variance, 10%, 90%) between 21 months with and without hyperintensity group. While in 5-year with and without hyperintensity group difference was shown by all 15 features except kurtosis when analysed at all time points together. In the 21 months groups, results of ROC analysis showed that nine texture features had an area under the curve (AUC) >0.7 (Fig.6.6, Table 6.6). In the 5-year PSC group, 12 features showed AUC >0.7 (Fig. 6.7, Table 6.7). For both groups, only two features (Skewness and Uniformity) showed AUC <0.5.

2 Conclusion: Radiomic texture analysis is a promising technique for assessing post-radiation changes in non-tumoral brain regions in paediatric brain tumours. The findings need confirmation in a larger patient cohort and should be related to patient and clinical outcome.

THESIS OUTPUT

Paper Presentations:

- A Correlation between longitudinal T2 MRI radiomic primary texture feature values and radiation dose in non-tumoral regions of the brain in paediatric brain tumours. P Sakhavalkar, S Avula, B Pizer, N Thorp, M Jenkinson. Presented at the Netherlands as Oral Presentation at the annual meet of the European Association of Neurooncology **(EANO)** Sept 2021

- Comparison Of Longitudinal MRI Radiomic Texture Features Between Protons And Photon Radiation Therapy In Non-tumoral Regions Of Brain At The Same Dose Levels In Paediatric Patients With Brain Tumours - An Exploratory Study. . P Sakhavalkar, S Avula, B Pizer, N Thorp, M Jenkinson. Presented at Chicago the US, Oral presentation at Radiological Society Of North America **(RSNA)** annual meet Nov 2021

Poster Presentation :

- Radiomic textural analysis of non-tumoral brain regions in paediatric medulloblastoma following radiotherapy. P Sakhavalkar, S Avula, B Pizer, N Thorp, M Jenkinson. European Congress of Radiology **(ECR)** March 2022 Vienna. Received **Magna Cum Laude Award 2022**

Publication

- OS03.5.A Correlation between longitudinal t2 MRI radiomic primary texture feature values and radiation dose in non-tumoral regions of the brain in paediatric brain tumours. P Sakhavalkar, S Avula, B Pizer, N Thorp, M Jenkinson **Neuro-Oncology** Sept 2021 (23):2: Page ii6. (Abstract)

DEDICATION

“This thesis is dedicated to all the children and their families who have fought, are fighting, or will fight brain cancer.

You are real Heroes!

I hope this research contributes to making your lives better."

Priyanka Umesh Sakhavalkar

Acknowledgements

“prakrteh kriyamánáni gunaih karmáni sarvasah
ahamkizravimicdhátm¿z kartáham iti manyale”
Bhagavat Gita Ch 3 Verse 27
All actions are universally engendered by the attributes (gunas) of primordial Nature (Prakriti). A man whose Self is deluded by egoity thinks, "I am the doer."

Firstly, I bow with reverence to thank "Lord Krishna and my Gurus". They enriched me with such a golden opportunity and infused the power in my mind to fulfil the task assigned to me.

With immense gratitude, I thank Prof. Michael Jenkinson for taking over as my primary supervisor at the most crucial stage of this project and putting forth every effort to transform my obstacles into stepping-stones for accomplishments and progress. I shall forever remain indebted to him for his kindness, faith in my work and support; without this, the research would not have been possible.

I am grateful to Prof. Barry Pizer for his supervision, insightful comments, encouragement, and the critical questions that incentivised me to widen my research from various perspectives. This study started with his insights by highlighting the burning clinical questions in paediatric neurooncology that need research work.

My gratitude extends to Prof Pizer, Alder Hey Children's Hospital and Institute of Systems, Molecular and Integrative Biology, University of Liverpool, for the funding opportunity to undertake my studies.

I am thankful to Dr Shivaram Avula for his supervision, radiological guidance, and support from Dept of Radiology at Alder Hey Children's Hospital. I am grateful to him for his help with radiological analysis, which has been an essential part of this research.

I want to express my gratitude to Dr Nicky Thorp for her advice and support that help me understand the radiotherapy work. I am also thankful to her for her time, comments, and guidance with the drafts and research work.

I am thankful to Prof. Ian Prior and Prof. Simon Keller for their help and guidance as IPAP assessors. I thank Mr Rhydian Caines, Ms Sarah Stead from Clatterbridge cancer centre, and Dr Katherine Cooper for their support with the clinical and radiation database. I am also thankful to colleagues from the University of Florida Health Proton Therapy Institute and Oklahoma Proton Centre for providing proton radiation maps.

I am thankful to Dr Shirley Cooper from Liverpool Doctoral College for the opportunity to work as PGR Tutor and conduct my workshops on mindfulness which was a very enriching experience during this PhD.

I would like to thank Mr Arturas Grauslys for his help with Machine learning and Mr David Hughes for his help with Statistics.

From the bottom of my heart, I would like to thank my family and friends, my parents, Mr Umesh and Mrs Ashumati, my grandparents, Ms Nalini, and the late Mr Sitaram, for their love, constant support, and presence throughout my writing this thesis and my life in general.

Lastly, I am grateful to all the paediatric patients and families who are part of this study and whose names I cannot mention.

Sincerely,

Priyanka Umesh Sakhavalkar

INDEX

ABBREVIATIONS

SR NO.	Abbreviation	Full Form
1.	MRI	Magnetic Resonance Imaging
2.	T1W	T1 Weighted
3.	T2W	T2 Weighted
4.	ROI	Region Of Interest
5.	PSC	Progressive Signal Change
6.	TA	Texture Analysis
7.	ROC	Receiver Operator Characteristic Curve
8.	AUC	Area Under Curve
9.	Ph	Photon
10.	Pr	Proton
11.	CNS	Central Nervous System
12.	RT	Radiotherapy
13.	MB	Medulloblastoma
14.	WNT	Wingless Activated
15.	SHH	Sonic Hedgehog
16.	CT	Computed Tomography
17.	fMRI	Functional Magnetic Resonance Imaging
18.	TE	Echo Time
19.	TR	Repetition Time
20.	FLAIR	Fluid Attenuated Inversion Recovery
21.	DWI	Diffusion Weighted Imaging
22.	MRS	Magnetic Resonance Spectroscopy
23.	ATRT	Atypical Teratoid Rhabdoid Tumour
24.	DTI	Diffusion Tensor Imaging
25.	BBB	Blood Brain Barrier
26.	GTV	Gross Tumour Volume
27.	IMRT	Intensity Modulated Radiotherapy
28.	PTV	Peritumoral Volume
29.	PBT	Proton Beam Therapy
30.	LET	Linear Energy Transfer
31.	SOBP	Spread Out Brag Peak
32.	PFS	Posterior Fossa Syndrome
33.	CSF	Cerebrospinal Fluid
34.	EG	Energy
35.	ETR	Entropy
36.	KR	Kurtosis
37.	MAD	Mean Absolute Deviation
38.	MDN	Median
39.	MIN	Min
40.	SK	Skewness
41.	TTE	Total Energy

42.	ANT.CC	Anterior Corpus Callosum
43.	L.CER	Left Cerebellum
44.	L.CS	Left Centrum Semiovale
45.	L.THALAMUS	Left Thalamus
46.	MED	Medulla
47.	POST.CC	Posterior Corpus Callosum
48.	R.CER	Right Cerebellum
49.	R.CS	Right Centrum Semiovale
50.	R.THALAMUS	Right Thalamus
51.	ANT.CC	Anterior Corpus Callosum
52.	L.CER	Left Cerebellum
53.	L.CS	Left Centrum Semiovale
54.	L.THALAMUS	Left Thalamus

Chapter 1 Introduction and Review of Literature

1.1. Chapter Overview

This chapter offers an overview of paediatric brain tumours, their classification, diagnosis, treatment, and the side effects of these therapies.

The chapter begins with a general overview and problem purpose statement of this research study. The chapter highlights the role of MRI in the diagnosis and treatment of these tumours. A summary of current evidence and a review of the literature is provided.

Radiomic texture analysis is a relatively new concept introduced in this chapter. Radiomics is a technique with massive potential in cancer research. Introduction to radiomics and the rationale for using it in analysing MRI images, and the need for research are discussed.

The chapter concludes with the aims and objectives of the thesis.

1.2. Problem Purpose Statement

About 50% of long-term survivors of paediatric brain cancers suffer from lifelong morbidity and disability due to the toxic side effects of cancer therapies. There is insufficient data to understand the tissue changes in affected brain regions uninvolved by tumours following radiation. These tissue changes are studied non-invasively by MRI in a qualitative manner. Quantitative MRI can provide a more detailed and objective analysis of tissue characteristics than routine qualitative methods, which are subject to bias and limitations of the human eye.

These quantitative MRI features can potentially be used as surrogates of underlying tissue changes following radiation, thus may provide a better understanding of radiation effects on non-tumoral brain structures.

This research describes quantitative MRI features of non-tumoral parts of the brain longitudinally in paediatric brain tumour patients treated with radiotherapy (RT), correlates them with the radiation dose and compares the effects of proton and photon therapy in different brain brain regions.

1.3. Introduction To Paediatric Brain Tumours

Central Nervous System (CNS – brain and spinal cord) tumours form the second most common group of tumours in children, accounting for more than a quarter (26%) of all childhood neoplasms worldwide [2]. Around 400 children are diagnosed with a CNS tumour every year in the UK [3]. CNS tumour is the most common cause of cancer death in children [3]. Over 60% of the paediatric survivors treated for brain tumours suffer from life-changing, long-term disability [4]. These comorbidities make the quality of life paramount in survivors treated for brain tumours.

Though these tumours were initially thought to have similar features to the corresponding adult variants, now it has been well established that they present in different locations and have other biological and histopathological features [5, 6]. For example, in 2021, the WHO classification of CNS tumours separates gliomas into adult-type and paediatric-type due to their molecular and genetic differences [7]. As growth and development are still occurring in children, paediatric patients have additional challenges with comorbidities. Hence, paediatric tumours should be studied as a separate class of tumours to optimise tumour-related outcomes and minimise treatment toxicity. For diagnosis, treatment planning and post-therapy assessment, non-invasive Magnetic Resonance Imaging (MRI) have a fundamental role. In the present study, we have explored the use of advanced image analysis of T2 MRI scans to understand the effects of treatment on paediatric brains.

With advancements in technology and therapies, overall long-term survival following paediatric brain tumour diagnosis has been improved to around 70-80% compared to previous treatment approaches [8, 9]. However, these tumours and their therapies are often associated with significant morbidity, including severe neuropsychological and neurological sequelae in about 50% of these long-term survivors [8]. Adverse effects on typical brain tissue result from tumours, surgery, chemotherapy and mainly radiotherapy. Toxicity impacts cognition, memory, intelligence, high-level brain function and attention [8] [10] [11]. Radiotherapy (RT) causes endothelial dysfunction and increases the risk of cerebrovascular complications such as stroke, microbleeds and Moya Moya syndrome [11], [12]. These effects are more pronounced

in children as their brain is still growing and developing. This warrants overall increased support for prevention and early detection, intervention, and long-term multidisciplinary and holistic care of these patients [13].

This review gives a brief clinical overview of paediatric brain tumours and the role of MRI, radiomics and texture analysis.

1.4. Aetiology / Pathogenesis:

Aetiologic factors for most brain tumours are unknown though multiple hypotheses have been postulated. Often genetic and environmental factors together lead to cellular alteration in the brain. Heredity may play a role as patients present with a history of a brain tumour in a family [14]. Genetic alterations are seen in these patients. Viral infections (JC or SV40), N-nitroso compounds, and head injury may be environmental factors causing childhood brain tumours [15]. Multiple factors act together in the aetiology of gliomas and other brain tumours.

Gliomas are the most common type of brain tumour. About 60% of paediatric gliomas occur in the infratentorial region. Paediatric gliomas arise from glial cells. Alteration in ependymal cells, a type of glial cell, causes ependymoma. It is most common in the fourth ventricle. Craniopharyngioma in the suprasellar region arises from the embryonic tissue related to the pituitary gland [16]. Children are more radiosensitive than adults. Therapeutic radiation used to treat other malignancies such as acute leukaemia is a well-known risk factor for glioma [17]. Tumours show an association with genetic conditions such as neurofibromatosis type 1 and 2, Gorlin's syndrome, basal cell nevus syndrome and Turcot syndrome [18]. Optic pathway gliomas are more likely to develop in patients with neurofibromatosis.

Remnants of primitive neuroectoderm can grow in the roof of the fourth ventricle and may arise as medulloblastoma [19]. Turcot syndrome, associated with germline mutations in the WNT signalling pathway, can predispose to medulloblastoma.

1.5. Clinical Presentation:

Patients with CNS tumours often present with non-specific symptoms of short duration due to increased intracranial pressure, for example, headache, vomiting, drowsiness, and confusion [20].

An increase in head circumference, vomiting and nausea are common non-specific symptoms in infants with CNS tumours. Infants may fail to thrive and show lethargy.

Table 1. 1 Signs and symptoms of brain tumours based upon location. Adapted from Abubakar et al. *[21]*

Location	Associated Signs and Symptoms
Cerebral Hemisphere	Hemiparesis, Seizures, Hemisensory deficits, Visual field defects, Headaches
Diencephalic	Visual loss/field defects, Endocrinopathy, Behavioural changes, Headaches
Posterior Fossa	Ataxia/dysmetria, Headaches, Nausea/vomiting, Neck pain, Extra ocular palsies
Brain Stem	Extra ocular palsy, Facial palsies, Swallowing difficulty, Hemi/quadriparesis, Ataxia/dysmetria
Pineal Region	Ataxia, Extra ocular palsy, Headaches

In children, tumours may cause behavioural changes and neurological symptoms. Seizures are seen in 30% of affected children with glioblastoma. Chorea, speech problems, or hemiparesis may also be seen in [20] and [22].

Tumours present with visual disturbances when they are located near the visual pathway. In contrast, they may present with endocrinal disorders such as diabetes insipidus and growth disturbances if they are located in the pituitary or hypothalamus regions [18]. Table 1.1 shows more specific signs and symptoms of brain tumours based on location.

1.6. Classification Of Paediatric Brain Tumours

Paediatric brain tumours are often considered idiosyncratic due to remarkable phenotypic variations. Recently, there have been many updates in classification due to a better understanding of developmental origins and genomic features.

Several classification methods exist for paediatric brain tumours. The location of the tumour, age of the patient and histological subtype have been used historically as key considerations when formulating diagnostic and therapeutic approaches [5].

80% of the brain tumours belong to 5 major histologic categories and are medulloblastoma (23%), astrocytoma (22%), juvenile pilocytic astrocytoma (20%), diffuse ependymoma (8%) and craniopharyngioma (7%) [23]. There are more than 100 histological subtypes of paediatric brain tumours, and their in-depth description is beyond the scope of this thesis. Location-based classification of tumours and their histological subtypes is given in Table 1.2.

This review will briefly discuss the latest updates in WHO 2021 classification.

Recent updates in the diagnosis and Classification of CNS tumours:

Conventionally, the treatment of brain tumours was determined by histopathological diagnosis. Histopathology is insufficient to be generally considered the gold standard for diagnosis [24]. Histopathology alone is inadequate to explain the clinical behaviour, biological profile and heterogeneity in treatment response by similar types of tumours [5].

Paediatric neurooncology has undergone a significant transformation with the invention of molecular diagnostics. Genomic and epigenetic data have revealed distinct tumour entities in virtually all paediatric tumours. Historical morphological classification based on histology is rapidly reclassified with additional molecular profiling based on genetics and imaging-based information. The most common malignant tumours are embryonal tumours with biologically variable histopathological appearances and molecular characteristics, e.g., the 2016 World Health Organisation (WHO) classification of medulloblastoma. Four genetically defined variants of medulloblastoma were introduced as subgroups – WNT, SHH, group 3 and group 4 [24]. These subgroups show differences in their clinical behaviours and outcomes. This classification system has tremendous potential in patient stratification and tailored therapies [24].

Table 1. 2 Classification of paediatric brain tumours based upon location adapted from an article by Koob ***[25]***

Location	Site	Tumour Type
Posterior fossa	Cerebellum/vermis/V4	Pilocytic astrocytoma, Medulloblastoma, Ependymoma, Rhabdoid tumour (ATRT)
	Brain stem	Infiltrating glioma Circumscribed glioma
Hemispheres	Superficial	Ganglioglioma, DNET, Pleomorphic Xanthoastrocytoma, Angiocentric glioma, Oligodendroglioma
	Deep	Embryonic tumour, Malignant glioma, Ependymoma
Deep grey nuclei		Malignant glioma, Germinoma
Intraventricular		Choroid plexus papilloma, Subependymal giant cell astrocytoma
Suprasellar		Craniopharyngioma, Optic tract glioma, Germinoma, Hypothalamic hamartoma
Pineal		Germinoma Pineoblastoma Papillary pineal gland tumour

ATRT: atypical teratoid rhabdoid tumour; DNET: Dysembryoplastic neuronal tumour; V4: fourth ventricle.

The 2021 WHO Classification of CNS tumours (CNS5):

Classification of CNS tumours was recently updated by WHO in 2021 and developed from its previous edition, published in 2016. This classification highlights the importance of integrating newer molecular knowledge and conventional histopathological approaches [7, 26].

Some of the essential highlights of CNS5 relevant to paediatric brain tumours:

- This CNS5 classification introduces newer tumour types and subtypes. The most salient feature of CNS5 classification relevant to the present study is that it has separated primarily paediatric gliomas from primarily adult-based gliomas upon distinct genetic profiling [26]. This was a long-awaited change as these are prognostically and biologically different entities. CNS5 classification has a vital role in therapeutic decision-making.
- Clinical tumour grading and grading within subtypes have been modified.
- Paediatric low-grade gliomas are subclassified based on histological features concomitant with the underlying genetic changes to understand gliomas better. Incorporating molecular markers in CNS5 has also enabled subclassifications of high-grade gliomas.
- Ependymoma classification should include anatomical sites along with histopathological grade and molecular features. The tumour's location has been added due to the difference in prognosis [7] [26, 27].
- CNS5 strongly encourages layered diagnostic reports to facilitate the provision of complete diagnostic information. This layered or integrated diagnosis combines different types of crucial information such as molecular, and histological information, and the grading of the tumour.

With the advancements in technology, newer molecular markers get added frequently. As further information is updated and knowledgebase gets more affluent, the classification of CNS tumours remains a work in progress and will continue to evolve.

Medulloblastoma (MB)

Medulloblastomas are the most common malignant brain tumours in children. They arise within the cerebellum and occur in all ages. These tumours are the most frequently studied

tumours [28]. Historically MB's were classified based on pathological appearance as classic, desmoplastic/ nodular and anaplastic variants[19].

Recent updates in molecular pathology and global consensus have classified them as wingless activated (WNT), Sonic hedgehog (SHH), group 3 and group 4 [29] [30]. A summary of the clinical and prognostic features of different subgroups has been given in Table 1.3.

High-risk cohorts and therapy to be administered are determined by age, the extent of tumour resection and metastatic status. Patients older than 3 years with localised disease and treated by gross or near-total resection (below 1.5 cm^2 of residual tumour) are categorised as a standard-risk group [28]. Following standard therapy, an excellent prognosis with above 90% 5-year progression-free survival is shown by standard-risk WNT MB. Beta SHH has a poor prognosis while gamma SHH shows good outcomes. Molecular heterogeneity results in variable prognosis in group 3 and group 4 MBs.

Standard-risk patients are primarily managed by maximal safe tumour resection with adjuvant craniospinal radiotherapy and combination chemotherapy. However, these patients suffer from the toxicities of these therapies with chronic neurocognitive and neuroendocrinal morbidities [28]. In chapter 6 of this thesis, MB patients with post-radiation effects on non-tumoral brain regions are assessed.

Table 1. 3 Medulloblastoma *subgroups summary of* clinical, histological, and molecular features. Adapted from an article by Doussouki **[29]. (**LCA: Large cell/anaplastic; SHH: Sonic Hedgehog; WNT: Wingless)

Subgroup	**WNT**	**SHH**	**Group 3**	**Group 4**
Frequency	10–15%	28–30%	25–28%	40–45%
Age range	6–12 (peaks at 10–12), 17(subgroup)	Bimodal (4, 16)	Infants and young children	All age groups (median 9)
Histology	Mostly classic, rarely LCA, never ND	Mostly ND, classic & LCA (less common)	Classic (most common), LCA	Classic and LCA (less common)
Subgroups	α & β	α , β, γ, δ	α,β &γ	α,β &γ
Anatomic location	Central, frequently Abutting brainstem and Infiltrating foramen of Lushcka	Hemispheric (rarely midline)	Midline (filling fourth ventricle), hemispheric cases reported	Midline (filling fourth ventricle)
Metastatic disease at diagnosis	8.6% α,21.4% β	20%α,33% β,8.9% γ, 9.4% δ	43.4% α,20% β 39.4% γ	40%α,40.7% β,38.7% γ
Genetics	CTNNB1, DDX3X, SMARCA4, TP53 and KMT2D	PTCH1, TP53 (high prognostic impact), KMT2D, DDX3X, MYCN, BCOR, LDB1, GLI	MYC, OTX2, SMARCA4, NOTCH, TGF-β	MYCN, CDKNA, SNCAIP duplications
Chromosomal abnormalities	Monosomy of 6 (diploid in older patients)	9q deletion, loss of 10q and 17p, gains of 3q and 9p	i17q, 1q gain, loss of 5q and 10q	i17q, loss of 8, 10, 11and gain of 4, 7, 17, and 18
Diagnosis	Exon 3 sequencing for CTNNB1 or both nuclear -catenin (IHC) and monosomy 6 (FISH)	Gene expression/methylation profiling and/or IHC for filamin A and YAP1 +/- GAB1	Genome wide methylation, expression array	Genome wide methylation, expression array
Prognosis	97% α 100% β	69.8% α, 67.3% β, 88%. Γ, 988.5% δ	66.2%α,55.8% β, 41.8% γ	66.8%α,75.4% β, 82.5% γ
Possible targeted therapies	Trichostatin A (HDAC inhibitor), other small molecules to inhibit WNT pathway in preclinical studies	Vismodegib, arsenic trioxide, bromdomain inhibitors, aurora kinase inhibitors	Bromdomain inhibitors, HDAC inhibitors, PI3K inhibitors	None

1.7. Role of Imaging:

Neuroimaging is indispensable for the diagnosis and management of CNS tumours. Imaging helps to confirm the diagnosis and eliminates other differential diagnoses such as abscesses, demyelinating lesions, and encephalitis, which may mimic brain tumours [25]. Most brain tumours are primarily treated by surgical resection and supplemented by radiotherapy and chemotherapy. Imaging helps to visualise these tumours, their appearances on CT and MRI, their position, and their relationship to essential structures in the brain and plan the biopsy, surgery, or radiotherapy accordingly. All these imaging findings, the clinical results, and the patient's age are considered in the diagnostic approach [25] [31]. The tumour's diagnosis and treatment are determined mainly by histopathological grading and molecular/genetic information, along with its imaging features. Conventional imaging such as CT and MRI provide structural information such as location, size, and appearance of the lesion on different imaging sequences. Initially, imaging had a limited role in visualising structural abnormality, while now it has greatly evolved to assessing physiological, functional, and haemodynamic alterations as a comprehensive diagnostic tool [32]. Advanced MRI - diffusion, perfusion or MR spectroscopy can provide information on the blood flow, blood volume/permeability and chemical composition. Functional MRI (fMRI) can provide information on motor or language function.

Intraoperatively, MRI enables safer surgery and ensures the completeness of tumour removal. Such intraoperative MRI is routinely performed at Alder Hey hospital.

Post-operative imaging is a non-invasive tool to evaluate the residual tumour volume, tumour response to therapy and possible new lesions/metastasis or pseudoprogression. Follow-up scans are part of routine brain tumour imaging protocol and present research is conducted on these follow-up scans. Selecting a suitable neuroimaging modality is essential to detect early tumour recurrence and treatment failures. Table 1.4 provides the use of imaging at different stages of brain tumour management. Different imaging modalities used in diagnosing and managing paediatric brain tumours are described below.

Table 1. 4 Role of imaging during different stages of brain tumour therapy. Adapted from a chapter by Zeleňák et al. [33]

Diagnosis	During Treatment	Post treatment
• Tumour Detection • Characterisation of tumour such as location, margins, size, extension, midline shift, adjacent important structure, vascularity, contrast enhancement, oedema, etc • Staging and differentiation	• Surgical planning • Intraoperative surgical assessment • Radiotherapy planning and delivery	• Post-operative assessment • Tumour recurrence • Radiation necrosis detection

1.7.1. Role of Computed Tomography (CT):

CT is often used as a preliminary technique for visualising brain tumours. It is a swift technique that is radially available to [18]. It is a screening tool to exclude intracranial pathologies during emergencies when access to MRI is limited. However, CT is more than a screening tool for the initial examination of brain tumours. CT provides information about the tumour's location, bony structures and the presence or absence of calcification within a few seconds. MRI is not an excellent tool to see calcifications. However, the information provided by CT is inadequate for the soft tissue visualisation, tumour boundaries and extent of brain tissue and tumour characterisation [18]. Contrast-enhanced CT may be taken to visualise tumour enhancement, but it is not necessary if MRI is scheduled.

1.7.2. Magnetic Resonance Imaging (MRI):

MRI is the most critical imaging technique in neuroimaging. MRI gives excellent 3D visualisation of soft tissues and the brain without harmful ionising radiation. MRI images are used for the present research work, and hence some basics of MRI and its role in paediatric brain tumour imaging will be briefly discussed.

MRI system comprises a giant magnet, gradient coils, and a radiofrequency coil (Fig.1.1). The patient is positioned in a big magnet bore. A constant, spatially localised, and strong magnetic field (B0) is generated by gradient coils using electric current [34]. Gradient coils are used sequentially for three-dimensional (along x, y and z plane) localisation of gradients and to create MR image [34]. The radiofrequency coil transmits the energy to the body and receives the body field signal [35]. This signal is digitalised and then sent to the computer in the control room. Complex mathematical algorithms are applied, and the image is reconstructed.

A solid external magnetic field is created when an electric current is applied. The hydrogen nuclei (also known as protons) from different body tissues align themselves along or opposite to this external field B0. When an RF pulse is applied perpendicular to B0, energy is absorbed by the nuclei, and they change their energy states and resonate. When this RF is stopped, tissues relax and emit this energy received by a receiver coil and transmitted to the computer as a voltage-current [36]. Different tissues have different relaxation times, and hence contrast is generated, and we can visualise other structures. TR (repetition time) is the time between successive pulse sequences, while TE (echo time) is the time between the application of the RF pulse and receiving the echo signal [37].

Figure 1. 1 MRI machine components and patient position. Adapted from *[35]*

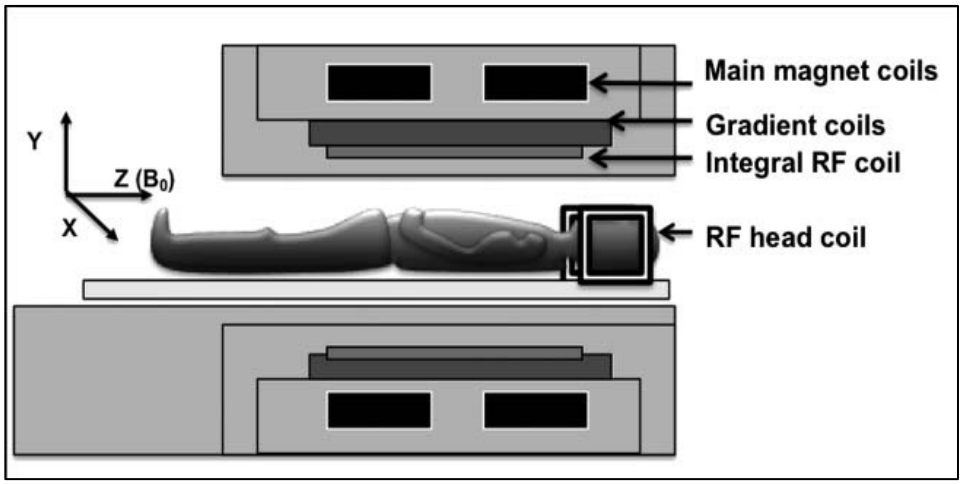

Tissue relaxation time is characterised by T1 (longitudinal relaxation) and T2 (transverse relaxation) times. T1 is represented by short TE and TR, while long TE and long TR describe T2.

These T1-weighted (T1W) and T2-weighted (T2W) along with the FLAIR (Fluid Attenuated Inversion Recovery) sequences are known as the conventional MR techniques. A gadolinium contrast agent is injected intravenously to enhance the visualisation of brain tumours in T1W imaging. These T1W post-contrast images can also detect breaches in the blood-brain barrier (BBB). These four conventional sequences are included in the basic neuroimaging protocol for brain tumour imaging. These images are obtained in all 3 planes – axial, coronal and sagittal. Images can be obtained as 3D volumes where images are captured in all 3planes or 2D for a particular plane. Indications of conventional MR sequences in brain imaging are summarised in table 1.5.

In this study, we have used 2D axial T2W images because they play an essential role in visualising white matter pathologies and cortical lesions. Also, T2W images were consistently available in all these patients with brain tumours.

Table 1. 5 Indications for Conventional MRI sequences in brain imaging

Imaging Sequence	**Indications**
T1 W and inversion Recovery	Anatomy, Structural abnormalities, T1 characteristics of lesions.
T2 W	Pathologies process leading to increase in water content for example: oedema, necrosis, or cystic lesions. White matter and cortical lesions. Evaluation of ischaemic changes, demyelination, degenerative diseases, trauma, vasculitis.
Fluid attenuated inversion Recovery (FLAIR)	Excellent contrast resolution at the brain-CSF junction and improves visualisation of white matter lesions, Differentiation of CFS and non-CSF containing structures
T1W post contrast	A breach in the blood-brain barrier (BBB) due to neoplasms, infections, or inflammation.
Diffusion weighted Imaging (DWI)	DWI measures the movement of water molecules. Without the need of external contrast agent [38]. It is more sensitive marker of cellularity than tumour size.
Perfusion Weighted Imaging [39]	Dynamic Susceptibility Contrast (DSC)-MRI and Dynamic Contrast-Enhanced (DCE)-MRI are two techniques. Useful to assess tumour grading and response to treatment
Magnetic Resonance Spectroscopy (MRS)	It helps in the quantification of neurochemicals. Useful for diagnosis of tumour and response assessment.

1.8 Role of MRI in the diagnosis of Paediatric Brain Tumours

MRI enables the non-invasive assessment of brain tumours that aid clinical decision making. MRI provides excellent tissue visualisation non-invasively. This helps with the diagnosis and includes essential information on response and progression, which serves as clinical endpoints in trials [40]. MRI is the heart of present neuroimaging, allowing excellent structural characterisation and cellular, molecular, vascular and functional information [41].

Structural MRI

Structural MRI is the foundation for brain tumour MRI examination. It provides information on the structural changes such as the location of the lesion, size, extent of involvement and associated changes in the surrounding brain parenchyma [41]. Classic appearances of some tumours on MRI provide a differential diagnosis to serve as a starting point for management, but it cannot provide accurate histological type in all cases. MRI provides superior visualisation of infiltrated tissue than CT. Intravenous gadolinium-based contrast agents shorten T1 relaxation time and increase tissue contrast. They enhance the visualisation of brain tumours. Enhancement only provides information on the leakiness of the BBB [20]. The type of enhancement seen after the injection of the contrast agent may provide important information about the type of tumour [42] [43]. The appearance of a tumour on different MR sequences together forms a basis for diagnosing a tumour type. Table 1.6 and Table 1.7 give information on the typical appearances of different paediatric brain tumours on different MR sequences.

Challenges in conventional MR imaging:

Conventional MRI is sensitive to structural brain changes and other mentioned tumour characteristics; however, it provides inadequate information about tumour physiology, function, and metabolism [33]. A significant number of paediatric brain tumours do not enhance gadolinium contrast. It is challenging to grade these tumours by conventional MRI [44]. The increasing evidence base suggests that assessment of the tumour response based upon the size of the tumour done with structural imaging has many limitations, such as poor reproducibility and inaccurate prognosis. Brain tumours have complex nature and are inherently heterogeneous, and multiparametric functional imaging can be helpful [45].

Differentiation between tumour recurrence and radiation necrosis is difficult to distinguish in conventional MRI [46].

This highlights the need for advanced multifunctional imaging modalities that can help to provide more information on evolving brain cancers.

Advanced MRI

Advances in MRI have enabled it to facilitate the evaluation of metabolic, functional, and biochemical changes. These techniques can complement genetics non-invasively. There is an association between genetic changes in tumour biology and advanced imaging features of the morphological phenotype [41]. Advanced MRI such as diffusion, perfusion, MR spectroscopy and functional MRI have provided practical quantitative tools correlating with diagnosis, treatment, and prognostic assessment of brain tumours by providing detailed information about tumour grading, cellularity, vasculature and microstructure[45] [47]. Table 1.8 shows the different advanced MRI techniques and their role in brain tumour imaging. Information from each modality is essential to understanding the complex cancer environment.

Table 1. 6 Conventional MRI diagnostic imaging chart for the most common glial and ependymal tumours ***[48]***

Tumour Type	Location	Imaging features
Pilocytic Astrocytoma	Cerebellum, Optic Pathway, other locations	CT: An isodense nodule that may show contrast enhancement with surrounding hypodense cyst T1W: iso or hypointense to grey matter, T2W; hyperintense -similar intensity with CSF. DWI: Restricted diffusion and Post- Contrast: avid gadolinium enhancement of solid portion or in the cystic walls
Pilomyxoid Astrocytoma	Suprasellar region	A cystic component may be present at the core. H shaped imaging feature T1W: Hypointense T2W: Hyperintense Post-contrast: homogenous or heterogeneous enhancement
Diffuse Midline Glioma	Brainstem, specifically pons but may infiltrate all other parts and spinal cord	Infiltrative pattern and presence of necrosis. Often displacing or engulfing the basilar artery. May present with exophytic features. T2W: variable intensity. Subtle areas of enhancement with a mild linear or punctate form. DWI: variable restriction mainly ranging from mild to normal restriction
Ependymoma	Posterior fossa. May occur supratentorial, infratentorial or spinal locations	Posterior fossa ependymoma extending through the foramen of Luschka and Magendie, heterogenous high T2W signal intensity and calcifications on susceptibility sequences. DWI – intermediate pattern of restriction. Postcontrast shows avid enhancement of solid components with several non-enhancing cystic and/or necrotic components.

Table 1. 7 Conventional MRI diagnostic imaging chart for the most common embryonal paediatric brain tumours ***[48]***

Tumour Type	**Location**	**CT Imaging features** **MRI features**
Medulloblastoma	WNT: lateral recess of fourth ventricle or cerebellopontine angle SHH: cerebellar cortex Group 3 and 4: Centre of four ventricle	CT: Hyperdense mass in the vermis/CP angle or cerebellar hemisphere. Intratumorally necrosis, haemorrhage, and calcifications may be seen. T1W: Low signal, T2W: Low signal, High FLAIR; Post-contrast: SHH: multinodular pattern with enhancement, WNT and group 3: moderate enhancement, Group 4: min or no enhancement DWI: the presence of restriction, MRS: aggressive metabolite pattern, elevated choline, lipid and lactate peaks
AT/RT(atypical teratoid/ rhabdoid tumour)	Cerebellum, midline. extra-axial and intra-ventricular locations, cranial nerve involvement	Heterogenous tumour with restriction of some parts on DWI. Leptomeningeal seeding may be observed. Necrosis, cystic formations, and haemorrhage are noted. Aggressive metabolite pattern on MRS,

Table 1. 8 Advanced MRI techniques used in brain tumour imaging *[49] [45]*

Advanced MRI Technique	**Provided Information/ Pathophysiological Correlates**
Diffusion-Weighted Imaging (DWI)	Cellularity and water movement
Perfusion-Weighted Imaging (PWI)	Angiogenesis and vascularity
Magnetic Resonance Spectroscopy (MRS)	Composition of metabolites such as choline: creatinine ratio
Intrinsic Susceptibility-Weighted MR Imaging	Level of tissue oxygenation
Diffusion Tensor Imaging (DTI)	White matter architecture, nerve tracts

1.9 Management of Paediatric Brain Tumours

Brain tumours are very challenging to manage, especially in the paediatric population. The diagnostic procedure is complex; the brain is protected by the blood-brain barrier (BBB), limiting the penetration of the drugs, and surgery is complicated [50]. It is essential to preserve brain function and limit morbidity while improving survival in these patients.

Treatment of children with brain tumours needs a multidisciplinary approach with several specialists such as a Paediatric Oncologist, Neurosurgeon, Neuroradiologist, Paediatrician, Radiation Oncologist, Endocrinologist, and Psychologist, Pathologist and Specialist Nurses. First and foremost, the therapy aims to cure or control the tumour and improve survival. Another important goal of the treatment includes preventing long-term complications and minimising the child and family [51].

Treatment of these tumours is dependent on location, age at diagnosis and the specific tumour type. Recent studies show the importance of molecular markers in the management and treatment planning [52]. Advances in molecular diagnostics have bought a transformation in approaching these tumours, and molecular classification is rapidly evolving. Genomics identifies newer tumour subtypes that can facilitate the personalised approach to treating these tumours; for example, medulloblastoma subtypes have different genetic and epigenetic markers that determine the prognosis and type and dose of chemotherapy.

At each time in the patient pathway, the decision is made for a more active or passive form or more enthusiastic or inactive treatment [53]. This is determined by age, histological diagnosis, molecular markers, survival scores and imaging-based assessment during different stages of the disease. Treatment may generally start with steroids to manage neurological symptoms. Depending upon the location and imaging features, the neurosurgeon decides whether to perform a biopsy or proceed with resection. After surgical excision, radiotherapy may be administered. Depending on diagnosis and treatment planning, chemotherapy is concurrently or separately given in a few cases if required.

1.9.a **Surgery:**

The neurosurgical opinion is essential in the early stages and decides the management line. Almost all brain tumours are treated with surgery as the first line of therapy except for a few tumours at specific locations and types. Neurosurgery is considered in patients where tumours can be safely resected [54]. Hydrocephalus, biopsy, and tumour resection are managed by neurosurgical` intervention. The primary surgical aim is complete resection, particularly in patients with infiltrative glioma, ependymoma, and medulloblastoma [52]. Adjacent neurovascular structures, the degree of infiltration and disseminated tumour, if present, are all factors that determine the extent of the tumour resection [55]. Maximal total resection can be compromised by the anatomical location of some tumours, for example, in the brainstem [56]. Significant morbidity is associated with large tumours near important brain structures such as the brain stem, optic tract, and hypothalamus. Some tumours show a high recurrence rate even after gross total resection. As a result, several other treatment modalities have evolved as an adjuvant or primary treatment of tumours when surgical management is restricted. For example, germ cell tumours are more sensitive to chemo-radiation.

Surgical planning starts with an initial examination and history at the presentation. Steroids are prescribed to provide symptomatic relief and antiepileptic agents in patients with seizures. As visualised by different neuroimaging techniques such as CT and MRI, the tumour's location can help plan neurosurgery. In some tumours, such as choroid plexus carcinoma, treatment is started with chemotherapy before surgical resection for the safer and total tumour resection [57]. Surgery is advised in the cases with raised intracranial pressure and deterioration and tumour progression, as evident on serial scans [58].

Neurosurgical intervention needs the excellent teamwork of experts for a successful surgery. These include anaesthetists, nurses, operating room technologists and neuroradiologists. Surgery is planned after discussion with all the team members about anticipated complications in each patient. Each patient requires a unique and personalised surgical plan depending upon presenting pathology [57], such as type of tumour, size of the tumour, location and presence or absence of metastasis. Most of the low-grade tumours and other non-metastatic tumours are treated by complete resection. Intraoperative MRI is an excellent modality to confirm the complete resection of tumours such as medulloblastoma and ependymoma. Tumours such as optic pathway glioma cannot be entirely

removed by surgery, and their location restricts removal. Subtotal resection or biopsy are the only goals of surgery in these cases.

Several patients included in this study have undergone surgical intervention before radiation. Post-surgical changes in these patients will also affect the specific brain areas under consideration. Additional care was taken during the image registration of these patients. These steps are discussed in detail in chapter 3.

1.9.b **Radiotherapy (RT)**

Radiotherapy (RT) is considered a cornerstone of the paediatric CNS tumours [59]. RT plays an important role, especially for brain tumours, because obtaining a sufficient surgical margin is difficult in brain tumours. RT is planned after considering the type of tumour, timing, required radiation dose, type of radiation modality, and anticipated toxicities of multimodal therapies [60]. RT is generally avoided in children less than three years of age. Advances in radiation technology enable safer, precise irradiation and reduced toxicity.

The rationale for the use of radiotherapy:

Selection criteria include age, tumour type and location, and other treatments received or planned. RT is indicated as definitive focal therapy where surgery is not an option due to morbidity concerns, e.g. infiltrative brainstem tumours and optic pathway gliomas. Focal RT is advised after near-total or complete resection to eliminate microscopic residual to reduce the risk of local recurrence, e.g. ependymoma. Focal RT is given after incomplete resection to reduce the risk of progression, e.g. craniopharyngiomas.

Wide field RT is prescribed to eliminate more widely disseminated micrometastases. e.g. whole ventricular RT for intracranial germinomas, craniospinal RT for standard-risk medulloblastoma. Wide field RT is also indicated for established metastases, e.g. medulloblastoma and ependymoma.

Biology of radiation therapy [61] [62]: As radiation travels through tissue, it causes the ionisation of water molecules to produce free radicals and reactive oxygen intermediates. These cause DNA damage, inducing cell death through mutations affected by radiation and present with demyelination, focal necrosis due to mutations, DNA damage, or apoptosis in a tumour cell (Fig.1.2). Normal brain regions are also vascular lesions, calcifications and gliosis. These effects lead to radiation toxicity.

Figure 1. 2 DNA damage caused by ionising radiation by ionisation of water. Adapted from *[62]*

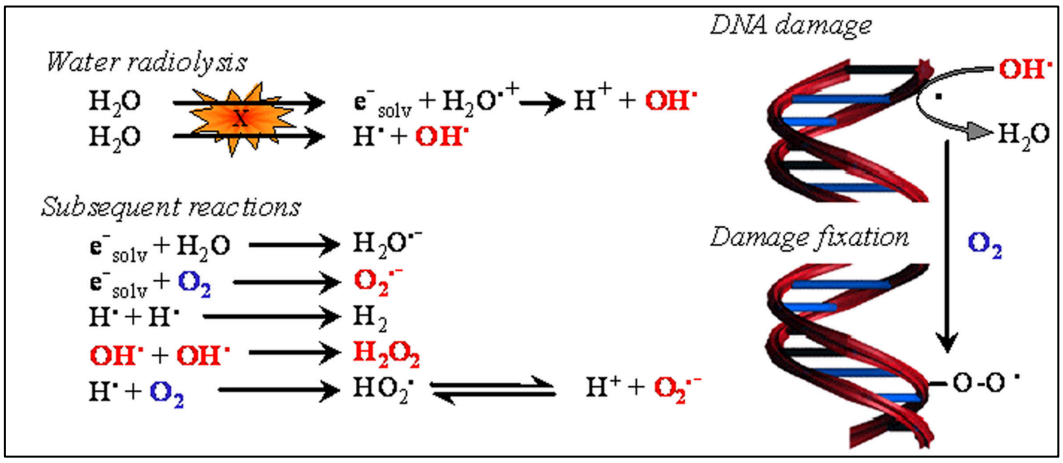

Radiation therapy is delivered by fractionation to reduce the damage to normal cells and limit toxicity. The process of radiation therapy fractionation can be summarised with the 4R's – repair, redistribution, repopulation and reoxygenation. Fractionation allows the restoration of sublethal damage to normal tissue. During the interval between fractions, redistribution of cancer cells to the radiosensitive phases of the cell cycle and reoxygenation of less sensitive cancer cells helps cell killing in the next cycle. These fractions aim to prevent the repopulation of tumour cells.

RT planning starts with 3D imaging of the tumour to get information about the extent and potential toxic effects on the child [61]. Both CT and MRI are used for contouring and volume definition. Steps of RT planning have been described in Fig. 1.3. CT is used for accurate dose calculation, while MRI is used for excellent soft-tissue visualisation and mapping of gross tumour volume (GTV).

Photon Radiation Therapy:

Most used photon (high energy x-rays) radiation therapies in paediatric brain tumours are 3D conformal radiation therapy (3DCRT) and intensity-modulated radiation therapy (IMRT).

IMRT provides better conformity around irregular tumour volumes but can adversely affect dose homogeneity. The decision upon selecting the type of photon radiotherapy is based on the balance between tumour area involvement, dose homogeneity vs dose to non-target tissue impacting neurocognitive function [63]. IMRT allows significant control to focus the radiation dose on minimising the amount to surrounding normal tissues. IMRT is the standard of care for many malignancies.

However, normal tissues next to target volumes still receive substantial radiation because of photons' physical properties, especially with the exit dose [64].

Figure 1. 3 Steps involved in radiotherapy from planning to delivery and adapted from an article by Carlos et al. *[65]*.

Immobilization	Image Acquisition	Planning	Patient Positioning	Treatment
•Reproducibility •Fewer errors due to pateint motion •Ensures correct position •patient comfort	•3D simulation •Evaluation of respiratory and internal tumour motion •Decistion to manage motion	•Definition of targets and organs at risk •Use of multiple radiation field •High gradients •Use of appropriate algorithms for dose callculation •Evaluation of dose distribution	•Image-guided patient positioning IGRT •Fewer random and systemic errors •Use of 3D corodinated of target tumour for radiation therapy delivery	•Management of interfraction motion •Use of strategies to manage respiratory motion - Gating and Tracking •IGRT monitoring

Figure 1. 4 shows a comparison of radiation plans in proton (a) and IMRT (photon) therapy (b). The red arrow indicated the hypothalamus. The figure is taken from an article by Mailhot Vega, R. et al. *[66]*

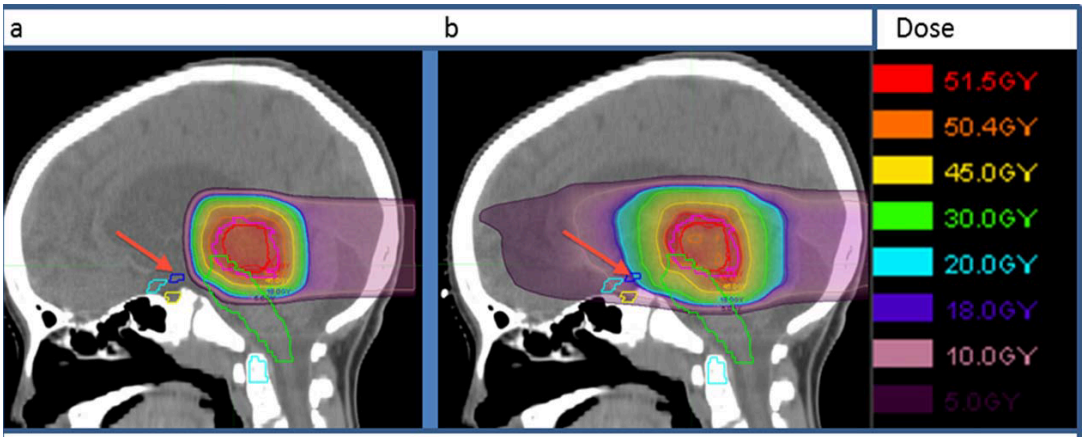

There is a trend toward restricting the normal part of the brain exposed to radiation to reduce these toxic effects. Another type of radiotherapy known as proton therapy was developed to reduce some of the above-mentioned harmful effects. There is still a need for evidence to understand the impact of

protons on tumours and standard parts of the brain. However, with increasing awareness about the side effects of radiation in children, treatment strategies are being developed to reduce the impact.

Proton Beam Radiation Therapy (PBT):

PBT is another popular modality that delivers a lesser peripheral radiation dose than IMRT (Fig 1.4). This therapy uses a beam of high energy protons. Protons are positively charged atomic particles that are heavier than electrons. These protons pass through normal tissues with negligible dose deposition till they reach the target [67]. This point of the highest dose is known as the Bragg peak (Fig 1.4). The depth of height is decided by initial energy. There is no exit dose as the dose beyond Bragg's peak falls to zero.

Proton therapy provides excellent dose localisation. Proton therapy reduces the radiation dose to the non-tumoural tissues and spares surrounding vital structures such as the pituitary gland and hippocampus [59, 68]. With the small field irradiation, proton therapy can reduce the volume of irradiated normal tissues by 2 to 3. Proton beam radiotherapy can reduce this volume by 6 to 11 in patients receiving craniospinal irradiation [69]. As adjacent normal tissue does not receive a large radiation dose, proton therapy can deliver a large dose of radiation to the tumour resulting in more excellent cure rates [70]. According to the NHS England clinical commissioning policy proposition on proton therapy, theoretically, PBT offers significant dosimetric advantages, which is more critical to children and young adults with developing and growing bodies and many years to live with the toxic effects of therapy [70]. PBT has been internationally accepted as a treatment of choice for the paediatric population.

The radiobiology of protons is different from that of photons due to differences in the type of DNA damage [67]. Relative biologic effectiveness (RBE) is the ratio of the physical dose of a reference photon radiation to the biological dose of protons required to achieve the same biologic effect [71].

This RBE of protons has been assumed to be 1.1 [72]. However, this was decided upon short term in-vitro studies, and there is increasing evidence questioning the accuracy of constant RBE 1.1 in normal living tissue [72]. Newer studies show this RBE to be 1.1-1.5 and higher in some situations. The dose prescribed to the patient during PBT is calculated based on this RBE (fig 1.5). Thus, incorrect RBE results in the incorrect physical dose.

This RBE was always measured at the centre of the spread-out Bragg peak (SOBP) (Fig. 1.5) and is likely to be different at different points of irradiated tissue. Thus, linear energy transfer (LET) levels are not uniform along the entire SOBP and are higher towards the end of the Bragg peak.

Figure 1. 5 *Depth Dose Curve demonstrating the relative dose delivered along with the tissue depth by each therapy. Photon delivers maximum dose at the entry while proton delivers maximum at the Bragg Peak. The figure* shows the proton Bragg peak at the tumour target delivering the highest dose. Proton radiation dose falls to zero beyond Bragg's peak. It was adapted from an article by Mohan et al. *[71]*. SOBP- spread-out Bragg peak *where maximum proton dose is delivered at the target tissue*.

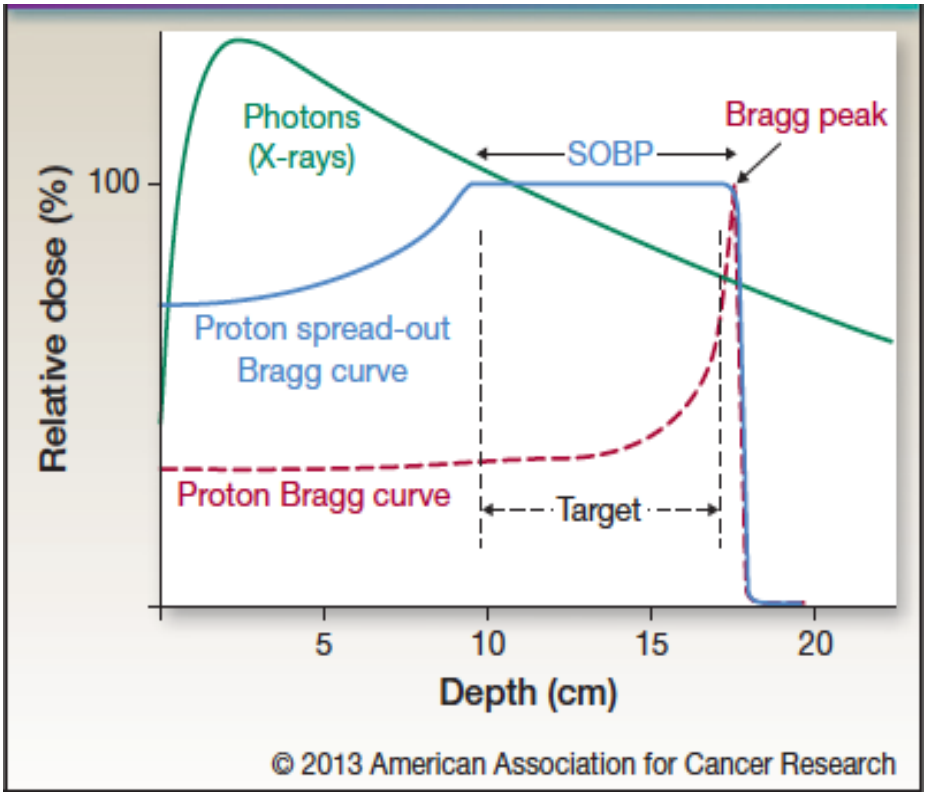

RBE is not a constant value and changes depending upon the type of tissue and radiosensitivity. A higher ionisation event within the Bragg peak causes increasingly clustered DNA damage, which is impossible to repair. Though this is beneficial for the tumour, it is highly toxic to the normal tissue closer to the tumour. If such delivered dose is higher, it can be toxic to normal tissue, while a lower amount will be insufficient to cure the tumour cells. This warrants more research for safer dosing of proton radiotherapy. The scientific community questioned the previous assumption of proton therapy dose as a 10% reduction of photon dose and seemed to be incorrect [72].

The major disadvantage of photon therapy is the requirement of a large dose that exits through normal body parts. Conventional therapy deposits the maximum dose in the subcutaneous tissue and targets the tumour, but it continues to impart the amount to normal tissue (Fig. 1.4,1.5). This exit dose affects larger volumes of adjacent normal tissues outside the primary radiation beam. This low dose radiation may increase the risk of late effects such as secondary malignancies, which occur at low doses.

Arguments against the use of Proton therapy:

Intensity-modulated radiation therapy (IMRT) is the newer development in the delivery of photon therapy with the advantage of a high degree of control over the dose distribution. This modulates the intensity of photon beams and reduces the dose received by surrounding normal tissue. Though proton therapy is advantageous concerning dose deposition, the financial cost is extremely high compared to IMRT. As described earlier, RBE, which is considered 1.1, may not be appropriate as per recent studies. High-quality studies about improved quality of life and long-term benefits of proton therapy over photon are still needed because the current literature is inadequate due to short follow up and lack of studies [69] [73] [70]. It may be unethical to design randomised control trials to compare proton vs photon directly. As per the NHS commissioning policy for proton beam therapy in children, there is insufficient evidence to determine if protons reduce the late risk of secondary malignancies. The current literature is based on a few studies, and long-term follow-up is required [70]. Some of the latest publications have shown the recurrence and survival rates to be comparable between the two. [74] [64] [16, 75]. The radiobiology of protons is unclear, with more physical and biological uncertainties. There is no quantitative evidence to support the reduced risk of toxicity with proton therapy than that of photon [16]. Patients present with different clinical manifestations following proton and photon therapy; for example, there is a higher incidence of radionecrosis following proton therapy than photon [76]. Radiobiology uncertainty makes it harder to predict clinical outcomes in proton therapy [73]. Considering the logistics, as it might be challenging for some families to stay away from home for up to 6-8 weeks, proton therapy still has limited availability and higher cost [77] [70] . There are only two centres (Manchester and London) in the UK that provide PBT for paediatric brain tumour patients. Patients might have to travel far and wait for an appointment which might worsen the outcome in some tumours [64]. Treatment planning for proton therapy needs more time for monitoring and replanning.

Radiotherapy is generally administered after surgical resection of the tumour. Hence, most tumour tissue is often removed along with some marginal tissue, and the irradiated area mainly includes normal

brain tissue. There is a need to understand the tissue changes induced by proton therapy dose at margins. Incorrect RBE assumptions can lead to the wrong proton beam dose at the Bragg peak, where very high energy is deposited because of the highest LET at the distal end of the proton beam, and LET may vary along the path. Hence, the end of beam range (Bragg Peak) should not fall within critical structures such as the brainstem. This highlights the importance of broader research surrounding the radiobiology of proton therapy, as the dose delivered may not be the same as the prescribed dose due to incorrect RBE calculation.

Long term follow-up data on the substantial clinical gain by PBT is still insufficient [70]. The theoretical benefit of PBT is a reduction in the risk of late and very late side effects. More research is required to understand the uncertainty in the long-term effects of proton therapy, and it is challenging. Due to ethical issues, randomised clinical trials to compare photon vs proton has not been possible. This is because proton therapy's dosimetric benefits are far superior, and parents would find randomisation unacceptable. It is essential to understand the tissue level difference between both therapies and their long-term effects. T2 MRI scans are helpful to visualise white matter changes in the brain. One of the aims of this study is to compare the longitudinal follow up T2 MRI images following proton and photon therapy at the same radiation dose. Quantitative changes seen on MRI in the non-tumour bearing brain areas may act as a surrogate for late effects. This will be discussed in chapter 5.

1.9.c **Chemotherapy**

Chemotherapy primarily serves as an adjuvant treatment for brain tumours. It has different roles during different stages of treatment. Chemotherapy is also administered to shrink a tumour size before surgery [57] or prevent its recurrence [78]. Chemotherapy is systemic therapy affecting all organs in the body in contrast to localised radiation therapy.

Chemotherapy can delay the timing of radiation therapy or replace radiotherapy in very young children, stabilise tumours, reduce radiation dose or as an alternative to the radiation [79].

Primary chemotherapeutic agents include alkylating agents, antimetabolites, anti-angiogenic agents, vinca alkaloids etc. Novel targeted therapies are currently under investigation by [51]. Average cure rates in patients with intermediate-risk medulloblastoma are increased with adjuvant chemotherapy. A retrospective study of 92 children with metastatic medulloblastoma showed improved treatment outcomes, increased total resection rate, and positive neuropsychological results without additional postoperative complications [80].

Chemotherapy is an additional factor causing tissue changes in our patient cohort. Unlike radiation, it will be responsible for overall changes in the entire brain. Side effects include white matter changes, neurocognitive changes, hair loss, reduced immunity etc. Recent advances in tumour biology and molecular markers have encouraged the discovery of novel agents with specific targets that have a role in tumour proliferation and survival [81]. Toxicity to the normal cells can potentially be considerably reduced with these targeted therapies.

1.10 Imaging-Based Treatment Response Assessment:

Response to the therapy is assessed by several clinical determinants such as a change in tumour size, volume on imaging and clinical symptoms [82]. Standard criteria such as McDonald, Response Evaluation Criteria in Solid Tumours (RECIST), and Response assessment in neuro-oncology criteria (RANO) have been developed by different study groups [83]. For pediatric patients, response assessment in pediatric neurooncology (RAPNO) was specifically developed [84].

These criteria are dependent on the change in the size of the tumour. However, research shows that the size of the tumour is not an accurate marker to measure the response to therapy. This might result from other confounding factors such as corticosteroids or the oedema [82]. Along with this significant drawback, they do not give a good idea about other pathophysiological (necrosis, haemorrhage, cavitation), functional or metabolic changes in response to therapy. An uptake of gadolinium on an MRI scan known as contrast enhancement is also not an accurate determinant of response. Pseudoprogression is radiologically described as a transient increase in the size of contrast enhancement that mimics tumour growth [ref]. This is histologically different from actual tumour progression [ref]. Pseudoresponse is described as radiological improvement without any associated biological response or clinical improvement. Differentiating accurate progression/response from pseudoprogression/ response can be challenging in structural MRI. These terms were previously described exclusively in adults; however, 21% of paediatric patients receiving radiation therapy have been reported with pseudoprogression [85].

Early assessment of treatment response to identifying nonresponsive tumours will help initiate effective second-line treatment at earlier stages. Still, it will also eliminate the unwanted toxicity of conventional therapies. Newer biomarkers are needed, and further studies should be directed to assess tumour response accurately. This timely treatment will save considerable time and cost of treatment in patients with brain tumours while reducing the side effects of inefficient therapies.

1.11 Complications Of Treatment Therapies And The Role Of MRI:

Paediatric brain tumours are treated with a multimodal approach, including surgery, chemotherapy, and radiotherapy. The intimate relationship of these tumours with critical structures within the brain and the ability to infiltrate locally with nervous tissue poses a significant challenge to treatment. Each therapy has its toxic effects, especially with earlier radiotherapy, including neurocognitive and neuropsychological changes, secondary cancers, and inadequate growth [68]. Surgery and chemotherapy have been shown to produce white matter changes in sites distant from tumours warranting attention to possible long-term effects of these treatments [86].

Surgical complications include CSF leak, meningitis, wound infections, and cranial nerve palsies. Posterior fossa syndrome (PFS) or cerebellar mutism is a common complication after removing posterior fossa tumours. It is characterised by diminished speech or mutism and emotional lability [87]. Young age, male gender, midline tumours, especially medulloblastoma and brainstem tumours, are predisposing factors [88]. This syndrome is characterised by mutism 1-4 days after surgery. Symptoms include mutism, oculomotor apraxia, emotional instability and cerebellar dysfunction [57]. These patients require long term rehabilitation and may develop long term cognitive and motor deficits.

Other side effects such as oedema, hydrocephalus, ischemia, neurological deficit, and haematoma significantly impact. Surgical complications and associated neuroimaging characteristics require further investigations in the case of cerebellar mutism. Initial MRI study in paediatric patients shows the association of post-operative periventricular ischaemia, calcification and haemosiderin deposition with cerebellar mutism [89]. Diffusion MRI abnormalities can serve as early markers for detecting children at risk of cerebral mutism [90].

As with any other cancer therapy, radiotherapy has several side effects. These side effects can be acute, early, delayed, or late depending on the time of presentation (Fig 1.6).

Acute side effects are seen in most of the children treated with radiation. These side effects involve – erythema, hyperpigmentation of the skin, loss of hair at the entry/ exit of radiation, headache, nausea, vomiting, otitis media, conjunctivitis, acute parotitis etc. [59]. However, late neuropsychological effects of radiation therapy have significant cognitive, academic and socioeconomic sequelae [91]. Paediatric patients treated with radiotherapy present with decreased white matter volume, radiation injury to

microvasculature and cognitive impairment leading to attention deficit and problems with visual perceptual skills and memory. High dose radiation in the hypothalamic region can lead to delayed onset of hormonal deficiency[55]. Radionecrosis is a devastating side effect that is seen as a late effect. There is an increased risk of secondary tumours after radiotherapy. Fig 4.1 in chapter 4 shows the Clinical manifestations and pathophysiology of progressive radiation brain injury.

Figure 1. 6 Types of radiation-induced brain injury based on the presentation time *[92]*.

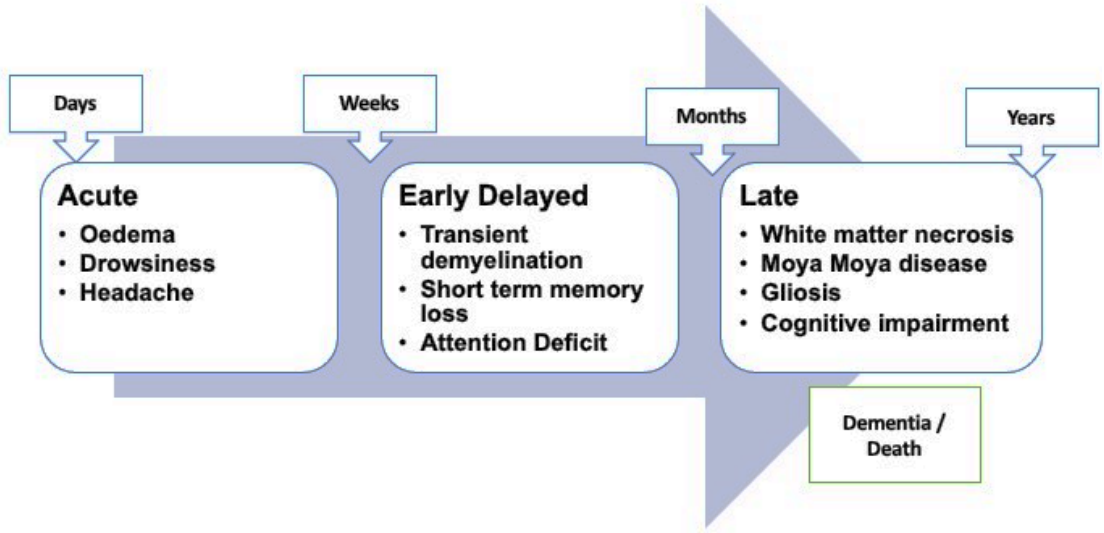

Radiation has immediate and late effects on CNS. Advanced MRI is a promising modality to study these changes. Functional anisotropy (FA) of a white matter seen on DTI represents the status of tissue microstructure and architecture. A cross-sectional study by Khong et al. demonstrated the association between a loss of FA after cranial irradiation and IQ score [93]. Magnetic Resonance Spectroscopy (MRS) studies show a reduction in N-acetyl aspartate ratios in the white matter in patients irradiated for leukaemia. Advanced MRI can demonstrate white matter changes, contrast enhancement, reduced FA and radiation-induced meningioma. Hyperintense foci are found to be progressing to peripheral regions[93]. Preliminary findings with 3D-EPSI (echo-planar spectroscopic imaging) and DTI have shown promising early detection of the subacute radiation injury in adults with lung cancer [94]. Radiotherapy also causes vessel wall thickening and damages endothelial cells resulting in cellular microbleeds and occlusions [92, 95].

Radiotherapy is responsible for multiple neurotoxic effects on the brain. White matter (WM) is most vulnerable. Even with low doses, impaired cognitive performance, lower IQ, poor growth, impaired

pubertal development and obesity are seen in [96]. Preclinical studies have shown damage to neuronal, glial, and vascular compartments of the brain leading to hampered molecular and cellular functions. Multiple studies affect the hippocampus after radiotherapy, impairing memory function and cognition [97]. Rodent studies reveal the more complex problems such as degeneration of axons and ischaemia, warranting analysis of several brain regions to display possible underlying side effects [98]. Clinical symptoms of radiation damage may be delayed and occur several months after the therapy. A reliable neurobehavioral assay to measure subacute injury is yet to be developed. There is a need for quantitative measures in the assessment [94].

Chemotherapeutic drugs are responsible for white matter damage, hearing loss, and other toxic effects. Concurrent cranial radiation compounds the poisonous effects of the chemotherapy [96]. Chemotherapeutic treatment with vincristine, cyclophosphamide, or cisplatin has decreased FA values in structures such as cerebellar hemispheres and brainstem on MRI scans. This was also associated with poor performance at school and mild to severe cognitive impairment [98].

While various therapeutic approaches have been developed to treat paediatric brain tumours, the response depends on the histological subtype, tumour location, and size.

Although with advances in therapies, overall long-term survival has improved, it is associated with morbidity and related neurological complications, including neurotoxicity. Neuronal toxicity impacts cognition, memory, intelligence, function, and attention. These symptoms may start to appear several months after the chemotherapy or radiotherapy. MRI has been effectively used to evaluate tumour growth and structural and functional changes in white matter architecture (diffusion tensor imaging). However, the clinical radiological workflow often uses these methods descriptively, which is insufficient for accurate assessment. Considering lifelong consequences and impact on quality of life in brain tumour survivors, there is an urgent need for an early, precise diagnosis of CNS complications.

Despite established treatment therapies and known side effects of radiotherapy in the paediatric population, current literature poses several limitations affecting survival and quality of life in children with brain tumours. Critical gaps in existing evidence:

2.1. Since protons do not have an exit dose, there is less radiation dose to the surrounding non-tumoral tissues. Thus, proton therapy reduces the risk of long-term effects, which could be considered theoretically safer in some children. Yet clinical data on long term effects in normal brain areas in children is insufficient [70].

2.2. Protons are physically different from x-ray photons, and research is needed to understand the differences in tissue reactions between the two. Proton therapy has an obvious advantage in patients with tumours near essential structures. However, the exact dose deposited at the margins and different areas of SOBP is still uncertain [67]. More studies are warranted to understand the radiobiology of proton therapy and its effects compared to photons at the same dose levels. This will enable better patient selection for each treatment.

2.3. Quantitative analysis of the normal part of the brain in paediatric patients treated with different radiotherapy modalities is a comparatively unexplored area. Further research needs to detect dose-dependent changes at earlier stages and longitudinally over a period.

2.4. Newer biomarkers are needed to estimate and predict post-treatment cerebellar white matter lesions in patients with medulloblastoma.

1.12 Quantitative Mri Analysis

By definition, quantitative imaging is the extraction of quantifiable features from medical images to assess the normal or the severity, degree of change, or status of a disease, injury, or chronic condition relative to a standard [99].

Quantitative MRI is a fundamentally different concept from routinely used qualitative MRI methods in the clinic. It complements traditional qualitative MRI analysis by providing measurements and interpretation of tissue-specific parameters independent of experimental design or subjective bias. It is the next advanced step in the evolution of MRI and can be measured with the same imaging equipment [100] [101] [102]. Qualitative MRI is dependent on visual interpretation of tissue contrast with the inherent limitation of subjective bias. Commonly measured quantitative parameters include proton density, T1 relaxation, T2 and T2* relaxation and magnetisation transfer.

Figure 1. 7 types of diffusion with their trajectories *[103]*

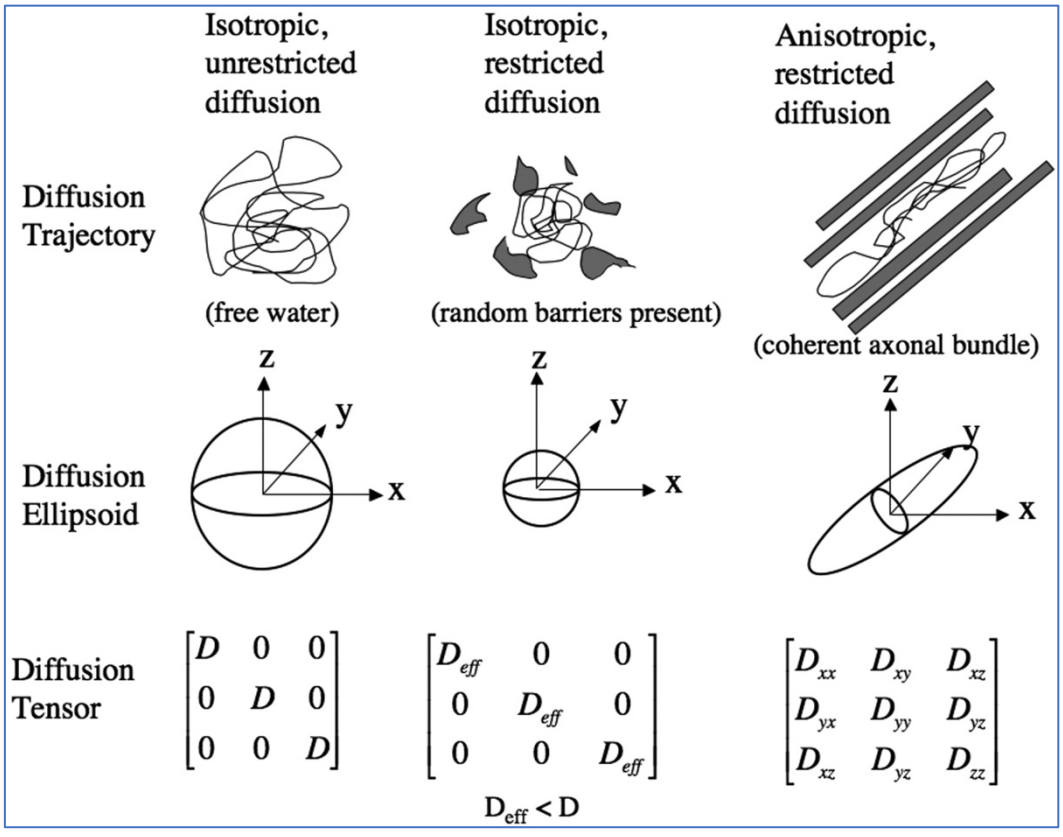

It is essential to understand that terms such as T1-weighted and T2 weighted in the qualitative analysis represent the difference in the timing of stages of the pulse sequence. T1 & T2 weighted images have signals related to T1 and T2 relaxation parameters and proton density. However, quantitative T1 and T2 maps characterise tissue properties independent of pulse sequence parameters like pixel values represent intrinsic relaxation value and not relative value [101].

In the case of diffusion MRI, diffusion data is collected by varying the strengths and directions of diffusion gradients. This data characterises the probability of water movement in each order over various spatial scales. Diffusion tensor imaging (DTI) can demonstrate the white matter tracts based on the direction of water diffusion (Fig.1.7). Quantitative parameters diffusion maps, Fractional anisotropy (FA), mean FA, and mean diffusivity have the potential to provide valuable objective information on the structural and functional characteristics of the underlying tissues. They can serve as a surrogate for disease activity. Tumours because of multiple mitosis and overpopulated cells generally show restricted diffusion.

Though these advanced MRI techniques are more helpful with structural MRI scans, they may not be available to all patients, especially from older databases. Traditionally, conventional MRI scans that are most commonly available in all patients are used for qualitative analysis. Extracting objective quantitative measures from these scans will provide better descriptors of tissues changes, thus enabling a better understanding of underlying tissue changes. In the present study, widely available T2 MRI scans are used to derive quantitative biomarkers.

1.13 MRI As An Imaging Biomarker And An Introduction To Radiomic Texture Analysis

"A biomarker is a characteristic that is objectively measured and evaluated as an indicator of normal biological processes, pathogenic processes, or a response to a therapeutic intervention" [104].

Requirements for a biomarker are threefold. Firstly, it is essential to define a disease. Secondly, it should be able to interpret the changes over time accurately, and finally, it should reliably serve as a surrogate for disease activity [105]. MRI can be used not just for morphology but also as a scientific measuring instrument for underlying pathophysiological processes. This can be achieved by extracting measurable, objective information from available scans and utilising it for diagnosis, therapeutic or prognostic purposes.

In radiomics, high-throughput imaging features are extracted from a radiological image to create a mineable database. 'Radio' refers to radiological images, while the suffix 'omics' characterises and quantifies biological properties that translate into clinically valuable parameters. The goal is to convert images into mineable data with high reliability and quantity. It is centred on advancements in image analysis, using automated high-throughput extraction of large amounts of quantitative data [106]. This allows correlation of these quantitative features with tumour genotypes, phenotypes, clinical behaviours, or treatment responses. They have shown to be successful for cancer patients in earlier studies [40]. Radiomics involved extracting image texture features from images by texture analysis.

When extracted, quantitative texture features are associated with patient information such as age, gender, location of the tumour, and other factors; it can be leveraged to provide relevant prognostic information. When statistically analysed, these datasets can provide a robust model to understand the factors influencing clinical outcomes [107]. Figure 1.8 demonstrates different steps in the radiomic analysis. We will be further discussing these in depth.

These features can enable the personalisation of cancer treatment strategies based on imaging-based phenotypes. Radiomics has the potential to predict tumour characteristics such as histology, genetic markers as well as response to the therapy [100]. Computer-extracted novel imaging features have

successfully demonstrated high-risk and low-risk post-therapy recurrence [108]. Analysis of pre-treatment scans has been able to identify patients that will respond to therapy.

Figure 1. 8 Steps in radiomic analysis adapted from [109]

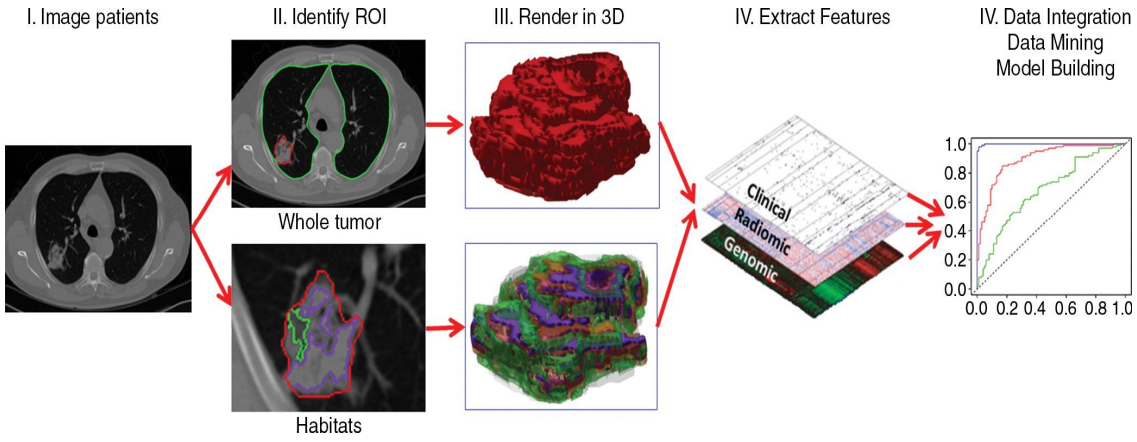

Delta-radiomics analysis compares the changes within extracted radiomic features of pre-treatment images with subsequent follow-up images. This has been shown to detect tumour responses such as progression, recurrence, and metastases at early stages in lung carcinoma and colorectal carcinoma [110]. Longitudinal analysis of percentage change of radiomic features such as textural components is related to prognosis. Intra-tumoral heterogeneity on imaging can identify sites for biopsy. In radiotherapy, these aggressive regions can be targeted with a radiation boost to improve outcomes [111].

Delta-radiomics provides a cost-effective response assessment tool as images are already available in the database. It can reduce invasive biopsy procedures to identify radioresistant areas of tumours earlier and give a boost. Delta radiomics can help assess the therapy-induced changes in standard parts of the brain. It has been shown to detect radiotherapy-induced pneumonitis in patients with oesophageal cancer [112].

Radiomic analysis of MRI of the non-tumoural brain following radiotherapy in children with brain tumours is comparatively unexplored, and successful identification of biomarkers may help refine treatment strategies.

Complete radiomic workflow requires complex study design and machine learning methods. This will also be discussed in detail in chapter 3. If found valid, these quantitative measures can potentially be used in future studies to predict the outcome with the help of machine learning techniques.

1.14 Texture Analysis (TA)

The texture is a local variation in intensity due to tissue heterogeneity. The term texture is widely used to describe the properties of images, food, and materials. The Oxford dictionary defines texture as "the feel, appearance, or consistency of a surface or a substance" [ref]. In biomedical sciences, texture represents micro and macro-structural properties of the tissue [113]. Radiologists are trained to identify visual image patterns and underlying cellular mechanisms. Many variations are seen in images due to differences in human anatomy and image acquisition and reconstruction protocols. Human errors and training (lack thereof) add to these errors. Qualitative descriptions of these patterns like smoothness, curiosity and roughness are often insufficient and subject to miscalculations [114]. Heterogeneity patterns inside a lesion can be captured and quantitatively measured by texture feature extraction analysis [115].

An image texture is a set of metrics calculated in image processing designed to quantify the perceived texture of an image.

Image texture gives us information about the spatial arrangement of colour or intensities in an image or selected region of an image. Texture Analysis (TA) is a method to evaluate the position of signal features, i.e. pixels/voxels, and their grey-level intensity, distribution and relationships in a digital image [116]. TA algorithms extract the distribution and relationships of different grey level pixels within the image by filtration and quantify them based on statistical methods [117]. TA has the potential as a promising biomarker for analysing biomedical images.

METHODS OF TEXTURE ANALYSIS[118] [119]

1. Shape-based :

These describe mainly the 3D size and shape of the mask image/segmented tumour. Examples are maximum 3D diameter, number of voxels, surface area, volume etc.

2. Statistical Methods:

In this study, we have used an intensity histogram-based statistical method for the textural analysis. They described the global distribution of intensity values.

Signal features are classified statistically as first-order, second-order and higher-order features. This depends upon whether they are classified as individual pixel values or as a group (matrix) of pixels considering their spatial relationship with adjacent pixels (Fig 1.9). First-order statistical features are directionally independent compared to higher-order features [117]. These statistics characterise image texture as a function of local variability of pixel intensity values. For example, smooth texture is characterised by a smaller range of pixel values in the neighbourhood around a pixel, while it might be rough in the more extensive coverage. Statistical parameters such as standard deviation indicate the local degree of pixel variability.

Examples of first-order texture features are Energy, total energy, entropy, grey level intensity (minimum, mean, maximum, percentile), median, interquartile range, range, mean absolute deviation, standard deviation, uniformity, and kurtosis [120]. Definitions of different texture features have been given in table 1.9

Figure 1. 9 Image showing the difference between first and second-order texture features. These three squares have the same distribution of first-order features (50% black and 50% white), while they differ in their correlation (second-order feature)

3. Grey Level Concurrence Matrix (GLCM):

GLCM is an example of a second-order texture feature. This matrix expresses the correlation of spatial location and grey level distribution of an image. GLCM calculates how often pairs of pixels with specific values in a particular relationship exist in an image as GLCM characteristic of a texture and extracts as statistical matric. They emphasise on the properties of homogeneity and randomness.

4. Gray Level Run Length Matrix (GLRLM): (GLRLM[121]):

They define texture in a specific direction with the same intensity value. The grey level run length is defined by the number of pixels with the same intensity and the run length value means the number of such occurrences.

Tissue heterogeneity is the local variations representing underlying pathophysiological processes, such as infection, inflammation, or malignancy. TA can be a potentially helpful tool to detect this process in routine clinical imaging.

TA can detect these underlying changes through routine clinical images at earlier stages before clinical manifestations, thus helping diagnosis, treatment response, and prognosis of tumours or treatment-related toxicities in the normal part of the brain. We will use image texture features as quantitative descriptors for dose-dependent tissue changes after radiation.

Texture analysis needs essential pre-processing of Images. These steps will be described again in depth in chapter 3, the methodology section.

Applications of Radiomic Texture analysis :

- Tumour staging
- Prediction of tumour response and prognosis
- Tumour genetics

Table 1. 9 gives information about the qualitative description of different textural features. These texture features were exported in excel format separately for each time point in each patient for statistical analysis.

Texture Feature	Definition [122] [123] [124] [120]	Qualitative meaning [120]
Mean	The average value of pixels in the selected ROI.	
Standard Deviation (SD)	The measure of deviation from the mean value	Deviation from average brightness / darkness
Skewness	Measures if there is a "wider" range of either darker or lighter pixels	● are the Texel intensities usually darker/lighter than average?) ● Measures if there is a "wider" range of either darker or lighter pixels
Kurtosis	Measure of the "peakedness" of the probability distribution of a variable	● how "uniform" is the grey level distribution?
Entropy	Entropy specifies the uncertainty/randomness in the image values. It measures the average amount of information required to encode the image values.	● how normal/nonnormal is the grey level distribution? ● Inhomogeneous scenes have low first-order entropy, while a homogeneous scene has high entropy.
Energy	Energy is a measure of the magnitude of voxel values in an image. A larger value implies a greater sum of the squares of these values.	● how much intensity variation is there in the region? ●
Total Energy	Total Energy is the value of Energy feature scaled by the volume of the voxel in cubic mm.	Intensity variation in cubic mm
Variance	Variance is the mean of the squared distances of each intensity value from the Mean value. This is a measure of the spread of the distribution about the mean.	Describes measures region "roughness")
Correlation	Correlation is a measure of gray level linear dependence between the pixels at the specified positions relative to each other.	
Contrast	Contrast is a measure of the local intensity variation, favoring values away from the diagonal	A larger value correlates with a greater disparity in intensity values among neighbouring voxels.

1.15 Overall Aim Of This Research Project

To evaluate the utility of radiomics in longitudinal analysis of paediatric brain tumours treated with radiotherapy.

Chapter 2 Data Collection, Ethical Approval And Creating A Radiological Database

2.1. Chapter Overview

The chapter provides the details of the study cohort, data collection, ethical approval, and radiological database.

2.2. Data Collection

This is a longitudinal retrospective study. The study cohort included paediatric patients diagnosed with primary brain tumours at Alder Hey Children's Hospital from the 1st January 2005 to the 1st January 2020. Ethical approval was obtained from the NHS health research authority (HRA) and health and Care Research Wales (HCRW).

- **Reorganisation, Renaming and Preparation Of The Clinical Database:**

The inclusion criteria were paediatric patients (Age <18) diagnosed with a primary brain tumour. A database was created, and 305 patients with primary brain tumours were screened for eligibility. Patients were anonymised and assigned a study identification (study ID). All patients had received some form of therapy, including surgery, chemotherapy, and radiation therapy. Patients were excluded if they did not receive the radiation therapy. A total of 105 patients treated with radiation therapy were identified (Fig 2.1). Demographic information includes age at diagnosis, gender, location of the tumour, histological diagnosis, date of diagnosis, presence of metastasis, date and type of surgery (biopsy or resection), use of chemotherapy, type of radiation therapy (photon or proton) and planned therapeutic dose was obtained from the medical records at Alder Hey Hospital and Clatterbridge Cancer Centre. An Excel sheet was prepared with all the available clinical information. Detailed demographics of the final eligible patients are shown in Table 2.1

Figure 2. 1 Screening and eligibility of patient cohort

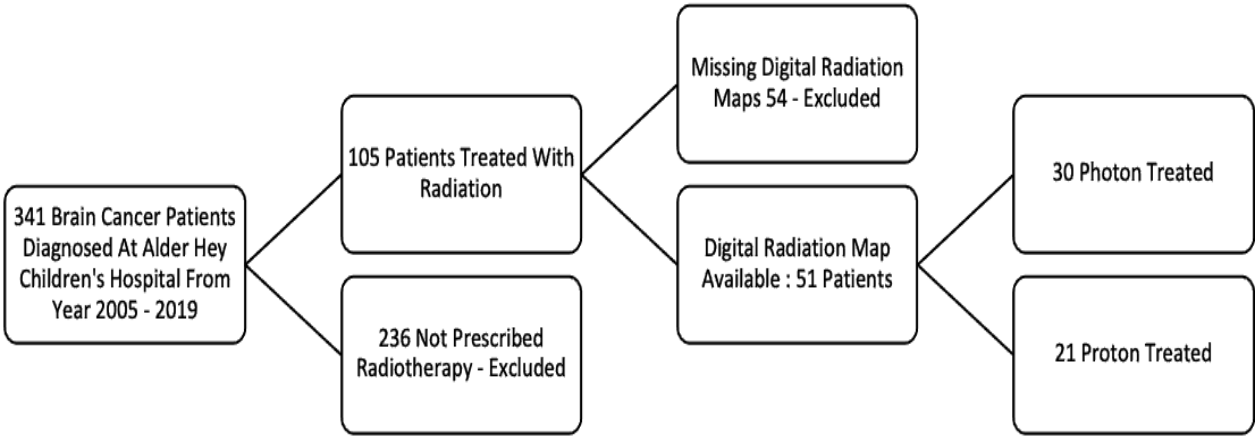

- **MRI Radiological Database:**

The Alder Hey Picture Archiving and Communication System (PACS) system, a digital radiology database, was searched for radiological information and MRI scans of the eligible patients were anonymised and renamed (pseudonymised) with the patient study ID from the clinical database. This pseudonymization was done by the inbuilt Siemens PACS software of the hospital. A detailed digital radiological database was created with information on the sequences used in the MR imaging for each patient at each time point during the study period (1st January 2005 to 1st January 2020). A date-wise sequential code was assigned for each scan for pseudonymisation, and used for further analysis. All the scans were always downloaded to a dedicated password-protected computer.

- **Radiation Maps:**

Digital radiation maps containing the radiation plan on CT scans were acquired from three treatment centres. Photon therapy maps were received from Clatterbridge Cancer Centre, Liverpool, while Proton radiotherapy maps were obtained from the University of Florida Health Proton Therapy Institute and Oklahoma Proton Centre. These maps held the details of GTV (Gross Tumour Volume), CTV (Clinical Target Volume) and Planning treatment volume (PTV), along with the radiation dose information for the entire brain volume (Fig 2.2).

These maps were also pseudonymised with the same patient code as those used for anonymised MRI scans. Photon and proton radiation maps were used for dose information and to generate a dose-volume-histogram (DVH). Only 51 patients had digital radiation planning maps available. Therefore, all other patients were excluded from this part of the study (Fig 2.1). Out of these 51 patients, one patient (BMS168) had a distorted baseline scan and hence it was not included in the study design.

<u>Reasons for study exclusion:</u>

1. Digital radiation maps are not available (most of the scans 54)
2. Patients with missing baseline MRI scans or poor-quality baseline scans with severe brain distortions or very high noise (BMS168).

Figure 2. 2 Digital radiation dose map showing PTV (pink), CTV (blue) and GTV (red) and dose-volume information histogram for photon radiation therapy

A supplementary database was created for the patients with available dose maps with patient demographics, diagnosis, treatments received, and longitudinal MRI scan dates using patient identification codes. One further patient was excluded due to inconsistent MRI scan information. Details of the final patient cohort are shown in Table 2.1

Table 2.1 Demographics and cohort information

Patient Characteristic	Age at the end of treatment	0-5 years: 6 5-10 years: 22 10-15 years: 18 15-20 years: 4
	Gender	F 27 M 23
Tumour Characteristics	Location	Brainstem 4 Cerebellar 19 Hemispheric cerebral (frontal/temporal/parietal/insular) 7 Supratentorial midline (thalamic/hypothalamic/suprasellar) 20
	Diagnostic Group	High Grade Glioma 3 Low Grade Glioma 9 Medulloblastoma 13 Ependymoma 9 Germ Cell Tumours 4 Meningioma 1 Rare Embryonal Tumours (Atypical Teratoid Rhabdoid Tumours / CNS PNET/Chordoma) 2 Tumours of the Sellar region (Pituitary tumours /Craniopharyngioma) 9
	Metastasis	No 41 Yes 9
Treatment Characteristics	Biopsy	No 37 Yes 13
	Surgery	GTR (Gross Total Resection) 24 NTR (Near Total Resection) 5 STR (Subtotal Resection) 15
	Chemotherapy	No 27 Yes 23
	Radiotherapy	Photon 30 Proton 20

2.3. Scan Selection, Pseudonymization And Reorganisation Of The Scans For Analysis

In the radiological database, information on the scans from the first postoperative MRI, radiotherapy planning MRI and all subsequent scans up to 24 months (732 days) were collated into the database (Table 2.2). The type of MR scan sequences used (e.g., T1, T2, FLAIR, Contrast-enhanced T1, Perfusion-weighted imaging, diffusion-weighted imaging, spectroscopy) and each patient's acquisition date were recorded in the database. T1, T2 and FLAIR images, which form the basic standard MRI protocol for brain tumour imaging, were available for most patients. In contrast, other advanced imaging sequences (e.g., diffusion/perfusion/spectroscopy) were not available in all patients.

T2W MRI scans:

T2-weighted (T2W) axial images were selected for the radiomics analysis due to their diagnostic advantage in detecting white matter lesions and consistent availability in the database. These are 2D scans with a slice thickness of 4 mm with a 0.4 mm or slice thickness of 5mm with a 1mm slice gap. This study aimed to look at the post-radiotherapy changes in the regular part of the brain, especially in the homogenous white matter regions, whenever possible. T2W imaging is helpful in pathological imaging processes in the white matter and grey matter areas. Ischaemic changes, inflammatory - demyelinating lesions, oedema, and necrosis, are better visualised on T2 sequences [125]. Vascular damage is the critical factor leading to brain damage after radiation therapy. Radiation-induced demyelination causes hyperintense white matter lesions on T2W images [126].

Nonetheless, T2W imaging in the axial plane is part of the routine imaging Field [3]. Therefore, T2 scans were consistently available in all the patients at all time points. This also adds to the broader application and potential generalisability of the radiomic analysis process for future validation studies. Since any advanced imaging modality is not used, this study can be performed and tested with a routine brain tumour imaging protocol at any hospital.

These scans were sequentially arranged and renamed based on the date of surgery and radiotherapy, as shown in Table 2.2

Table 2.2 Sequential reorganisation and renaming of longitudinal T2 MRI scan

Scan Name	Details
Scan A (Baseline Scan)	Last T2 (axial) scan in the system after the surgery and before the date of initiation of radiotherapy was selected as a baseline scan
Scan B	First scan after end of radiation therapy
Subsequent scans (Scans C -I)	All the axial T2 scans in the system after scan B up to 24 months (730-740 days approx.). They were sequentially named as per their date of acquisition. These scans do not have fixed time points since they were acquired based on the clinical need and the patient response at the time of the scan. A minimum of 3 and a maximum of 9 scans (Named C..... I) were available for each patient.

Chapter 3 – Image Preprocessing Methodology (Registration, Bias correction, Dose calculation) and Texture Analysis

3.1 Chapter Overview

This chapter gives a theoretical background and the image processing pipeline (Fig 3.1 & 3.2). MRI provides detailed images of body structures and is an indispensable modality for diagnosing and managing brain tumours. However, MRI data is often large and is constantly subjected to image noise and signal intensity changes. The effects of changes in the scanning parameters, scanner manufacturer and patient positioning at each scan need to be considered, and standardisation steps should be carried out to make these images comparable in large datasets. In this study, we have used the steps described in the Imaging Biomarker Standardization Initiative (IBIS) [127]. Texture analysis is a relatively recent technique of MRI data analysis that is inherently subject to low repeatability, which needs to be addressed by by pre-processing. [109] [128] In this chapter, we will be describing the specific challenges of our study and our techniques to overcome these challenges.

3.2 What is Image Pre-processing?

Pre-processing encompasses different steps of analysis carried out to transform images, reduce noise and improve their quality, enabling more repeatable statistical results. It also helps the standardisation of each scan so that results are comparable after the statistical analysis. [129] Pre-processing is an essential part of every radiomic study. In the present study, we used the following pre-processing steps before performing textural analysis: Image registration, Bias correction, and Region of interest (ROI) drawing.

3.2.1 Image Registration

Multimodal imaging is widely used in the diagnosis and management of brain tumours. Image registration is an essential step in integrating the information obtained from multiple modalities. Image registration, also known as image fusion, matching or warping, can be defined as the process of aligning two or more images. An image registration method aims to find the optimal transformation that best aligns the structures of interest in the input images. It helps determine the correspondence of anatomical structures between two images. [130]

There are two types of image registration methods (Fig 3.3):

- Affine (Rigid) Registration is also known as affine alignment. Affine registration aims to find the affine or linear transformation that best maps one data set (e.g., image, set of points) onto another. [131] This is a simple process involving linear change or rotation of an image.
- Non-rigid (Deformable) registration: This is a more complicated registration method. This is used when simple rotation is insufficient, and some image stretching is required for correspondence to compensate for biological or scanning differences. [130] The B-spline model of non-rigid registration is one of the efficient techniques for registering images with deformations, e.g. follow-up scans for monitoring brain tumours in patients [132]. The main disadvantage of the B-spline is that it may fail to preserve topography.

Figure 3. 1 Image Processing Pipeline showing main steps

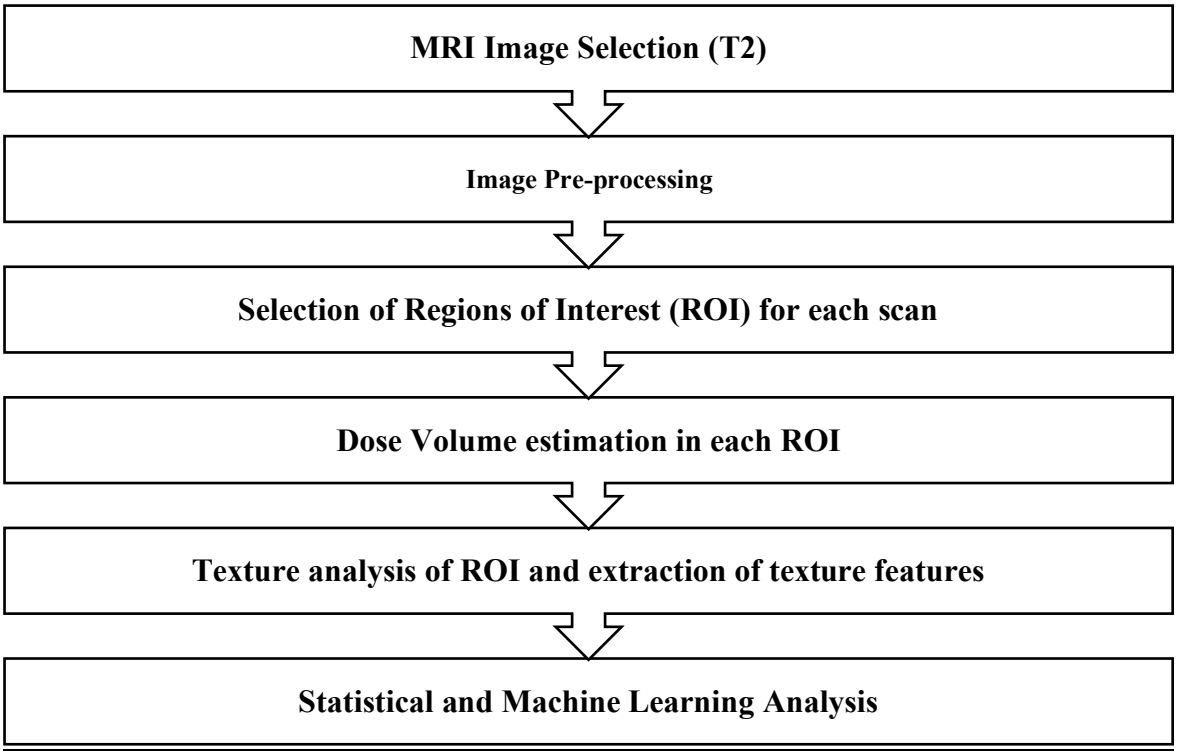

In this study, it was essential to align the CT dose maps with MRI images so that accurate radiation doses can be measured in each ROI. Each MRI scan was taken at different time points, using other scanning parameters and with different patient positioning. It was essential to align accurately to facilitate the selection of ROI in the same region across all time points.

Specific challenges in the present study:

- Software selection: Several software programmes were assessed (e.g., Freesurfer, SPM, FSL, etc). Most commonly used software for MRI image processing, such as Freesurfer or FSL, is primarily designed for adult brain MRI. Thus, we needed software that allowed customised registration and was user friendly for clinicians without programming expertise.

Figure 3. 2 . Detailed Image Processing Pipeline

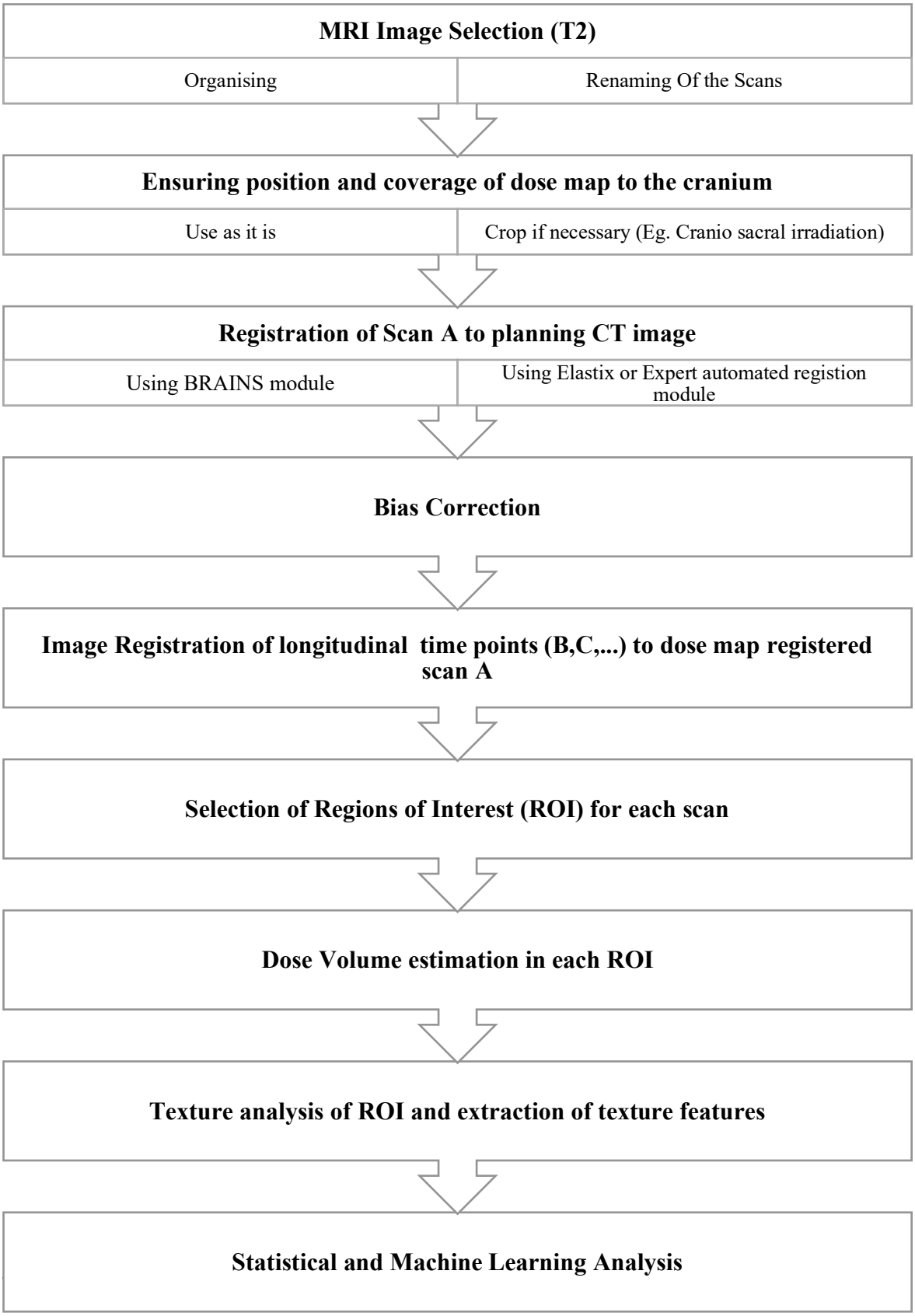

Figure 3. 3 Schematic representation of image registration methods by Crum et al. Eyes and face represent internal structures [5]. In the image on the right side, MR images show alignment of the midline after registration.

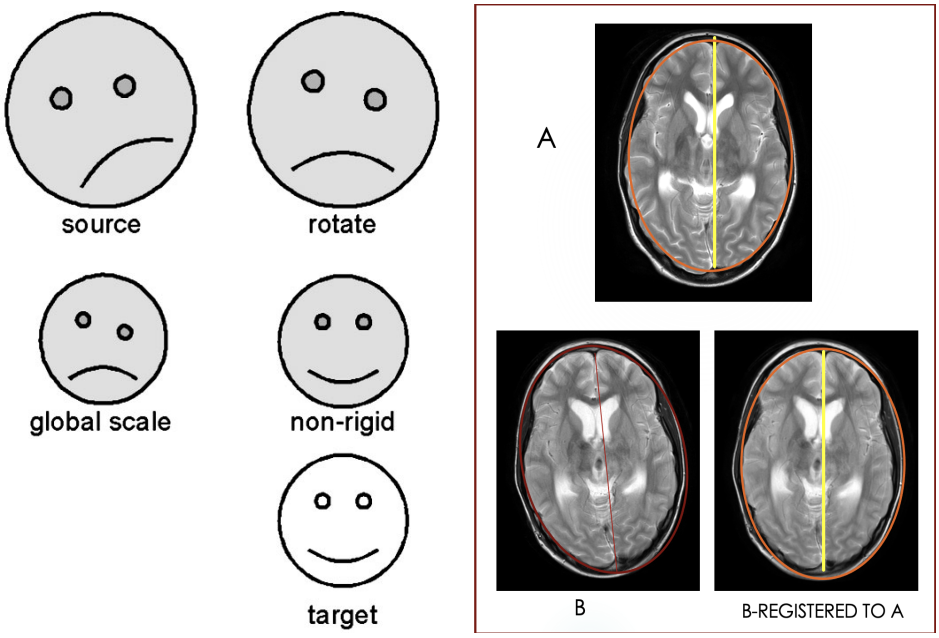

Figure 3. 4 shows the CT dose map registration steps with the baseline T2 scan. B:3 Anon is the original craniospinal CT used for planning. B:3 Anon is cropped cranial image from the CT planning, B: 153AT2

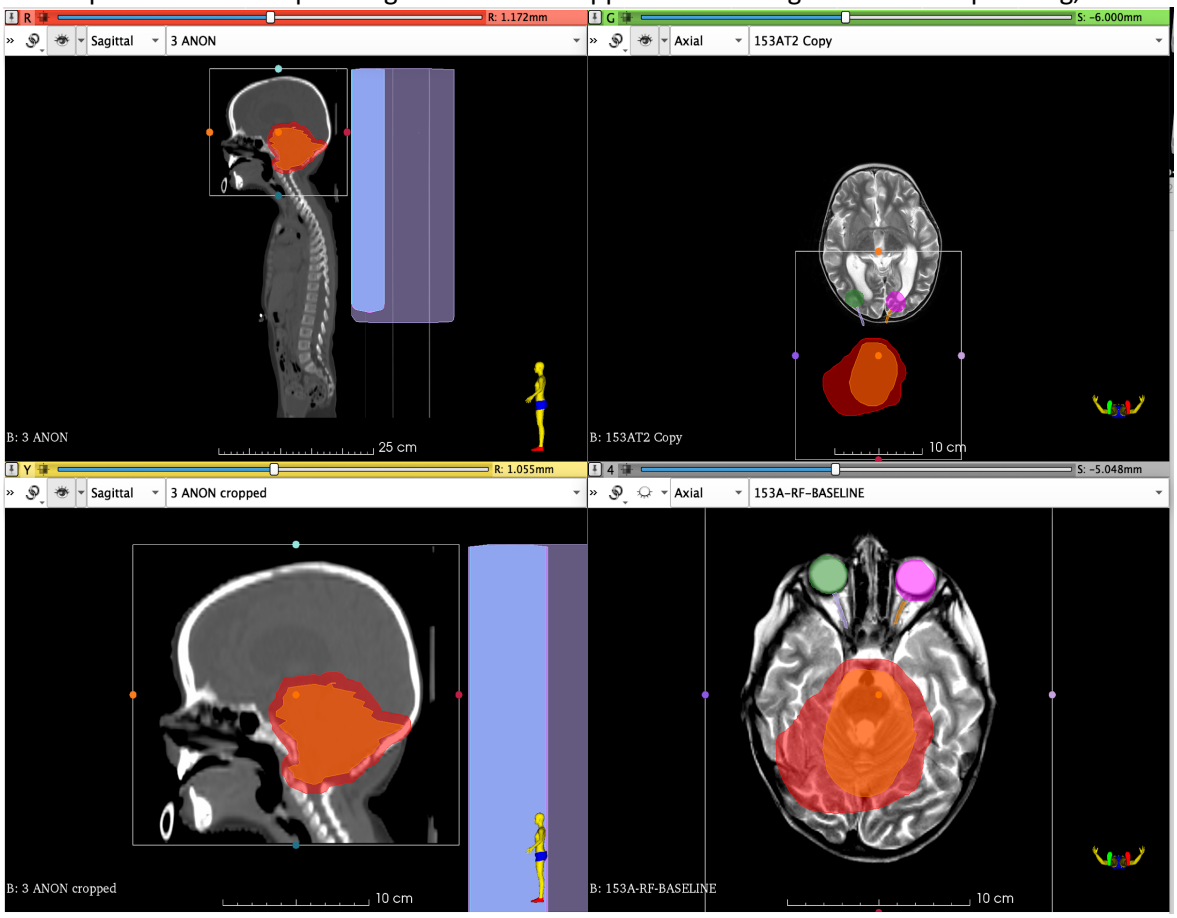

- Challenges due to brain distortions: MRI scans with brain tumours before and after surgery can show considerable distortions of the normal brain. This poses challenges that do not usually occur with undistorted brain registrations, e.g., in idiopathic epilepsy or Alzheimer's disease. This factor also limits using the software above (FSL, Freesurfer) that is generally used in image pre-processing.
- Brain Growth, Development and Other changes: This longitudinal study in a paediatric population between 3 and 8 years. In young children, 90-95% of adult brain weight is acquired by 2-3 years, and structural maturation occurs between 4-11 years of age. [133] Patients also showed other MRI differences, such as post-surgical brain shift. This required a flexible approach for longitudinal registration in each patient.

Specialised techniques for image registration were selected to overcome the challenges above.

To take advantage of both (Affine and Non-rigid) techniques and improve our registration results, we combined these techniques as the method of choice suggested by the Slicer Registration Library Case #37 : [134]: Intra-subject Brain MRI: T1 Tumour Growth / Resection Assessment.

<u>The steps of registration used are as follows:</u>

A. Registration of the baseline MR scan with the CT dose map

The baseline axial T2 MRI scan (BMS-N- A) was registered with the CT scan used for radiotherapy planning using an expert automated registration module of a 3D slicer in default mode. For the patients who underwent craniospinal irradiation, CT was cropped to select only the cranial region to ensure better alignment with brain MRI. (Figure 3.4) After CT registration, the baseline scan (e.g. 153AT2) was converted into a registered scan and assigned a new label (e.g. 153AT2-R). This registration was verified by examining superimposed radiation dose maps, tumour position, PTV position, and other anatomical landmarks.

B. Registration of follow up T2 scans with the CT registered baseline MR scan:

This step was particularly challenging due to the previously mentioned issues, such as post-surgical brain distortion and subsequent healing/resolution of brain shift on the follow-up MRI scans. To facilitate the selection of the same region of interest (ROI) across all time points, subsequent scans (e.g., B, C, ...I) were registered with the registered and bias-corrected baseline scan. They were re-named accordingly (BMS-N-T2A-RF) (Fig. 3.4). These scans were registered in 2 steps using the General registration module (BRAINS) of the 3D slicer with the specialised technique to compensate for post-surgical changes in the brain. This was done by initial affine registration followed by non-rigid registration B-spline. It is important to note that this step was performed on the bias-corrected image of the CT registered baseline scan (e.g. 1563AT2-RF). Bias correction will be described in the next section.

3.2.2 Bias Correction

MRI images are subjected to the regions of non-uniform intensity, which is known as bias or inhomogeneity (Fig. 3.5). The nonparametric nonuniformity normalisation (N3) method of bias correction is a commonly used method due to the simplicity and automation of the process and the fact that it can be used without prior knowledge of the algorithm. ***[135]*** This method was recently updated and made available for public use via the National Health Institute Insight toolkit known as N4ITK. ***[136]*** We used the N4ITK module of the 3D slicer to reduce confounding due to image MR bias.

Registered scans were bias-corrected using the N4ITK filtration module of the 3D slicer and renamed (BMS-N T2A-RF) (Fig 3.6). This was subsequently used as a baseline scan for further analysis.

Figure 3. 5 MR image showing bias. The image on the right shows the algorithm for the estimation of bias. Source image by Tustison et al[11]

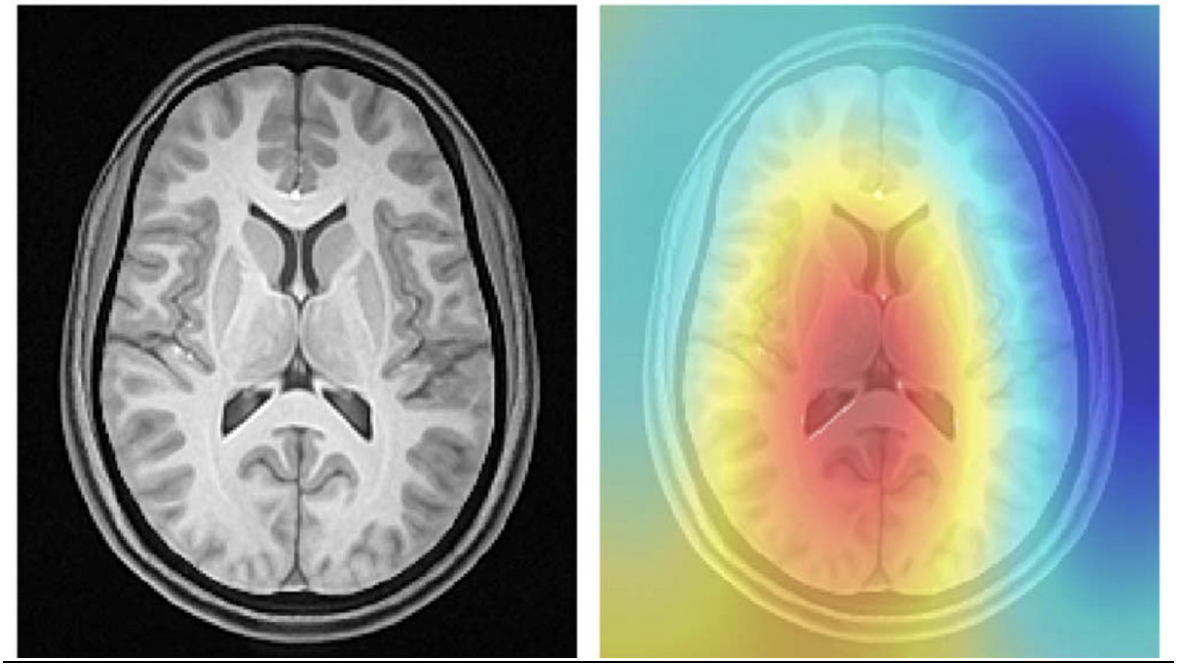

Figure 3. 6 Bias correction was performed in the present study. The image on right is filtered using the N4ITK filtration module. Though these images look the visually identical, finer image irregularities are filtered in this process for more reliable analysis.

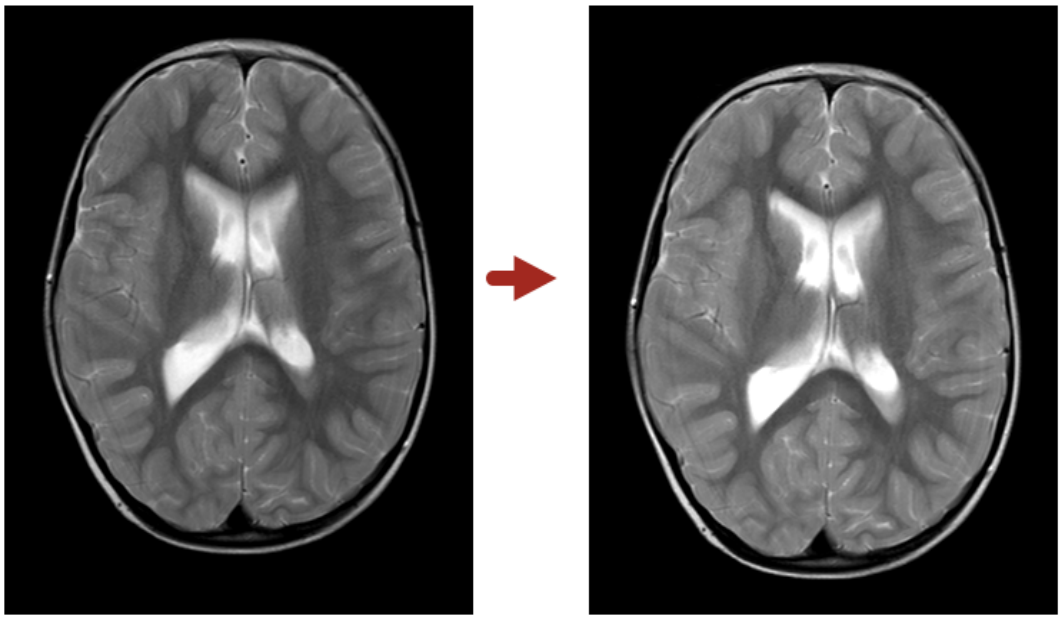

3.2.3 **Region of Interest (ROI) selection**

During post-surgical and post-radiotherapy follow up of paediatric patients with brain tumours, brain changes are frequently observed. These patients present with clinical symptoms that are not limited to the anatomical area of the tumour and can occur in other parts of the brain.

Patients treated for brain tumours often develop white matter lesions in the peritumoral and other areas of the brain. These lesions may cause transient signal abnormalities visible on T1 and T2 MRI sequences [137]. They may represent demyelination or oedema [138]. Acute brain injury due to RT generally does not show early changes on MRI. Radiotherapy and chemotherapy cause T2 hyperintense areas and new enhancement patterns as early delayed effects within six months. These lesions are known as pseudoprogression [139]. These lesions are more common in adult glioblastoma patients but may be seen in paediatric gliomas [140].

Considering this clinical question, we wanted to explore the effects of radiation dose on the whole brain. Each brain region has specialised neural function and tissue composition and is different from other areas, e.g., corpus callosum versus medulla or pons. Texture analysis generates millions of features for each region, and segmentation the whole brain in a surgically distorted brain is technically challenging. Also, each part receives a different dose of radiation. To overcome this challenge, a 2D small circular areas of interest (ROI) was selected for analysis to cover eleven other anatomical areas (Table 3.1) of the brain after consultation with the clinical expert supervisors. This helped to:

i. Understand the effects of radiation in each region of the brain separately
ii. To calculate radiation dose in specific ROIs and correlate with the textural changes over time.

Table 3. 1 Particulars of ROIs

Sr. No	Anatomical Brain Region	Particulars of the position & Size	Role in normal brain function	No. Of ROIs
1.	Medulla (MED)	Centre of pyramid 5mm	Medulla has an important role in monitoring autonomous body functions such as cardiac, respiratory, vomiting and vasomotor centre.	1 (Fig 3.7)
2.	Pons (PONS)	Centre 5mm	Pons is the relays and monitors the pain sensation. It has important role in balance and coordination. Pons has nuclie that monitor swallowing, sleep, facial expressions and sensations.	1 (Fig 3.8)
3.	Corpus callosum (CC)	Genu and Splenium along the midline(A, P)3mm each	CC connects left and right hemispheres of the brain and mainly contains white matter tracts. It helps both sides of teh brain to communicate and send signals to each other.	2 (Fig 3.9)
4.	Centrum Semiovale (CS)	At the centre of the white matter at the frontoparietal junction (R, L),5mm	This is a part of brain cortex located superior tot he lateral ventricles & corpus callosum. It has projection, commissural & association fibres.	2 (Fig 3.10)
5.	Thalamus (T)	posteromedial (R,L) 5mm	Thalamus has role in memory, sleep, consciousness, sleep, etc All the sensory information (vision, touch, taste, balance) is passed through thalamus.	2 (Fig 3.11)
6.	Cerebellum (CER)	Dentate nucleus of the cerebellum (R, L) 5mm	Cerebellum controls voluntary movements such as walking, balance, posture, coordination,etc. It also has a role in cognitive functions such as language and attention.	2 (Fig 3.12)
7.	PTV (Peri-Tumoral Volume)	Best available homogenous brain tissue 5mm	This is the part of brain which is surrounding the tumour. This is a non-tumoral region which receives the highest amount of radiation dose, same as tumoural region.	1 (Fig 3.13)

Figure 3. 7 ROI drawn in the medulla. The low resolution in the sagittal and coronal images results from reconstructing them from non-volumetric 2D axial scans.

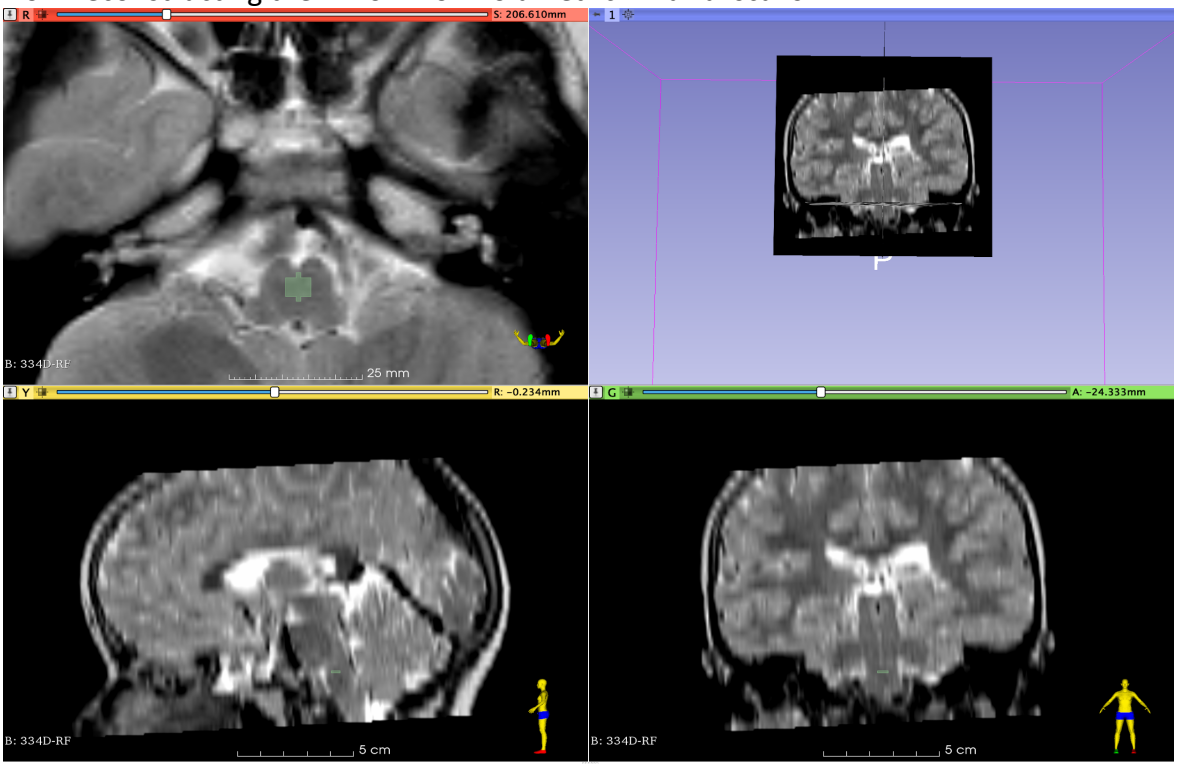

Figure 3. 8 ROI in the Pons (yellow)

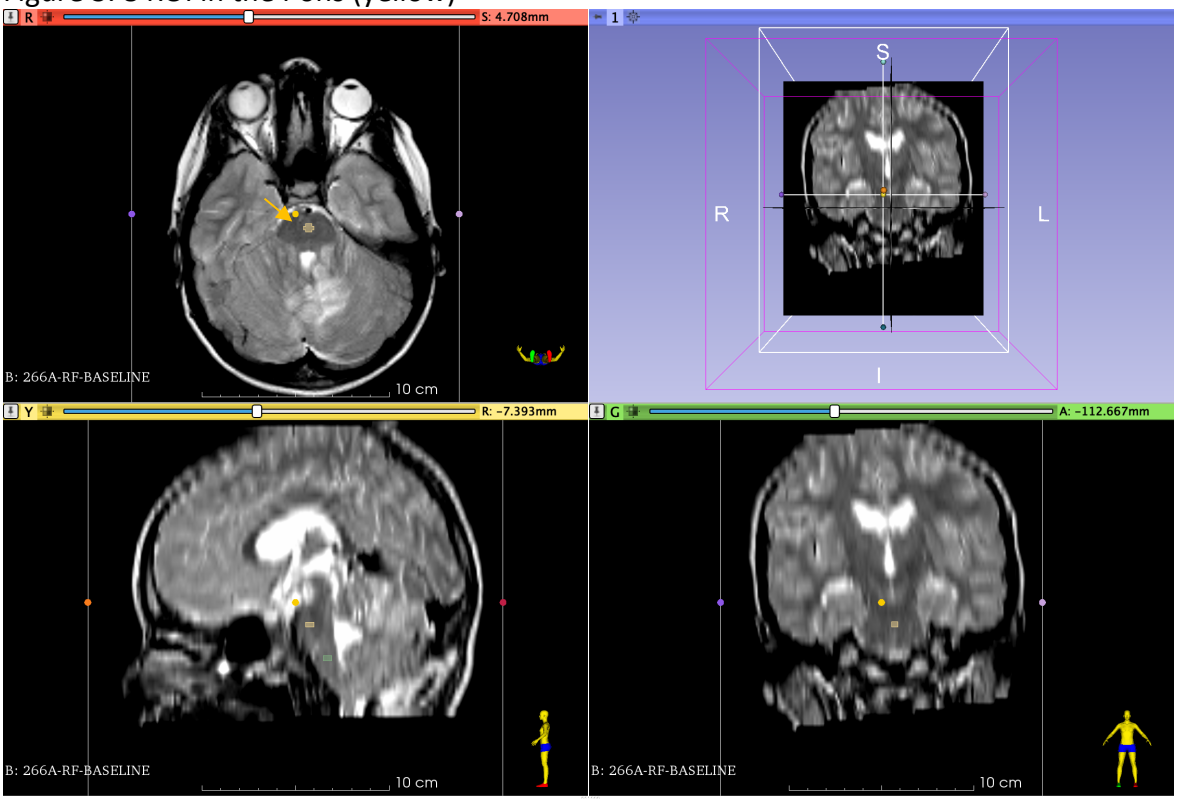

Figure 3. 9 ROI in anterior (ACC) and posterior corpus callosum (PCC)

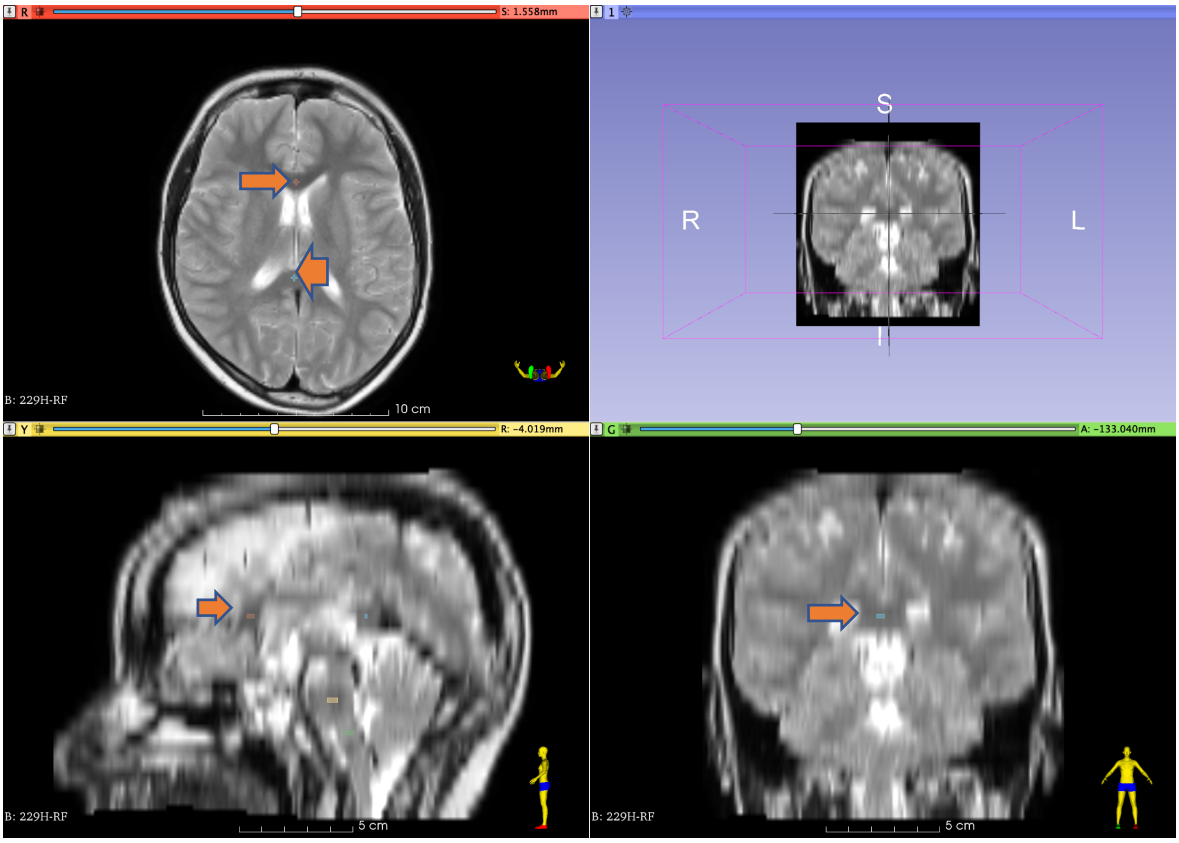

Figure 3. 10 ROI in the right and left centrum semiovale (RCS) & (LCS)

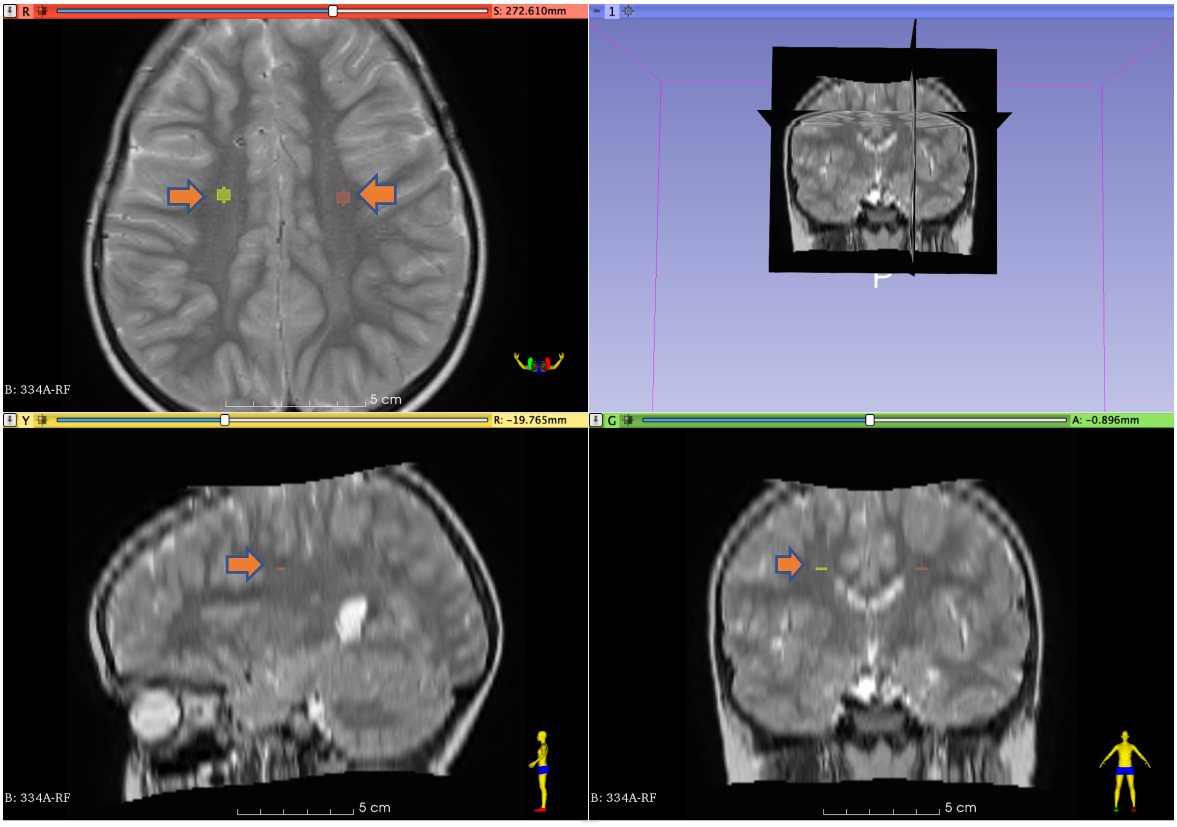

Figure 3. 11 ROI in the right (RT) and left thalamus (LT)

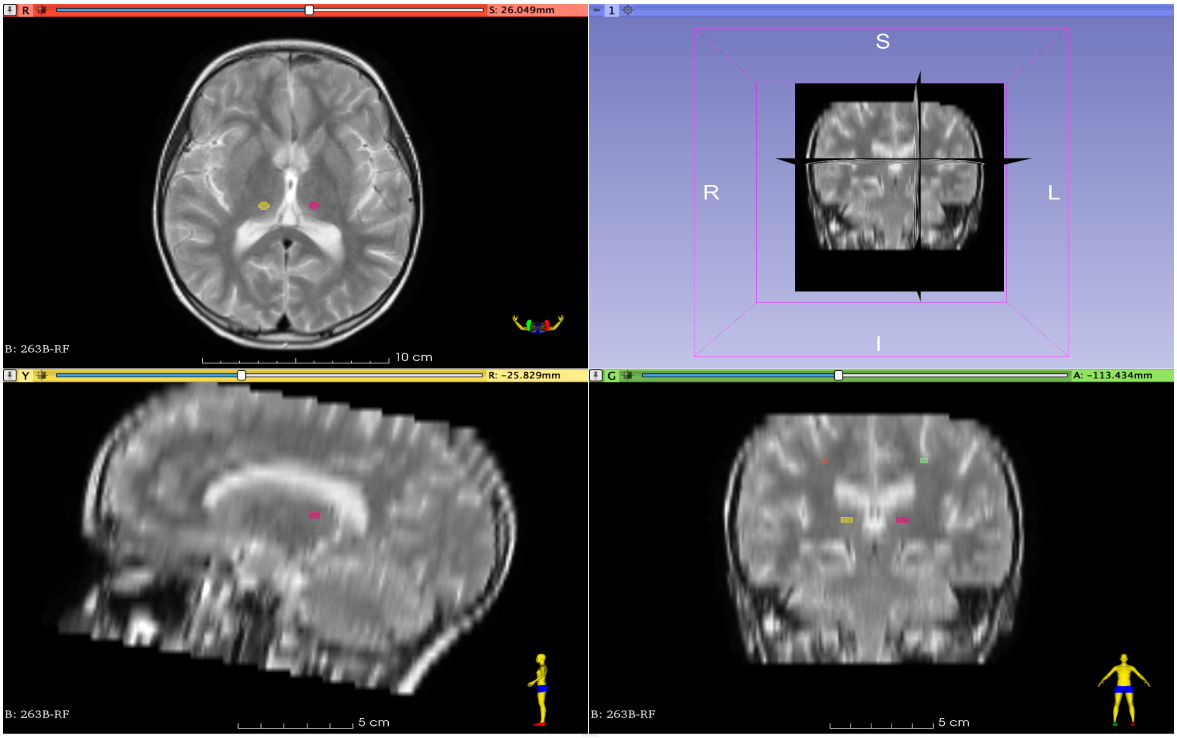

Figure 3. 12 ROI in the right (R CER) and left cerebellum (L CER)

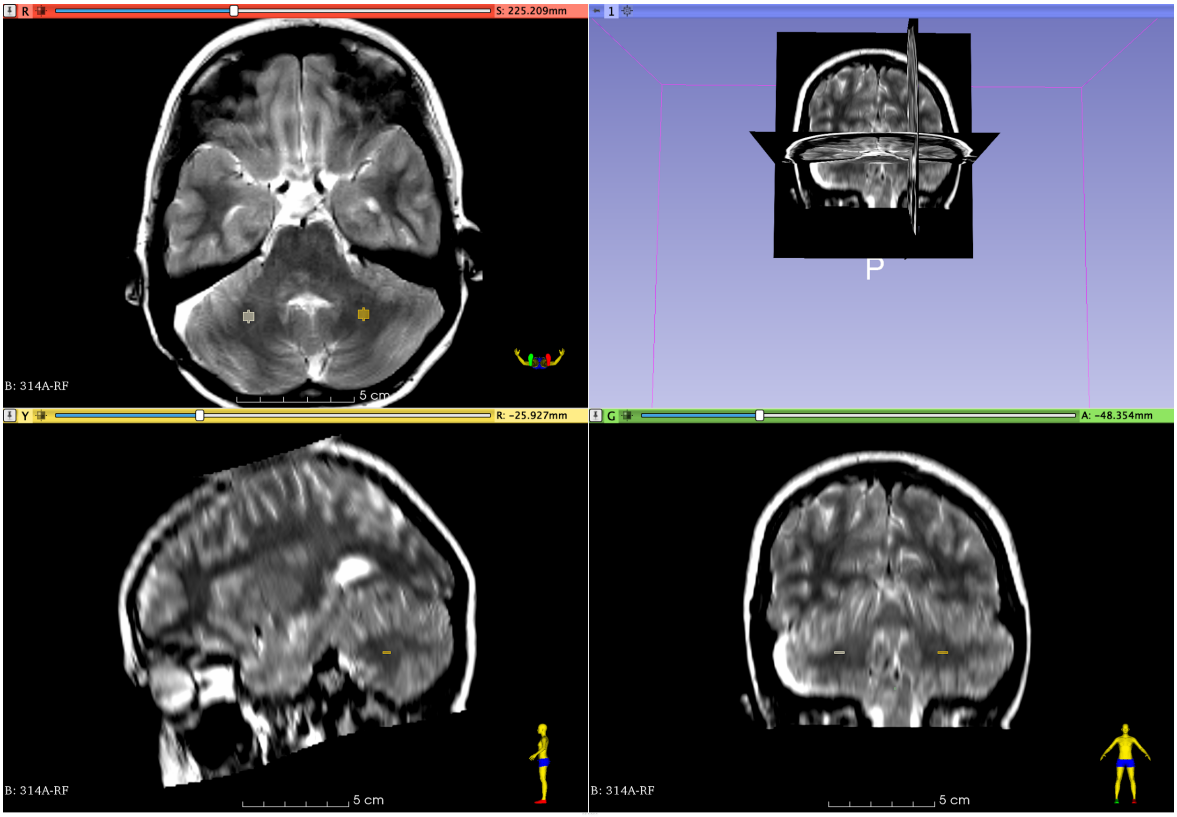

Figure 3.13 SEQ Figure_3. * ARABIC 13 ROI (Yellow arrow) showing PTV (Red arrow). Please note this region changes as per location of tumour and planning e.g. BMS 293 (panel A) and 255 (panel B)

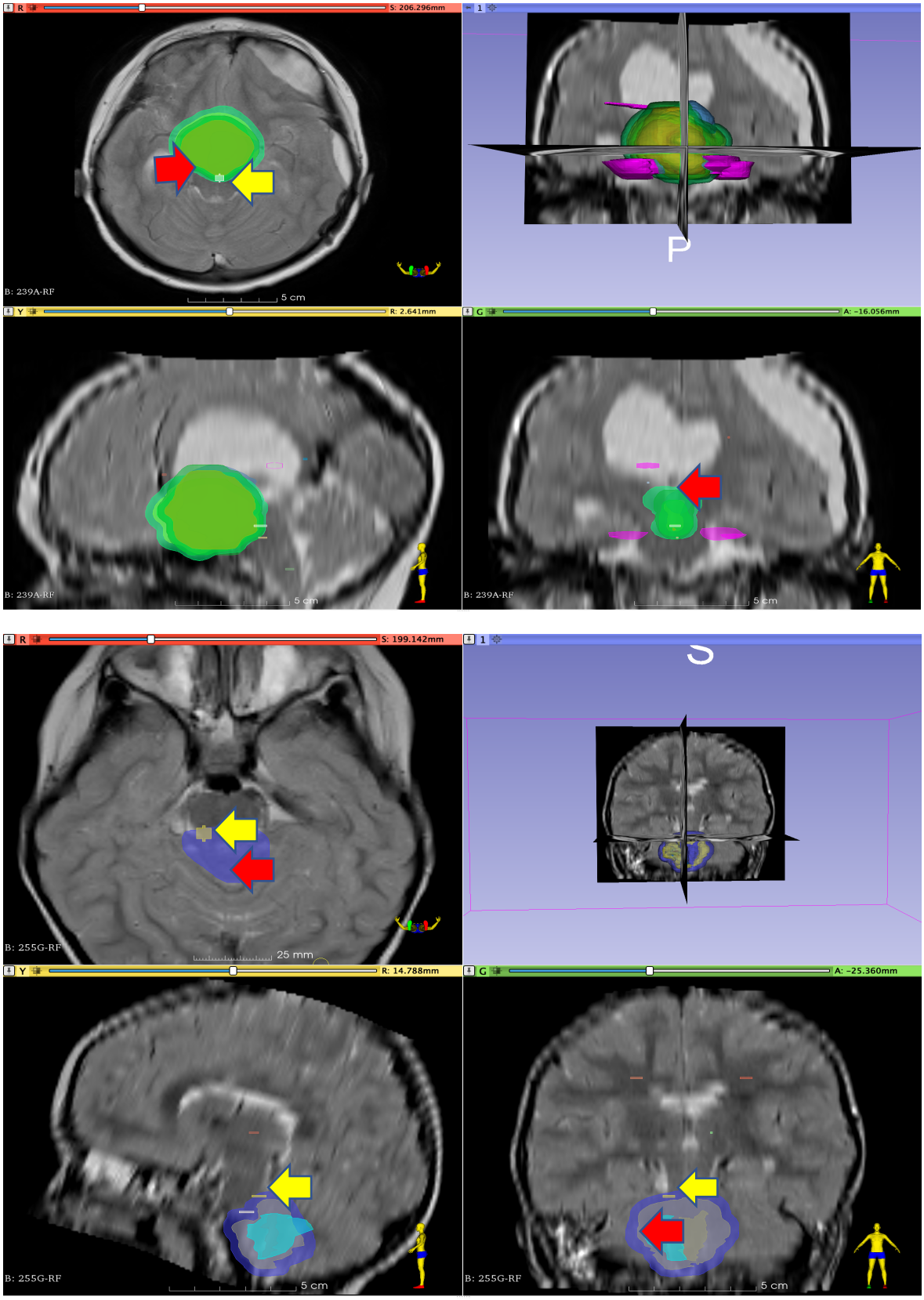

In this study, we started with multiple ROIS covering multiple areas of interest. Initially we had about 24 ROIS, Corpus Callosum – 4 (2 anterior, 2 posterior – bilaterally)Centrum Semiovale – bilateral – 2Medulla -1Pons – 1Basal Ganglia – 2Thalamus – 2Hippocampus – 2
Occipital lobe – 2Temporal – 2 Frontal – 2 Peritumoral – 4. However, radiomics generates millions of features, and to make this exploratory study manageable as these nos of ROIs were reduced to the least number of ROIs with maximum coverage. ROIs were drawn on the BMS -N- T2A-RF scan using a 2D circular tool from the segment editor module of the 3D slicer. These were preferably drawn in the region of homogenous white matter where possible to improve comparability on textural analysis. The diameter was selected as 3mm or 5mm depending upon the availability of homogenous tissue in the ten anatomical regions.

We preferred homogenous white matter because it is more susceptible to radiation tissue damage due to vasculature. We preferred the homogenous centre of different parts of the brain. ROIs in the Peri-tumoural volume (PTV) region were drawn pragmatically in the best available brain tissue region. This ROI was carefully placed in the homogenous white or grey matter, and areas such as bone, Cerebrospinal fluid (CSF), or non-brain regions were avoided.

Standard anatomical ROI placement for all cases regardless of anatomical tumour location to ensure consistency across all cases. This ROI segmentation was saved as a default for each patient to analyse subsequent MRI scans to ensure the selection of the same regions of interest at all time points. However, in some areas of interest in some patients, we found default ROI to be misplaced. e.g. ROI placed in the anterior Corpus Callosum in scan A might appear on CSF or grey matter in scan C or scan F. To rectify this error, each scan (scan B to scan I) was examined separately for the positioning of ROI, and ROIs were redrawn when necessary. These newly drawn ROIs were used for analysis.

3.2.4 Intraclass Correlation Coefficients Analysis (ICC) for the reliability of ROI's:

For testing the reliability of ROI placement by the single observer (PS) additional ICC analysis was performed. All 11 ROI's were redrawn by the primary investigator (PS) on the same scan 8 times with a delay of minimum 24 hours. Textural analysis was performed and features were extracted in all of these ROIs. ICC analysis was carried out on these extracted values. Results of these ICC analysis are shown in Table 3.2. Details of ICC analysis is added as Appendix 5

Table 3.2. Summary table of obtained ICC values :

Feature Value/ Parameter	**ICC Average Measure**	**Reliability**
10 Percentile	0.980	Excellent
90 Percentile	0.975	Excellent
Energy	0.589	Moderate
Entropy	0.921	Excellent
Kurtosis	0.631	Moderate
Mean	0.887	Good
Mean Absolute Deviation	0.928	Excellent
Median	0.980	Excellent
Minimum	0.978	Excellent
Total Energy	0.589	Moderate
Uniformity	0.915	Excellent
Variance	0.897	Good
Range	0.916	Excellent
Sum Squares	0.889	Good

ICC analysis shows moderate to excellent reliability.

3.3 Radiation Dose calculation:

This is a post-radiation study. So all the scans except baseline were after radiotherapy. No patient received any radiotherapy later. Radiation dose that was calculated , was total dose received to the particular ROI as per planned radiation maps.

Dose Volume Histograms (DVH) were obtained at all the 11 ROIs using available radiation dose maps used for radiotherapy planning. These maps contained the total amount of dose received by the patient at the end of radiotherapy. The mean radiation dose was considered for each volume of ROI. This dose information was exported in Excel format for each patient using a 3D slicer. Radiation dose maps and dose values are shown in Fig 2.2 of the previous chapter and also in fig 3.14

Verification: To ensure that the 3D slicer measures and calibrates the correct dose value from the dose map, the maximum dose received at the PTV region were cross-checked with the prescribed radiation dose to ensure accurate maps are used for the dose estimation.

Figure 3. 14 CT dose map superimposed on the T2 MRI scan. The Orange area shows CTV (clinical tumour volume), and the red indicates PTV.

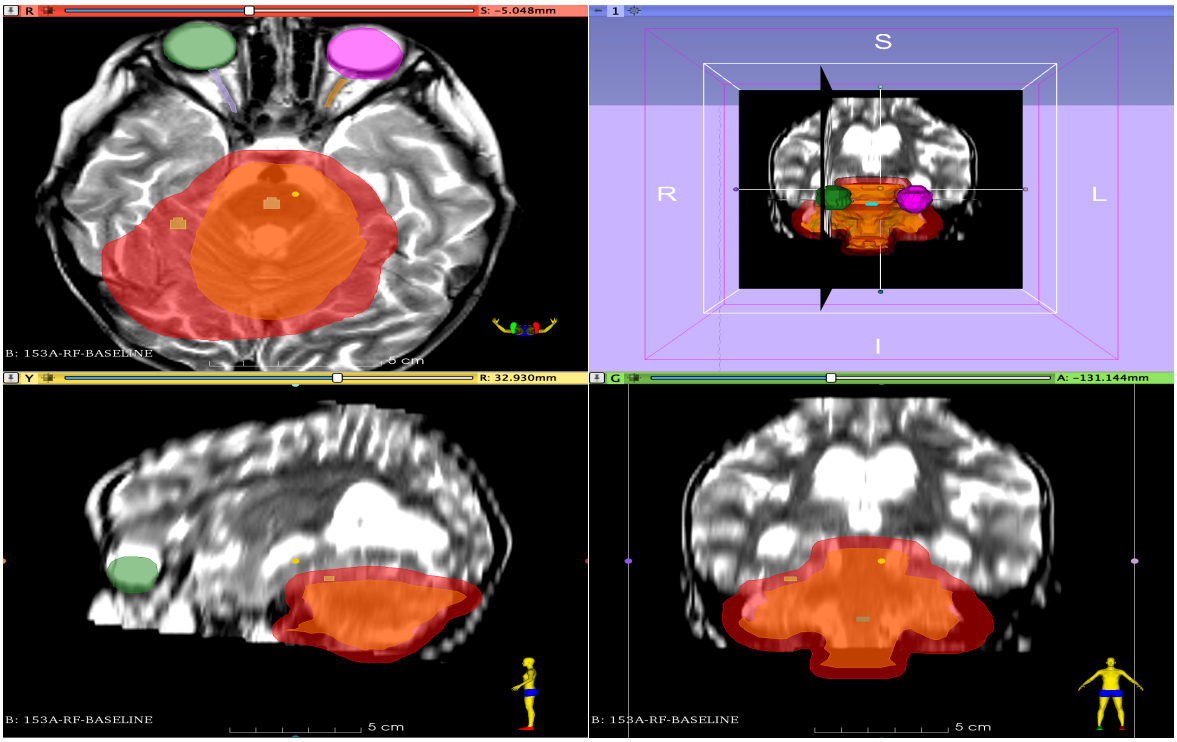

3.4 Texture Analysis:

Texture analysis is the heart of this project. During the initial stages of this study, few pilot studies were carried out to evaluate different software and validate the process.

Life X software was [141] was initially used to generate histograms and analyse if these features change over time. ROIs were selected in random brain areas, and feature values were exacted (Fig. 3.15). This histogram analysis aimed to test the software features generation and format usability. This initial analysis was performed only to check the feasibility of the software and prepare a processing pipeline; hence any T1, T2 or FLAIR were used in this analysis. The decision to carry out this analysis on T2 scans was finalised at the later stages of this study.

Figure 3. 15 Random ROI's selected with Red (HR1), magenta (CC1) and purple (HL1) circles. The graph shows intensity histograms in the same colour.

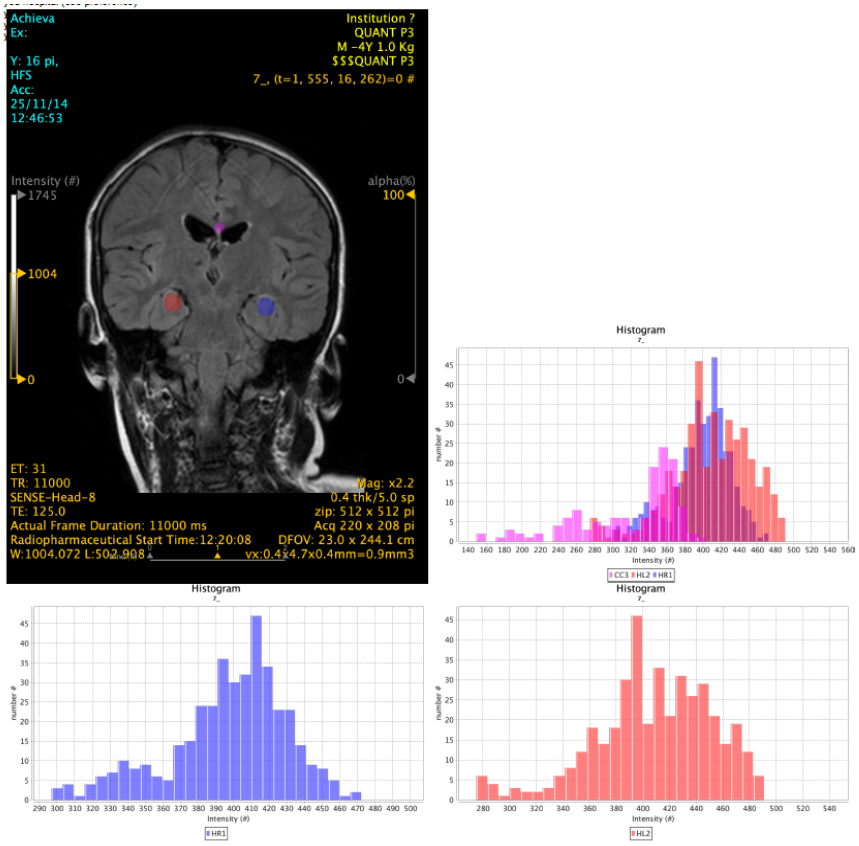

It was found that LifeX software designed primarily for PET image analysis can be used for MRI images, is very user-friendly, and features can be generated very quickly. Normalisation parameter was used to simulate MRI images' filtration and fixed bin sizes.

Life X was further used in one patient; T2 axial scans were selected at sequential time points A (21/06/2017), B 30/08/2017 and time point C (21/02/2018). Multiple ROIs were drawn at random points in all three scans. Intensity normalisation and manual alignment were performed in all three scans. Texture analysis was performed using filtration, and fixed gb values and bins at random ROI and graphs were plotted. (Fig. 3.16)

Figure 3. 16 Panel shows example images of the same ROI selected at 3-time points A, B, and C. Texture features were extracted using LifeX. Graphs show changes in textural features over time. The exact dates of these scans are given on the right side of the chart.

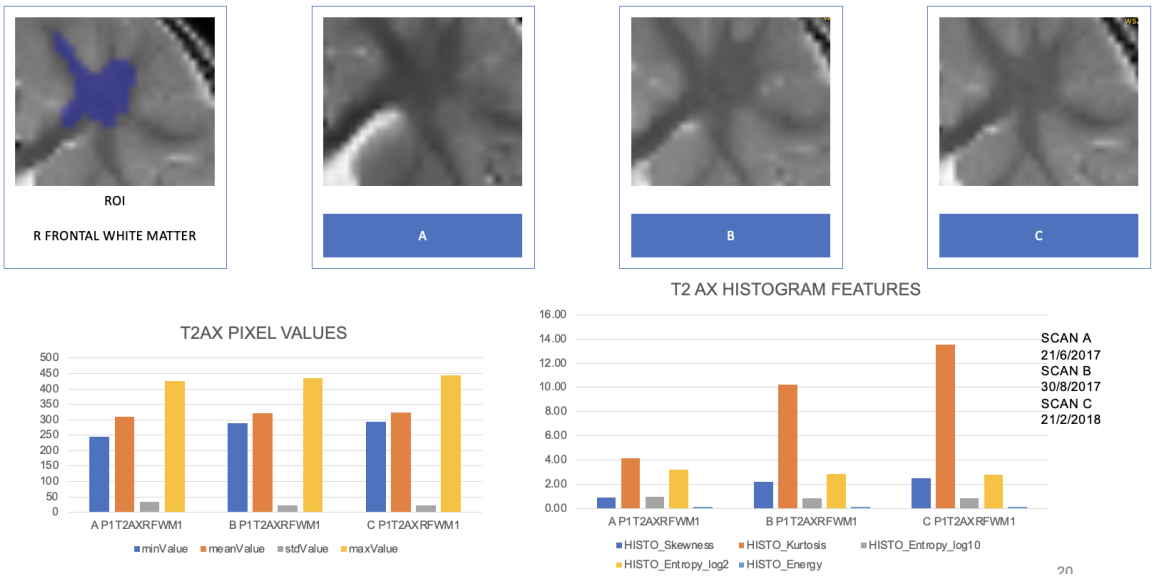

As discussed before, pre-processing steps such as image registration of subsequent scans, filtration, bias correction, etc., were required. Hence, I searched for software that allows all these functions to be performed easily.

3D slicer software with the added pyradiomics module supplied all the necessary functions. 3D slicer provided an active online support community and guidance links to cater to the specific registration needs in surgically treated paediatric patients. Hence, I tested this software for the final analysis.

Figure 3. 17 A. Chart showing the methodology of an exploratory study 2 carried out in the initial stages comparing texture features between photon and proton therapy. B. Chart showing image processing pipeline of the exploratory study 2

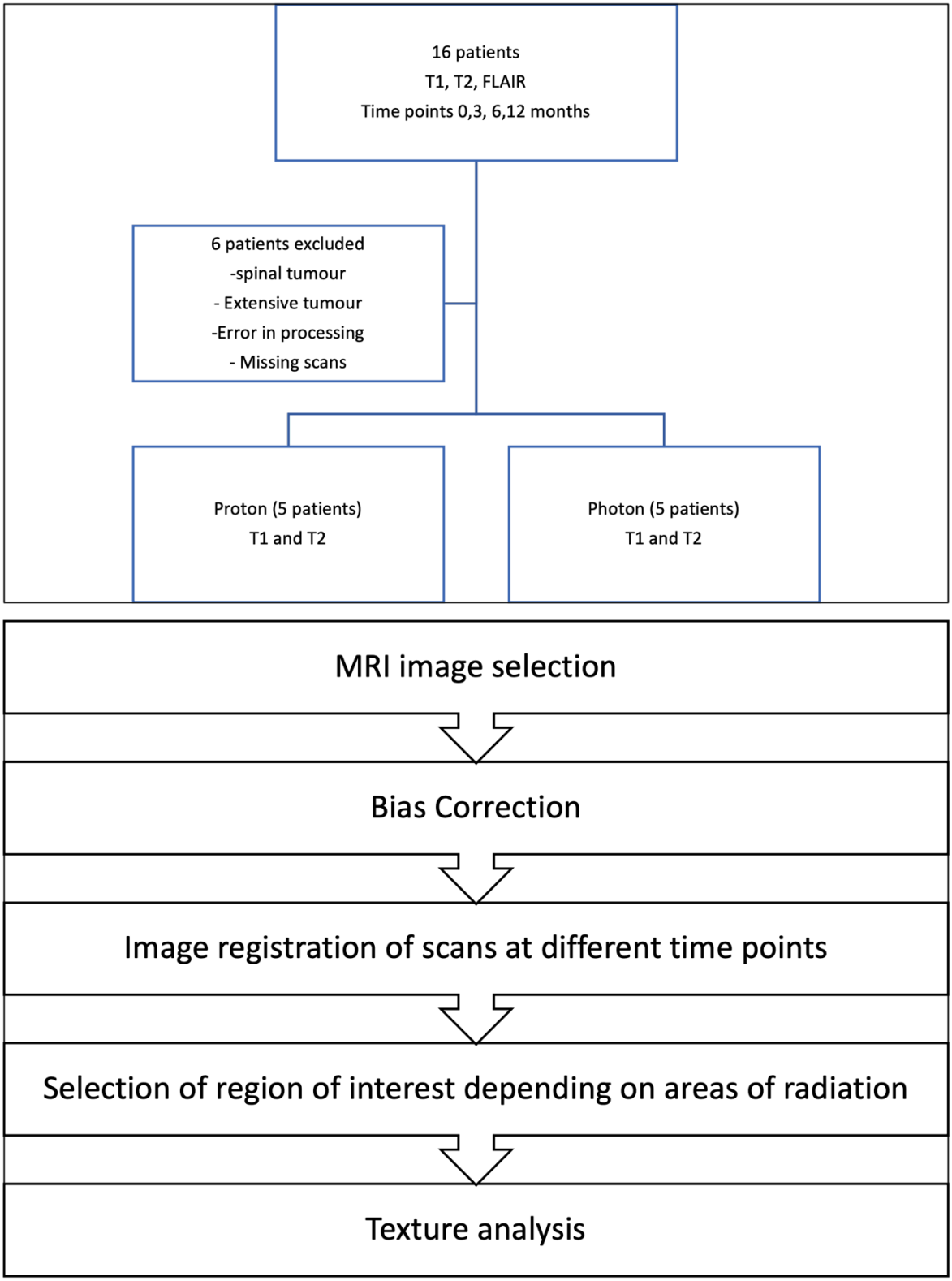

After a preliminary trial of the pyradiomics module, another exploratory analysis (study2) was carried out with 3D slicer software to test if there is any difference in these trends between proton and photon therapy. ROIs were drawn at different structures (Fig 3.18). This exercise was carried out on T1 and T2 scans of 16 patients at fixed time points. The method is shown in figures 3.17 A & B.

Figure 3. 18 Panel shows the location of each ROI and the role of that brain part in the normal functioning of the brain.

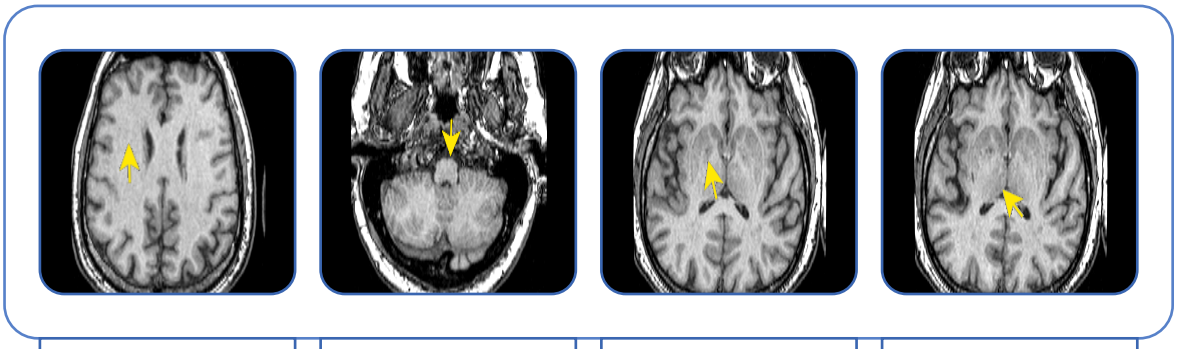

Centrum Semiovale	**Medulla**	**Basal ganglia**	**Thalamus**
White matter tracts	Brainstem - Organs at risk , generally preserved	normal brain function and behaviour, voluntary actions	Role in Cognitive functions – consciousness , alertnss

Initial graphs (Fig. 3.19 A & B) showed the differences between the two therapies. Thus, the decision was made to go ahead and explore texture analysis to understand the post-radiation brain changes and possible differences after proton and photon radiation therapy.

<u>The rationale for using texture analysis.</u>

We hypothesise that texture features represent brain structures and their underlying tissue composition and that any change in this structure will change the textural values. When visually different regions of interest in the brain are compared to the textural values, there is a clear difference in texture values (Fig 3.20,3.21).

Figure 3. 19 A. Graphs show differences in texture feature values changes (Skewness, Entropy, Energy) over time between photon and proton therapy in patients with different brain tumours. A,B,C,D are scans taken at 0,3,6 & 9 months following radiation in the thalamus region

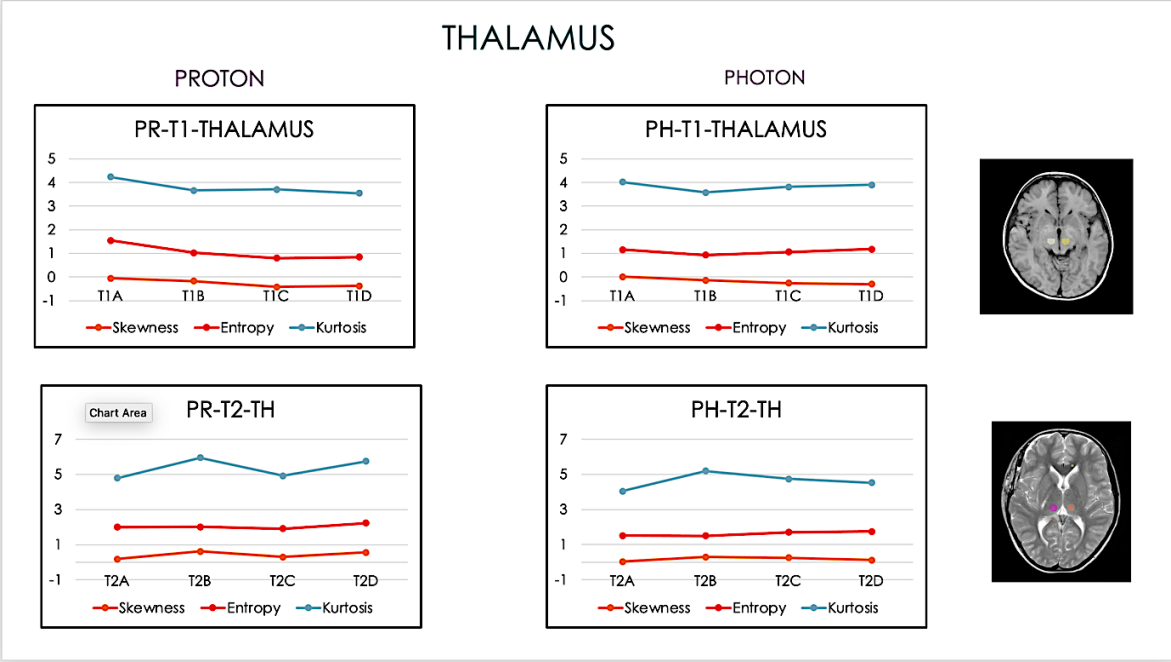

3.19 B. Graphs showing differences in changes of texture feature values (Median, variance, Mean) over time between photon and proton therapy in a patient with different brain tumours. A,B,C,D are scans taken at 0,3,6 & 9 months following radiation in the thalamus region

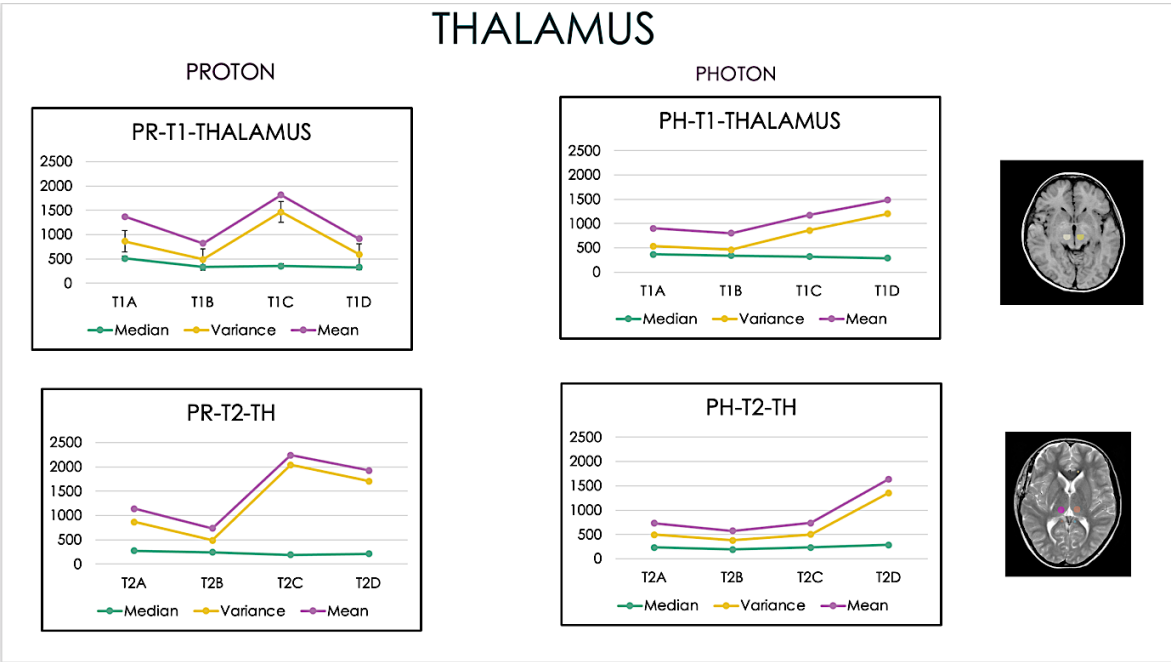

Figure 3. 20 Axial T1 MRI shows the difference in primary texture feature values in homogenous white 1 (green), mixed - more grey matter 2 (Yellow) and mixed with white matter 3 (light blue) ROIs. The X-axis shows feature value, and ROIs are shown on Y-axis.

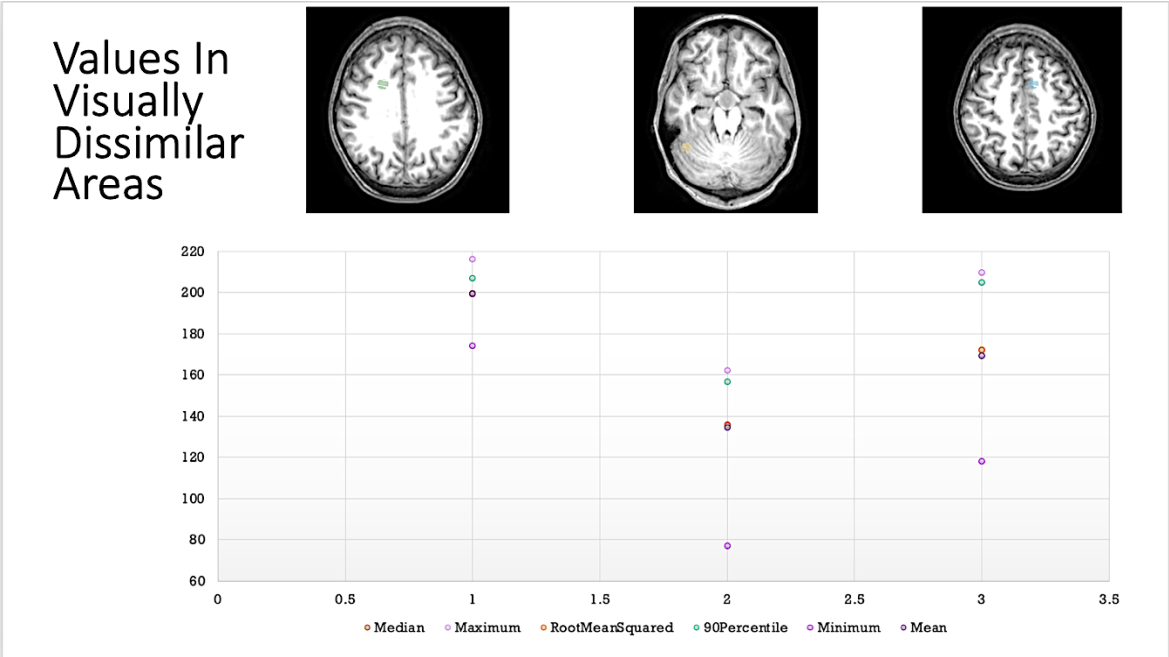

Figure 3. 21 Axial T1 MRI with ROI in white matter in a visually similar area (Right & Left). The graph shows the difference in primary textural values in visually identical brain areas. Please note that this difference is less than that of previous visually dissimilar regions of the brain. The X-axis shows feature value, and ROIs are shown on Y-axis.

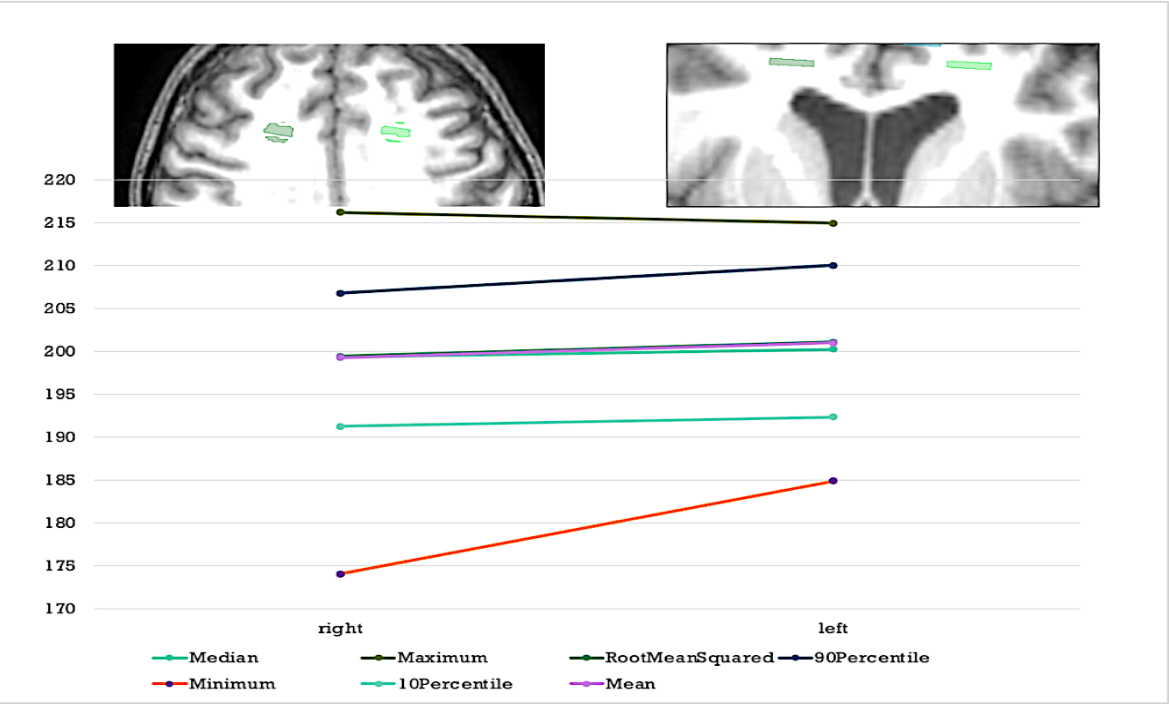

Quantitative texture analysis provides objective values in different areas, which the human eye can differentiate. However, the visual perception of the human eye has limitations, and slight changes in pixel intensity are not appreciated. Figure 3.21 shows a visually similar region (to the human eye), indicating differences in texture values after texture analysis. However, the difference was less than the difference between visually different areas, as seen in Fig 3.20.

Image-processing pipeline

All eligible patients and MRI scans were subjected to the pre-processing image pipeline using the techniques and methods described above, as illustrated in figure 3.1B. ROI segmentation previously used for dose calculation was also used for texture analysis using the pyradiomics module of the 3D slicer. First-order and GLCM features were extracted at altime pointsts, including baseline T2 scans (A-I). Definitions of these texture features have been given in chapter 1 in the texture analysis section. Some of the texture features that were selected are also suggested by IBIS for T1 w MRI texture analysis [127].

Figure 3. ***22*** Schematic representation of all 11 ROI's in different parts of the brain.

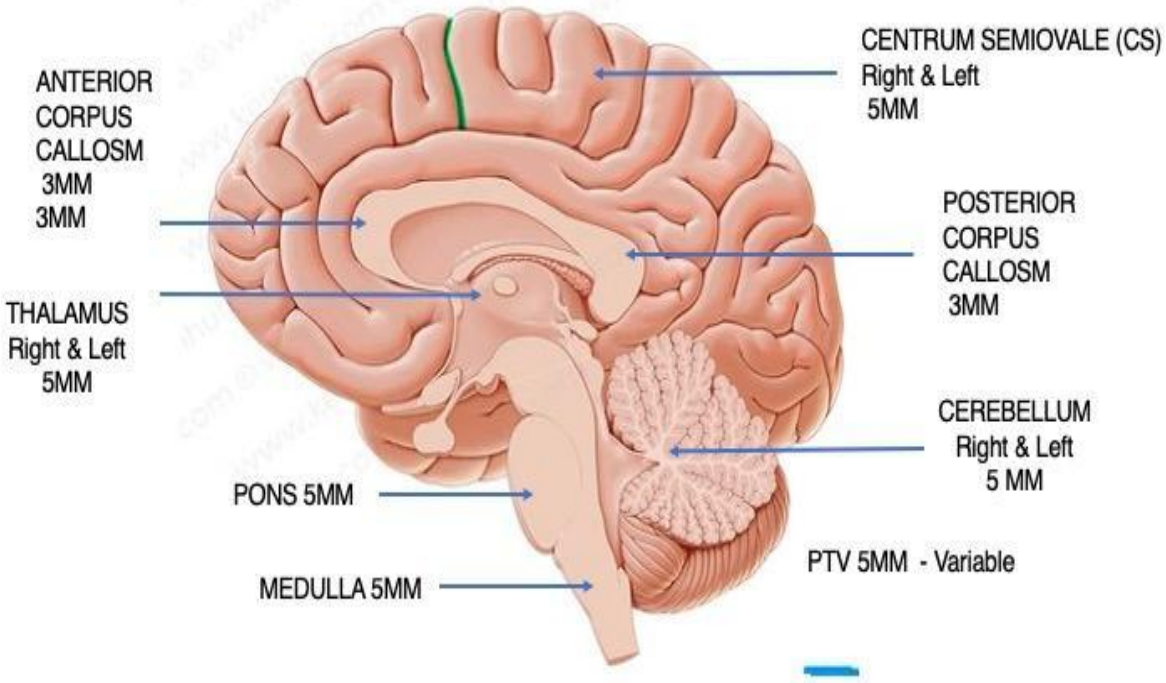

3.5 Limitations

The patients in this study were acquired retrospectively, and existing available data limited the methodology and analysis. The limitations and mitigation measures are detailed in table 3.3.

Table 3. 3. Limitations of image processing and measures taken to mitigate them

Methodology Step	Limitation	Measure to correct if possible
Data Collection	Missing scans / time points Patients with brain tumours are clinically and radiologically followed up based on the need for assessment and appointment schedule. It was difficult to find scans on fixed time durations in this clinical study.	Use of machine learning methods of analysis to compensate for these changes. Instead of considering scans at fixed time points, we analyzed all the scans taken over a period of 732 days from the date of end of radiotherapy. Thus, maximum possible data is available for each patient in given time duration. For statistical analysis, scans were selected from fixed time points and scans in between these fixed time points were not included.
	Missing digital radiation maps. Scans are obtained from the database from last 10-15years. There has been changes in system and development in the process of delivery of radiotherapy. Radiotherapy maps were searched in the databases of 3 different institutions – Clatterbridge, Florida, Oklahoma. We could not find digital maps for all the	Digital radiation maps help to calculate the exact dose given to the specific region of interest. Since it is not possible to estimate this dose exactly with hard copies, patients with no available digital radiation maps were excluded from the study. Only patients with available digital maps where exact dose can be estimated were used for the analysis.

	patients treated with radiotherapy.	
	Missing clinical information. It was difficult to find clinical corelates such as IQ, or other indices to assess cognitive function	Study was designed to focus on the available information – dose-based toxicity over time. Meticulous efforts were made to obtain maximum possible clinical information from the AH clinical records. Qualitative radiological assessment is also incorporated to increase reliability of this study in the medulloblastoma group
Image Analysis	MR Bias field effect MR images have uneven intensities due to bias field effects of high strength magnets. Texture analysis is sensitive to these changes in bias field.	N4ITK Bias Field Correction was used to filter all MR scans. This reduces inhomogeneities due to uneven magnetic fields.
	Difficulties with the registration of images Radiotherapy is planned on CT images. Registration of baseline MR scans on CT images need multimodality registration. Post-surgical MR scans show distortion and lot of variation on scans making registration difficult with the scans at subsequent time points.	Post-surgical, pre radiotherapy brain scan was used as a baseline. Several different modules of registration were tried for each individual MR scan to register with CT scan. Method that gives was most accurate feasible image registration was selected in each patient. Specialized registration technique was used to register longitudinal scans over baseline scans to compensate for the gross brain changes. Details in methodology section.

	Repeatability of TA TA is a very sensitive technique. Low repeatability of TA is known measure drawback widely reported in the literature.	Inherent problem of TA can be minimized by standardization, registration, and filtration. All scans are registered carefully, and maximum efforts are made to ensure same ROI is selected in all the scans of each patient. However possible errors due different registration techniques across the whole cohort are unavoidable due to clinical limitations. ICC analysis was carried out.
Results	Data presentation – Huge data	Specific charts and graphs were selected

Chapter 4 Effects of radiation dose, time and dose*time on longitudinal T2 MRI radiomic primary texture feature values in non-tumoral regions of the brain in paediatric brain tumours

4.1. Chapter Overview:

This chapter discusses the effects of radiation dose on the textural feature values in the normal parts of the brain over the two years following radiotherapy. This chapter explores the effects of time and time dose on the change in different primary texture features.

The chapter starts with an introduction to the side effects of radiation therapy in paediatric brain tumours, along with the effects of dose and time. The hypothesis follows this for using textural analysis as a methodology to study these effects.

Details of the developed application for the comprehensive data visualisation to study confounding factors such as age, gender, diagnosis, location, and surgery are described. The results of machine learning analysis with the random forest method demonstrate that the total energy is a useful feature for showing the relationship between dose and time in different regions of interest.

This is followed by the discussion of the results of statistical analysis using a general linear mixed model (GLM) demonstrating the effects of dose, time, and dose*time with the change in texture features over two years.

Finally, results are discussed with the evidence from the related studies in the literature and concluded with the future directions for research.

4.2. Introduction

Radiation therapy is a very effective treatment for brain tumours and is associated with high rates of survival. Hence, it is administered along with surgery and chemotherapy for the majority of paediatric posterior fossa tumours [142]. However, radiotherapy is neurotoxic and affects the quality of life in paediatric patients [93]. It affects cognition, memory, and speech and can cause long-term motor deficits [92]. A wide range of radiation doses can result in radiation toxicity. Combined chemotherapy and radiation effects manifest differently in paediatric patients than in adult populations [76]. It is essential to investigate radiation toxicity in paediatric patients to understand the susceptibility of non-tumoral parts of the brain in these patients. There are several factors influencing the severity of impairment, such as demographic factors (age, gender), radiation dose, time, diagnosis and location of the tumour, chemotherapy, type of radiation, etc. (Table A1.1, Appendix 1). Demographic details of the study population have been added in Appendix 5.

The clinical manifestations and pathophysiology of radiation toxicity and general introduction have been discussed in Chapter 1. In this chapter effects of dose, time and dose*time will be addressed.

4.2.a. Radiation brain injury and the effect of radiation dose on brain tissue

Dose, the volume of the irradiated brain, and the irradiation region are important factors affecting the incidence of radiation necrosis after radiosurgery [143]. It is well known that high doses of ionising radiation to the growing human brain affect myelination and neuronal development, leading to overall impaired brain development involving IQ and memory. In addition, even low doses of ionising radiation to the infant's brain can influence cognitive abilities in adulthood [144]. Posterior Reversible Encephalopathy Syndrome (PRES), which was seen in the adult population, is increasingly being seen in children. It manifests as cortical T2 hyperintensities, headaches, seizures, vision loss, and loss of consciousness [145].

According to a dose-escalation study by The Radiation Therapy Oncology Group, after whole-brain irradiation, radiation damage was dependent upon the size of the target. 15Gy was the maximum tolerated dose for target 31-40mm, and 18Gy was for target 21-30Gy. >24Gy was the maximum tolerated dose for targets <20mm. Radiation necrosis and asymptomatic radiological changes were associated with the radiation dose >/= 12 Gy [143].

4.2.b. Effect of time on radiation brain injury (Figure 4.1)

Brain injuries following cranial irradiation are mainly classified into three groups depending on the manifestation timing after the irradiation [92].

- Acute Radiation Brain Injury: a reversible type of reaction that presents within days to weeks after irradiation
- Early delayed brain injury: a severe reaction that occurs within 1-6 months after irradiation
- Late, delayed brain injury: these are progressive and irreversible injuries presenting over six months after irradiation and can result in radiation necrosis.

4.2.c. Radiation dose to different brain parts

Most post-radiation studies focus mainly on one or a few selected more significant parts of the brain, such as the hippocampus or corpus callosum. Memory decline or cognitive impairment can present even without hippocampal injury due to damage to white matter tracts [146]. Whilst most studies consider constant dose across the whole brain; there is growing evidence that the radiation dose/volume effect of smaller brain structures shows a more vital link to cognitive impairment than larger structures, e.g., memory loss is more associated with irradiation of the left hippocampus than the whole of the left temporal lobe [147]. Different brain parts receive different radiation doses depending upon the type of therapy (photon or proton), distance from the tumour and radiation plans. Different studies show that different brain parts may be necessary for assessing cognitive decline, e.g. supratentorial area [148]. In a retrospective study to assess post-treatment MRI changes in 44 children with primary malignant tumours, white matter lesions were associated with the supratentorial location of tumours [149].

maximum radiation dose constraints are also set for brain parenchyma, though cortex and grey /white matter are different structures within parenchyma [146]. The hippocampus, cerebral white matter and subventricular zones all show differing levels of radiosensitivity [150]. The volume of the corpus callosum is generally used as a surrogate of whole-brain parenchyma because of the white matter volume of the corpus callosum. However, such a correlation between the two is yet to be demonstrated.

Whole-brain volume and corpus callosum volume loss, which are used interchangeably may be unrelated and need separate assessments . Cortical thickness and volume are affected by radiation

dose . This has been reported in a voxel-wise MRI analysis showing that cortical thickness reduces with an increase in radiation dose . This contrasts with the study by Szychot et al. where dose did not show a correlation with brain volume loss in the corpus callosum and whole-brain .

4.2.d. The rationale for texture analysis (TA):

Clinical manifestations of irreversible brain changes appear late. These changes are rarely visible to the naked eye in the early period after radiation, and recent studies have shown that patients may have significant cognitive abnormality without any visible anatomical changes on MRI [151].

Figure 4.1 Clinical manifestations and pathophysiology of progressive radiation brain injury (Chu et al) [1]

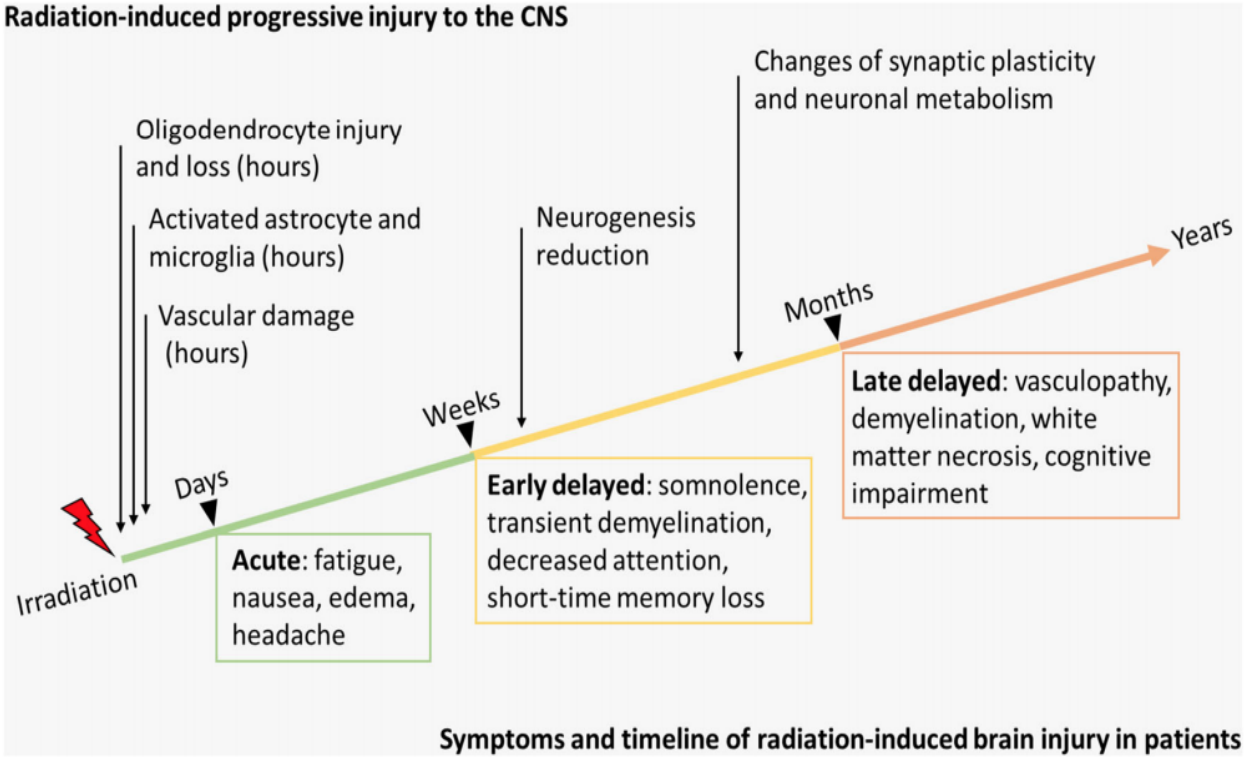

Texture analysis can quantitatively detect the changes in MRI signals that are not visible to the naked eye, thus potentially enabling objective assessment of these scans at earlier stages after radiation. This chapter aims to determine the effect of radiation dose on texture feature values over time.

TA can generate millions of features. Considering all of them might lead to overfitting error hence dimension reduction is frequently employed in these studies.

First-order texture features are considered more robust and less affected by the types of scanners used. Also, this was an exploratory study and hence basic features were selected. Other features will be considered in future studies.

4.2.e. Need for research:

Paediatric brains are different from adults with more myelination and neurogenesis in the white matter. Most studies of radiation-induced neurotoxicity are focused on adult brains, and more evidence is still needed in paediatric patients with more sensitive brain regions [147] [76]. The incidence of radionecrosis is increased by concurrent chemotherapy, which is commonly given after photon radiation in paediatric patients [147]. Diagnosis of brain toxicity is mainly made with radiological and clinical findings, and biopsy is rarely performed. Hence it is essential to have quantitative tools for earlier assessment of brain toxicity with routine MRI scans. These results may help investigate differences in clinical findings among groups of patients moving forward.

Primary objective of this exploratory study was to understand the effect of the radiation therapy in non-tumoral parts of brain. Hence all patients were assessed first.

4.2.f. Hypothesis:

We hypothesised that MRI texture features could act as a surrogate of underlying tissue changes following radiation therapy.

4.3. Primary Research Question:

Is there any effect of radiation dose, time, and dose* time when considered together on longitudinal T2 MRI radiomic primary texture feature values over 24 months and in non-tumoral regions of the brain in paediatric patients with primary brain tumours?

4.4. Aims and Objectives:

- To create a data visualisation app to facilitate the visualisation of different clinical parameters such as demographic features, tumour characteristics and treatment details for the entire database.
- To understand the effects of time, dose, and time dose together on the change in longitudinal T2 MRI radiomic primary texture feature values

4.5. **Methods**

4.5.1. Texture Analysis

Patient selection and image processing methods (Fig 3.1 A & B) have already been described in chapters 2 & 3. Image pre-processing steps were performed, and subsequent scans were registered with the baseline scan. All the steps from the first pre-processing of cropping and CT registration until the complete extraction of textural features from each scan were manually performed separately for each patient.

Eleven ROIs were drawn in the pre-determined areas on each baseline scan of all 50 patients. After registration, these locations were visually inspected on each subsequent scan and repositioned if necessary. Texture analysis was carried out in each ROI (out of 11) in each scan (from baseline A to the last scan for patient B-I over two years).

First-order texture features were extracted (Fig. 4.2) at all time points, including baseline T2 scans (A-I). Feature extraction was done separately by the pyradiomics module of the 3D slicer, and an Excel sheet was used to record the patient code and scan name. (e.g. 154A-TA.csv, 154B-TA.csv). Extracted dose files (Eg.154dvh.csv) were available for 50 patients.

4.5.2 Machine Learning Analysis Rationale and Methods:

This is a longitudinal analysis with huge data generated from 50 patients x 11 ROIs x 5-10 scans, one at each time point. And about 16 primary features were generated from each ROI. For example, if one patient has 5 follow-up scans, that patient-generated 5x11x16 = 240 values. And this becomes a minimum 240x50 = 12000 values (N). Machine learning analysis was used primarily to organise all the data by the exploration app.

Entire data including clinical and radiological information was combined in the single database and used for further analysis. This huge data needs a dimension reduction, and the random forest method was employed as a method of choice. The random forest method can handle large data sets for regression and classification purposes. It's a supervised learning method that generates decision trees. Details have been described in the discussion.

Figure 4. 2 . 3D slicer pyradiomics module for texture feature extraction.

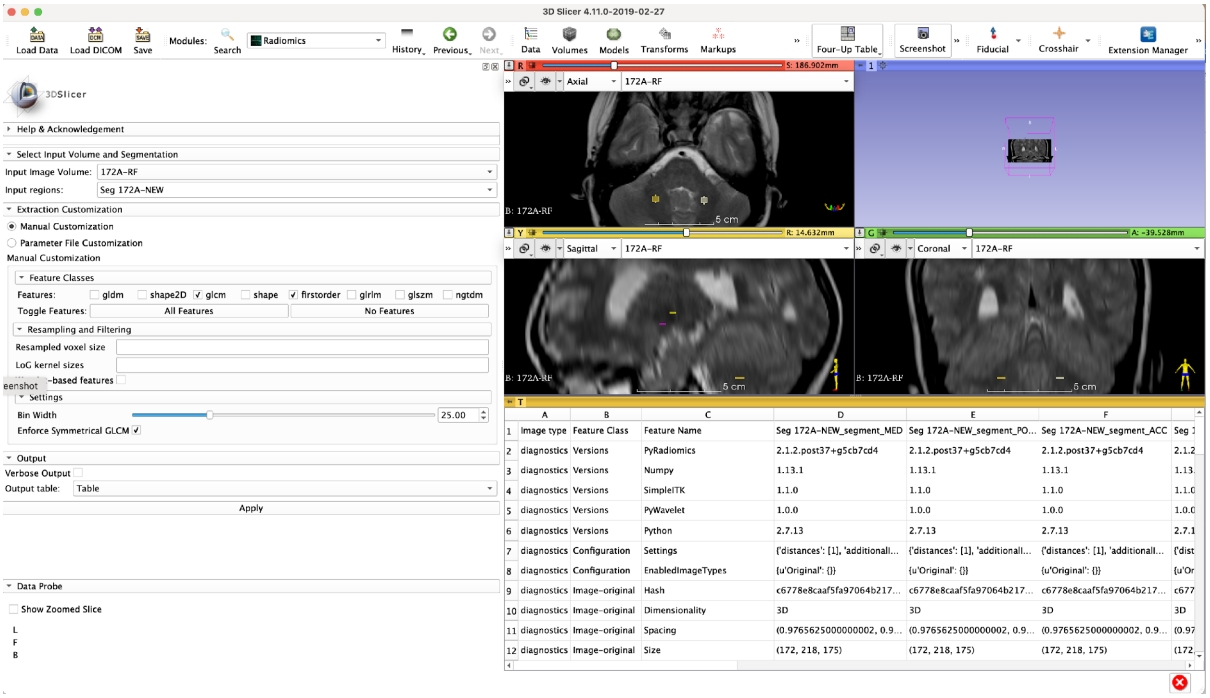

4.5.2.a Data processing

The data used had a collection of comma-separated value (CSV) files. Each file contained either a set of calculated texture features (one per scan) or the values of radiation doses for each region (one per patient). The files were matched by a unique patient identifier and merged. Region identifiers were unified to allow automatic filtering of all data. Fields with incorrect calculations (containing only values of 0 or 1) were removed from the feature table. Feature deltas (rates of change) were calculated and stored. The patient clinical data table was reformatted to accommodate filtering and plotting. Patient date of birth was replaced with age at treatment start/end and age at diagnosis.

4.5.2.b Data exploration app

An online dashboard-style app was built and hosted. The app utilised the formatted and filtered data for several visualisations. The results of some data modelling and analysis are presented in the app. Details of all the app features are described in the results section below and in appendix 1.

4.5.2.c Methods

The project aimed to find patterns relating changes in values of texture features over time to a dose of exposure, with the implication of this being associated with radiation-caused alterations in the brain matter.

Two approaches were explored: using the feature ‘rates of change’ at different times and an alternative including modelling the time courses to align time points and using predicted values of texture features at these time points. Random forest algorithms were used as the primary tool for exploring patterns in the data. The smoothing was added to moderate the variation between conditions (MRI setup). A set of 3rd-order polynomial functions have been fitted to each sequence of data points consisting of values of one texture feature over time in one region and one patient. This allowed interpolating texture feature values at times that were not present in the data, which enabled the use of methods that did not apply to data with unaligned time points.

Time points ranging between 0 and 540 days with gaps of 30 days were selected, and using the fitted splines, texture feature values were calculated at these times (Fig.4.3). This way, data at consistent time points were obtained. Additionally, “descriptions” of trends were calculated using the splines' first and second-order derivatives in the intermediate intervals between the time points. This allowed us to automatically assign the values to different trends, e.g., “Increasing," “decreasing," “flat," “concave," and “convex”. These additional features were used for clustering the trends. This hierarchical clustering was investigated to discover the subgroups.

Hierarchical clustering is an unsupervised clustering algorithm that aims to detect groups in the data that are not predefined. Using the Euclidean distance (absolute distance between points data points; there are alternatives) as the similarity metric between the data points, it finds the most similar data points and combines them into clusters. The clusters are then compared further to combine the most similar ones into larger clusters. This results in a hierarchical similarity structure between data points.

By investigating of this hierarchical structure (normally plotted as a dendrogram) we can discover subgroups of data points that show high similarity within the groups but are dissimilar between groups.

Figure 4. 3 Time points location of each scan in the dataset

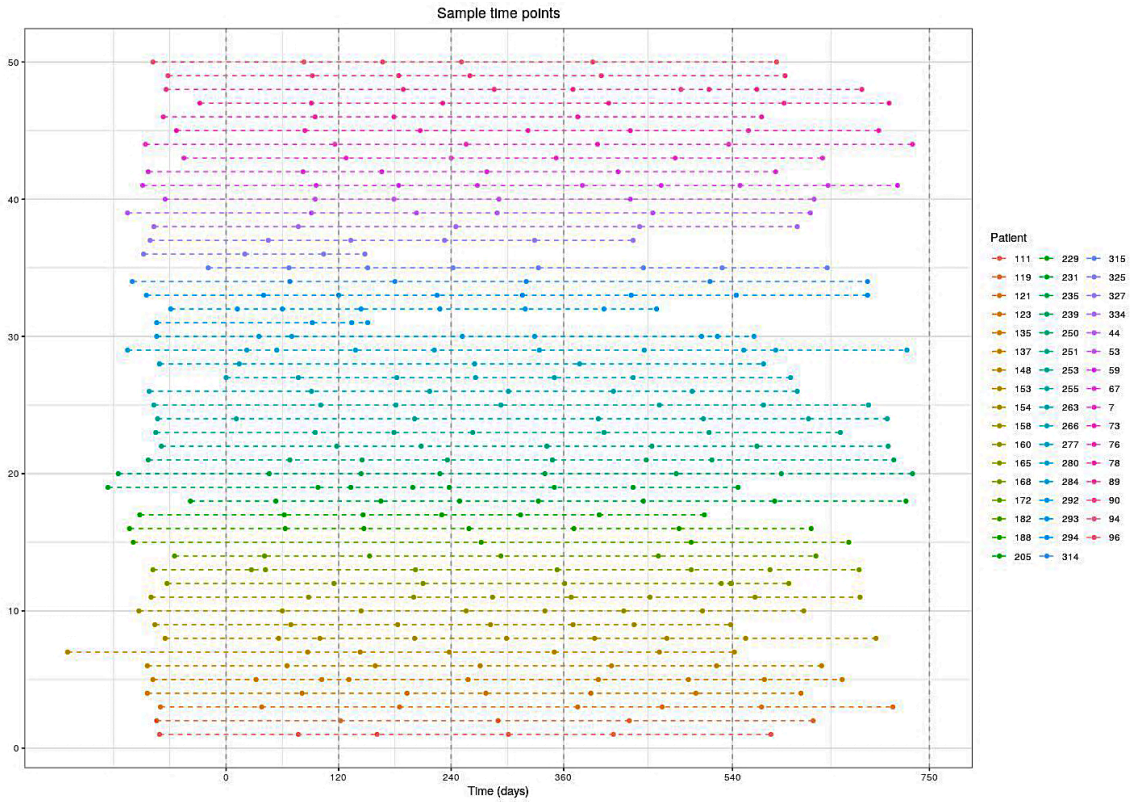

4.5.3 Statistical Analysis

General Linear Model (GLM) statistical model was used in SPSS . The GLM Multivariate procedure provides an analysis of variance for multiple dependent variables by one or more factor variables or covariates. The factor variables divide the population into groups.

Multivariate analysis of variance (MANOVA) is a statistical analysis used when a researcher wants to examine the effects of one or more independent variables (IVs) on multiple dependent variables (DVs). This method is an extension of the analysis of variance (ANOVA) model and is the most used multivariate analysis in the social sciences. MANOVA tests, whether they are statistically significant or not, produce differences among levels of the IVs for multiple DVs. MANOVA tests belong to a larger family of statistical techniques known as the general linear model, which includes analyses such as ANOVA, multiple types of regression, and repeated-measures designs. Independent variables – time and dose both are the main effects (time as covariate, dose in groups as fixed factor) and time with a dose interaction effect.

The dose was grouped in 6 groups for the GLM analysis

Table 4. 1 Shows dose groups for analysis

dose (Binned)	Gray
1	0-10.55
2	10.56-20.55
3	20.56-30.55
4	30.56-40.55
5	40.56-50.55
6	50.56-60.55

Effect of dose, time and dose with time interaction effect on dependent variables TA features

Selected textural features used for correlation are as follows:

- 10Percentile
- 90Percentile
- Energy (EG)
- Entropy (ETR)
- Kurtosis (KR)
- Mean
- Mean Absolute Deviation (MAD)

- Median (MDN)
- Minimum (MIN)
- Skewness (SK)
- Total Energy (TTE)
- Uniformity (UNI)
- Variance (VR)
- Range (RG)
- Sum Squares (SS).

Analysis was carried out in all ROIs across the whole brain together and in each ROI separately. TA can generate millions of features. Considering all of them might lead to overfitting error hence dimension reduction is frequently employed in these studies.

First-order texture features are considered more robust and less affected by the types of scanners used. Also, this was an exploratory study and hence basic features were selected. Other features will be considered in future studies. IBIS study recommends some of these texture features for MRI textural analysis[127].

A similar analysis was performed separately for all the 11 ROIs across the entire brain and later for each ROI separately. The significance of these effects was tested with Pillai's Trace. Pillai's trace is a test statistic produced by a MANOVA. It is a value that ranges from 0 to 1. The closer Pillai's trace is to 1, the stronger the evidence that the explanatory (independent) variable has a statistically significant effect on the values of the response (dependent) variables.

4.6. Results

T2-weighted (T2W) axial images with a slice thickness of 4 mm with a 0.4 mm or slice thickness of 5mm with a 1mm slice gap were selected for texture analysis.

Results of Machine Learning Analysis:

4.6.1 Data Exploration App: MRI Diagnostics and Machine Learning Analysis

A dedicated weblink https://pgb.liv.ac.uk/shiny/agraus/MRIanalysis/ can be used to open this app. Details of the application and all its features are shown in Appendix 1.

An online dashboard-style app was built and hosted as proposed in the project plan. The app utilises formatted and filtered data for several visualisations. It includes several features agreed upon beforehand and devised during the project. Results of some data modelling and analysis are also presented in the app.

Summary of data as a table and counts of patients based on categorical clinical features. A
A separate section has been added for exclusively medulloblastoma patients.

Texture feature plots (Fig. A1.18) show the change in each texture feature over time for all patients in each region of the brain. These include the functionality of removing outliers (points further than 2 standard deviations from the mean).

Texture feature delta plots (Fig. A1.9) show the relative change of texture features – the difference between consecutive time points divided by the length of time between the scans. The options are analogous to the texture feature plots.
3D feature plot (Fig. A1.18) is a dynamic 3-dimensional plot showing the change of features over time and dose.

Heatmaps (Fig. A1.11) of texture features and feature deltas are included for an alternative visualisation of the data all at once. The samples are grouped by patient and ordered by time of scan. The features are reordered by a clustering algorithm to group similarly behaving features together.

Feature deltas against dose plots and feature correlation to dose heatmaps were included to enable exploration of the idea that the secondary effects observed later in the patient's history would manifest as increasing correlations of feature deltas and radiation dose in the region when calculated in different time windows. Plots include linear model fits, absolute and relative slope figures are shown. Feature deltas over time plots (Fig A1.9) were included to allow investigation of linear relationships between feature deltas at different times at various windows of dose. The plots include linear model fits, and absolute and relative slopes are shown.

A linear model was fit (Fig. A1.14) to evaluate the influence of clinical features as well as time and dose to predict each feature deltas. The coefficients of the model are shown in the Clinical feature heatmap. Unfortunately, none of the features showed significant association.

The Splines tab of the app includes results of further data modelling and is described in the following section.

4.6.2 Statistical Analysis

General Linear Model (GLM) model was used in SPSS with dose as a fixed factor, texture feature as a variable and time as a covariate. Effects of Dose, time and Dose*Time on the texture feature values were calculated.

4.6.2.A Whole Brain Analysis

Results were obtained by applying the multivariate test to assess overall effects when all features were considered together (Table 4.1) and the effects of textural features on dose, time and dose*time. All remaining tables are given in Appendix 2 (Table A2.1, A2.2, A2.3).

The table shows that dose level in groups has a statistically significant effect on Texture features @10percentile, @90percentile, contrast, Correlation, Energy, Entropy, Maximum, Mean, Mean Absolute Deviation, Median, Minimum, Range, Total Energy, and Uniformity.

Time has a statistically significant effect on Texture features at 10percentile, 90percentile, Correlation, Energy, Entropy, Maximum, Mean, Mean Absolute Deviation, Median, Minimum, Range, Total Energy, and Uniformity.

It is also seen that the interaction effect of dose levels in groups with time has a statistically significant effect on Texture features Correlation, Energy, and Total Energy.

Table 4. 2 summary table shows the effect of time , dose and dose * time on the number of texture features

Effect of IV	Presence of effect	
	Yes	No
Time	13	4
Dose	14	3
Dose*Time	3	14

Figure 4. 4 Graph showing number of texture features showing significant effects of dose, time and dose*time. X axis is the factor and y-axis is the number of texture features.

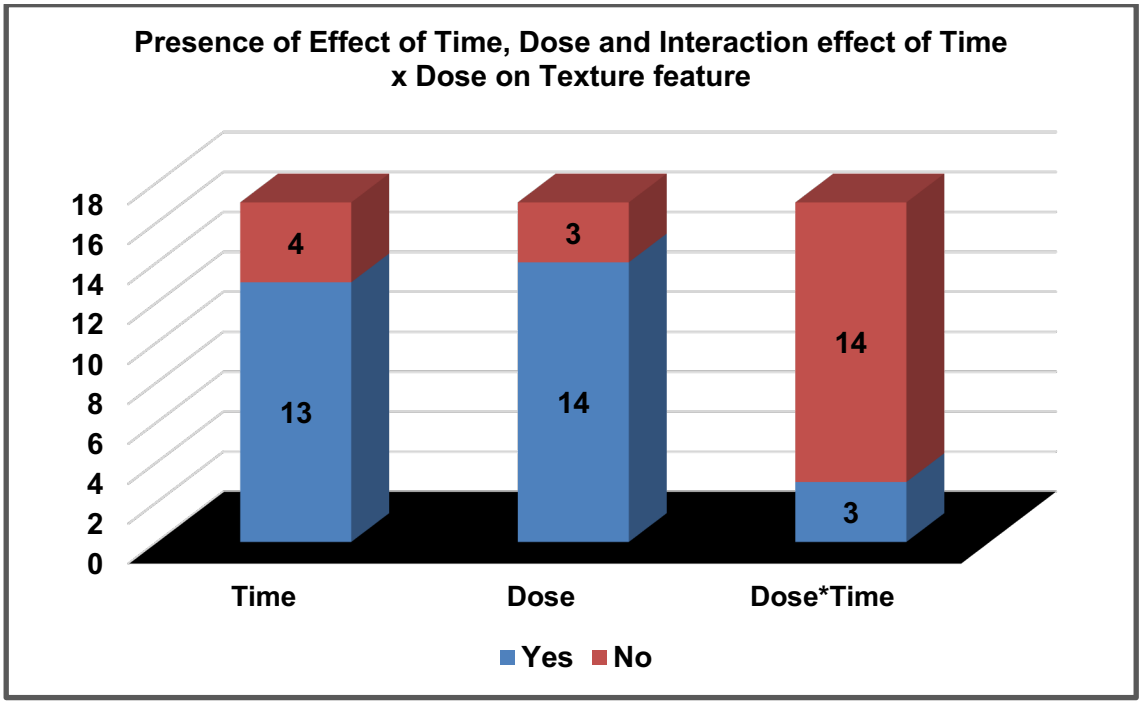

Table 4. 3 Effect of time on texture feature (Tests of Between-Subjects Effects)

Texture feature	Signifance	P value
@10Percentile	Y	P <0.001**
@90Percentile	Y	P <0.001**
Contrast	N	0.054
Correlation	Y	0.019*
Energy	Y	P <0.001**
Entropy	Y	P <0.001**
Kurtosis	N	0.211
Maximum	Y	P <0.001**
Mean	Y	P <0.001**
Mean Absolute Deviation	Y	0.012*
Median	Y	P <0.001**
Minimum	Y	P <0.001**
Range	Y	P <0.001**
Skewness	N	0.253
Total Energy	Y	P <0.001**
Uniformity	Y	P <0.001**
Variance	N	0.569

Presence of effect	Frequency
Yes	13
No	4

Figure 4. 5 Pie chart showing number of texture features showing significant effects of time

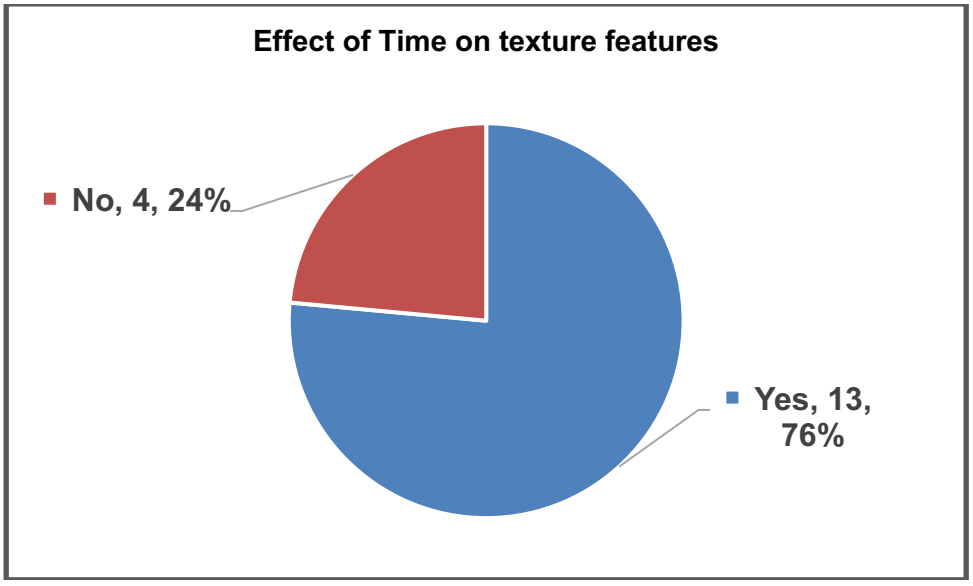

Table 4. 4 Effect of dose level on texture feature (Tests of Between-Subjects Effects)

Texture feature	Signifance	P value
@10Percentile	Y	P <0.001**
@90Percentile	Y	P <0.001**
Contrast	Y	P <0.001**
Correlation	Y	0.004*
Energy	Y	P <0.001**
Entropy	Y	P <0.001**
Kurtosis	N	0.212
Maximum	Y	P <0.001**
Mean	Y	P <0.001**
MeanAbsoluteDeviation	Y	P <0.001**
Median	Y	P <0.001**
Minimum	Y	P <0.001**
Range	Y	P <0.001**
Skewness	N	0.055
TotalEnergy	Y	P <0.001**
Uniformity	Y	P <0.001**
Variance	N	0.063
Presence of effect	Frequency	
Yes	14	
No	3	

Figure 4. 6 Pie chart showing number of texture features showing significant effects of dose

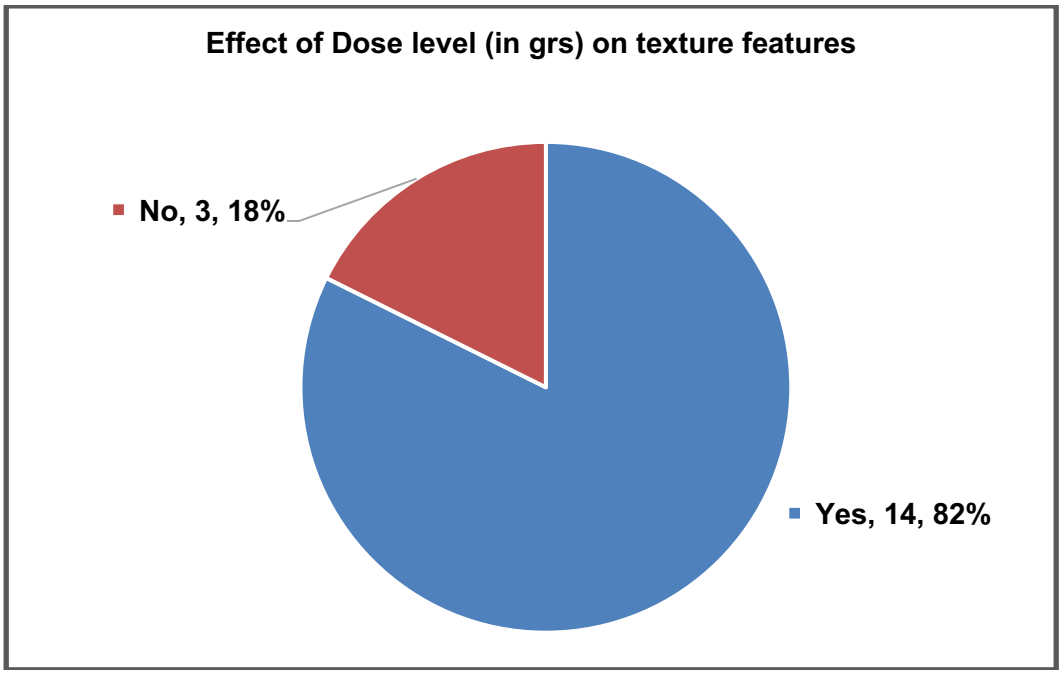

Table 4. 5 Interaction Effect of dose X time on texture feature (Tests of Between-Subjects Effects)

Texture feature	Signifance	P value
@10Percentile	N	0.214
@90Percentile	N	0.194
Contrast	N	0.998
Correlation	Y	0.048*
Energy	Y	0.028*
Entropy	N	0.486
Kurtosis	N	0.817
Maximum	N	0.173
Mean	N	0.169
Mean Absolute Deviation	N	0.884
Median	N	0.147
Minimum	N	0.237
Range	N	0.783
Skewness	N	0.384
Total Energy	Y	0.005*
Uniformity	N	0.327
Variance	N	0.998
Presence of interaction effect	Frequency	
Yes	3	
No	14	

Figure 4. 7 Pie chart showing number of texture features showing significant effects of time*dose

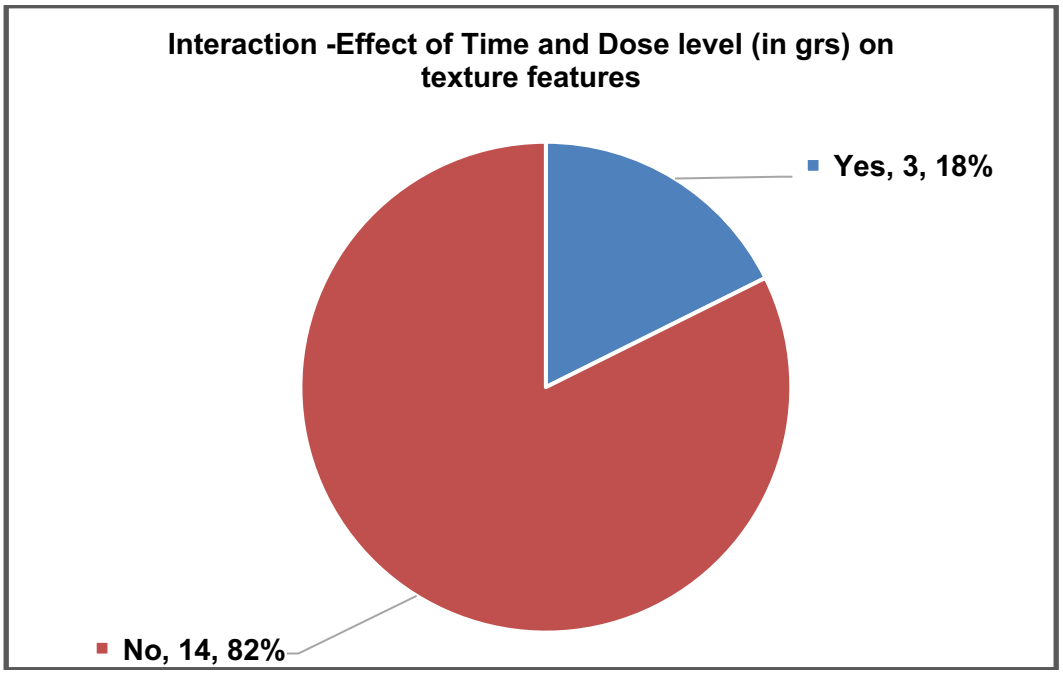

Figure 4. 8 The graph shows the number of ROIs showing a significant effect of dose on textural features. X-axis shows the name of the feature and the Y-axis shows the number of ROIs. Eg. 10 percentile shows a significant effect of dose in 2 ROIs

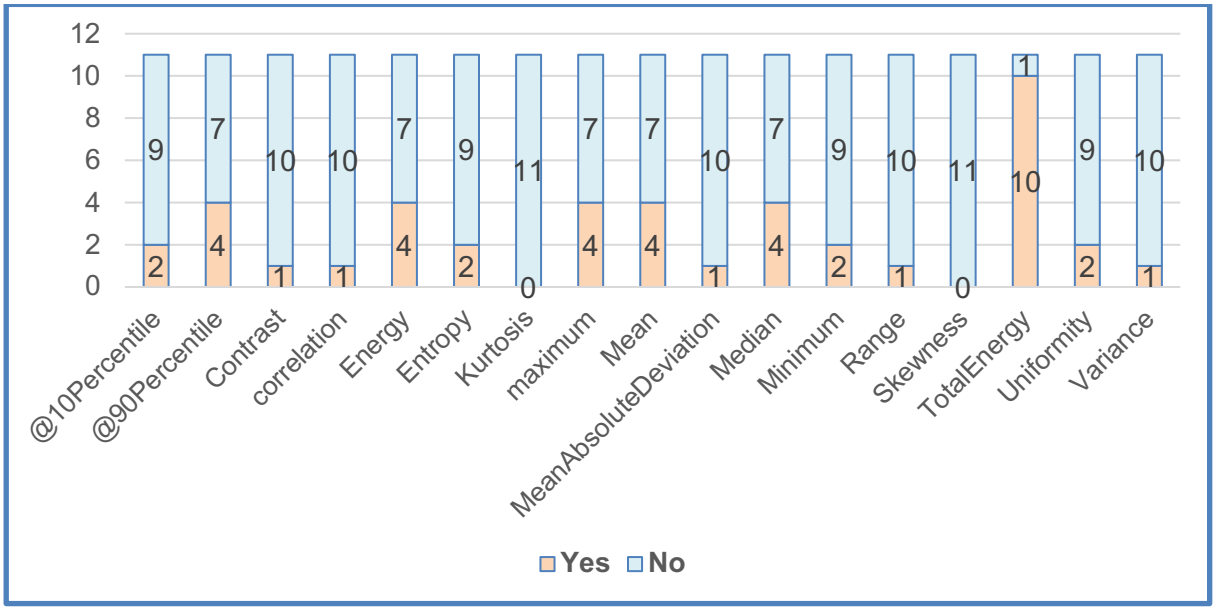

Figure 4. 9 The graph shows the number of ROIs showing a significant effect of time on textural features. X-axis shows the name of the feature and the Y-axis shows the number of ROIs. Eg. 10 percentile shows a significant effect of dose in 4 ROIs

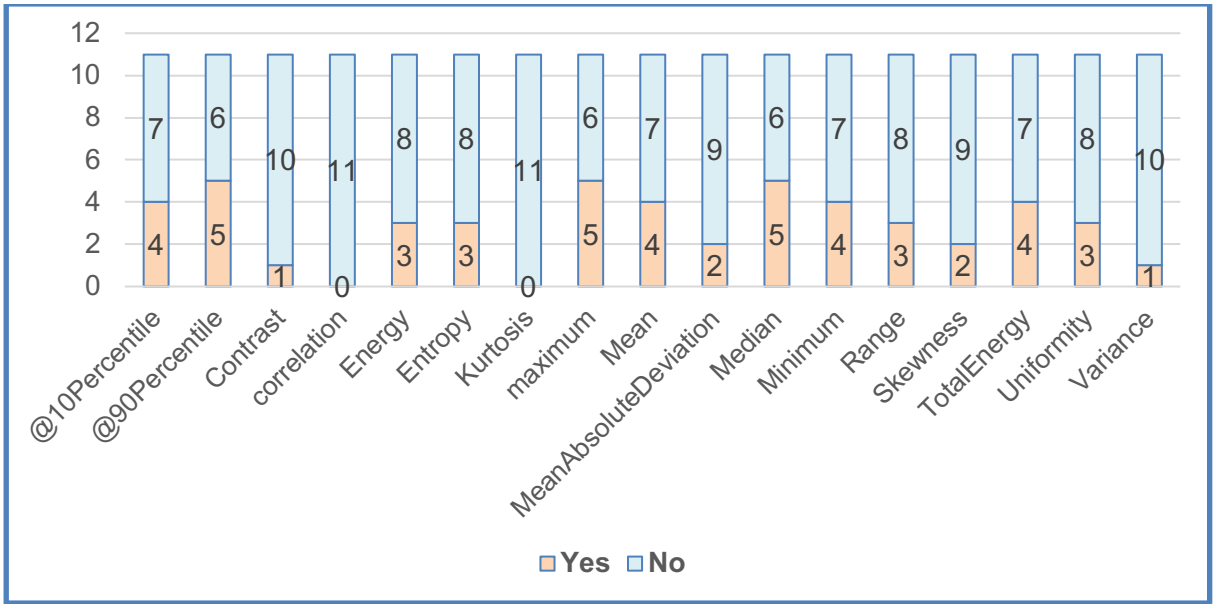

Figure 4. 10 The graph shows the number of ROIs showing a significant effect of dose* time on textural features. X-axis shows the name of the feature and the Y-axis shows the number of ROIs. Eg. 10 percentile shows a significant effect of dose in 2 ROIs

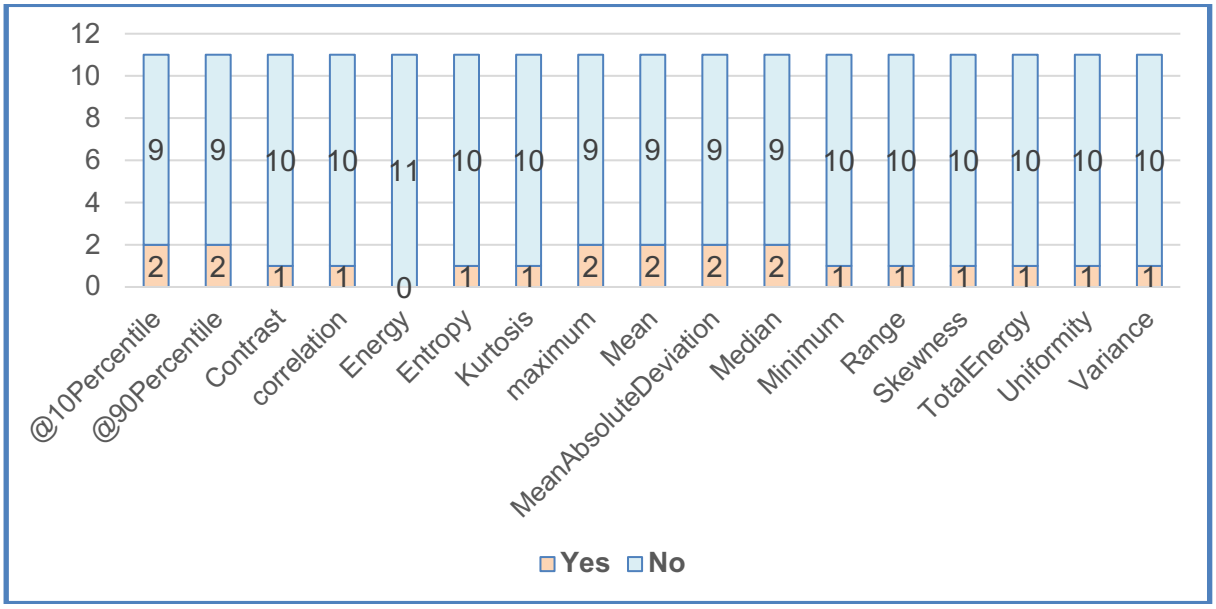

4.6.2.B Region-wise Analysis

After analysing all ROIs together, each ROI was separately analysed to understand the correlation between textural features and dose. Individual values in the tables are added in Appendix 2. Summary Table 4.9 and effect-wise tables 4.6, 4.7, 4.8 and graph 4.12 show the overall relationships in each ROI.

Figure 4. 11 Shows a simple bar graph showing mean dose values in each region of interest. X axis is a ROI and Y axis depicts the mean dose received by each ROI.

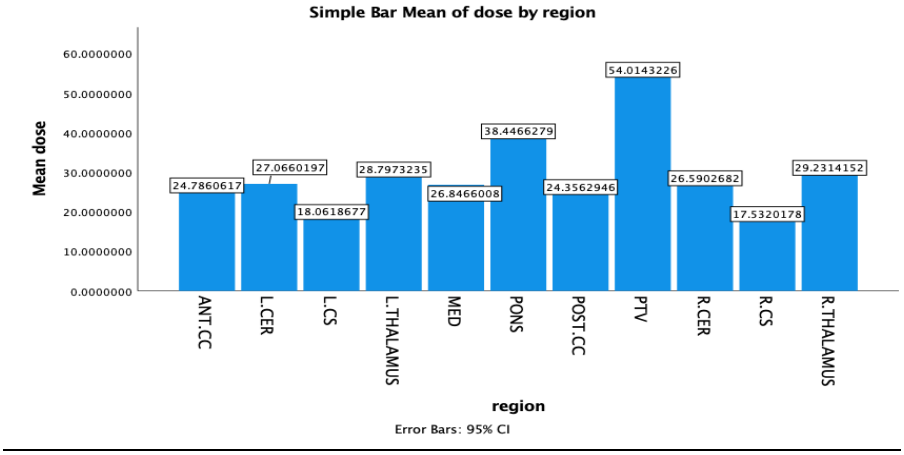

Table 4. 6 Summary table showing the significance values effect of dose in each ROI

R.CS	R.CER	PTV	POST.CC	PONS	MED	L.THALAMUS	L.CS	L.CER	ANT.CC	Region of Interest	
0.072	0.98	0.138	0.08	0.359	0.054	0.005	0.244	0.975	0.54	@10Percentile	Effect of dose levels in group upon texture feature
0.099	0.991	0.097	0.009	0.216	0.047	0.005	0.238	0.947	0.40	@90Percentile	
0.876	0.988	0.773	0.275	0.026	0.686	0.322	0.251	0.115	0.23	Contrast	
0.42	0.995	0.074	0.391	0.109	0.403	0.414	0.294	0.117	0.04	correlation	
0.068	0.603	0.182	0	0.584	0.091	0.002	0.044	0.692	0.32	Energy	
0.84	0.882	0.19	0.369	0.007	0.257	0.221	0.456	0.223	0.02	Entropy	
0.508	0.082	0.668	0.51	0.953	0.709	0.274	0.807	0.959	0.50	Kurtosis	
0.089	0.988	0.072	0.011	0.216	0.033	0.004	0.304	0.931	0.53	maximum	
0.083	0.986	0.109	0.02	0.289	0.046	0.004	0.242	0.965	0.46	Mean	
0.332	0.852	0.352	0.718	0.002	0.168	0.205	0.684	0.071	0.69	Mean Absolute	
0.08	0.986	0.132	0.011	0.287	0.047	0.005	0.226	0.96	0.44	Median	
0.076	0.979	0.114	0.082	0.393	0.061	0.005	0.301	0.988	0.56	Minimum	
0.237	0.538	0.294	0.492	0.005	0.129	0.218	0.754	0.053	0.67	Range	
0.727	0.288	0.076	0.678	0.651	0.934	0.762	0.249	0.155	0.62	Skewness	
0.001	0.001	0.682	0.025	0	0	0	0.001	0	0.00	Total Energy	
0.897	0.747	0.26	0.371	0.019	0.37	0.324	0.341	0.266	0.04	Uniformity	
0.623	0.888	0.648	0.747	0.005	0.358	0.331	0.931	0.11	0.54	Variance	

R.THALAMUS
0.019
0.024
0.955
0.235
0.017
0.829
0.975
0.027
0.022
0.243
0.024
0.026
0.104
0.825
0
0.953
0.177

Table 4. 7 Summary table showing the significance values effect of time in each region of interest on each texture feature.

Region of Interest	Effect of time on texture feature																	
	@10Percentil	@90Percentil	Contrast	correlation	Energy	Entropy	Kurtosis	maximum	Mean	Mean Absolu	Median	Minimum	Range	Skewness	TotalEnergy	Uniformity	Variance
ANT.CC	0.14	0.11	0.74	0.89	0.11	0.44	0.77	0.15	0.11	0.82	0.09	0.17	0.80	0.04	0.06	0.50	0.95
L.CER	0.18	0.12	0.38	0.22	0.27	0.60	0.67	0.11	0.15	0.07	0.16	0.16	0.08	0.10	0.10	0.90	0.14
L.CS	0.01	0.01	0.53	0.21	0.04	0.40	0.47	0.01	0.01	0.56	0.01	0.01	0.38	0.67	0.01	0.58	0.98
L.THALAMUS	0.06	0.05	0.25	0.14	0.11	0.41	0.89	0.05	0.05	0.11	0.05	0.07	0.17	0.96	0.05	0.82	0.34
MED	0.00	0.00	0.06	0.82	0.03	0.00	0.21	0.00	0.00	0.08	0.00	0.01	0.02	0.60	0.00	0.00	0.13
PONS	0.34	0.32	0.83	0.46	0.49	0.77	0.87	0.36	0.35	0.72	0.37	0.38	0.53	0.88	0.51	0.77	0.96
POST.CC	0.00	0.00	0.08	0.55	0.00	0.09	0.18	0.00	0.00	0.39	0.00	0.01	0.14	0.43	0.03	0.10	0.92
PTV	0.81	0.99	0.90	0.05	0.97	0.17	0.95	0.99	0.94	0.70	0.96	0.71	0.70	0.33	0.99	0.09	0.95
R.CER	0.13	0.10	0.05	0.22	0.32	0.06	0.13	0.08	0.12	0.04	0.12	0.14	0.03	0.00	0.06	0.10	0.09
R.CS	0.04	0.04	0.34	0.35	0.08	0.05	0.34	0.03	0.04	0.16	0.04	0.05	0.07	0.54	0.01	0.04	0.50

R.THALAMUS
0.12
0.07
0.03
0.67
0.13
0.00
0.97
0.06
0.09
0.01
0.09
0.13
0.02
0.25
0.08
0.00
0.03

Table 4. 8 Summary table showing the significance values effect of dose*time in each region of interest on each texture feature.

Region of Interest	ANT.CC	L.CER	L.CS	L.THALAMUS	MED	PONS	POST.CC	PTV	R.CER	Interaction Effect of dose X time on texture feature
@10Percentile	0.98	0.322	0.476	0.383	0.019	0.041	0.231	0.676	0.847	
@90Percentile	0.95	0.243	0.592	0.491	0.023	0.028	0.075	0.823	0.885	
Contrast	0.58	0.137	0.579	0.985	0.445	0.024	0.57	0.984	0.764	
correlation	0.54	0.028	0.064	0.771	0.732	0.912	0.507	0.102	0.542	
Energy	0.96	0.253	0.801	0.497	0.061	0.066	0.133	0.792	0.671	
Entropy	0.76	0.258	0.82	0.991	0.158	0.015	0.871	0.392	0.85	
Kurtosis	0.72	0.835	0.816	0.845	0.524	0.961	0.895	0.892	0.015	
maximum	0.92	0.244	0.623	0.518	0.016	0.027	0.068	0.819	0.897	
Mean	0.97	0.278	0.52	0.434	0.018	0.034	0.104	0.736	0.871	
Mean Absolute Deviation	0.99	0.043	0.94	0.814	0.608	0.023	0.911	0.961	0.945	
Median	0.97	0.273	0.507	0.465	0.015	0.032	0.088	0.723	0.879	
Minimum	0.98	0.348	0.462	0.32	0.025	0.05	0.259	0.582	0.835	
Range	0.99	0.06	0.983	0.932	0.24	0.035	0.768	0.96	0.645	
Skewness	0.38	0.168	0.931	0.771	0.985	0.79	0.386	0.57	0.025	
Total Energy	0.42	0.118	0.29	0.177	0.043	0.171	0.76	0.809	0.532	
Uniformity	0.63	0.305	0.552	0.957	0.077	0.036	0.796	0.187	0.777	
Variance	1.00	0.112	0.999	0.912	0.753	0.045	0.993	0.998	0.939	

R.THALAMUS	R.CS
0.639	0.345
0.726	0.353
0.975	0.681
0.084	0.333
0.827	0.592
0.931	0.45
0.746	0.772
0.751	0.334
0.678	0.354
0.997	0.1
0.688	0.36
0.689	0.366
0.918	0.242
0.585	0.978
0.808	0.279
0.854	0.604
0.979	0.345

Table 4. 9 Summary of Overall Multivariate Analysis (test) of each ROI By p-value. Table shows effect of dose, time and diose*time in each ROI on texture features considered together.

Region of Interest	dosegr (main effect)	time_days (main effect)	dosegr * time_days (Interaction effect)
ANT.CC	0.00	0.29	0.80
L.CER	0	0.027	0.36
L.CS	0	0.317	0.916
L.THALAMUS	0	0.348	0.596
MED	0	0.005	0.081
PONS	0.003	0.576	0.143
POST.CC	0.001	0.15	0.756
PTV	0.457	0.562	0.897
R.CER	0.002	0.023	0.128
R.CS	0	0.043	0.525
R.THALAMUS	0	0.378	0.931

Figure 4. 12 The graph shows the overall summary of number of ROIs showing a significant effect of dose, time and dose* time on textural features. X-axis shows the name of the factor and the Y-axis shows the number of ROIs. Eg. Dose group shows significant effect in 10 ROIs

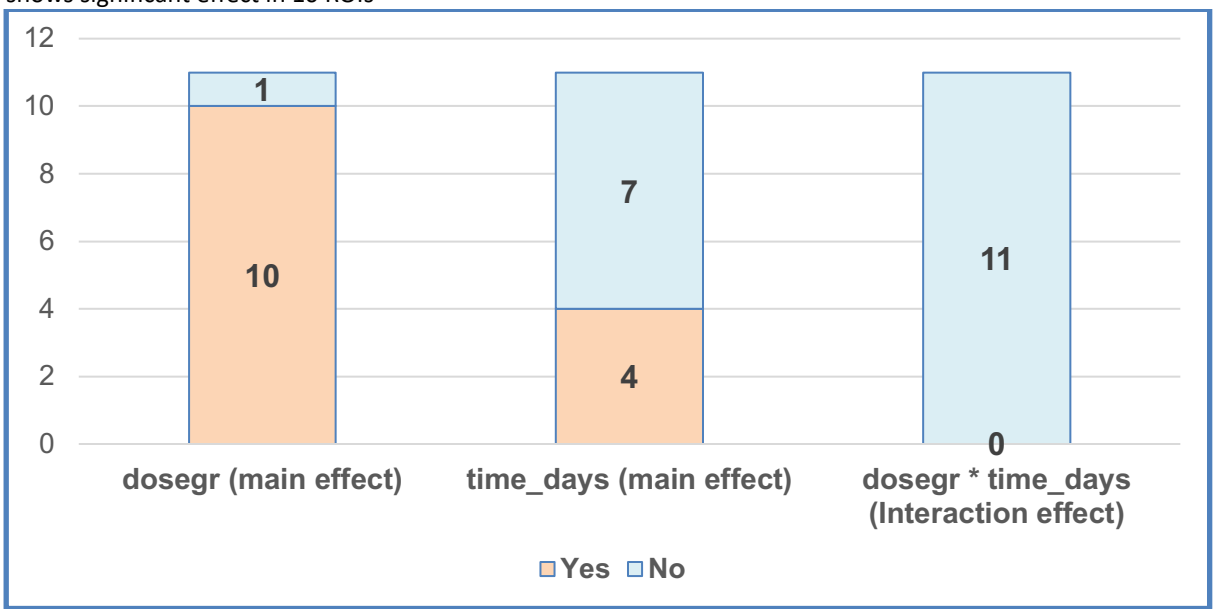

4.7. Discussion

This chapter aimed to assess the effect of individual radiation doses in 11 different regions of the brain to assess the T2 signal changes following radiation. These changes could be secondary to the underlying structural changes.

The database consisted of 341 brain cancer patients diagnosed with primary brain tumours.

out of which 105 were treated with radiation, and 51 patients had a digital radiation map available. 50 patients were finalised for this study. They showed different tumour characteristics. 11 different ROIs were selected for texture analysis. The dose was also calculated in each 11 ROI.

In this chapter, the texture analysis of non-tumoral brain regions has shown that the effects of interaction between dose, dose*time and time and textural features. Several techniques were assessed during the study, including machine learning and statistical analysis using GLM.

4.7.1. Machine Learning Analysis

Random forest is a supervised learning algorithm based on the automatic creation of many decision trees. A decision tree is a stepwise branching path with a condition at each branching point (e.g., Entropy > 1.3). A positive answer directs the process onto one branch while a negative response to another. Following the branches in this manner (evaluating a condition at each split in the path) leads to an endpoint (a leaf in the tree) that suggest an answer — a group assignment in a classification model or a predicted value in a regression model. However, each decision tree is prone to overfitting the data (fitting to noise and the signal). Random forest is a solution to this problem by fitting many trees (hundreds or thousands) on various subsets of samples and variables and taking the consensus predictions of all the trees. This has the effect of mitigating overfitting and improving the model's overall performance.

Smoothed splines are piecewise polynomial functions that allow the modelling of sequence data. The smooth spline interpolation was used to address the issue of variable time points, and a varying selection using random forest was used to elucidate predictive features.

Total Energy (TTE) which represents the pixel intensity variation in cubic volume seemed the most robust feature in predicting dose in each region of the brain (Appendix 1, Figure A1.24). It might be a consequence of it being the least susceptible to the various sources of noise present in the data, such

as varying conditions of data acquisition, varying age (and development speed) of patients, and differing brain tumour diagnoses.

Hierarchical clustering is an unsupervised clustering algorithm that aims to detect groups in the data that are not predefined. Using the Euclidean distance (absolute distance between points data points; there are alternatives) as the similarity metric between the data points, it finds the most similar data points and combines them into clusters. The clusters are then compared further to combine the most similar ones into larger clusters. This results in a hierarchical similarity structure between data points. By studying this hierarchical structure (see Figure A1.24, Appendix 1 for an example of a normally plotted dendrogram,) we can discover subgroups of data points that show high similarity within the groups but are dissimilar between groups.

Visualisation of the TTE values across different regions split by clustering results showed that variation in the TTE was significantly higher in the regions exposed to high-dose radiotherapy (>20 Gy). This suggests observable changes in the TTE of the MRI scan regions in patients irradiated with doses higher than 20Gy. These changes are mainly visible in the first year after radiation treatment.

Repeatability and reproducibility are the desirable qualities for any quantitative biomarker. However, textural analysis is affected by changes in scanners, vendors, and other parameters of the MR imaging [152, 153]. Several studies have evaluated the robustness of different radiomic texture features with different results. The robustness of texture features can be improved with pre-processing [154]. In a study using a virtual phantom for analysis, the following first-order features were robust: 10th percentile, 90th percentile, Energy Entropy, Kurtosis, Maximum, Mean, Median, Minimum, Skewness, Root mean squared, Total energy and Uniformity [154].

Furthermore, ROIs with the same diameter have been shown to have more reliability in the texture features when compared to the homogenous phantoms [155]. This study selected ROIs of fixed diameter and used a standard pre-processing protocol, including the N4ITK filter, to improve our results. Other radiomic studies have shown that when texture features are obtained from images from different scanners, total energy and energy were the primary texture features that showed excellent reproducibility across all scanner types [152], a finding also observed.

The Random Forest models were used to try and find features that would be predictive of high/low doses used in the treatment (high being >20Gy). The idea was that if we could fit a model that was able to predict the dose from the calculated features well, we could then find out which of the features were the most important to make those predictions and subsequently narrow down the feature list to the ones that are worth looking at (potentially different for different regions). Unfortunately, no model could predict the dose well enough.

4.7.2. Statistical Analysis:

When feature values over two years were analysed with the radiation dose, time, and dose*time in the ROIs across the entire brain, most of the features showed a significant effect with dose and time separately. Most of them did not show a significant effect of time and dose when considered together (Table 4.2).

Dose shows a significant effect on all 13 features (Table 4.4) when each feature was individually considered. The qualitative meaning of different texture features has been described earlier in Chapter 1, in the last part of texture analysis. Energy is one of the determinants of heterogeneity and provides information on the local intensity variation .

Our findings were consistent with Cunliffe et al. [156], who studied oesophageal cancer and found a significant correlation between dose and change in texture features. They showed that with an increase in radiation dose, there was a significant increase in Δ feature value and that Δfeature value was significantly related to radiation pneumonitis development. In a study of head-neck cancers, textural analysis (TA) correlated with mean dose, severe chronic xerostomia and volume of the parotid glands [157]..Textural parameters such as mean intensity and dimensions have been shown to predict parotid gland shrinkage at the end of the radiotherapy [158].

<u>Effects of radiation on different brain regions:</u>

The radiation dose to different brain regions varied depending on the tumour location and type in this study. Tables 4.6,4.7 and 4.8 show the number of ROIs showing the effects on different textural features. Fig 4.11 shows the mean dose received by each ROI across the entire dataset. Different areas

of the brain have other structures and different susceptibilities to radiation. e.g., white matter shows more sensitivity and vascular changes after radiation. Hence this analysis was also carried out separately in each brain region.

A study measuring a change post-radiation in cortical thickness of 54 primary brain tumour patients showed that the cerebral cortex shows selective vulnerability and radiation-related atrophy was associated with dose in entorhinal and inferior parietal ROIs while it was not significant in the primary cortex. They showed that the areas responsible for the higher-order neurological function are more susceptible to radiation dose-dependent atrophy [159]. Loss of volume in the corpus callosum and whole-brain volume loss are affected by different factors and should not be used interchangeably [142]. Further studies need to be conducted to identify the reason for the inconsistent effect of time on different texture features. Dose* Time showed a significant effect with very few textural features (Table 4.5).

4.8. Limitations, Clinical Relevance and Future Scope

While rich in data, this study presented a unique set of challenges. The patient cohort was diverse in terms of age, treatment type and diagnoses, and conditions of collection of the scans. This limited the standardisation and grouping based on clinical characteristics due to fewer patients. Additionally, the time course included data collected at variable intervals with a variable number of time points. This posed specific challenges to applying several standard approaches to data modelling.

Registration of post-operative brain scans was challenging, as discussed in Chapter 3. Measures were taken to reduce the inherent limitations of texture analysis by filtration and bias correction. Data processing was performed manually, and hence the study is subjected to human errors for ROI selection and placement. Registration was performed to select the same region of interest across all the follow-up scans and specific areas and guidelines were made to ensure the ROI placement to reduce these human errors. The utilisation of automated techniques for precise inter-scan registration was prohibited due to two factors: 1. the presence of postoperative intracranial changes due to surgery, and 2. variation in postoperative MRI data quality (e.g. lack of brain/skull coverage, no volume scans). However, such a longitudinal study would be challenging to administer without data acquired from

clinical evaluation. Thus, clinically acquired data, which is widely available, has been exploited in this study. Therefore, the manual placing of ROIs was necessary to overcome partial volume effects. This approach also eliminated the need for additional measurements or image acquisitions beyond the clinical routine. ICC analysis was carried out for the manual ROI drawing. Results can be found in Chapter 3.

Although no independent validation cohort was available for machine learning analysis, the model was validated using cross-validation with different subsamples, a standard procedure for model validation with a limited number of samples. The combined model proved valid in the cross-validation yielding high diagnostic accuracies above 80%.

This study supports the hypothesis that radiation dose-related non-tumoral brain changes that are not detected by the neuroradiology imaging assessment can be seen objectively and earlier by radiomic texture analysis. Detecting the sensitivity of individual brain regions towards radiation-induced damage may provide insights into future cognitive-sparing radiotherapy. Radiomics may help detect the group of patients who are more likely to manifest neurotoxicity. The present study did not have useful clinical outcome data e.g. cognitive function, and level of schooling achieved, which was important to relate the radiomic changes to clinical outcomes. Radiomic changes should be correlated with such clinical neurological outcomes in future research.

4.9. Conclusion

Radiomic texture analysis is a promising modality to understand dose and time-related T2 signal changes in the normal parts of the brain in paediatric brain tumour patients. Dose-related signal changes can be detected earlier by texture analysis than by visual inspection by a neuroradiologist. The lack of neurological outcomes data in this study limits the impact of these findings. Future studies should be designed with these considerations since the ability to predict these changes before clinical manifestations may contribute to a better quality of life after radiotherapy.

Chapter 5. Comparison Of Longitudinal MRI Radiomic Texture Features Between Protons And Photon Radiation Therapy In Non-tumoral Regions Of Brain At The Same Dose Levels

5.1. Chapter Overview

This chapter explores the important clinical question pertaining to the main radiotherapy modalities used in the treatment of paediatric patients with primary brain tumours. Photon radiation has been conventionally used for the radiotherapy in these patients. Proton therapy is a comparatively newer and more expensive modality that is increasingly used as it has a lower exit dose and therefore fewer long-term adverse radiation effects [160]. They both are used in the treatment of brain tumours, and NHS patients are selected based on clinical criteria, stage, and prognosis of the tumour [70]. Photon and proton are fundamentally different, in terms of physical characteristics, and the brain may react differently to each type of radiation. This difference in their mode of action and underlying biological process after proton therapy is still unknown and needs to be evaluated [73].

The aim of this chapter is to assess and compare if there are differences in the MRI signal changes between proton and photon therapy following each therapy using radiomic texture analysis. The chapter begins with the brief introduction to each radiotherapy modality and the rational of this part of the study with the need for research. The methodology of texture analysis is the same as the describing in Chapters 3 and 4.

Finally, the results are discussed in the context of related studies from the literature and concluding with the future directions for research.

5.2. Introduction

The late effects of radiotherapy in children have been described in detail in chapter 1. These effects are mainly dependent upon radiation dose, age, tissue volume, and other important organs in the radiation field. Newer radiation therapy known as proton beam therapy (PBT) is being increasingly used due to its dosimetric advantage over conventional photon radiation therapy. However, there are many unanswered questions regarding proton radiotherapy, its radiobiology, and long-term effects on the quality of life. In this chapter, the effects of proton radiotherapy on T2 signal change in the brain are compared with the effects of conventional photon radiotherapy.

5.2.1 Short Introduction to Proton therapy and its advantages over photon therapy

Proton therapy has been discussed in detail in the chapter 1. Proton therapy is the type of radiation therapy where charged proton particles are used. The most important characteristic of protons is their minimal dose deposition at entry and along the path until they reach the target towards end of their path. Maximum energy is deposited at the end of their path which is known as the Bragg Peak [73]. Thus, proton therapy enables better depth distribution over photon therapy with virtually no dose of radiation beyond targeted tissue [75, 161] . This is a major advantage over conventional photon therapy where radiation dose is deposited beyond tumour (Fig. 1.4) irradiating normal tissue surrounding the tumour [70]. Proton beam therapy delivers a reduction in radiation dose to normal tissue and facilitates higher dose delivery to the tumour tissue [77] . This in turn, in theory leads to improved quality of life due to greater local control and sparing of normal tissue. This is advantageous especially in paediatric patients because of their higher susceptibility to the toxic effects of radiation [77]. Several organs are subjected to high radiation doses when craniospinal radiation is administered to children [162] Proton therapy can also be advantageous to deposit large dose of radiation in radioresistant tumours. [64] [73] We have already discussed the arguments against proton therapy in 1.

The proton versus photon debate continues since the introduction of proton therapy. Despite having dosimetric advantages, the radiobiological and clinical benefits of proton therapy still need quality evidence. This study compared the T2 signal changes over 2 years in proton and photon therapy with radiomic texture analysis as a quantitative tool. Textural changes are the quantitative statistical determinants of the pixel values in an MRI image. There are structural changes in irradiated brain

tissues following radiation therapy which present as changes in MRI signal on subsequent scans. These changes may not be visible with the naked eye in early stages of radiation toxicity. Texture feature values are combinations of local intensities with respect to specific location in given ROI. These are objective quantitative measures derived by extraction of collection of statistics of local distribution of grey values in any ROI [163]. Post radiation necrosis can present with varied radiological features and a heterogenous pattern on the MRI scan [164]. Texture analysis can help to identify if there is any pattern of signal change. Comparing texture feature values in these two therapies essentially facilitates comparing the patterns of T2 signal intensities in the given ROI which are secondary to the underlying tissue changes following radiotherapy.

5.2.2 Need for research:

Protons are physically different from photons and there is a need to understand the differences in tissue reactions between the two. At present, the radiobiology of proton beam therapy is still not very clear and needs exploration. As explained in chapter 1, section 1.9, the current RBE of 1.1 with respect to photon is just an approximation and not an absolute [73]. For developing optimal therapeutic strategies, it is essential to understand the difference between radiobiology of the two therapies [75, 160]. Though there are studies suggesting possible differences in the radiobiology of the two therapies, the exact mechanism is yet to be known. Proton radiobiology is likely to be changing depending upon tissue and fraction size [73]. Potential side effects that are more prevalent with proton therapy should be identified and dose dependent tissue changes need to be described. This is more relevant with respect to personalised medicine. More research is required with follow up studies to understand the long-term clinical benefits of proton therapy. Understanding these differences might also help to identify the patients who are more likely to manifest radiation toxicity as a long-term side effect of the therapy.

5.2.3 Hypothesis

We hypothesized that quantitative MRI texture features can potentially be used as surrogates of underlying structural tissue changes. Textural feature values after photon and proton therapy will be different due to the difference in radiobiology of the two therapies. This could be better explored in the non-tumoural brain regions that are inadvertently irradiated along with the tumour. These changes are likely to be comparable at the same dose levels.

5.2.4 Aim of Chapter 5

The aim of this chapter was to compare quantitative T2 MRI textural features in different regions of the brain longitudinally over 24 months in paediatric brain tumour patients treated with photon and proton radiotherapy at the same dose level and to assess if there is any difference in these features.

5.3. Methodology

This is a retrospective comparative analysis aimed to understand the differences in the texture feature values between two therapies at the same dose level. Non-parametric test for comparison – Mann Whitney test is used for statistical analysis. And data was also compared using machine learning methods.

Data collection and image preprocessing have been described in chapters 3 & 4 (pipeline is shown in figure 5.2). Texture analysis was carried out in the same 11 ROIs (MED: Medulla, PON: Pons , ACC: Anterior Corpus Callosum, PCC: Posterior Corpus Callosum, L CS: Left centrum semiovale, R CS : right Centrum semiovale, L Thal: Left Thalamus, R Thal: Right Thalamus, L CER: Left cerebellum, R CER: Right Cerebellum, PTV: Peri-tumoral volume) as previous chapter 4 and texture features were extracted using pyradiomics. To reduce the time and cost of computation 16 primary texture features were selected for comparative analysis, and full details are described in Chapter 4. These features are 10^{th} percentile, 90^{th} percentile, mean, median (MDN), mean absolute deviation (MAD), Contrast (CR), Energy (EG), Entropy (ETR), Kurtosis (KR), Maximum (MAX), Minimum (MIN), Range (RG), Skewness (SK), Total energy (TTE), Uniformity (UNI) and Variance (VR) were selected for comparison.

Figure 5. 1 Methodology to compare radiomic texture features between proton and photon radiotherapy.

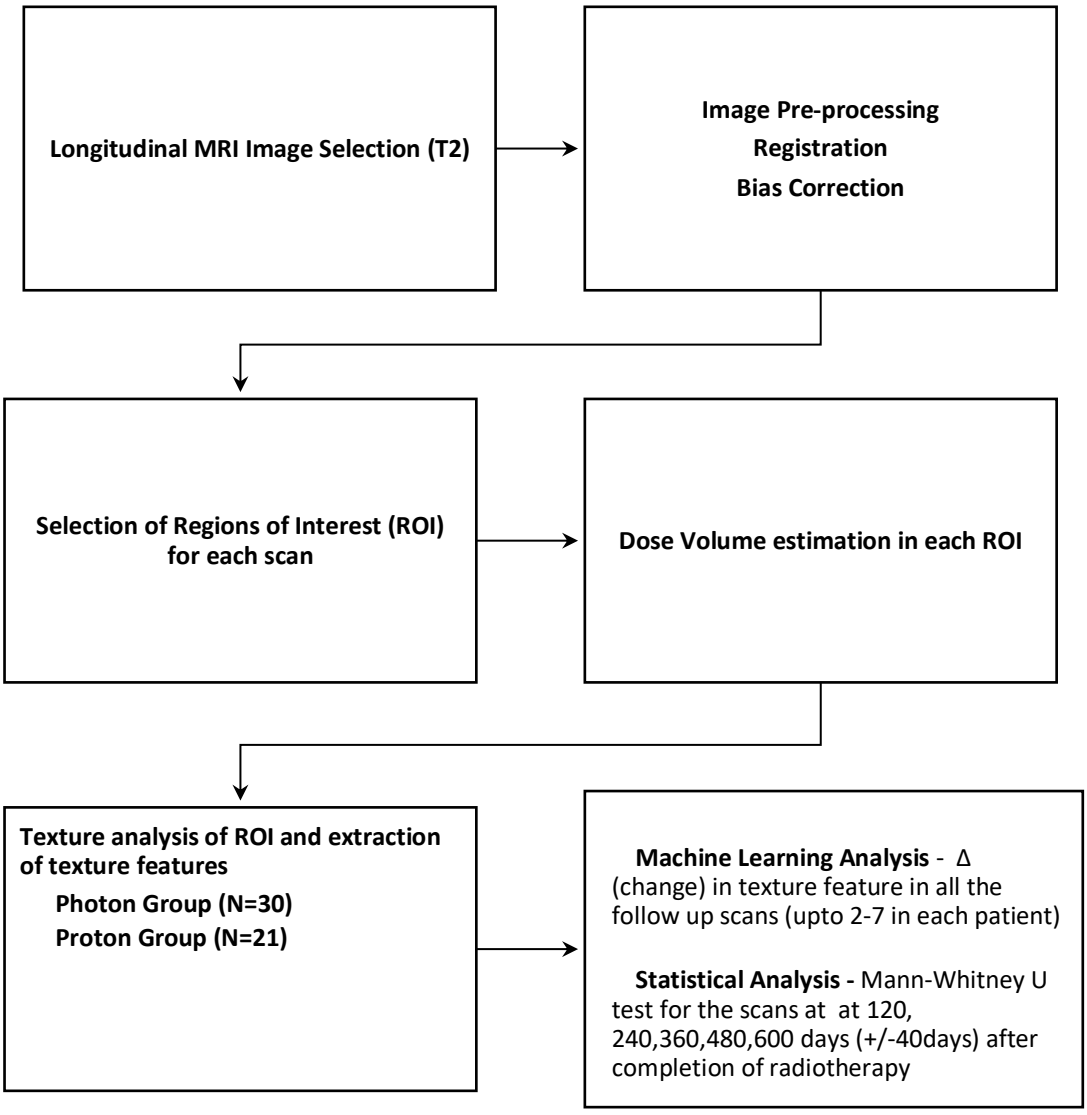

Machine learning and statistical analysis:

Results were analyzed using machine learning techniques to visualize the difference in rate of change of textural feature (Delta Radiomics) and feature value by statistical analysis using SPSS.

Mann-Whitney U test was used to compare primary texture features between proton and photon therapy – all ROIs across the whole brain and each ROI separately at the same dose levels. Man Whitney test is used to compare two groups of independent observations.

5.4. Results

The patient cohort and types of tumours have been described in detail in chapters 2 and 4. The database consisted of 341 patients with primary brain tumours. Of the 105 patients treated with radiation, 51 patients also had a digital radiation planning map available. Out of these 51 patients, one patient (BMS168) had a distorted baseline scan and hence it was not included in the study design. The number of patients treated by photon were 30 while those treated with proton were 20. This was a group of different locations of tumours with Brainstem tumours 4 , Cerebellar tumours 19, Hemispheric cerebral (frontal/temporal/parietal/insular) tumours 7, Supratentorial midline tumours (thalamic /hypothalamic / suprasellar) 10. The number of ROI analysed was 833 for photon (30 patients) and 631 for proton therapy (20 patients).

5.4.i Results – Machine Learning Analysis

Graphs were plotted for data visualization with the help of data exploration app as described in the previous chapter. Figure 5.3 shows TTE values over a period in all patients. While Figure 5.4 shows rate of change of TE at different dose levels.

Figure 5. 2 Showing TTE values in the medulla (MED) region in all patients. X axis represents time. Each colour denotes the value of TTE in each patient. Difference in the spread of TTE values (range) between proton and photon therapy can be noted. Points show wider distribution in the photon therapy.

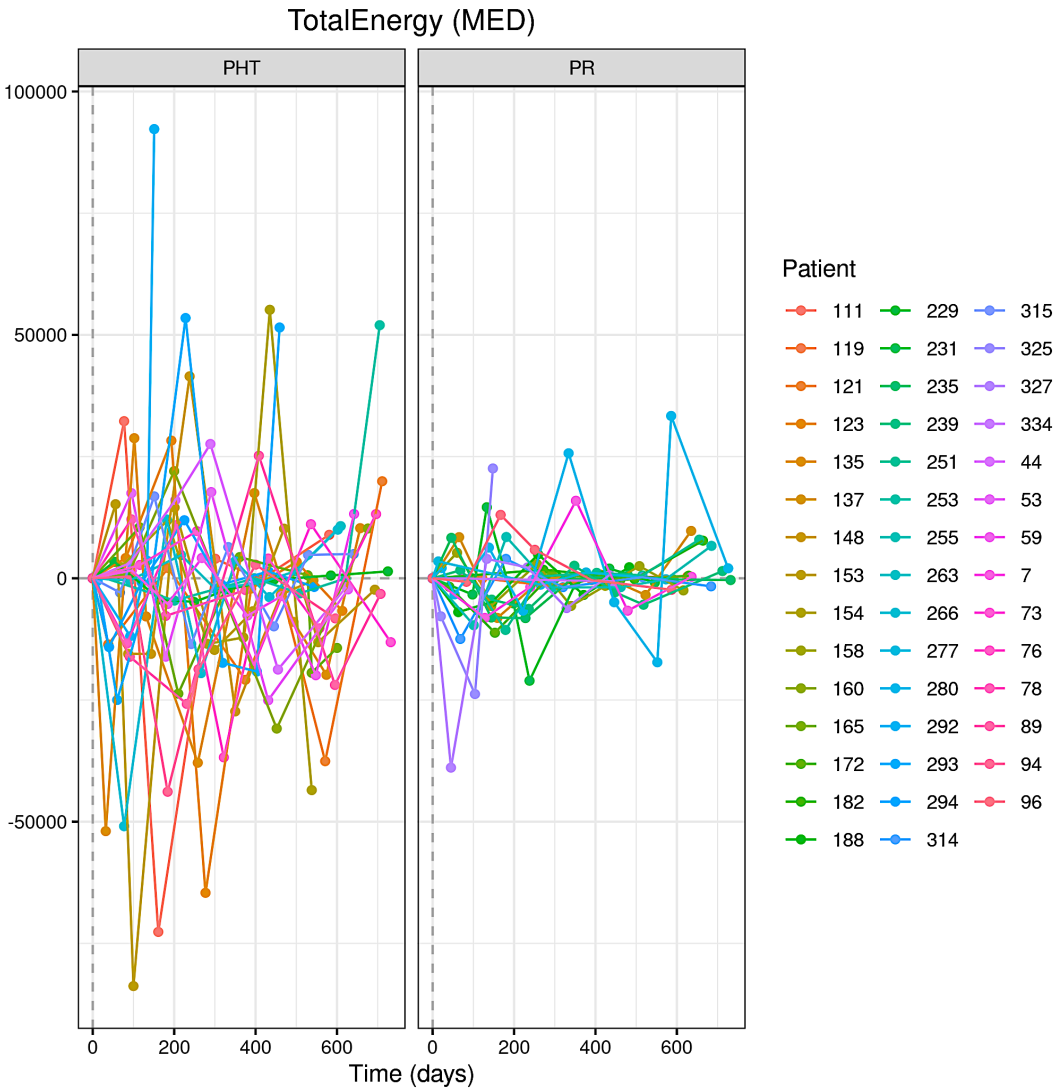

Figure 5. 3 Showing the difference in the rate of change of total energy (Delta Radiomics) over a period of 2 years between proton and photon therapy in the posterior corpus callosum region. Slopes of lines are different between the therapies for each dose group represented by different colour. Difference in the relative slope values between two therapies can be noted. Dots representing value of TTE in each scan are more scattered in photon therapy. Dose line representing dose rage of 30-40 Gy is not seen in the proton therapy graph.

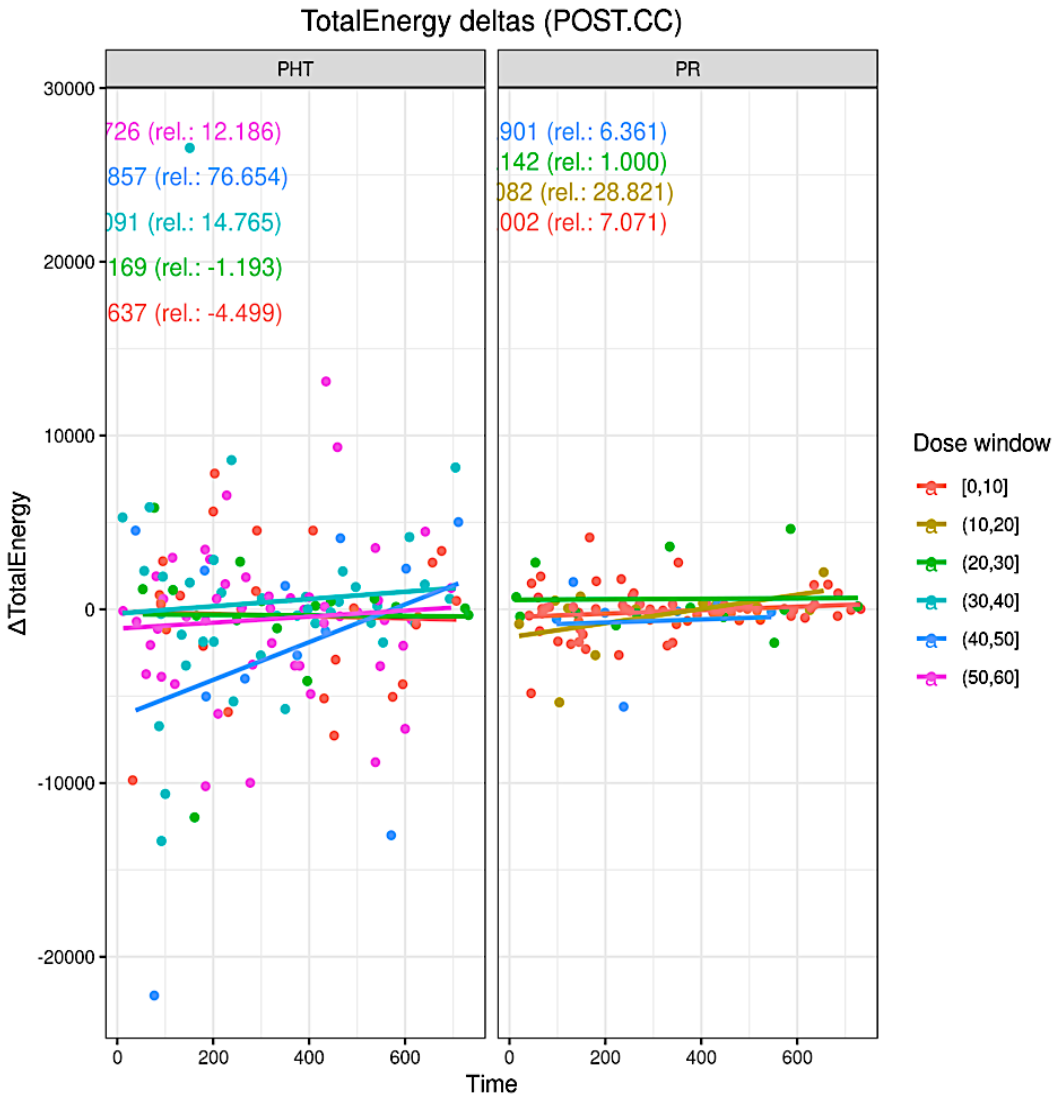

5.4.ii Results: Statistical Analysis:

ROIs across the whole brain (Table 5.1):

When all 11 ROIs were analyzed together, different dose levels showed significant differences in textural features across different therapies at each dose level. Radiation dose distribution was different between the two therapies (fig.5.5). It was found that the number of observations (N) was different in each therapy due to the difference in dose distribution between the proton and photon therapy across the whole brain. Fifteen features showed a significant difference at dose group A & C, 1 feature at B &E, 3 features at dose D and 11 features showed a significant difference at dose F (Table 5.1).

Figure 5. 4 Difference in dose distribution between photon and proton therapy. Dose showed a wider distribution on the left side of the graph while it is more concentrated in proton therapy.

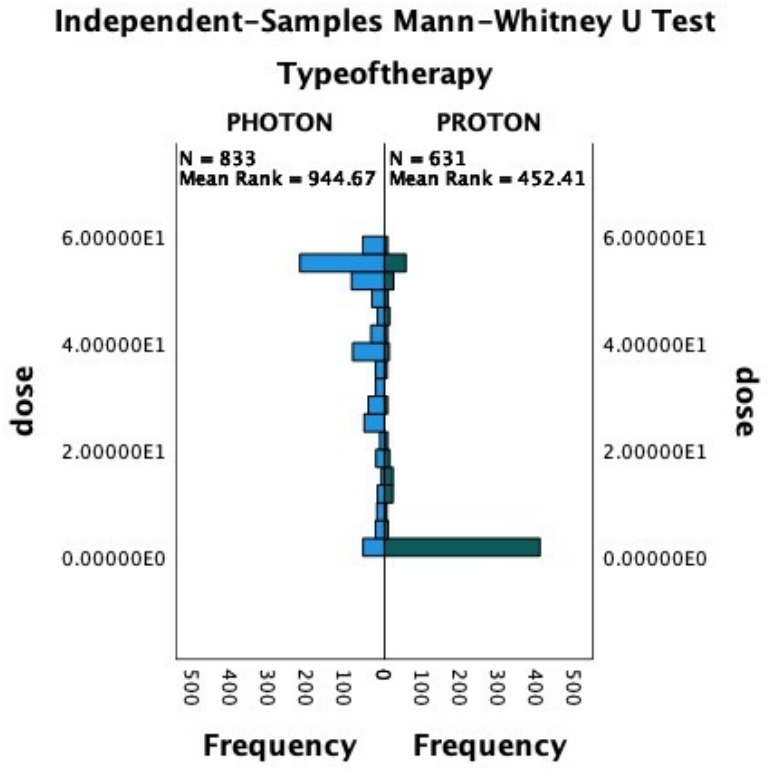

Table 5. 1 Showing N (No. Of observations) and list of features showing significant differences between therapies at each dose level across whole brain over a period of 2 years following radiotherapy

Dose Group	N Total	N Photon	N Proton	Features Showing Significant Difference Between Two Groups
A (0- 10.55Gy)	753	144	609	All 15 features except kurtosis
B (10.56- 20.55Gy)	141	58	83	Only TTE
C (20.56- 30.55Gy)	198	172	26	All 15 except skewness
D (30.56- 40.55Gy)	223	196	27	Energy, skewness, total energy
E (40.56- 50.55Gy)	150	108	42	Only TTE
F (50.56-60.55Gy)	642	514	128	Contrast, Energy, Entropy, Kurtosis, Maximum, MAD, Range, Skewness, TTE, Uniformity, Variance

Figure 5. 5 Graph shows difference in mean frequency of 90% between two therapies at dose group A. Table on right shows the summary of the independent Mann Whitney U Test.

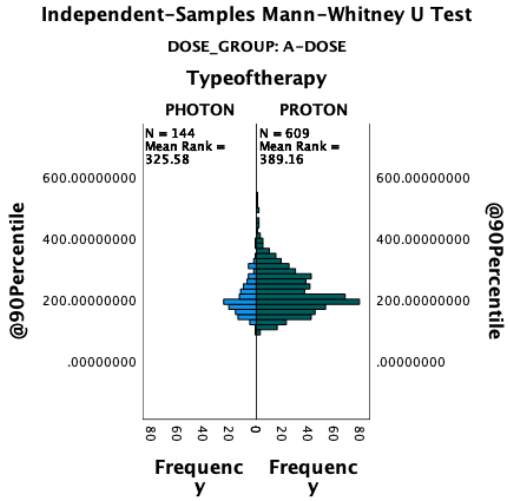

Independent-Samples Mann-Whitney U Test Summary

Total N	753
Mann-Whitney U	48987.500
Wilcoxon W	234732.500
Test Statistic	48987.500
Standard Error	2346.391
Standardized Test Statistic	2.190
Asymptotic Sig.(2-sided test)	.028

Figure 5. 6 Graph shows the difference in mean frequency of entropy between two therapies at dose group F. The table on right shows the summary of the independent Mann-Whitney U Test.

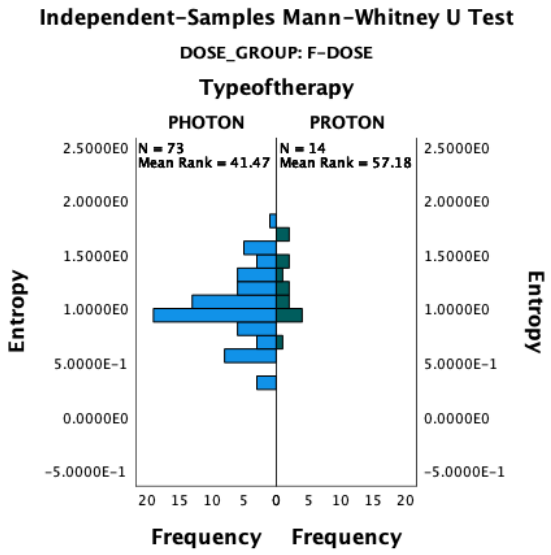

Independent-Samples Mann-Whitney U Test Summary

Total N	87
Mann-Whitney U	695.500
Wilcoxon W	800.500
Test Statistic	695.500
Standard Error	86.526
Standardized Test Statistic	2.132
Asymptotic Sig.(2-sided test)	.033

Table 5. 2 Shows the summary of texture features showing significant differences between Proton (PR) and Photon (PH) therapy at each region of interest at each dose group over a period of 2 years following radiotherapy (All other factors are matched between two groups) [N: No. Of observations over 2yr, DD: Dose Distribution, ND: No Significant Difference, NA: Not Applicable, SF: significant features, Red highlights show groups with similar no of observations in each group, Blue highlights shows groups with min 20 observations in both groups]

DOSE GROUP	**N**	**MED**	**PON**	**ACC**	**PCC**	**L CS**	**R CS**	**L THAL**	**R THAL**	**L CER**	**R CER**	**PTV**
A (0-10.55 Gy)	N PH PR	79 10 69	NA	70 9 61	83 24 59	91 22 69	102 35 67	60 3 57	59 3 56	87 20 67	90 19 71	NA
	Features	TTE	NA	TTE	DD TTE	DD ND	DD SK	DD ND	DD ND	TTE SK	DD MAX, MADTE, RG, VR	NA
B (10.56-20.55 Gy)	N PH PR	19 15 4	11 6 5	NA	NA	16 6 10	21 4 17	18 9 9	23 9 14	7 3 4		NA

	Features	SK TTE	ND	NA	NA	DD TTE	TTE	TTE	MAD TTE	ND		NA
C (20.56 - 30.55 Gy)	N PH PR	NA	10 4 6	NA	21 11 10	NA	NA	13 9 4	NA	19 16 3	13 10 3	NA
	Features	NA	ND	NA	10%, 90% CR, MAX, MEAN , TTE, MDN	NA	NA	DD ND	NA	DD 10% 90%, CR, EG, ETR, MAX, MEAN ,MDN, MIN, UNI	10% 90% EG, MAX, MEAN MAD, MDN, MIN, VR	NA
D (30.56 - 40.55 Gy)	N PH PR	NA	29 15 14	38 35 3	NA	NA	NA	27 20 7	23 20 3	NA	NA	NA
	Features	NA	TTE			NA	NA	DD TTE	TTE	NA	NA	NA

E (40.56 - 50.55 Gy)	N PH PR	NA	23 11 12	26 16 10	12 7 5	NA	NA	26 19 7	28 20 8	NA	NA	NA
	Features	NA	TTE	EG KR, TTE	TE	NA	NA	TTE	TTE	NA	NA	NA
F (50.56 - 60.55 Gy)	N PH PR	64 53 11	87 73 14	20 16 4	NA	9 4 5	NA	NA	51 48 3	80 70 10	69 63 6	169 94 75
	Features	10% KR, MEAN , TTE, MDN, MIN	DD,10 % 90% EG, TTE ETR MAD, MDN, VR	TTE	NA	DD TTE	NA	NA	DD SK TTE	DD TTE	DD, 10% 90%, MAD, TTE,ET R, MIN, MDN, RG VR	DD, CR, MAD, RG (fig5.8), TTE, VR

Figure 5. 7 Simple Boxplot Showing significant difference in the range between therapies at Dose F in PTV region (p<0.005)

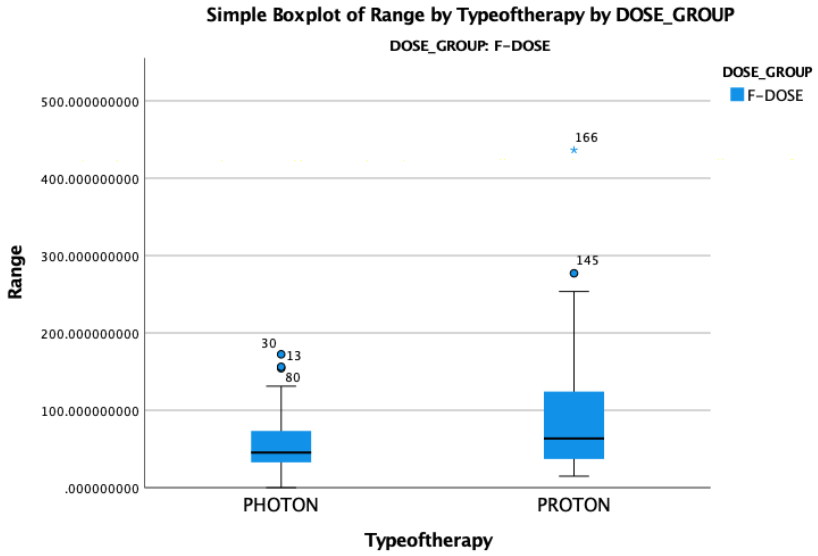

In each ROI (Table 5. 2):

When similar ROI was selected in each scan of the patients, different texture features showed significant difference between the therapies at each ROI. Fig 5.6, 5.7 and 5.9 are graphs showing statistically significant difference at different doses and different ROI's. Table 5.2 gives the details of number of scans analysed in each ROI at each dose level and texture features showing statistical difference between two therapies. Different colour codes were used because of variation in the N value in each column.

5.5 Discussion

Although the number of patients in this chapter was small, follow up scans were used at multiple time points. Further analysis was done after grouping each region on brain by the radiation dose received. N values after this grouping are given in table 5.1 for whole brain and table 5.2 for each ROI.

It is well established that the photon dose is distributed over a larger area and beyond tumour target while the proton dose is more confined in the target tumour region (Bragg Peak). We could clearly see this in our statistical analysis (fig 5.5). In fig 5.4 each dose group is represented by colour, and we see more colours in the graph of photon therapy. This difference was more obvious in the superior regions such as LCS: left centrum semiovale and RCS right centrum semiovale because they were further from PTV as most of the tumours were in the posterior fossa region and less likely to receive radiation dose with protons confirming the difference in distribution. Additional graphs are added in the appendix 3 showing results in each ROI. The dose delivered to the non-tumoral tissue was either close to zero Gy or it was maximum in the case of proton therapy because of the Bragg peak. Dose was widely distributed with photon therapy. The texture feature energy is a measure of magnitude of pixel grey value intensity in each voxel while total energy is the volumetric measure. It is one of the determinants of homogeneity of the MRI image. TTE is highly related with the volume of ROI and changes with change in a volume. Interestingly, the range of values of TTE was also seen to be spread in photon therapy than that of proton therapy (figs. 5.3 & 5.4) when plotted with the machine learning method. Thus, there is difference in change of tissue homogeneity after proton and photon therapy.

When graphs were plotted by machine learning analysis, there was a difference in the rate of change of some texture feature in each ROI at the same dose level (fig.5.4). For example, the rate of change of total energy which is one of the determinants of tissue homogeneity was different between proton and photon therapy over 2 years as denoted by different slopes of lines. This difference in slope of lines could not be tested to determine if this difference is statistically significant due to complexity of the technique and time limitation even though there are visible changes.

Machine learning analysis demonstrated high correspondence of low exposure dose with the proton therapy type. TTE changes were observed to be associated with the high dose of radiation in the regions surrounding PTV. Thus, most of the regions containing the observed changes in TTE are also corresponding to photon therapy type since photon delivers high radiation dose even beyond PTV. In a study performed to compare 2-year cumulative T2 changes following proton and photon therapy in patients with meningioma, it was found that higher rates of T2 changes such as white matter lesions or signal abnormalities were seen in patients with photon therapy [165]. This is consistent with the findings of this study where TE (grey value magnitude) changes or change in tissue homogeneity were more prominent in patients treated with the photon therapy.

It was found that entropy levels which denoted the randomness in pixel value which is the representative of tissue disorder or variability [166] is seen to be higher with photon therapy patients in this study (fig. 5.7). In a study of patients with glioblastoma, it was found that 3- & 6-months brain volume loss after chemoradiation was greater in patients treated with photon therapy than that of proton [95]. This was secondary to the radiation dose delivered to healthy tissue and thus was greater in photon therapy. Thus, tissue irradiated with proton shows lower rate of change entropy meaning smoother or uniform pattern than that of coarse pattern due to high entropy of photon perhaps reflecting a higher tissue change after photon. In a study evaluating application of texture analysis to study small blood vessels showed higher mean entropy and higher white matter hyperintensity in lacunar stroke. [166]

On statistical analysis most of the texture feature values over 2 years following radiotherapy showed significant differences at dose levels A, C and F. TTE was the only feature that showed significant difference between two therapies at dose levels B and D. In the previous part of this study, it was found that TE showed maximum correlation with dose and was found to be the consistent feature showing correlation by both machine learning and statistical analysis in all the ROI's. Total energy is considered as one of the parameters for homogeneity and is less sensitive to changes in scanner manufacturers as reported in previous studies [155] [154] [152]. This was consistent with the study on investigation of MRI based radiomic model where TTE was found to be an important feature to distinguish between lymphoma and squamous cell carcinoma of the sinonasal region [167].In this study machine learning analysis was performed on both primary and secondary texture features. For statistical analysis primary texture features were selected since they are less affected by changes in scanners and scan parameters

. Features that are more related with the image homogeneity such as energy, total energy, 10% and variability such as variance, entropy, uniformity etc,. were selected for the analysis. However, there is no consensus in the literature about selection and usefulness of any specific group of texture features for diagnosis. This could be because radiomic studies are performed in different types of tumours using different modalities such as CT, PET, MRI etc and there is still a paucity of studies to standardise the selection of texture features in paediatric brain tumours. To our knowledge, there is no published radiomic study to evaluate effect of radiation therapy in non-tumoral brain regions.

Each part of brain shows different sensitivity to therapeutic radiation. Cortical areas responsible for higher order cognition show greater susceptibility to post-radiation atrophy [159]. Also, dose received by each brain region was different in each patient and in each therapy. Hence each ROI was also analysed and compared separately. When neuropsychological outcomes after radiotherapy were assessed in adult survivors of paediatric CNS malignancies, the risk of memory impairment was associated with high dose exposure to the temporal region [10]. Radiation dose to the frontal region resulted in greater association of general health and physical performance issues suggesting the importance of targeted delivery of radiation [10]. This is consistent with the findings of the present study where textural features showing a significant difference in different regions of brain were not the same. Table 5.2 shows total N for each region as per dose and therapy received. To make these comparisons more reliable we performed statistical analysis separately in each region of brain at the same dose level. As mentioned before N values differ in each group. Table 5.2 summarises the features showing significant difference between two therapies as different dose groups. Similar analysis was performed by addition subgrouping with time, but N values were very small and helps results were excluded from further consideration.

In some columns of table 5.2, no texture feature showed significant difference between therapies e.g., dose group A for L CS, L thalamus and R thalamus. These regions had received a larger dose with photon therapy and hence N was extremely low than that of proton therapy. In contrast, N was lower for proton therapy in dose groups B, C, D, and E. Some comparisons could not be performed in these dose groups due to the absence of proton data. This again highlights the difference in dose distribution between two therapies.

It was observed that in high dose groups such as D, E and F where N was comparable in proton and photon therapy e.g., Pons D groups (PH 15, PR 14), E group (PH 11, PR 12), PCC E group (PH 7, PR 5) and

LCS F group (PH 4 PR 5); TTE was the feature showing significant difference between these two groups. This is again consistent with the previous findings of this study.

Analysis was also carried out at the PTV region where maximum dose (Dose F) is delivered in both the therapies and the proton Bragg peak is located. However, the location of this region was different based upon anatomical position of the tumour. As mentioned before this region was selected more pragmatically in the visually homogenous brain tissue region where ROI was drawn according to the radiation dose maps. Contrast, mean absolute deviation, variance, range, and total energy were the features that showed a significant difference between the two therapies at dose F. Fig 5.8 shows the simple box plot of the difference in range values at PTV at dose level F. All these features are representative of variation or heterogeneity of pixel intensities in ROI. Thus, at maximum radiation dose (Dose F) MR signal changes over 2-year period differ between two therapies. Such difference in one or more texture features were observed at each dose level in different ROI's. This could possibly point towards difference in tissue response after irradiation with each therapy at different dose levels.

Lack of knowledge on radiobiology after proton therapy prevents use of this therapy to its full potential. Specific biomarkers expressing underlying tissue changes and pathophysiology when found will help to select patients who will benefit most from this therapy [168]. Radiomic texture features if established and supported by further good quality evidence-based studies may serve as these potential biomarkers for patient selection enhancing the benefits of both therapies based upon individual patient needs.

5.6 Limitations, Clinical Relevance and Future Scope

It is important to note that number of patients treated with photons or protons was not balanced in this study. However, the values were averaged while performing Man Whitney U test reducing the effect of this unequal grouping.

While assessing the toxic effects after radiation therapy, concurrent chemotherapy plays important role. This simultaneous use of chemotherapy and surgery along with other clinical factors such as diagnosis and anatomical location of tumour were the confounding factors of this study which were not considered in the analysis.

MRI scan data was collected about over a period of 20 years from different local and international centres. The variety of machines could have an impact on the texture analysis, however additional pre-processing steps such as filtration and bias correction methods were used to mitigate this effect.

Further investigation is needed to understand the difference in textural features between proton and photon therapy and to determine whether advanced machine learning algorithms could contribute to validate the results.

In this study, several features showed significant difference between the two therapies. Clinico-radiological correlation of these changes in future studies will bring clinical meaning to the values and changes in each texture feature. Correlating these findings with neuropsychological outcome measures in a larger prospective dataset will improve the reliability of these preliminary results. Such correlation will help to resolve the uncertainties regarding the radiobiology of proton therapy and might help to answer the questions on long term quality of life and give rationale for therapy selection in each individual patient.

5.7 Conclusion

Quantitative image analysis of normal brain in paediatric patients treated with different radiotherapy modalities is relatively unexplored and needs further research to detect pathological changes at earlier stages of follow up. The results of this study showed that there are statistically significant differences in some of the primary textural feature values at the same dose levels between proton and photon therapy. These differences could be potentially representing different underlying biological/structural tissue changes at the same dose levels following different types of radiation therapies. Understanding the difference in the radiobiology of each therapy can help to select personalised therapy suitable for a particular patient.

In this study we used T2 weighted imaging that is a part of routine brain tumour imaging protocols, and this texture analysis methodology can be applied to a wider paediatric population and does not need the use of advance imaging techniques that are often challenging in children.

To our knowledge this is the first radiomic study to demonstrate the differences in changes to normal brain following proton and photon radiation therapies. Further research is needed to validate these findings in a larger dataset and to understand the long-term effects of these therapies and potentially enable early prediction of these imaging changes.

Chapter 6 : Radiomic Textural Analysis Of Non-Tumoral Brain Regions In Paediatric Medulloblastoma Following Radiotherapy

6.1. Chapter Overview

Paediatric patients with medulloblastoma suffer from lifelong consequences because of the side effects of cancer therapies. This chapter explores the essential clinical questions regarding the treatment-related side effects in paediatric patients with medulloblastoma.

The chapter begins with an introduction and the need for research. In this part of the study, the radiomic textural features have been compared in post-treatment T2 follow up MRI scans in patients with and without 21 months and 5-year cerebellar T2 progressive signal abnormality.

The methodology for qualitative and quantitative analysis has been described, followed by the results and discussion with the evidence from the related studies in the literature and conclusion with the future directions for research.

6.2. Introduction

Medulloblastoma is the most common malignant brain tumour in children [169].Medulloblastomas arise in the cerebellum and are prone to disseminate throughout the central nervous system (CNS). Histopathological and imaging characteristics of medulloblastoma have been described in Chapter 1, table 1.3. Treatment consists of surgical resection, radiotherapy to the craniospinal axis (CSA) with a boost (additional dose) to the tumour bed and multiagent chemotherapy. The prescribed dose of craniospinal radiation standard-risk MB is 23.4 Gy and in high-risk MB is 35-40Gy plus a boost up to a total dose of 54-55.8Gy with concurrent and adjuvant chemotherapy [170]. Five-year survival for standard risk, non-metastatic medulloblastoma is currently 70-80%. Possible targeted chemotherapeutic agents are Trichostatin A for WNT, Vismodegib, arsenic trioxide, Bromdomain inhibitors, for SHH, and Bromodomain inhibitors, HDAC inhibitors, for Group 3MB. Prognosis is dependent upon the molecular classification group and survival varies from 55.8%(Group 3 β to 100% (WNT β) [29] (table 1.3).

Radiotherapy plays a vital role in the treatment of patients with brain tumours, however, when radiotherapy is delivered to the tumour, the surrounding non-tumoral brain regions also inevitably get irradiated. Although the dose to the non-tumoral brain region is generally lower, it can affect cognitive abilities, IQ, memory, sleep and other brain functions[171]. All patients treated for medulloblastoma suffer from the side effects of these therapies to some extent and up to 33% of patients suffer from severe neurotoxicity due to these anticancer therapies [172]. As described in previous chapters, this often results in severe lifelong neurocognitive deficits, which significantly and adversely impact their quality of life [173, 174].

Post-treatment white matter lesions and potential clinical implications:

The effect of radiotherapy on the white matter has been explained in Chapter 3 section 3.2.3 for ROI selection and analysis. Patients treated for brain tumours often develop white matter lesions in the peritumoral and other areas of the brain. These lesions may cause transient signal abnormalities visible on T1 and T2 MRI sequences [137]. They may represent demyelination or oedema [138]. Acute brain injury due to RT generally does not show early changes on MRI. Radiotherapy and chemotherapy cause

T2 hyperintense areas and new enhancement patterns as early delayed effects within six months. These lesions are known as pseudoprogression [139]. These lesions are more common in adult glioblastoma patients but may be seen in pediatric gliomas [140].

Late, delayed reaction to the RT can be vascular or parenchymal. Vascular injury can manifest as progressive cerebral arteriopathy leading to narrowing of blood vessels. This may be associated with Moya Moya disease. Radiotherapy induced capillary telangiectasis and cavernous malformations manifest as T2 hypo intensities on MRI[172]. Periventricular T2 hyperintensity in the white matter is seen because of parenchymal injury, also known as leukoencephalopathy or diffuse radiation injury [137, 172].

Transient focal T2 hyperintense and enhancing lesions are seen in the cerebellum, posterior cerebral hemisphere and pons with a snowflake or curvilinear appearance [172]. One uncommon, delayed complication associated with unilateral T2/FLAIR hyperintensities is seen in the temporal, occipital or parietal lobe. These patients present with stroke-like migraine attacks [175].

Chemotherapeutic agents (such as methotrexate) may lead to acute or chronic encephalopathy. This is seen as bilateral periventricular and subcortical T2/FLAIR hyperintensity of white matter with no contrast enhancement [172]. Symmetric subcortical T2 hyperintensities are seen in the occipital and parietal lobe due to posterior reversible encephalopathy syndrome [176]

In one prospective study to understand the effects of white matter lesions on 134 paediatric patients after craniospinal irradiation and conformal boost to the tumour bed, followed by four high-dose chemotherapy and associated neurocognitive symptoms, it was found that patients with white matter lesions showed a greater neurocognitive decline and poorer maths scores [137]. MRI monitoring is performed to check for recurrence. However, suggests the need for more monitoring of the patients who present with lesions on the follow-up MRI than those who do not offer these hyperintensities in the brain.

The cerebellum has a definite role in higher cognitive function. Radiation toxicity in the posterior fossa region or cerebellum is associated with disturbances of verbal memory, attention, learning and visual-spatial functions **[137]**.

Need for research:

Although some neurocognitive deficits are related to hippocampal and other irradiation during the CSA phase of radiotherapy treatment, the cerebellum also plays a vital role in higher cognitive function [177]. Damage to cerebellar white matter is observed as T2 hyperintensity on serial MRIs performed following treatment for medulloblastoma, and these white matter lesions have been demonstrated to correlate with more severe neurocognitive deficits[137, 178]. These changes are thought to result from radiation toxicity, possibly compounded by chemotherapy. They are not widely reported in the literature, are often transient, are challenging to diagnose accurately and may mimic tumour[149] [137]. The underlying biological cause is unknown. The routine qualitative radiological analysis is subjective and suffers from the human eye's limitations, which may not identify early changes and distinguish between treatment-related imaging changes and tumour recurrence in some instances. An objective quantitative assessment may facilitate a more accurate and earlier identification of these lesions, although currently, there are no practical interventions to prevent these changes.

Radiomics may have the potential to predict these changes earlier so that strategies can be designed for patients who are more likely to manifest such abnormalities in the future.

Hypothesis

We hypothesised that quantitative MRI texture features could be used as surrogates of underlying tissue changes. There is a difference between cerebellar changes in patients who show progressive T2 signal abnormality and those who do not develop these changes after 21 months and 5-years following radiation. These changes are subtle at the early stages, making them difficult to identify with the routine qualitative radiological examination due to the human eye's limitations. However, quantitative texture analysis can potentially identify subtle changes in MRI images. There will be a difference in the textural features in patients with and without post-radiation T2 cerebellar hyperintensity 21 months and 5 years after radiation in patients treated for medulloblastoma.

Aim

To determine if the 21-month radiomic texture features can differentiate those patients with medulloblastoma who develop T2 progressive signal change (PSC) in the cerebellar on qualitative

analysis at 21 months and 5 years, compared to those who do not. Also, to determine the diagnostic ability of radiomic textural features in differentiating groups with/without qualitative signal changes.

6.3. Methodology

The rationale for focusing on the medulloblastoma patients and the qualitative features is that they comprised the largest single group of patients. In this study, we chose the most homogenous tumour group for a more detailed analysis and comparison of radiomics with qualitative features. This is a retrospective review of nine paediatric patients (total 78 scans) with medulloblastoma treated with surgery, radiotherapy, and chemotherapy. A schematic representation of the methodology is shown in fig 6.1. The previous chapters have described the data collection and image preprocessing pipeline (Chapters 2 and 3).

Figure 6. 1 Patient inclusion/ exclusion flow chart

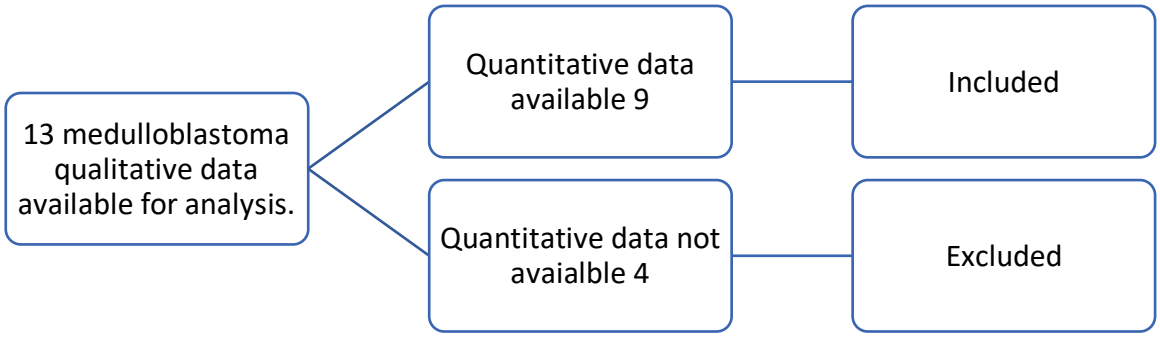

This is a comparative analysis where brain changes were noted, and groups were formed based on qualitative analysis. Here qualitative analysis by an expert neuroradiologist was considered a primary criterion and standardization to decide a group. Later quantitative features between groups with and without changes were compared to see if there is any difference between the two groups. Later

Receiver operating characteristic (ROC) curve was plotted to determine the diagnostic accuracy of this binary classification.

Qualitative Analysis:

An experienced Paediatric Neuroradiologist (SA) qualitatively analysed 21 months- and five-year follow-up MRIs based on the preoperative, postoperative, and one-year follow-up scans. The T2 scans were evaluated for the presence or absence of progressive T2 signal hyperintensity and volume loss in different brain regions, including the pons, medulla, cerebellum, thalamus, corpus callosum and centrum semiovale. Figure 6.2 shows these changes. A score from 0-4 was given depending upon hyperintensity progression and volume loss (Table 6.1) at 21 months and five years after radiotherapy. (Scoring: 0, none, 1. present, 2. stable since previous, 3. progression since previous, 4. reductions since previous).

Most of the patients showed these changes only in the cerebellum region. Hence values from the cerebellum region were considered for further analysis. Patient BMS 284, 292, 168 and 90 were not included in the final analysis due to the absence of quantitative data.

After scoring, these patients were grouped into two categories (Table 6.2) based on the presence or absence of 21 months - and five-year progressive signal abnormality (PSC) in the cerebellum. These groups were used for statistical analysis and comparison with quantitative analysis.

Quantitative Radiomic Texture Analysis:

The pipeline for texture analysis is stated in Figure 5.3 of the previous chapter. After completing image preprocessing (registration and bias correction), 5mm diameter circular ROIs were drawn (Fig 6.4) at the right & left cerebellar white matter on the visibly normal-appearing homogenous regions of the cerebellar white matter on all the follow- -up T2 scans over 21 months. Areas with signal abnormality were avoided in the baseline scan while placing these ROIs. The same region was selected in all the follow-up scans after registration with the baseline scan. The radiation dose was calculated in all these 78 ROIs and was 50-60Gy. Texture analysis was performed. Sixteen primary textural features (contrast, energy, entropy, kurtosis, maximum, mean, mean absolute deviation, median, minimum, range, skewness, total energy, uniformity, variance, 10%, 90%) were extracted.

Texture feature values were compared separately between groups with or without qualitative changes (PSC) at 21 months and 5-year follow-ups. Feature values between the 21 months groups were compared with Mann Whitney U test at different time points: Baseline, A, B, C, D, E and cumulatively all the time points together as described in table 6.4 & table 6.5. Receiver Operator Characteristic Curve (ROC) analysis was carried out to determine the diagnostic performance of the radiomic features to distinguish between patients with PSC at 2 and 5 years.

Figure 6. 2 Schematic representation of the methodology

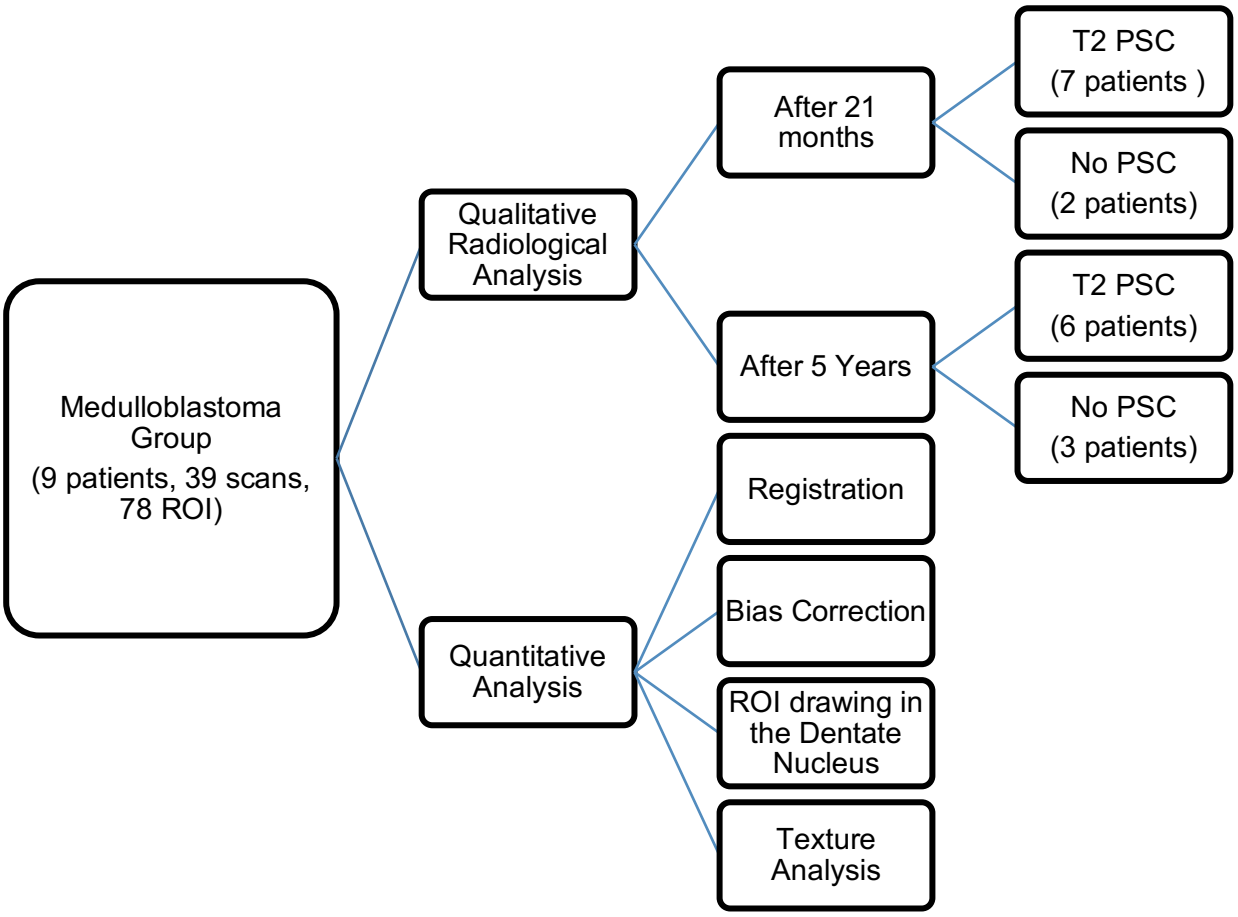

6.4. Results:

6.7.1. Qualitative analysis:

After 21 months seven patients qualitatively showed PSC and two did not. At five years, six patients qualitatively showed PSC compared to the 21 months scan, while three did not (Table 6.3).

6.7.2. Comparison of textural feature values in PSC / non-PSC groups at each time point:

When different time points after radiation were analysed, various texture features significantly differed between the two groups (Tables 6.4 and 6.5). There was no significant difference in feature values at time points C and E in the 21 months PSC group and at time points B, C and E in the 5-year PSC group. The graph on the left in Figure 6.5 shows the difference in the '10 percentile' value between groups at different time points.

6.7.3. Comparison of textural feature values in PSC / non-PSC groups cumulatively at all time points together:

When textural features were compared by Mann Whitney test at all time points together, a statistically significant difference ($p<0.05$) was shown by all 16 primary textural features (contrast, energy, entropy, kurtosis, maximum, mean, mean absolute deviation, median, minimum, range, skewness, total energy, uniformity, variance, 10%, 90%) between the 21 monthswith and without PSC group. While in the 5-year with and without PSC group, a difference was shown by 15 features except for kurtosis when analysed cumulatively at all time points together. The results are shown in tables 6.4, 6.5 and Figure 6.4. Figure 6.5 (right side) shows the differences in the feature – "10 percentile" values between the two groups.

6.7.4. Results of ROC and AUC:

In the 21 monthsgroups, results of ROC analysis showed that nine texture features had an area under the curve (AUC) >0.7 (Figure 6.6, Table 6.6). In the 5-year PSC group, 12 features showed AUC >0.7 (Figure 6.7, Table 6.7). For both groups, only two features (Skewness and Uniformity) showed AUC <0.5.

Table 6.1. Scores of hyperintensity by qualitative analysis in different brain regions Scoring: 0, none, 1. present, 2. stable since previous, 3. progression since previous, 4. reductions since previous.

	Hyperintensity												Volume Loss					
Bms	Pons			Medulla			Cerebellum			Centrum Semiovale			Cerebellum			Centrum Semiovale		
YEAR	**1**	**2**	**5**	**1**	**2**	**5**	**1**	**2**	**5**	**1**	**2**	**5**	**1**	**2**	**5**	**1**	**2**	**5**
153	0	0	0	0	0	0	1	3	3	0	0	1	0	0	1	0	0	1
165	0	0	0	0	0	0	0	1	3	0	0	0	1	2	2	0	0	1
284	0	0	0	0	0	0	1	2		0	0		1	2		0	0	
315	0	0	0	0	0	0	1	2	3	0	0	0	1	2	2	0	0	0
76	0	0	0	0	0	0	1	3	3	0	0	0	1	3	2	0	0	0
266	0	0	0	0	0	0	0	0	0	0	0	0	1	2	2	0	0	0
90	0	0	0	0	0	0	1	3	2	0	0	0	1	2	2	0	0	0
253	0	0	0	1	2	4	1	2	3	1	4	0	1	3	2	1	2	2
294	0	0	0	0	0	0	1	2	2	0	0	0	1	2	2	0	0	0
292	1			0			1			0			0			0		
121	0	0	0	0	0	0	1	2	3	0	0	0	1	2	2	0	0	0
263	0	0	0	0	0	0	0	0	0	0	0	0	1	0	0	0	0	0
168	0	0	0	0	2	2	1	2	3	0	0	0	1	3	2	0	0	0

Table 6. 2 Showing grouping of *patients* by presence or absence of PSC

Patient	**121**	**153**	**165**	**253**	**263**	**266**	**294***	**315**	**76**
21 months PSC	YES	YES	YES	YES	NO	NO	YES	YES	YES
5 YEAR PSC	YES	YES	YES	YES	NO	NO	NO	YES	YES

*In patient 294, there was PSC at 21 months while it was stable at 5 years qualitative analysis.

Figure 6.3. T2 scan showing a qualitative increase in cerebellar hyperintensity on successive scans (153AT2 – baseline, 153FT2 393 days post-irradiation, 153IT2 – 693 days post-radiation approx. two years and 153w- five years post-radiation)

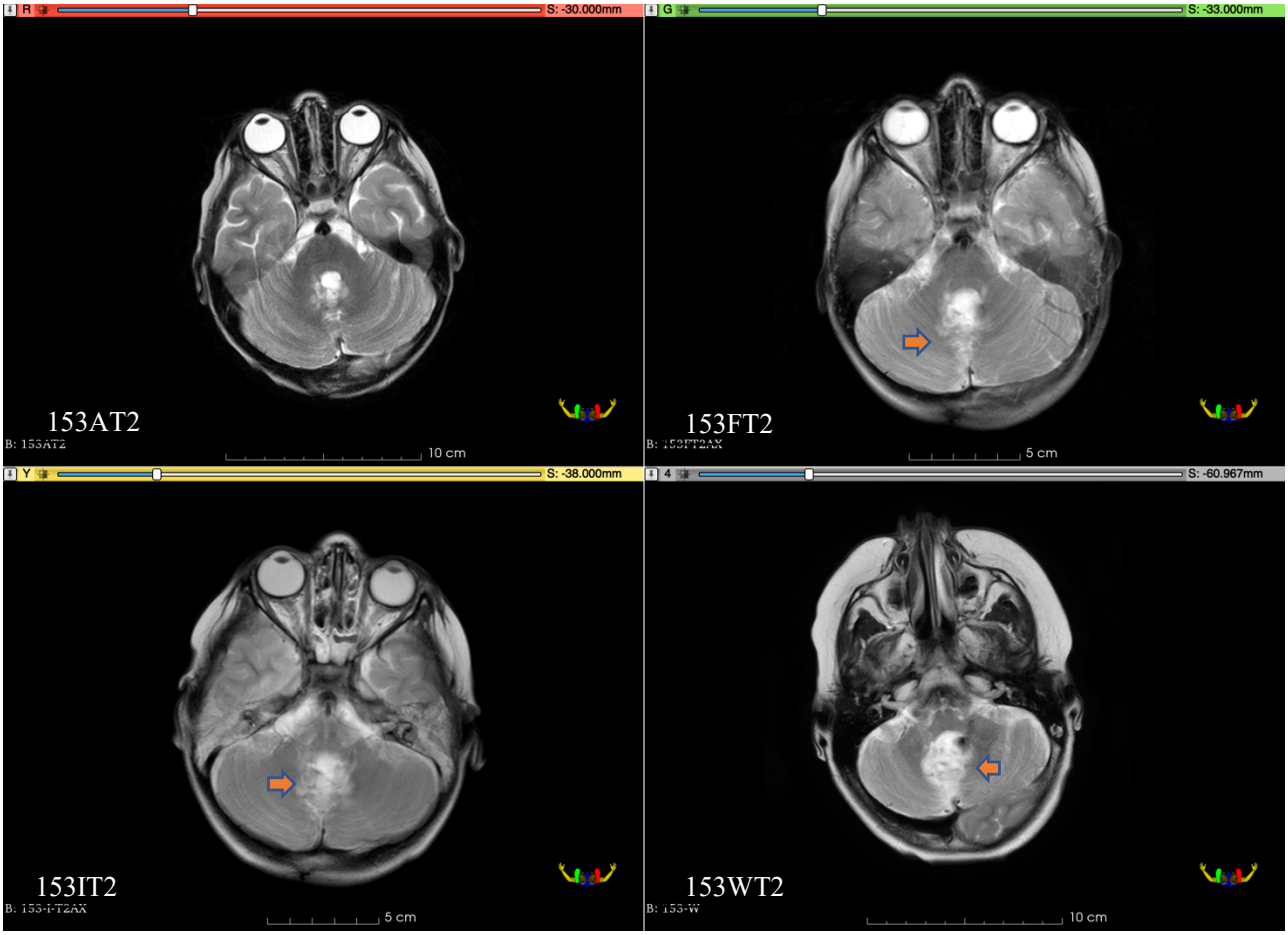

Figure 6.4. Axial and Coronal T2 scans showing ROIs in the cerebellar white matter of right and left cerebellum

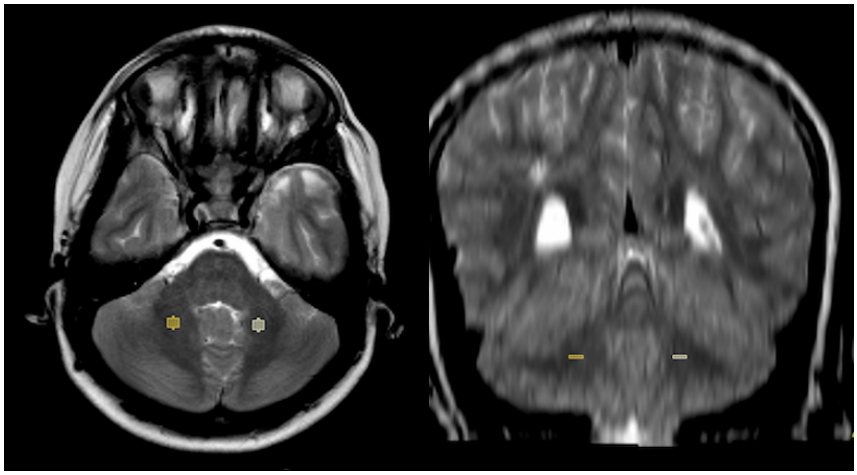

Table 6. 3 Results for the group at 21 months showing qualitative progressive signal change. Nunber of ROIs are dependent upon the presence or absence of a follow-up scan at each time point.

Time Point	Total No. Of ROIs (N)	No PSC (No. Of ROIs)	PSC Present (No. Of ROIs)	Features Showing Significant Difference Between Two Groups
Baseline (Last T2 (axial) scan in the system after the surgery and before the date of initiation of radiotherapy was selected as a baseline scan)	18	4	14	Skewness
Time A (120 +/- 40 Days)	12	2	10	Maximum, Energy, 10percentile, 90percentile , Mean, Median, Minimum
Time B (240 +/- 40 Days)	14	4	12	Maximum, Energy, 10percentile, 90percentile , Mean, Median, Minimum, Total Energy, Range
Time C (360 +/- 40 Days)	12	2	10	No Difference
Time D (480 +/- 40 Days)	10	2	8	Maximum, Energy, 10percentile, 90percentile, mean, median, skewness, total energy
Time E (600 +/- 40 Days)	10	4	6	No Difference
Overall Cumulative At All-Time Points	78	18	60	All 16 primary textural features

Table 6. 4 Results table showing the group 5-year qualitative Progressive Signal Change. No of ROIs are dependent upon the presence or absence of a follow-up scan at each time point.

Time Point	**Total No Of ROIs (N)**	**No PSC (No. Of ROIs)**	**PSC Present (No Of ROIs)**	**Features Showing Significant Difference Between Two Groups**
Baseline (Last T2 (axial) scan in the system after the surgery and before the date of initiation of radiotherapy was selected as a baseline scan**)**	18	6	12	Kurtosis, Mean Absolute Deviation
Time A (120 +/- 40 days)	12	4	8	Maximum, Energy, 10percentile, 90percentile, Mean, Median, Minimum, Total Energy, Range, Mean Absolute Deviation, Entropy, Uniformity, Variance
Time B (240 +/- 40 days)	16	6	10	No Difference
Time C (360 +/- 40 days)	12	2	10	No Difference
Time D (480 +/- 40 days)	10	2	8	Maximum, Energy, 10percentile, 90percentile, Mean, Median, Total Energy
Time E (600 +/- 40 days)	10	4	6	No Difference
Overall cumulative at all time points	78	24	54	15 primary textural features except Kurtosis

Figure 6.5. Categorisation and overall cumulative quantitative analysis results at all time points at 21 monthsand 5-year.

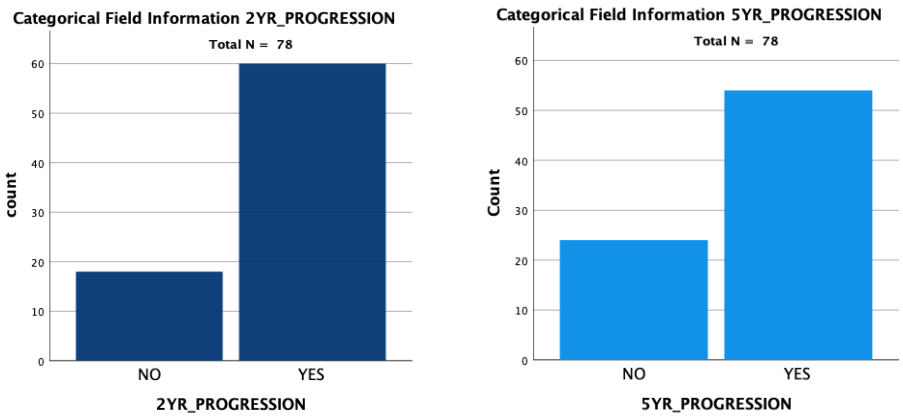

Figure 6.6. Boxplot showing significant differences in the feature '10 percentile' between 21 months and 5-year with and without qualitative PSC groups when analysed at different time points (left side) and when analysed cumulatively over two and five years (right).

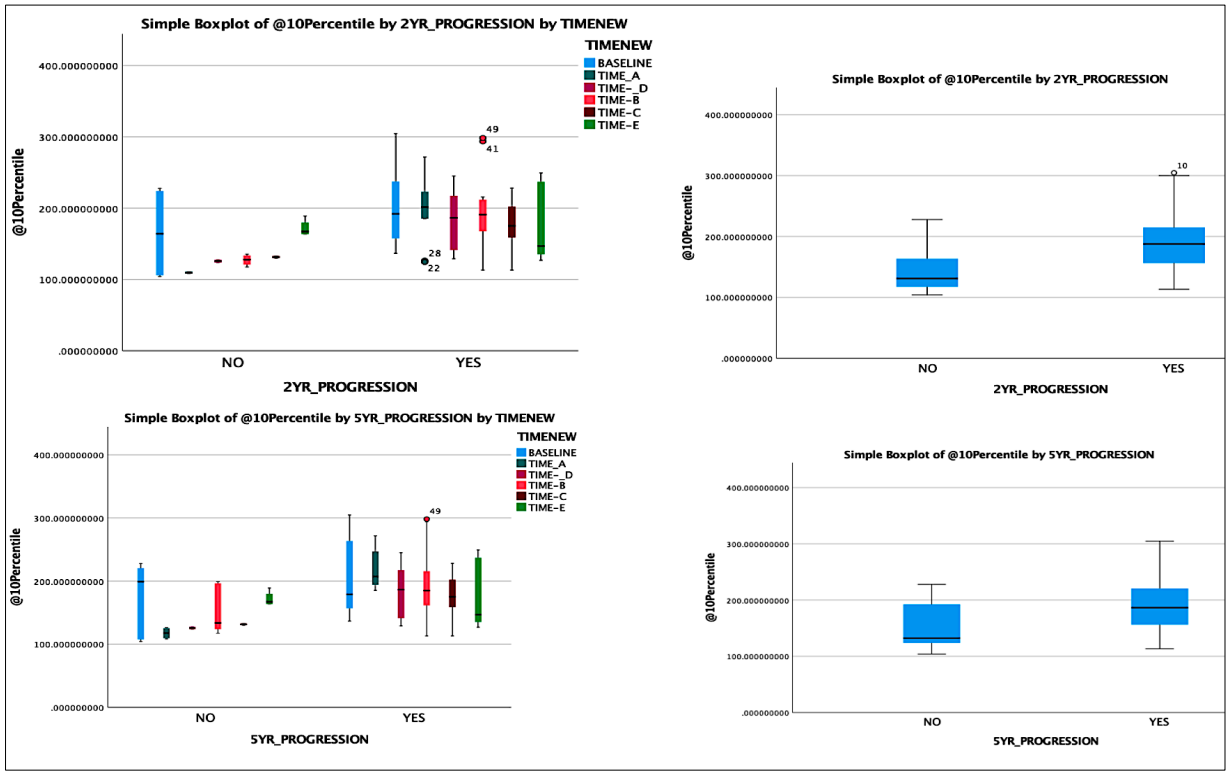

Figure 6.7. ROC curve for 21 months qualitative PSC group

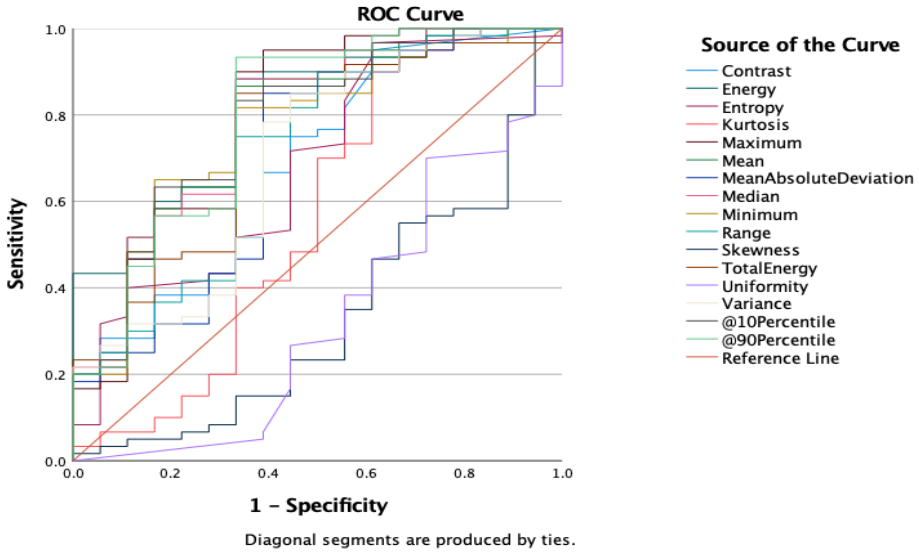

Table 6.5. AUC table for 21 month squalitative PSC group

Area Under the Curve

Test Result Variable(s)	Area	Std. Error[a]	Asymptotic Sig.[b]	Asymptotic 95% Confidence Interval	
				Lower Bound	Upper Bound
Contrast	.686	.074	.017	.540	.832
Energy	.810	.056	.000	.700	.920
Entropy	.682	.075	.020	.535	.829
Kurtosis	.556	.091	.477	.377	.734
Maximum	.794	.070	.000	.657	.930
Mean	.787	.066	.000	.658	.916
MeanAbsoluteDeviation	.694	.079	.013	.540	.848
Median	.788	.066	.000	.659	.917
Minimum	.766	.065	.001	.638	.893
Range	.716	.074	.006	.570	.861
Skewness	.331	.076	.031	.183	.480
TotalEnergy	.740	.070	.002	.603	.877
Uniformity	.331	.078	.030	.178	.484
Variance	.696	.076	.012	.547	.846
@10Percentile	.781	.065	.000	.654	.909
@90Percentile	.792	.068	.000	.658	.926

The test result variable(s): Contrast, Entropy, Uniformity has at least one tie between the positive actual state group and the negative actual state group. Statistics may be biased.

a. Under the nonparametric assumption

b. Null hypothesis: true area = 0.5

Figure 6.8. ROC curve for 5-Year qualitative PSC group

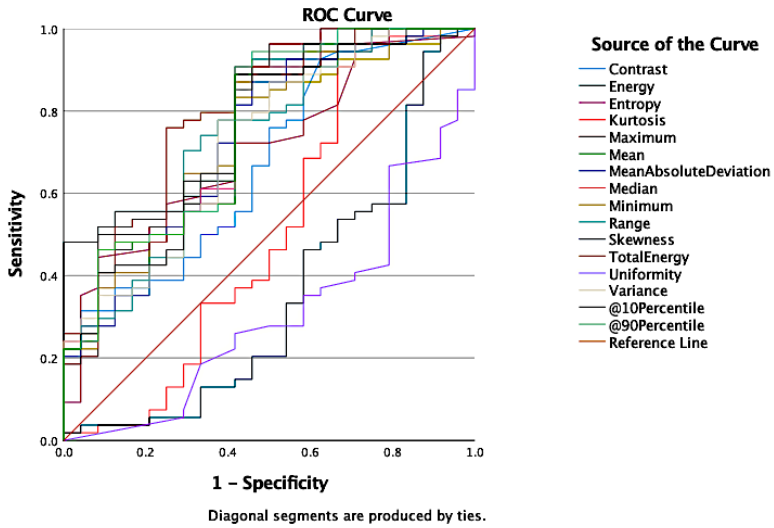

Table 6.7. Table showing AUC for 5-year qualitative PSC group.

Area Under the Curve

Test Result Variable(s)	Area	Std. Error[a]	Asymptotic Sig.[b]	Asymptotic 95% Confidence Interval	
				Lower Bound	Upper Bound
Contrast	.673	.066	.015	.544	.803
Energy	.796	.053	.000	.692	.899
Entropy	.703	.062	.004	.582	.824
Kurtosis	.504	.082	.957	.343	.664
Maximum	.764	.062	.000	.643	.885
Mean	.752	.061	.000	.633	.871
MeanAbsoluteDeviation	.728	.064	.001	.603	.853
Median	.752	.061	.000	.633	.871
Minimum	.725	.062	.002	.603	.846
Range	.728	.063	.001	.605	.852
Skewness	.350	.073	.036	.206	.494
TotalEnergy	.793	.056	.000	.684	.903
Uniformity	.309	.064	.007	.184	.434
Variance	.723	.063	.002	.599	.847
@10Percentile	.740	.062	.001	.619	.861
@90Percentile	.759	.062	.000	.638	.880

The test result variable(s): Contrast, Entropy, Uniformity has at least one tie between the positive actual state group and the negative actual state group. Statistics may be biased.

a. Under the nonparametric assumption

b. Null hypothesis: true area = 0.5

6.5. Discussion

To the best of our knowledge, this is the first radiomic study to assess post-treatment changes qualitatively and with radiomic quantitative analysis in paediatric patients with medulloblastoma. ROIs were placed in the visibly normal-appearing parts of the cerebellum to remove the bias and increase the reliability .

The qualitative radiological analysis is the usual way of assessing radiological images. Radiologists examine MRI scans for changes in different brain regions and compare them with subsequent serial follow-up scans. However, a qualitative assessment is generally subjective. In the present study, the cerebellum showed progression of white matter hyperintensities in some patients (Fig 6.2), while there was no change in other patients. These areas were initially scored according to the transition from the previous scan. The presence or absence of volume loss was also assessed in these patients.

White matter lesions in the patients treated for medulloblastoma are inconsistent and are not seen in every patient [137, 138, 179]. The causes of these lesions are unknown and could be due to cancer therapies' toxicity. A preclinical study on an animal model has shown that even very low dose radiation may cause a change in gene expression, leading to behavioural deficits [180]. According to a descriptive study to assess the qualitative imaging changes in young children, these white matter changes can be transient and appear at different times after therapy [138]. Different time points were considered for analysis in our study. Our quantitative assessment results are consistent with these findings, and we also found that different textural features showed significant differences between the groups at different time points (Tables 6.4 & 6.5, Figures 6.4 & 6.5). There was no difference in the textural features between the 21 months and 5-year PSC and non-PSC groups at time points C and E. Timepoint B showed no difference in textural features only in the 5-year PSC and non-PSC groups. At baseline, the 21 months groups only showed a difference in skewness, while the 5-year group showed a difference in kurtosis and mean absolute deviation. Though only one patient is different between the groups, no of scans differed more (i.e. 2 vs 10 and 4 vs 8). This could be the reason for the significant difference in other features.

At time points C and E where the number of scans remained the same, there was no difference which was consistent in both tables. Also, the overall difference was comparable (15 features and 16 features). Further research is needed to determine the exact cause of this difference at baseline. It could be because of post operative oedema or difference in the concurrent medicines given to each patient. However, it could also be because of the difference in the time between surgery and the start of radiotherapy.

When analysed cumulatively over 21 months years, all textural features showed a significant difference between the 21 months PSC and non-PSC groups. The region of the cerebellar white matter appeared to be normal in all patients where ROI was taken, and the observer was blind to the qualitative scoring of scans at the time of textural analysis. This increases the reliability of our study and highlights that there are subtle intensity differences in the cerebellar white matter between two groups that are invisible to the human eye within the first 21 months years after radiotherapy. Similarly, when groups with 5-year qualitative PSC and non-PSC were compared, 15 textural features were able to show significant differences within the first 21 months years when analysed cumulatively. Kurtosis was the only feature that could not show the difference between these two groups.

Good predictive ability (AUC. 0.7) to distinguish between PSC and non-PSC groups was shown by nine texture features for the 21 months group and 12 features for the 5-year groups when ROC and AUC were carried out. Skewness and uniformity were not helpful (AUC< 0.5) for distinguishing the groups with or without PSC in 21 months as well as 5-year groups, while kurtosis showed borderline performance (AUC 0.5).

Our results are like a study on the classification of brain metastasis where support vector machine-based classification could distinguish between radiation necrosis and brain metastasis with high accuracy of AUC >0.94[181]. In this study very high accuracy was obtained where support vector machine could differentiate radiation necrosis. Our study shows AUC value of 0.7 which even though is a good predictive ability, it is lower than this high accuracy.

6.6 Limitations, Clinical Relevance and Future Scope

In the present study, we could show the difference between five-year qualitative changes within the first 21 months years by radiomic textural analysis of 21 months follow up scans in these patients. The dentate nucleus and surrounding cerebellar region play important role in planning and voluntary movements [181]. At the base line it appears that skewness (21 months) and kurtosis, mean absolute deviation (year 5) are significantly different. We do not know the exact reason for this. The fact textual features show significant differences between groups at baseline (i.e. before RT) is a potential weakness of this study . This result may have been a temporary phenomenon related to peritumoral oedema and post-surgical changes that resolved subsequently. Also, we tried to avoid the peritumoral oedema or post-surgical changes as much as possible about this is may not be possible in all cases as this is a small area.

On qualitative analysis, the radiologist considered the post operative changes when commenting on PSC. The ROIs were places in what appeared as normal brain tissue, but it is possible that there are subtle differences in the signal intensity that can only be identified by TA and not by the naked eye. We speculate that this could be due to white matter changes in the peritumoral region. In routine clinical practice the radiologist will describe PSC on each sequential MRI for patients. Some patients may show PSC on MRI at 1 and 2 years, which then stabilises and therefore by 5 years would not be defined as further PSC. Since the study was using 'real world' clinical data from routine practice we must accept and acknowledge this limitation. The rationale for this chapter was to investigate if we could see changes in radiomics that predict the subsequent development of PSC.

Another concern showed that individual TA features showing differences between two groups are different at different time points. This questions the potential reliability of textural features. However, this could be associated clinical changes or other confounding factors (such as patients on medication or other brain changes).

Presently this study being more image based, has a limited direct clinical application. Results of this study are based upon qualitative and quantitative MRI changes and this study has not considered clinical outcomes or level of impairment in these patients. Correlating these findings with clinical outcomes in future studies will help to understand the clinical significance of these findings.

6.7 Conclusion

In this initial study, longitudinal texture analysis at 21 months showed a difference between patients with and without qualitative signal changes in visibly normal-appearing brain regions. Radiomic texture analysis is a promising tool to distinguish patients with and without qualitative progressive signal changes even in visibly normal-appearing areas and possibly predict 5-year signal changes such as T2 hyperintensity within the first 21 months years after radiotherapy in paediatric patients with medulloblastoma at different time points and cumulatively. Anticipating these changes earlier may help identify children likely to manifest these changes in the future. A more extensive study is needed to examine the wider normal brain and correlate radiomic findings with clinical features.

Chapter 7. Summary, Final Remarks, And Recommendations For Future Work

7.1. Chapter Overview

This chapter aims to discuss the research's main points and summarises the highlights of each chapter of this thesis. The chapter mentions the overall contribution of this research work and provides several recommendations for future work.

7.2. Summary:

The overall aim of this research was to explore and evaluate the utility of radiomics in longitudinal analysis of non-tumoral brain regions in patients with paediatric brain tumours treated with radiotherapy. The first chapter provides a brief review of existing literature on paediatric brain tumours, classification, diagnostic imaging, treatment, and side effects of different treatment therapies in paediatric patients. This introductory chapter describes the gaps in the existing literature and the need for research. The chapter introduces the concept of radiomics, the rationale behind its usage and its potential as a biomarker to assess MRI brain tissue changes following radiotherapy.

Chapter 2 provides information on the study cohort, ethical considerations, and demographic data of scans.

Technical details of the methodology and challenges with image processing, especially in paediatric brain scans, have been described in Chapter 3. This chapter also includes the established image processing pipeline, trials with different software, technical limitations and measures undertaken to overcome them.

Chapter 4 describes the first hypothesis of this research, understanding the effects of dose, time and dose and time together on textural features. This study showed a significant effect on some radiomic texture features and radiation dose and time. Some of the features did not show any correlation with time. Here results of machine learning analysis and details of data exploration apps have also been discussed.

Chapter 5 is the first study to show the significant difference in the texture feature values between proton and photon therapy at the same dose levels, pointing toward the possible difference in radiobiology between the two.

Finally, Chapter 6 shows the difference in feature values between patients showing the 21 months and 5-year qualitative signal change in the cerebellar region of paediatric patients treated for medulloblastoma. Texture features offering good diagnostic reliability were also identified. Radiomics shows some interesting results, but the importance of PSC needs to be correlated with clinical patient

outcomes, and confirmed in a larger study to determine whether it is a useful approach to monitor patients and predict future changes.

7.3. **Advances Made and Clinical Relevance**

This thesis has contributed to the radiation oncology field as a research effort focused on deriving novel non-invasive quantitative imaging biomarkers to assess the underlying tissues following therapeutic radiation. In this multidisciplinary effort, technical areas such as image processing, machine learning, statistics, and clinical specialities such as paediatric neuro-oncology, radiation oncology, neurosurgery and radiology were integrated towards solving clinically important problems. Most of the work in this study was focused on exploring radiomic textural features as a quantitative marker and T2 MRI as the primary neuroimaging modality.

These quantitative measures can potentially be used in future studies to predict the outcome with the help of advanced machine-learning techniques. Predicting the biological toxicities of different therapies on different brain regions will form the foundation of personalised medicine by delivering tailored approaches to each region.

Clinical relevance of this project

i. A non-invasive imaging-based biomarker has been derived to assess dose-dependent changes in standard parts of the brain longitudinally at different time points.

ii. In clinical practice, scans are advised based on the clinical need. Having scans at fixed time points for the planned clinical trial in paediatric patients with brain cancer is challenging. Such scans with fixed parameters increase cost and are less feasible. The present study has overcome this problem.

iii. Complete information has been obtained from existing clinical scans as a large amount of data is available to explore. In this study, structural MRI images have been used that are part of routine brain tumour imaging protocol. This allows the broader utility of derived potential biomarkers in secondary and tertiary level treatment centres. This is more significant in paediatric brain tumours as advanced imaging is not always possible in children.

iv. Because this method is based on routine brain MRI studies, the expected improved efficiency of the diagnostic procedure is not associated with additional technical setups for image acquisition. This reduces the cost of study as the existing database can be exploited to get results.

v. This study encompasses quantitative analysis of non-tumoral brain regions of several T2 scans in a paediatric patient treated with all treatment modalities. Understanding the effects of radiation dose and time can help assess the overall effect of radiation over time at different dose levels and in

different brain regions. Presently there is minimal published literature in this area.

vi. This study helps to understand and compare the difference between underlying tissue changes after photon and proton therapy. This is the first radiomic study to compare these differences, pointing toward the difference in underlying radiobiology. Understanding the biological underpinning of these significant differences, where possible, can strengthen the conclusion, provide additional validation, and provide further opportunities for investigation.

vii. A part of the study shows the role of radiomics in differentiating groups of patients showing 5-year T2 cerebellar changes within the first two years after radiotherapy in paediatric patients treated for medulloblastoma. When developed further, this might help identify the more likely patients to manifest these changes over time.

7.4. Limitations and Future Directions:

This present study is a clinical retrospective study; with existing non-available data-limited methodology and analysis. We have made active efforts to increase the reliability of this study by modifying technical methods and eliminating errors wherever we could. The list of technical limitations and measures taken to mitigate the effects that have been given in Chapter 3 (Table 3.2). Limitations, clinical relevance, and future scope of each aim of the study have been mentioned in more detail in chapters 4, 5 and 6.

Presently radiomic analysis is in the developing stages with minimal information on validation. This is complicated by poor reproducibility resulting in limited impact. The association of these radiomic findings with clinical data will enhance their reliability and put them in a more biological context. The correlation of textural features with IQ scores, memory testing, brain volume etc will help to identify the exact relationship between these features and clinical manifestation of brain toxicity. Designing a study with age-matched control groups will increase reliability.

In this study, the random forest method of machine learning was used to study the correlation between textural features and radiation dose and a clear relationship could not be observed. Using another machine learning method such as principal component analysis (PCA) to reduce the dimensions of data and having a heatmap with all the clinical factors might be able to give a list of useful textural features. Due to time limitations, only first-order texture features were included in this study. Including higher-order texture, features may help to get additional information.

In this study, brain changes were also associated with concurrent chemotherapy and surgery thus confounding the study results. In future studies, a separate analysis of the patients who received concurrent chemotherapy will help to overcome this limitation.

Preclinical models can also analyse and correlate the underlying biological mechanisms causing toxicity after each therapy. Such studies will enable the comparison of proton vs photon therapy in a more controlled condition related to radiation dose. It will also be possible to take scans at fixed time points and note clinical changes in an animal. Fundamental differences in the radiobiology of the two therapies might be demonstrated in these studies by simultaneous cellular and histopathological analysis. Having clinical-radiological and histopathological correlation will increase the validity of the results in a more clinical context.

Moving forward, radiomic analyses might be tested in future studies to understand the post-radiation changes in the tumour and correlate with the prognosis and survival. Radiomics has the potential to be a more objective biomarker than tumour size and other qualitative markers.

The results of this study are taken from a single institution and thus had a smaller sample size. Developing a multinational and multicentric study on a larger dataset will obtain more reliable results with higher statistical power.

7.5. Conclusion:

Radiomic texture analysis is a valuable and promising tool to explore post-radiation MRI changes in non-tumoral brain regions. This thesis has explored its usage as a potential biomarker of toxicity and its importance in predicting this toxicity in paediatric brain tumour patients. Some of the textural features showed significant effects of radiation dose and time and demonstrated differences in photon and proton therapy. Textural features showed differences between patients pre-identified to have progressive signal change. This suggests the features may be able to predict progressive signal change in the future. . The role of radiomics in routine oncology care requires further investigations through prospective studies with patient and clinical outcomes. Radiomics remains a research tool for the time being.

APPENDIX 1: DATA EXPLORATION APP

Table A1. 1 Table showing different variables used to assess brain changes in paediatric patients with primary brain tumours

Demographic data
- Gender
- Age At diagnosis

Location of Tumour
- Brainstem
- Cerebellar
- Hemispheric cerebral (frontal /temporal /parietal /insular)
- Supratentorial midline (thalamic /hypothalamic /suprasellar)

Diagnosis
- Medulloblastoma
- Low Grade Glioma
- High Grade Glioma
- Ependymoma
- Rare Embryonal Tumours (atypical teratoid rhabdoid tumours / CNS PNET/Chordoma),Tumours of the Sellar region (pituitary tumours /craniopharyngioma)
- Germ Cell Tumours
- Meningioma
- Unclassified

ROI (11)
- Medulla 1
- Pons 1
- Corpus Callosum 2- Ant , Post
- Centrum Semiovale 2- R L
- PTV 1
- Thalamus 2 R L
- Cerebellum 2 Centre (R L)

Chemotherapy
- Yes
- No

Biopsy
- Yes
- No

Surgery
- Subtotal Resection
- Gross Total resection
- Near Total resection

Time
- Multiple scans over 720 days post radiation (2 years approx)

Radiological Data
- Radiation Dose/volume brain tissue
- No of fractions
- Texture Features
  - First Order
  - GLCM
- Therapy
  - Proton
  - Photon

4.6.1.a First tab: Info: Provides information on updates during the process of data analysis. (Figure A1.1)

4.6.1.b The second tab summary (Figure A1. 2) gives a birds-eye view of the entire dataset. It has three additional tabs: meta data, counts and medulloblastoma. Metadata tab demographic information of the patients and the location, metastasis, diagnosis, type of radiotherapy, chemotherapy tab, and the information of biopsy and surgery.

4.6.1.c The count tab (Figure A1. 3, A1.4, A1.5, A1.6) helps to instantly get information on the number of patients as per any clinical variables and grouping. We can select the variable in columns 1 and 2 for a more detailed overview.

4.6.1.d Lastly, the medulloblastoma tab (Figure A1. 7) was added later to analyse patients in the medulloblastoma group. This analysis will be discussed in the upcoming chapter on medulloblastoma.

4.6.1.e Texture feature plots (Fig. A1.8) show the change in each texture feature over time for all patients in each brain region. These include the functionality of highlighting outliers (points further than two standard deviations from the mean).

4.6.1.f Texture feature delta plots (Fig. A1.9) show the relative change of texture features – the difference between consecutive time points divided by the length between the consecutive follow up scans. The options are analogous to the texture feature plots.

4.6.1.g 3D feature plot (Fig. A1.10) is a dynamic 3-dimensional plot showing features changes over time and dose. All the three variables, texture feature, dose and time, can be seen at once in this plot.

Figure A1. 1 Showing information about the application and updates.

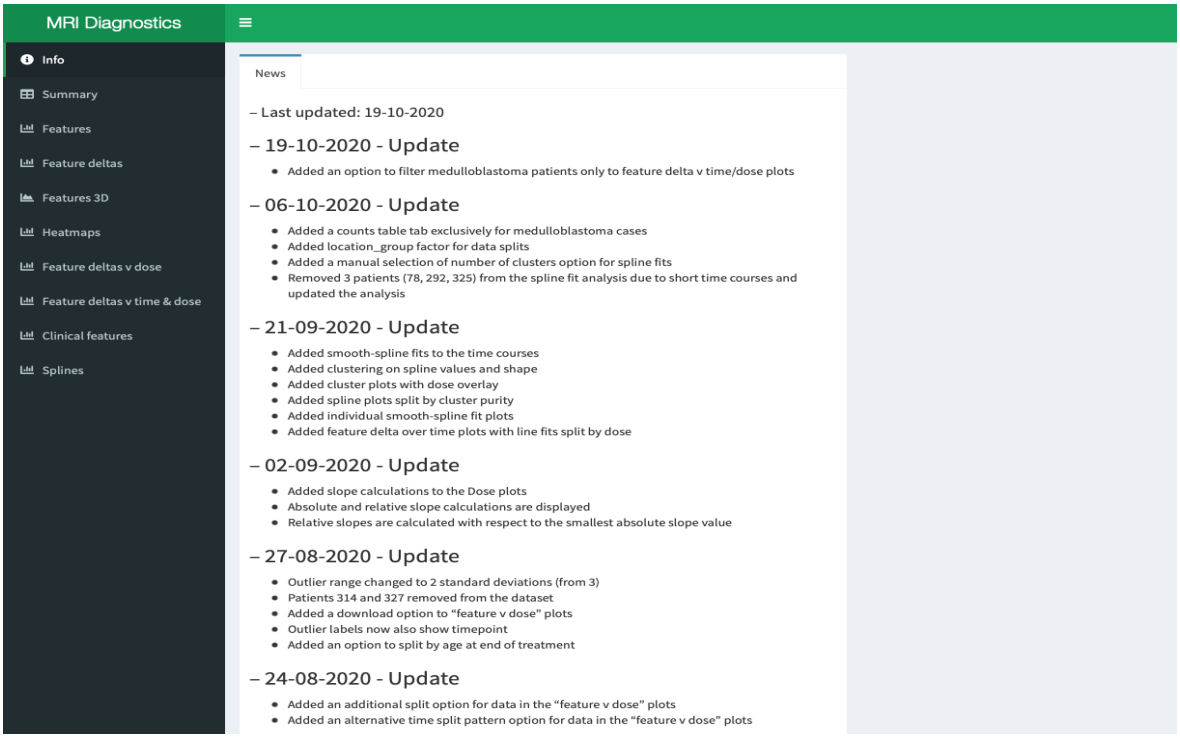

Figure A1. 2 Patient cohort with database information given in the summary – metadata tab of the application

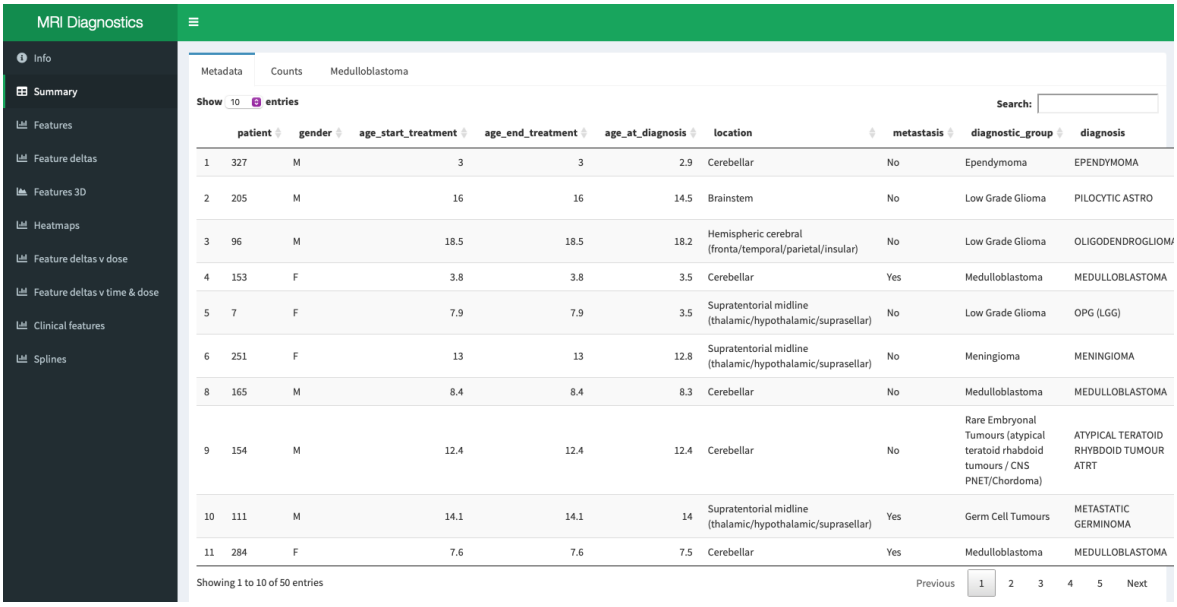

Figure A1. 3 Count tab showing information of number of patients based upon gender and diagnostic group.

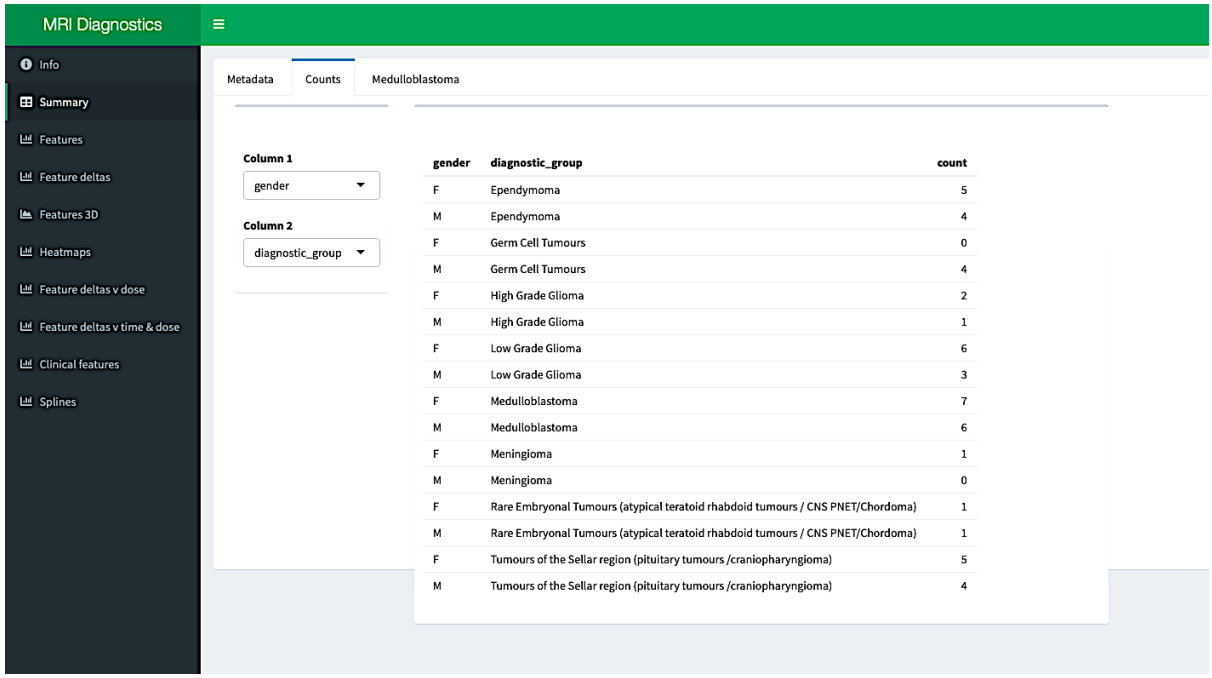

gender	diagnostic_group	count
F	Ependymoma	5
M	Ependymoma	4
F	Germ Cell Tumours	0
M	Germ Cell Tumours	4
F	High Grade Glioma	2
M	High Grade Glioma	1
F	Low Grade Glioma	6
M	Low Grade Glioma	3
F	Medulloblastoma	7
M	Medulloblastoma	6
F	Meningioma	1
M	Meningioma	0
F	Rare Embryonal Tumours (atypical teratoid rhabdoid tumours / CNS PNET/Chordoma)	1
M	Rare Embryonal Tumours (atypical teratoid rhabdoid tumours / CNS PNET/Chordoma)	1
F	Tumours of the Sellar region (pituitary tumours /craniopharyngioma)	5
M	Tumours of the Sellar region (pituitary tumours /craniopharyngioma)	4

Figure A1. 4 Count tab showing information of a number of patients based upon location and therapy type.

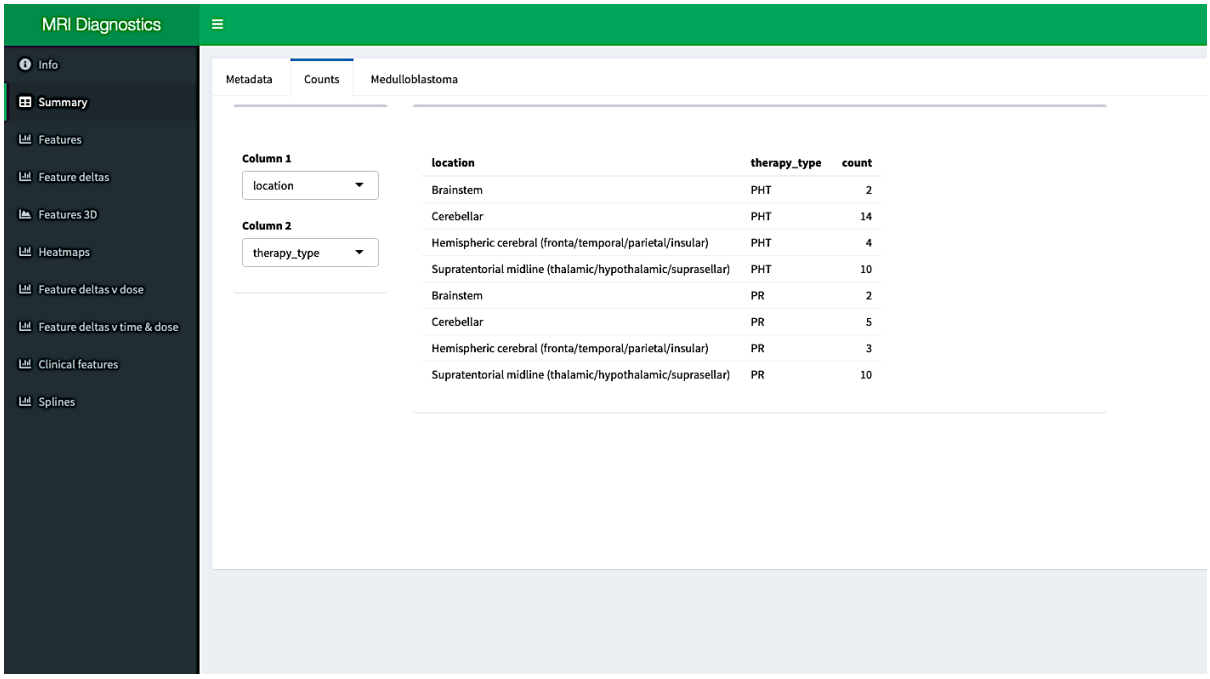

location	therapy_type	count
Brainstem	PHT	2
Cerebellar	PHT	14
Hemispheric cerebral (fronta/temporal/parietal/insular)	PHT	4
Supratentorial midline (thalamic/hypothalamic/suprasellar)	PHT	10
Brainstem	PR	2
Cerebellar	PR	5
Hemispheric cerebral (fronta/temporal/parietal/insular)	PR	3
Supratentorial midline (thalamic/hypothalamic/suprasellar)	PR	10

Figure A1. 5 Count tab showing information of number of patients based upon age at the end of radiotherapy and location group.

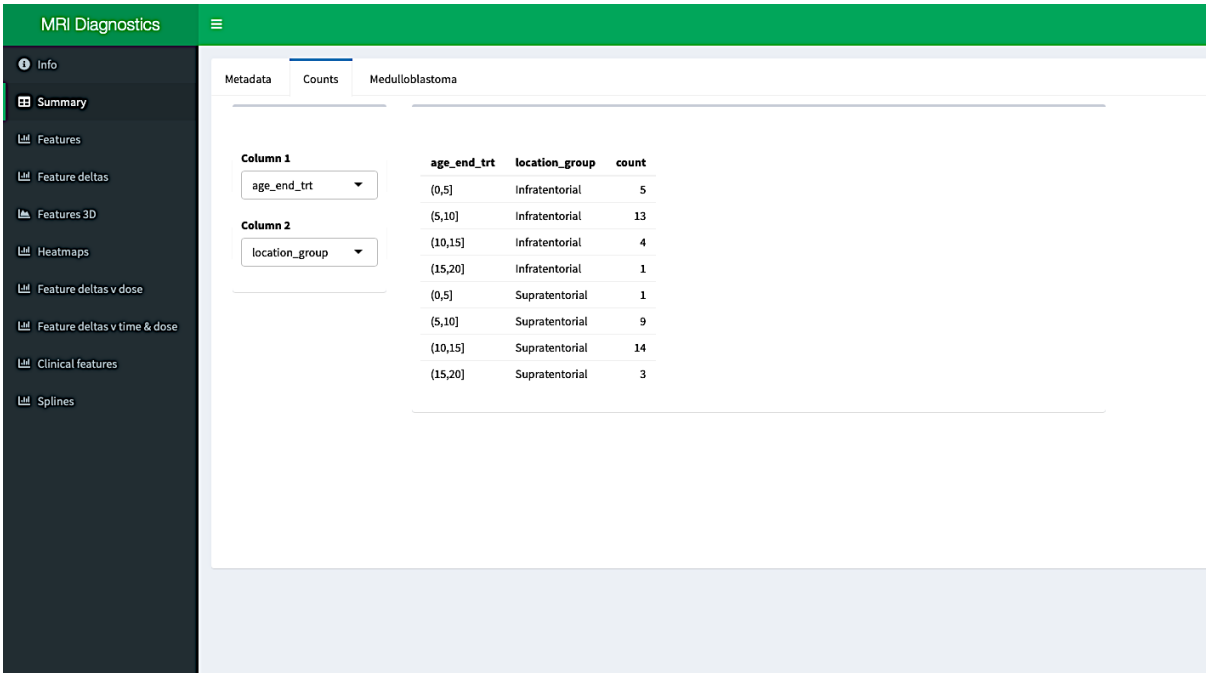

Figure A1.6 Count tab shows the number of patients based on gender and surgery type.

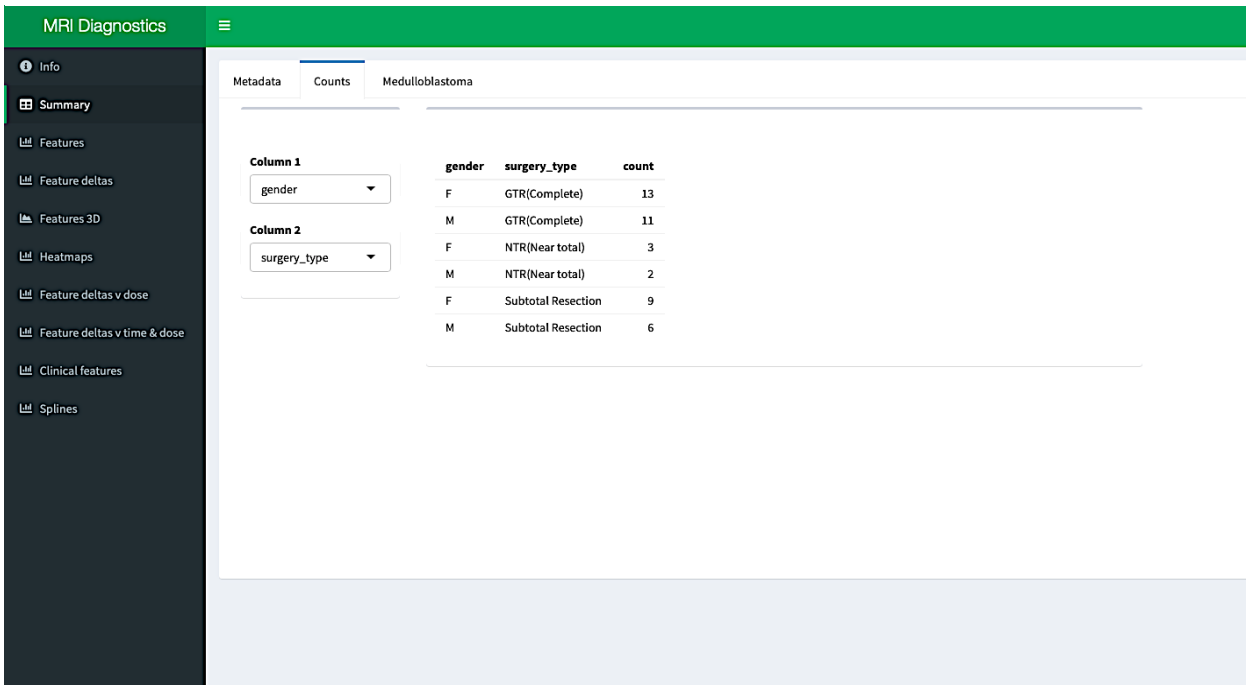

Figure A1. 7 Medulloblastoma section for the information of patients with medulloblastoma

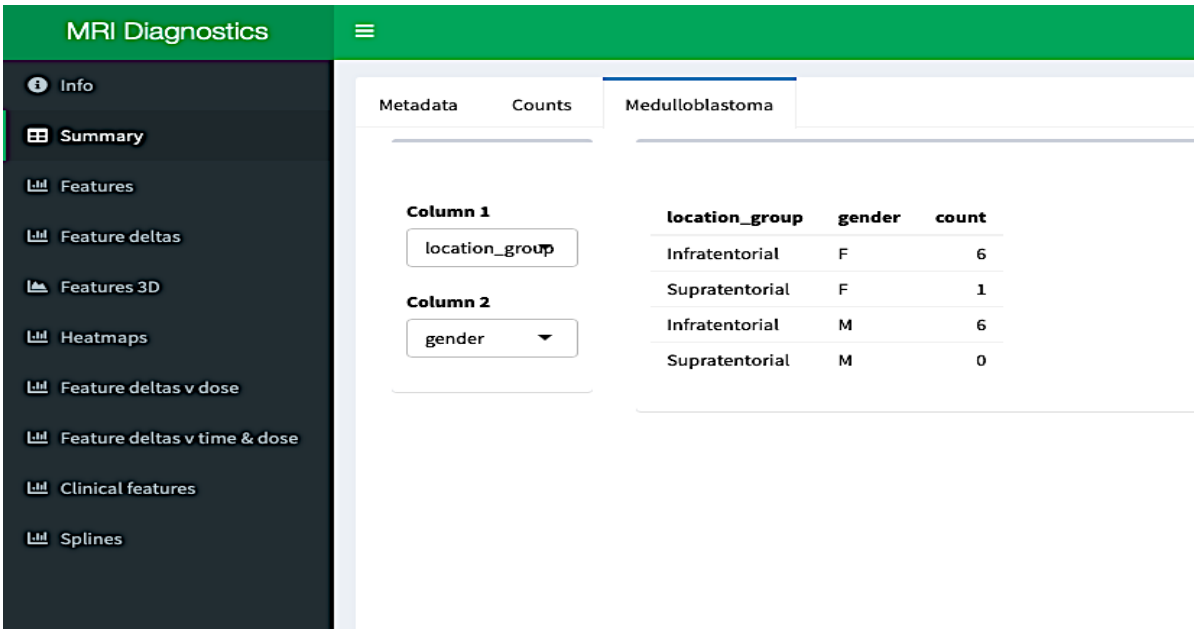

Figure A1. 8 Feature tab with graphs of feature values of all patients. Each colour represents selected feature in each patient. Y axis shows feature value and x axis shows time in days. Please note the additional tabs for selection of other parameters such as region, feature, etc.

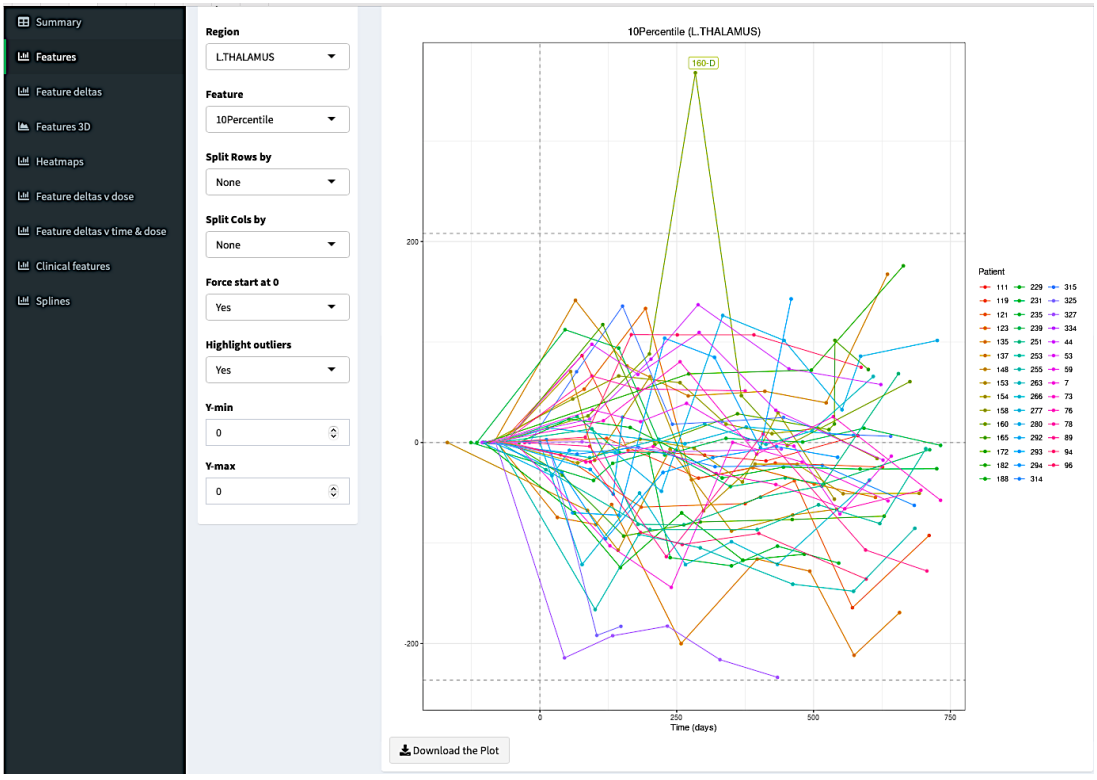

Figure A1. 9 Texture feature delta plot with selected parameters to compare different groups. Left side graphs show patterns in female groups, right side graphs show a pattern in the male group. The upper row is the photon group and the lower is the proton group. X and Y axis, colours are similar to the previous graph.

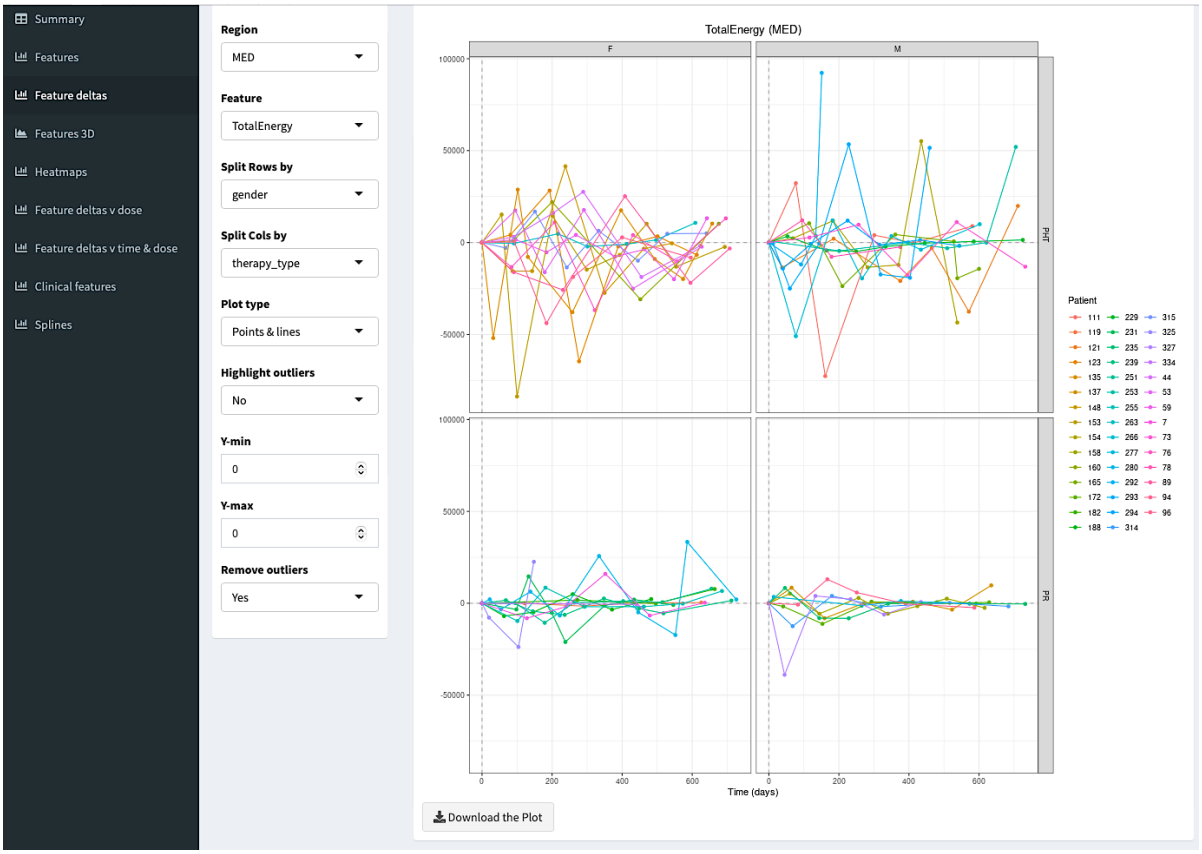

Figure A1.10 showing 3D dose map showing entropy, time, and dose values of right cerebellum region for all patients in a single graph.

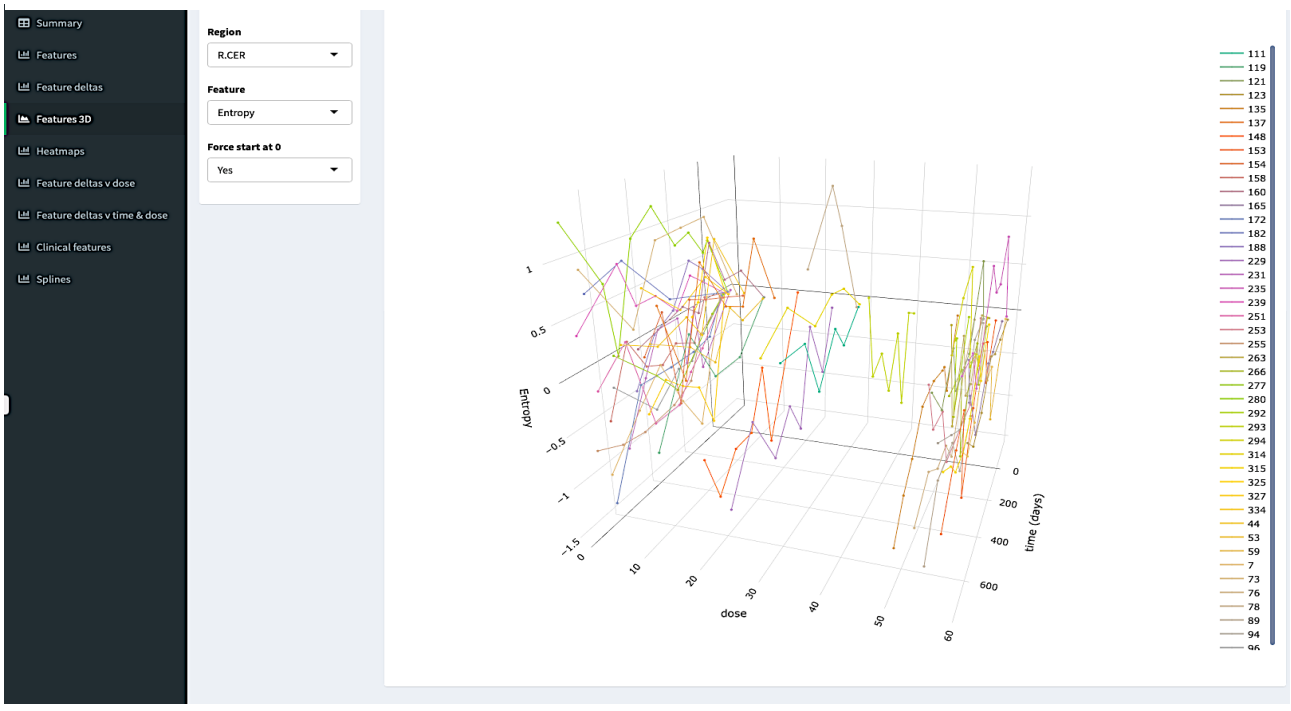

4.6.1.h Heatmaps of texture features (Fig. A1.11) and feature deltas are included for an alternative visualisation of the data all at once. The samples are grouped by the patient and ordered by the time of the scan. The features are reordered by a clustering algorithm to group similarly behaving features together.

4.6.1.iFeature deltas vs time plots allow visualisation of change in textural features against time. This also allowed us to understand how these lines differ at each radiation dose. Like previous graphs, additional tabs allow the selection of parameters for visualization of group-specific data e.g., gender, type of therapy, region, feature, etc. Feature deltas against dose plots and feature correlation (Fig. A1.12) to dose heatmaps (Figure A1. 13) were included to enable exploration of the idea that the secondary effects observed later in the patient's history would manifest as increasing correlations of feature deltas and radiation dose in the region when calculated in different time windows. Plots include linear model fits, and absolute and relative slope figures.

4.6.1.jFeature deltas vs time and dose (Figure A1. 14) are included to allow the investigation of linear relationships between feature deltas at different times at various windows of dose. The plots include linear model fits, and absolute and relative slopes are shown.

4.6.1.k A linear model was fit to evaluate the influence of clinical features as well as time and dose to predict each feature deltas. The coefficients of the model are shown in the clinical feature heatmap (Figure A1. 15).

4.6.1.l Finally, a dendrogram (Figure A1.16) was created for the visualisation of the correlation between feature value and radiation dose. This was the dendrogram of the hierarchical clustering results of interpolated feature data and trend descriptions. Each branch is annotated with the dose level: red - dose >20, green - dose <= 20.

Figure A1.11 Heatmap of features deltas over time for the posterior corpus callosum region. Each column represents each patient, and rows represent the rate of change of texture feature value. Similar colours

s values in

nd proton

Figure A1 12 Heatmap showing correlation of texture features with dose in the Pons region. Each row represents time in days, while rows represent each textural feature. The scale representing colour for the correlation index is

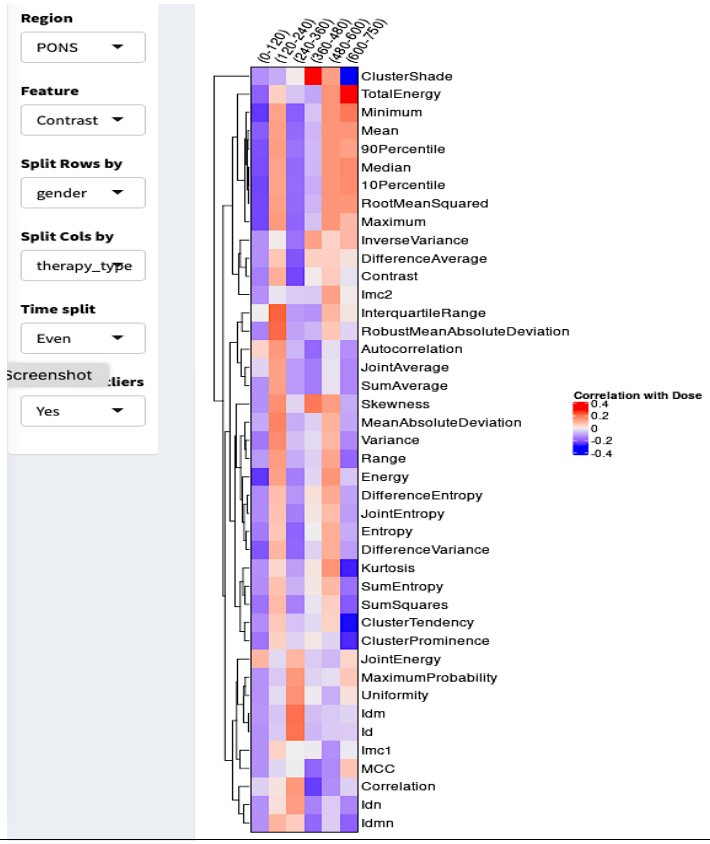

Figure A1. 13 Graphs represent a change in the contrast value vs dose in the pons region. The upper row represents values in females while the lower row shows values in males. The Left and right columns show photon and proton therapy graphs, respectively. Each colour in the graph represents the time window, as presented in the scale.

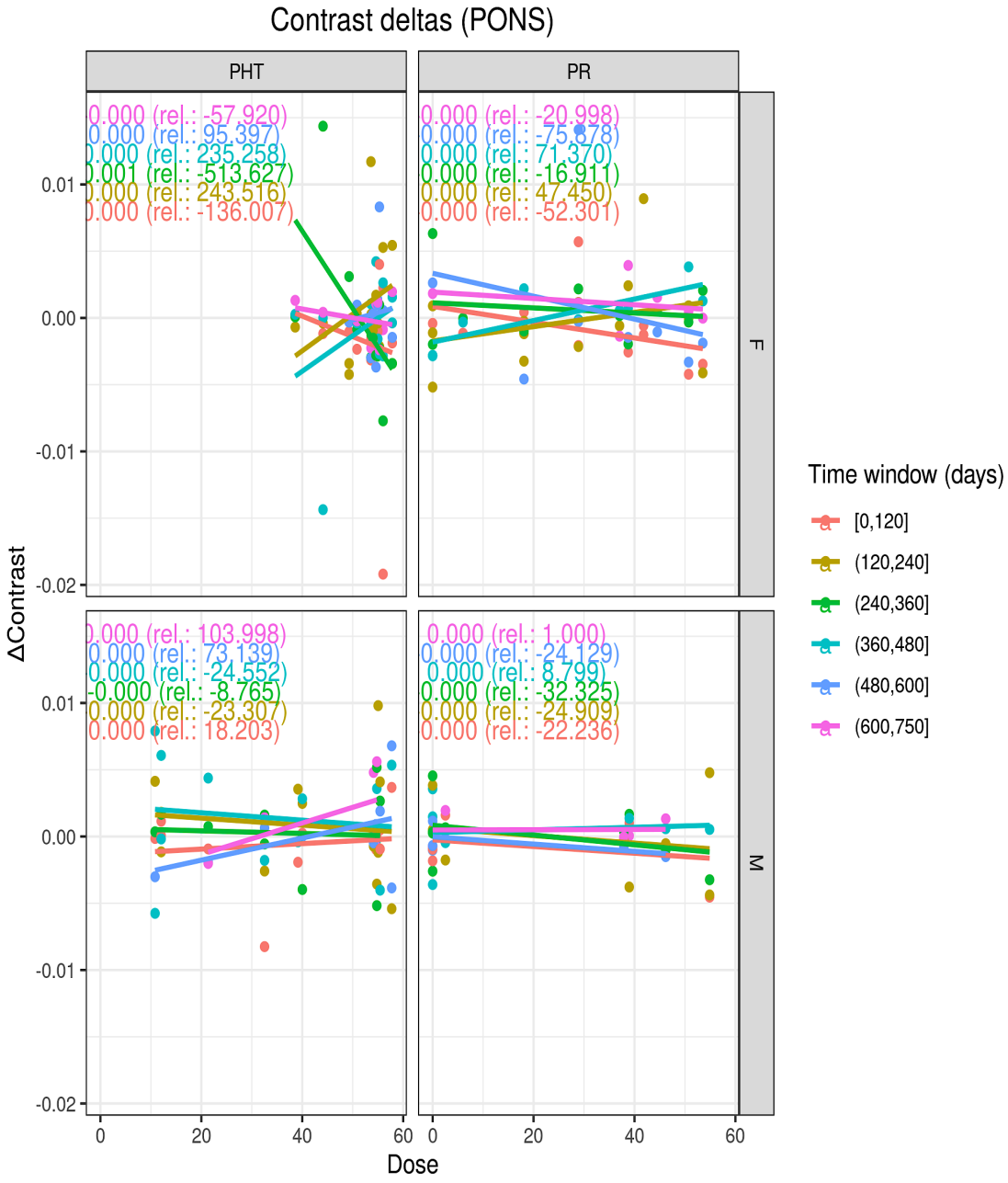

Figure A1. 14 Graph shows the rate of change of uniformity in the right cerebellum region. Y-axis represents a change in uniformity (delta), and the x-axis represents time. Each dose is demonstrated with a specific dose group, as shown in the dose window. Addition splits were done so that each row represents the age group and the column represents the therapy type. Each dot represents a value of uniformity at a time in one patient. The line represents the overall trend when all such dots are considered together at each dose window.

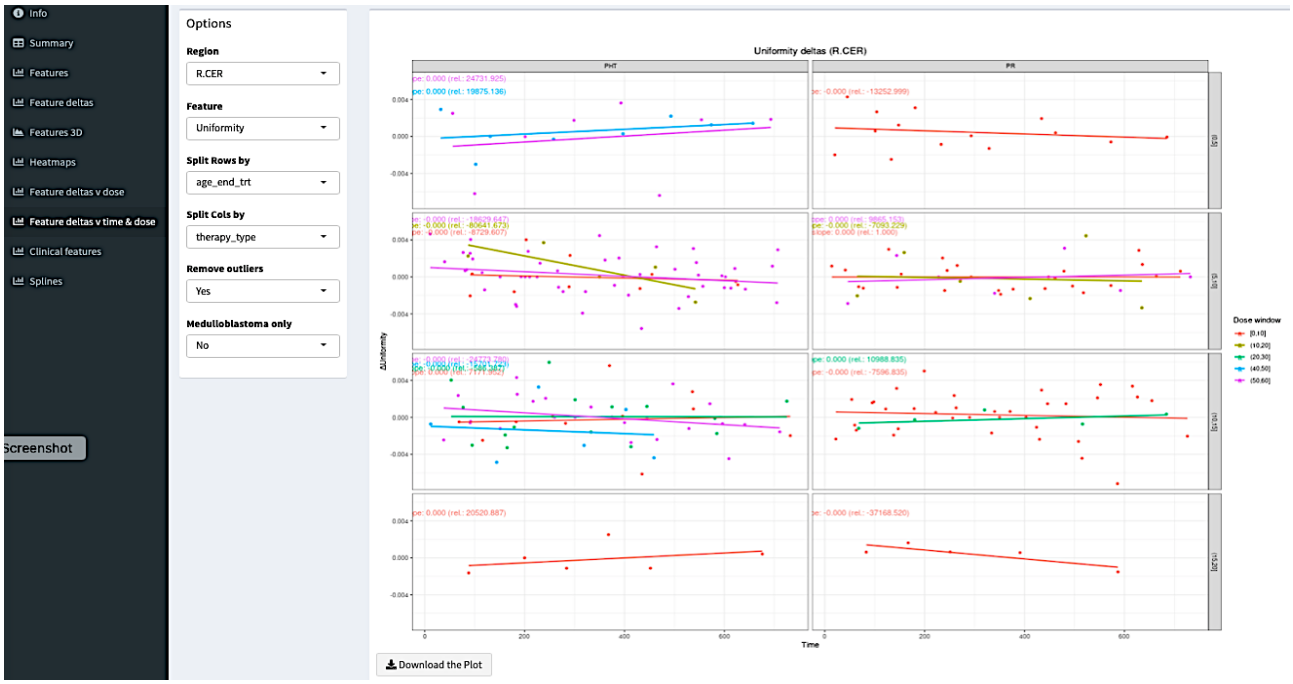

Figure A1. 15 Heatmap showing correlation each clinical feature with the feature value over time in anterior corpus callosum region. Each column represents each clinical feature and each row represent each texture feature. Corelation scale has been given on the right side with red regions shows maximum correlation.

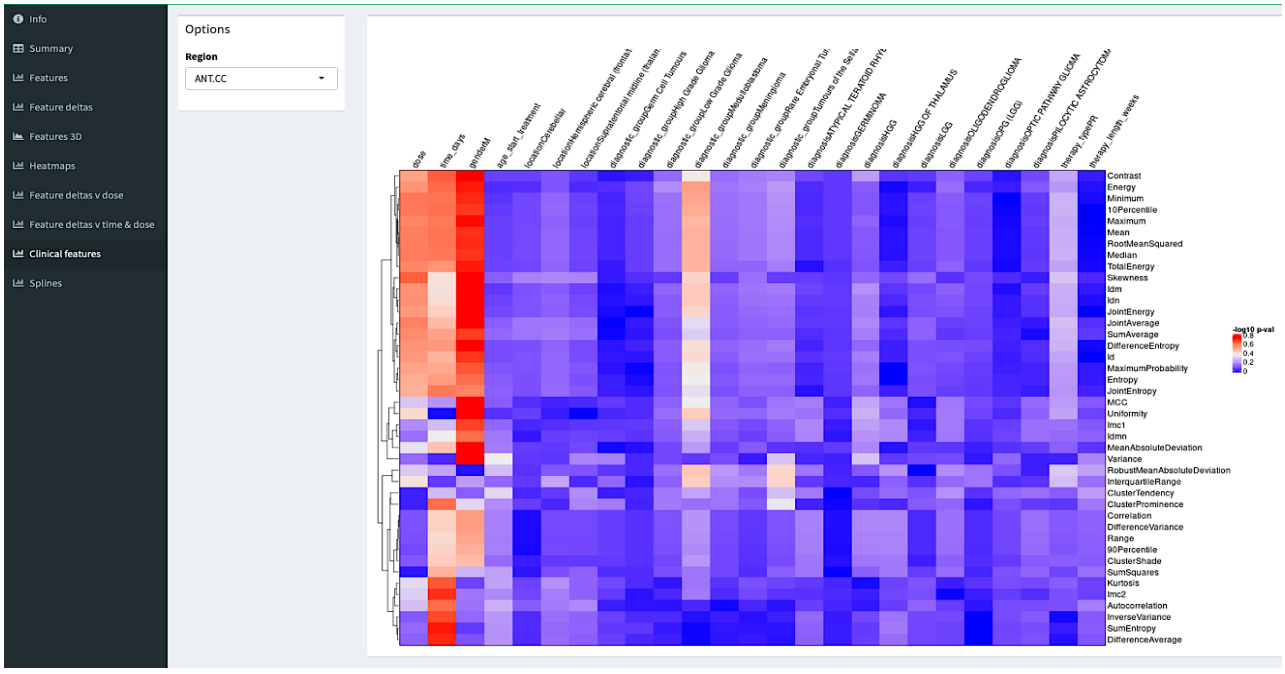

Figure A1.16 Dendrogram shows the radiation dose relationship with total energy in the anterior corpus callosum region. Red dots represent patients that received a high dose (>20Gy), while green dots represent a low dose (<= 20Gy). The X-axis has patient codes, while Y-axis represents the distance between the nodes. The more downward distance between the nodes shows a close relationship, e.g., BMS 7 and 280 are interchangeable. The overall picture shows the majority of the green dots on the left branch, while the red dots on the right unit show a correlation of total energy with the dose. TE values of the patients receiving low radiation dose are more closely related than those with high radiation dose. Total Energy was the best predictor by far in most of the regions. This supported the observations in the clustering results.

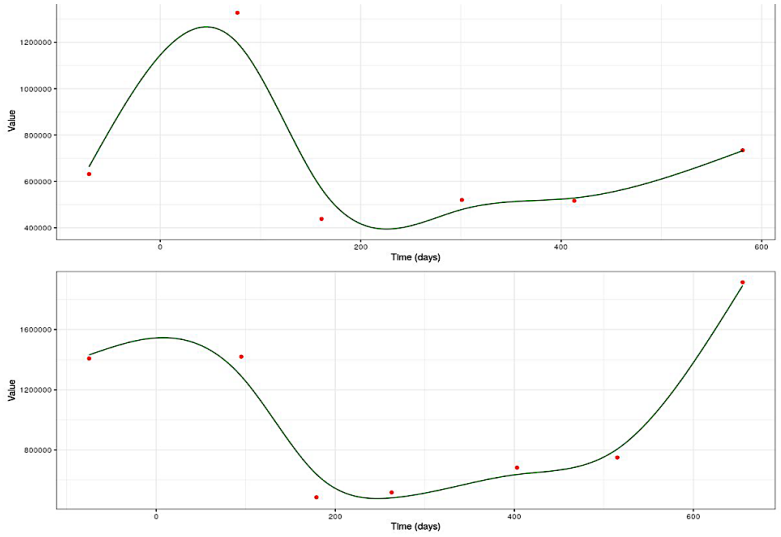

Figure A1. 17 Example spline fits the values of the "Energy" texture feature in the medulla region for two patients. Red dots indicate measured values; the green line shows smooth spline interpolation.

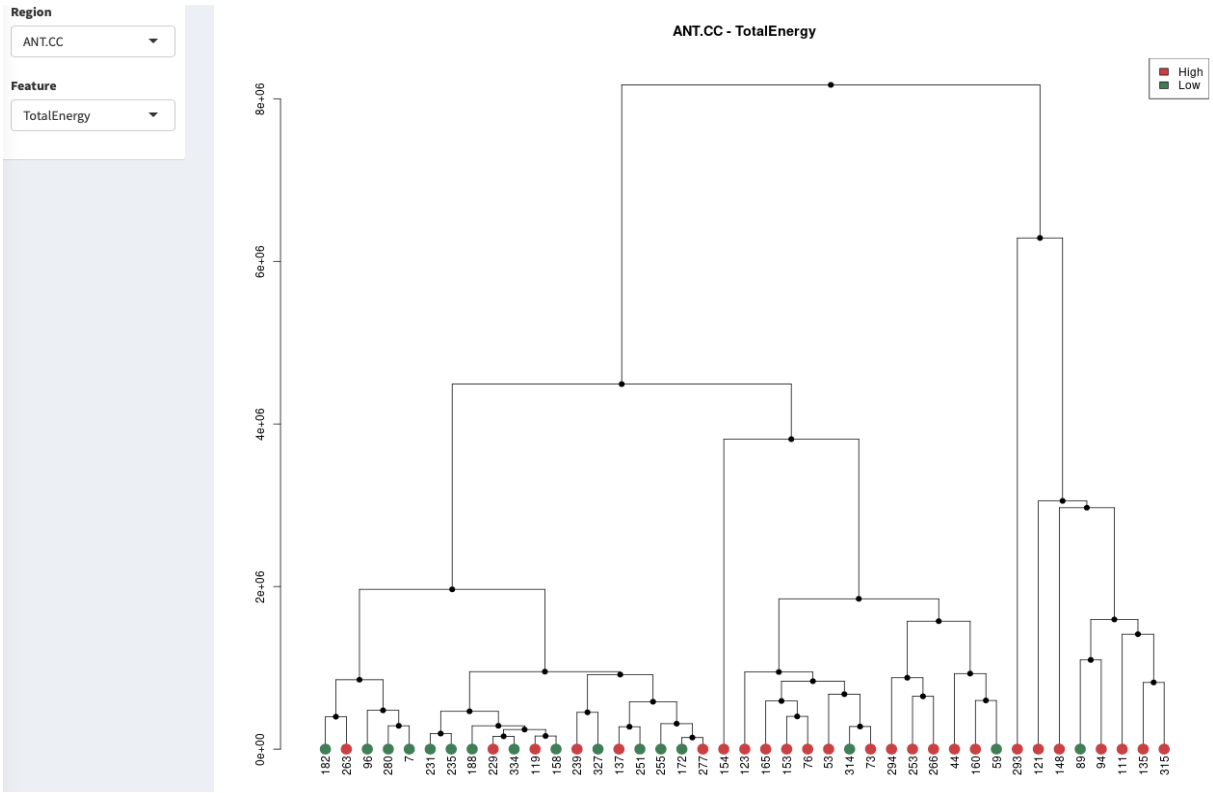

4.6.1.m Most machine learning algorithms require all samples to have the same variables (features). In this study, each patient had scans taken at variable intervals (Fig. A1.3) making data not directly comparable. To make the time points comparable, smoothing splines were used to interpolate the data and obtain approximate intermediate values (Fig. A1.20). This allowed direct comparison of data between patients.

4.6.1.n Another tab (Fig. A1.18) visualised the spline interpolation to see the variation in feature values over time in high-dose and low dose groups initially represented in the dendrogram.

Other random forest algorithms were used to find the top 20 most predictive features based on their frequency to predict the dose-effect in each brain region. This model was built over ten iterations, and the results are shown in (Figure A1. 19). Total energy (TTE) seemed the most robust feature to predict dose in each brain region.

Figure A1. 18 Plot of two clusters of smooth spline fits derived from the interpolated data, and trend descriptions of Total Energy in the medulla region show a clear difference in variation in the feature in the first half of the time course. The left column mainly represents values in patients with high doses, and the right shows values in patients with low doses.

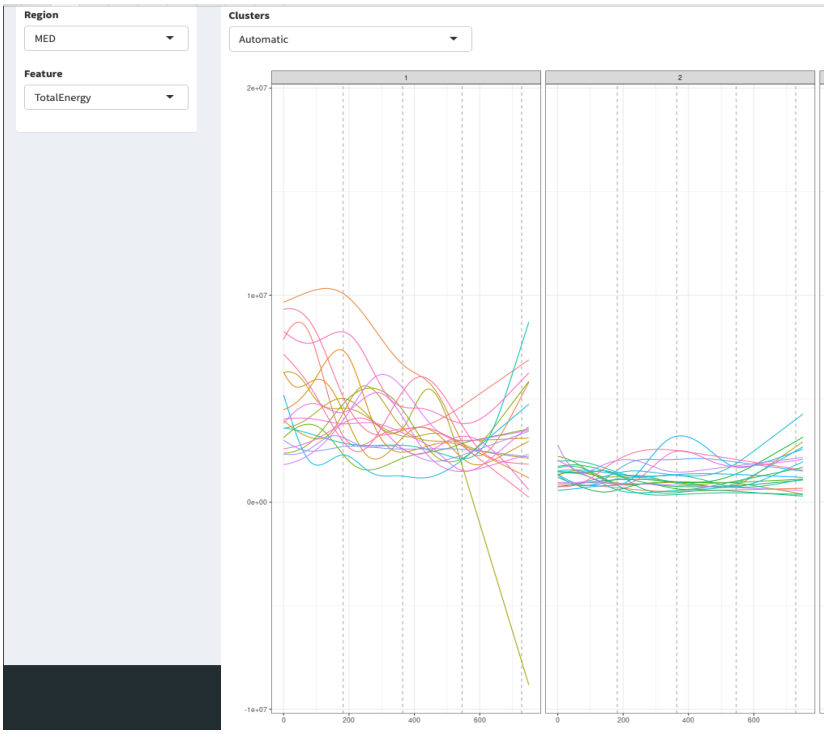

Figure A1. 19 Frequencies of each feature selected in the top 20 most predictive features by a random forest model over ten iterations in each region.

	MED	PONS	ANT.CC	POST.CC	L.CS	R.CS	L.THALAMUS	R.THALAMUS	L.CER	R.CER
TotalEnergy	129	58	144	153	112	96	127	129	97	115
MaximumProbability	21	0	0	0	0	0	0	0	0	0
ClusterShade	20	0	0	0	0	0	0	0	0	0
JointEnergy	20	0	0	0	0	0	0	0	0	0
Uniformity	19	0	0	0	0	0	0	0	0	0
Correlation	0	28	0	0	0	0	0	0	0	0
Skewness	0	21	0	0	0	0	0	46	0	0
Energy	0	20	0	0	0	0	21	0	18	0
Idn	0	18	0	0	0	0	0	0	0	0
Variance	0	0	23	17	0	0	0	0	0	0
InterquartileRange	0	0	21	0	25	0	0	0	0	0
MeanAbsoluteDeviation	0	0	21	0	0	0	0	0	21	0
Imc1	0	0	19	22	0	0	0	16	0	21
Kurtosis	0	0	0	18	0	31	0	30	0	25
ClusterProminence	0	0	0	17	0	0	0	0	0	0
RobustMeanAbsoluteDeviation	0	0	0	0	24	0	0	0	0	24
Minimum	0	0	0	0	21	0	0	0	0	0
10Percentile	0	0	0	0	20	0	0	0	0	0
MCC	0	0	0	0	0	25	0	0	0	0
Idmn	0	0	0	0	0	19	0	0	0	0
DifferenceAverage	0	0	0	0	0	14	0	0	0	0
SumAverage	0	0	0	0	0	0	35	0	0	0
JointAverage	0	0	0	0	0	0	32	0	18	0
Autocorrelation	0	0	0	0	0	0	24	0	0	0
Imc2	0	0	0	0	0	0	0	19	0	23
Range	0	0	0	0	0	0	0	0	26	0

APPENDIX 2: STATISTICAL GRAPHS EFFECTS OF RADIATION DOSE, TIME, AND DOSE*TIME ON TEXTURAL FEATURES

GLM statistical model was used in SPSS with dose as a fixed factor, Texture feature as a variable and time as a covariate. The effects of radiation dose, time, and dose *time with the texture feature values was calculated. The text for these graphs is in chapter 4.

WHOLE BRAIN ANALYSIS

Between-Subjects Factors		
dose (Binned)	Value Label	N
1	0-10.55	1092
2	10.56-20.55	209
3	20.56-30.55	319
4	30.56-40.55	334
5	40.56-50.55	229
6	50.56-60.55	1005

Descriptive Statistics				
	dose (Binned)	Mean	Std. Deviation	N
@10Percentile	0-10.55	202.23	70.29	1092
	10.56-20.55	199.66	68.75	209
	20.56-30.55	177.21	54.93	319
	30.56-40.55	177.44	56.72	334
	40.56-50.55	178.90	58.93	229
	50.56-60.55	195.96	59.78	1005
	Total	193.31	64.11	3188
@90Percentile	0-10.55	224.82	73.62	1092
	10.56-20.55	221.54	77.60	209
	20.56-30.55	193.40	58.15	319
	30.56-40.55	198.03	61.01	334
	40.56-50.55	201.92	65.04	229
	50.56-60.55	224.19	70.44	1005
	Total	216.81	70.63	3188
Contrast	0-10.55	0.37	0.36	1092
	10.56-20.55	0.43	0.47	209
	20.56-30.55	0.30	0.24	319
	30.56-40.55	0.42	0.56	334
	40.56-50.55	0.55	0.96	229
	50.56-60.55	0.58	1.11	1005
	Total	0.45	0.75	3188
Correlation	0-10.55	0.19	0.35	1092
	10.56-20.55	0.15	0.32	209
	20.56-30.55	0.24	0.43	319
	30.56-40.55	0.20	0.38	334
	40.56-50.55	0.11	0.34	229
	50.56-60.55	0.20	0.31	1005
	Total	0.19	0.35	3188
Energy	0-10.55	1048700.00	817864.00	1092

	10.56-20.55	1096700.00	1052860.00	209
	20.56-30.55	634490.00	559434.00	319
	30.56-40.55	698470.00	652570.00	334
	40.56-50.55	686000.00	680893.00	229
	50.56-60.55	1012800.00	872362.00	1005
	Total	936350.00	823028.00	3188
Entropy	0-10.55	0.82	0.46	1092
	10.56-20.55	0.86	0.45	209
	20.56-30.55	0.65	0.42	319
	30.56-40.55	0.81	0.46	334
	40.56-50.55	0.87	0.44	229
	50.56-60.55	1.00	0.53	1005
	Total	0.86	0.49	3188
Kurtosis	0-10.55	2.69	1.04	1092
	10.56-20.55	2.72	0.79	209
	20.56-30.55	2.58	0.87	319
	30.56-40.55	2.57	1.04	334
	40.56-50.55	2.61	0.83	229
	50.56-60.55	2.76	1.56	1005
	Total	2.69	1.19	3188
Maximum	0-10.55	231.37	76.34	1092
	10.56-20.55	228.53	82.41	209
	20.56-30.55	198.07	59.29	319
	30.56-40.55	204.86	66.07	334
	40.56-50.55	208.06	66.88	229
	50.56-60.55	234.39	78.25	1005
	Total	224.35	75.31	3188
Mean	0-10.55	213.41	70.97	1092
	10.56-20.55	210.33	72.63	209
	20.56-30.55	185.22	56.39	319
	30.56-40.55	187.61	58.44	334
	40.56-50.55	190.21	61.65	229
	50.56-60.55	209.50	63.93	1005
	Total	204.78	66.49	3188
MeanAbsoluteDeviation	0-10.55	7.96	10.22	1092
	10.56-20.55	7.45	4.66	209
	20.56-30.55	5.60	2.55	319
	30.56-40.55	7.30	4.71	334
	40.56-50.55	8.02	5.49	229
	50.56-60.55	9.73	8.38	1005
	Total	8.19	8.12	3188
Median	0-10.55	213.67	70.58	1092
	10.56-20.55	209.94	71.89	209

	20.56-30.55	185.00	56.32	319
	30.56-40.55	187.36	58.26	334
	40.56-50.55	190.01	62.00	229
	50.56-60.55	208.41	63.60	1005
	Total	204.44	66.20	3188
Minimum	0-10.55	196.78	68.41	1092
	10.56-20.55	193.64	68.14	209
	20.56-30.55	173.30	54.17	319
	30.56-40.55	172.59	55.78	334
	40.56-50.55	173.27	57.20	229
	50.56-60.55	189.52	58.28	1005
	Total	187.71	62.60	3188
Range	0-10.55	34.59	27.48	1092
	10.56-20.55	34.88	20.68	209
	20.56-30.55	24.77	12.25	319
	30.56-40.55	32.27	24.58	334
	40.56-50.55	34.80	20.49	229
	50.56-60.55	44.87	38.53	1005
	Total	36.64	30.03	3188
Skewness	0-10.55	0.08	0.55	1092
	10.56-20.55	0.07	0.56	209
	20.56-30.55	0.09	0.57	319
	30.56-40.55	0.10	0.59	334
	40.56-50.55	0.07	0.60	229
	50.56-60.55	0.18	0.66	1005
	Total	0.11	0.60	3188
TotalEnergy	0-10.55	1336400.00	1707180.00	1092
	10.56-20.55	1961500.00	3158110.00	209
	20.56-30.55	1848800.00	1678850.00	319
	30.56-40.55	1935700.00	1680790.00	334
	40.56-50.55	1972600.00	2265610.00	229
	50.56-60.55	2570000.00	2021230.00	1005
	Total	1926000.00	2032240.00	3188
Uniformity	0-10.55	0.65	0.19	1092
	10.56-20.55	0.63	0.18	209
	20.56-30.55	0.71	0.20	319
	30.56-40.55	0.65	0.19	334
	40.56-50.55	0.63	0.18	229
	50.56-60.55	0.59	0.20	1005
	Total	0.63	0.20	3188
Variance	0-10.55	202.73	1015.50	1092
	10.56-20.55	114.99	186.83	209
	20.56-30.55	57.39	59.86	319

	30.56-40.55	125.09	415.37	334
	40.56-50.55	135.97	285.69	229
	50.56-60.55	246.63	783.73	1005
	Total	183.34	759.49	3188

Multivariate Tests(c)						
Effect		Value	F	Hypothesis df	Error df	Sig.
Intercept	Pillai's Trace	0.995	4.325E4a	16	3161.00	0
Dosegr	Pillai's Trace	0.184	7.578	80	15820.00	P <0.001**
time_days	Pillai's Trace	0.02	4.123a	16	3161.00	P <0.001**
dosegr * time_days	Pillai's Trace	0.029	1.136	80	15820.00	0.191
a. Exact statistic						
b. The statistic is an upper bound on F that yields a lower bound on the significance level.						
c. Design: Intercept + dosegr + time_days + dosegr * time_days						

Note : * indicates p value is significant at 0.05 means P <0.05
**** indicates p value is significant at 0.05 means P <0.001**

In this table : Effect of dose on Texture features is significant. P value of test statistic pillai's trace is <0.001
Effect of Time on Texture features is also significant. P value of test statistic pillai's trace is <0.001

There was a statistically significant differences in TA feature based on a dose level in groups, F (80, 15820) = 7.578, p < .001; Pillai trace = 0.184,

statistically significant differences also found in TA feature based on a Time , F (16, 3161) = 4.12, p < .001; Pillai trace = 0.02

Tests of Between-Subjects Effects						
Source	Dependent Variable	Type III Sum of Squares	df	Mean Square	F	Sig.
Corrected Model	@10Percentile	628148.094a	11	57104.37	14.54	0
	@90Percentile	883634.787b	11	80330.44	16.99	0
	Contrast	36.478c	11	3.32	6.03	0
	Correlation	4.124d	11	0.38	3.12	0
	Energy	1.264E14e	11	11490000000000.00	17.96	0
	Entropy	45.033f	11	4.09	18.12	0
	Kurtosis	20.288g	11	1.84	1.30	0.217
	Maximum	1.031E6h	11	93703.10	17.46	0
	Mean	742205.422i	11	67473.22	16.06	0
	MeanAbsoluteDeviation	5873.279j	11	533.93	8.30	0
	Median	741225.071k	11	67384.10	16.18	0
	Minimum	571620.566l	11	51965.51	13.85	0
	Range	148545.769m	11	13504.16	15.74	0
	Skewness	8.739n	11	0.79	2.23	0.011
	TotalEnergy	1.055E15o	11	95900000000000.00	25.16	0
	Uniformity	5.623p	11	0.51	13.71	0
	Variance	1.273E7q	11	1157219.79	2.01	0.024
Intercept	@10Percentile	35170000.00	1	35170000.00	8955.00	0
	@90Percentile	44040000.00	1	44040000.00	9314.00	0
	Contrast	204.49	1	204.49	372.02	0
	Correlation	23.11	1	23.11	192.20	0
	Energy	815000000000000.00	1	815000000000000.00	1274.00	0
	Entropy	717.36	1	717.36	3176.00	0
	Kurtosis	6486.53	1	6486.53	4578.00	0
	Maximum	47100000.00	1	47100000.00	8775.00	0
	Mean	39400000.00	1	39400000.00	9375.00	0
	MeanAbsoluteDeviation	60054.70	1	60054.70	933.66	0
	Median	39280000.00	1	39280000.00	9432.00	0
	Minimum	33110000.00	1	33110000.00	8826.00	0
	Range	1228249.14	1	1228249.14	1432.00	0
	Skewness	12.30	1	12.30	34.57	0

	TotalEnergy	4373000000000000.00	1	4373000000000000.00	1147.00	0
	Uniformity	341.66	1	341.66	9163.00	0
	Variance	22390000.00	1	22390000.00	38.95	0
Dosegr	@10Percentile	164026.50	5	32805.30	8.35	P <0.001**
	@90Percentile	266979.07	5	53395.82	11.29	P <0.001**
	Contrast	14.02	5	2.81	5.10	P <0.001**
	Correlation	2.08	5	0.42	3.45	0.004*
	Energy	49910000000000.00	5	9982000000000.00	15.60	P <0.001**
	Entropy	16.57	5	3.31	14.67	P <0.001**
	Kurtosis	10.09	5	2.02	1.42	0.212
	Maximum	333542.27	5	66708.45	12.43	P <0.001**
	Mean	206871.17	5	41374.24	9.85	P <0.001**
	MeanAbsoluteDeviation	2631.89	5	526.38	8.18	P <0.001**
	Median	199981.94	5	39996.39	9.61	P <0.001**
	Minimum	146744.37	5	29348.87	7.82	P <0.001**
	Range	66702.98	5	13340.60	15.55	P <0.001**
	Skewness	3.86	5	0.77	2.17	0.055
	TotalEnergy	598500000000000.00	5	119700000000000.00	31.40	P <0.001**
	Uniformity	1.75	5	0.35	9.40	P <0.001**
	Variance	6017477.66	5	1203495.53	2.09	0.063

time_days	@10Percentile	148096.93	1	148096.93	37.71	P <0.001**
	@90Percentile	197552.39	1	197552.39	41.78	P <0.001**
	Contrast	2.04	1	2.04	3.72	0.054
	Correlation	0.67	1	0.67	5.55	0.019*
	Energy	12850000000000.00	1	12850000000000.00	20.08	P <0.001**
	Entropy	5.76	1	5.76	25.51	P <0.001**
	Kurtosis	2.22	1	2.22	1.56	0.211
	Maximum	221688.77	1	221688.77	41.31	P <0.001**
	Mean	172346.93	1	172346.93	41.01	P <0.001**
	MeanAbsoluteDeviation	409.86	1	409.86	6.37	0.012*
	Median	171948.38	1	171948.38	41.29	P <0.001**
	Minimum	133204.80	1	133204.80	35.50	P <0.001**
	Range	11207.62	1	11207.62	13.06	P <0.001**
	Skewness	0.47	1	0.47	1.31	0.253
	TotalEnergy	113800000000000.00	1	113800000000000.00	29.86	P <0.001**
	Uniformity	0.86	1	0.86	23.17	P <0.001**
	Variance	186119.83	1	186119.83	0.32	0.569
dosegr * time_days	@10Percentile	27876.52	5	5575.31	1.42	0.214
	@90Percentile	34898.98	5	6979.80	1.48	0.194
	Contrast	0.14	5	0.03	0.05	0.998
	Correlation	1.34	5	0.27	2.24	0.048*
	Energy	8052000000000.00	5	1610000000000.00	2.52	0.028*
	Entropy	1.01	5	0.20	0.89	0.486
	Kurtosis	3.16	5	0.63	0.45	0.817
	Maximum	41401.10	5	8280.22	1.54	0.173

	Mean	32727.14	5	6545.43	1.56	0.169
	MeanAbsoluteDeviation	111.94	5	22.39	0.35	0.884
	Median	34022.70	5	6804.54	1.63	0.147
	Minimum	25469.92	5	5093.98	1.36	0.237
	Range	2107.23	5	421.45	0.49	0.783
	Skewness	1.88	5	0.38	1.06	0.384
	TotalEnergy	64770000000000.00	5	12950000000000.00	3.40	0.005*
	Uniformity	0.22	5	0.04	1.16	0.327
	Variance	172825.20	5	34565.04	0.06	0.998
Error	@10Percentile	12470000.00	3176	3927.14		
	@90Percentile	15020000.00	3176	4728.15		
	Contrast	1745.82	3176	0.55		
	Correlation	381.83	3176	0.12		
	Energy	2032000000000000.00	3176	639900000000.00		
	Entropy	717.41	3176	0.23		
	Kurtosis	4500.46	3176	1.42		
	Maximum	17050000.00	3176	5366.84		
	Mean	13350000.00	3176	4202.54		
	MeanAbsoluteDeviation	204285.50	3176	64.32		
	Median	13230000.00	3176	4164.18		
	Minimum	11920000.00	3176	3751.79		
	Range	2724983.33	3176	857.99		
	Skewness	1129.82	3176	0.36		
	TotalEnergy	12110000000000000.00	3176	3812000000000.00		
	Uniformity	118.43	3176	0.04		
	Variance	1826000000.00	3176	574818.04		
Total	@10Percentile	132200000.00	3188			
	@90Percentile	165800000.00	3188			

	Contrast	2435.77	3188			
	Correlation	503.24	3188			
	Energy	4954000000000000.00	3188			
	Entropy	3138.74	3188			
	Kurtosis	27508.50	3188			
	Maximum	178500000.00	3188			
	Mean	147800000.00	3188			
	MeanAbsoluteDeviation	423751.09	3188			
	Median	147200000.00	3188			
	Minimum	124800000.00	3188			
	Range	7153553.17	3188			
	Skewness	1179.93	3188			
	TotalEnergy	24990000000000000.00	3188			
	Uniformity	1400.95	3188			
	Variance	1946000000.00	3188			
Corrected Total	@10Percentile	13100000.00	3187			
	@90Percentile	15900000.00	3187			
	Contrast	1782.29	3187			
	Correlation	385.96	3187			
	Energy	21590000000000000.00	3187			
	Entropy	762.45	3187			
	Kurtosis	4520.75	3187			
	Maximum	18080000.00	3187			
	Mean	14090000.00	3187			

	MeanAbsoluteDeviation	210158.78	3187			
	Median	13970000.00	3187			
	Minimum	12490000.00	3187			
	Range	2873529.10	3187			
	Skewness	1138.56	3187			
	TotalEnergy	131600000000000000.00	3187			
	Uniformity	124.05	3187			
	Variance	1838000000.00	3187			

a. R Squared = .048 (Adjusted R Squared = .045)
b. R Squared = .056 (Adjusted R Squared = .052)
c. R Squared = .020 (Adjusted R Squared = .017)
d. R Squared = .011 (Adjusted R Squared = .007)
e. R Squared = .059 (Adjusted R Squared = .055)
f. R Squared = .059 (Adjusted R Squared = .056)
g. R Squared = .004 (Adjusted R Squared = .001)
h. R Squared = .057 (Adjusted R Squared = .054)
i. R Squared = .053 (Adjusted R Squared = .049)
j. R Squared = .028 (Adjusted R Squared = .025)
k. R Squared = .053 (Adjusted R Squared = .050)
l. R Squared = .046 (Adjusted R Squared = .042)
m. R Squared = .052 (Adjusted R Squared = .048)
n. R Squared = .008 (Adjusted R Squared = .004)
o. R Squared = .080 (Adjusted R Squared = .077)
p. R Squared = .045 (Adjusted R Squared = .042)
q. R Squared = .007 (Adjusted R Squared = .003)

Note : * indicates p value is significant at 0.05 means P <0.05
**** indicates p value is significant at 0.05 means P <0.001**

REGIONWISE ANALYSIS

1.Region = ANT.CC

Between-Subjects Factors[a]			
		Value Label	N
dose (Binned)	1	0- 10.55	104
	2	10.56- 20.55	6
	3	20.56- 30.55	45
	4	30.56- 40.55	59
	5	40.56- 50.55	43
	6	50.56-60.55	34
a. region = ANT.CC			

Descriptive Statistics[a]				
	dose (Binned)	Mean	Std. Deviation	N
@10Percentile	0- 10.55	157.42	66.37	104.00
	10.56- 20.55	198.35	45.74	6.00
	20.56- 30.55	157.99	64.68	45.00
	30.56- 40.55	138.27	41.49	59.00
	40.56- 50.55	150.71	37.79	43.00
	50.56-60.55	149.30	41.15	34.00
	Total	152.53	55.49	291.00
@90Percentile	0- 10.55	182.06	60.12	104.00
	10.56- 20.55	221.22	44.38	6.00
	20.56- 30.55	172.04	66.41	45.00
	30.56- 40.55	155.94	46.64	59.00
	40.56- 50.55	176.80	48.08	43.00
	50.56-60.55	171.59	48.11	34.00
	Total	174.02	56.20	291.00
Contrast	0- 10.55	0.35	0.33	104.00
	10.56- 20.55	0.68	0.54	6.00
	20.56- 30.55	0.30	0.27	45.00
	30.56- 40.55	0.42	0.93	59.00

	40.56- 50.55	1.18	1.99	43.00
	50.56-60.55	0.54	0.68	34.00
	Total	0.51	0.97	291.00
correlation	0- 10.55	0.25	0.50	104.00
	10.56- 20.55	0.15	0.43	6.00
	20.56- 30.55	0.26	0.55	45.00
	30.56- 40.55	0.25	0.49	59.00
	40.56- 50.55	-0.04	0.40	43.00
	50.56-60.55	0.26	0.51	34.00
	Total	0.21	0.50	291.00
Energy	0- 10.55	285590.00	216056.00	104.00
	10.56- 20.55	364550.00	149041.00	6.00
	20.56- 30.55	217650.00	222013.00	45.00
	30.56- 40.55	202670.00	147986.00	59.00
	40.56- 50.55	198460.00	141960.00	43.00
	50.56-60.55	234330.00	136609.00	34.00
	Total	241040.00	188545.00	291.00
Entropy	0- 10.55	0.69	0.47	104.00
	10.56- 20.55	1.01	0.65	6.00
	20.56- 30.55	0.55	0.43	45.00
	30.56- 40.55	0.66	0.47	59.00
	40.56- 50.55	0.97	0.50	43.00
	50.56-60.55	0.74	0.58	34.00
	Total	0.71	0.50	291.00
Kurtosis	0- 10.55	2.32	0.87	104.00
	10.56- 20.55	2.84	0.95	6.00
	20.56- 30.55	2.19	0.70	45.00
	30.56- 40.55	2.29	1.00	59.00
	40.56- 50.55	2.52	0.77	43.00
	50.56-60.55	2.18	0.77	34.00
	Total	2.32	0.85	291.00

maximum	0- 10.55	186.42	60.64	104.00
	10.56- 20.55	230.15	47.64	6.00
	20.56- 30.55	174.51	66.95	45.00
	30.56- 40.55	160.45	49.02	59.00
	40.56- 50.55	182.60	51.02	43.00
	50.56-60.55	176.58	51.40	34.00
	Total	178.50	57.73	291.00
Mean	0- 10.55	169.37	59.72	104.00
	10.56- 20.55	209.09	45.12	6.00
	20.56- 30.55	165.16	65.39	45.00
	30.56- 40.55	146.97	43.67	59.00
	40.56- 50.55	163.46	41.30	43.00
	50.56-60.55	159.67	43.81	34.00
	Total	162.99	53.95	291.00
MeanAbsoluteDeviation	0- 10.55	10.20	19.71	104.00
	10.56- 20.55	8.94	4.65	6.00
	20.56- 30.55	5.29	2.74	45.00
	30.56- 40.55	6.68	4.30	59.00
	40.56- 50.55	10.04	10.00	43.00
	50.56-60.55	8.56	6.31	34.00
	Total	8.49	12.88	291.00
Median	0- 10.55	168.56	59.55	104.00
	10.56- 20.55	207.49	46.39	6.00
	20.56- 30.55	165.64	65.13	45.00
	30.56- 40.55	146.50	43.04	59.00
	40.56- 50.55	162.91	41.73	43.00
	50.56-60.55	157.59	42.41	34.00
	Total	162.32	53.66	291.00
Minimum	0- 10.55	154.90	65.77	104.00
	10.56- 20.55	192.60	46.96	6.00
	20.56- 30.55	155.20	64.16	45.00

	30.56- 40.55	135.53	41.47	59.00
	40.56- 50.55	145.55	37.25	43.00
	50.56-60.55	146.25	41.63	34.00
	Total	149.40	55.12	291.00
Range	0- 10.55	31.52	42.23	104.00
	10.56- 20.55	37.55	21.49	6.00
	20.56- 30.55	19.31	11.14	45.00
	30.56- 40.55	24.92	16.77	59.00
	40.56- 50.55	37.05	31.99	43.00
	50.56-60.55	30.33	19.67	34.00
	Total	29.10	30.66	291.00
Skewness	0- 10.55	0.21	0.64	104.00
	10.56- 20.55	0.34	0.89	6.00
	20.56- 30.55	-0.07	0.58	45.00
	30.56- 40.55	0.14	0.61	59.00
	40.56- 50.55	0.06	0.78	43.00
	50.56-60.55	0.19	0.58	34.00
	Total	0.13	0.65	291.00
TotalEnergy	0- 10.55	325920.00	282040.00	104.00
	10.56- 20.55	347660.00	142136.00	6.00
	20.56- 30.55	822280.00	912140.00	45.00
	30.56- 40.55	538060.00	356210.00	59.00
	40.56- 50.55	464710.00	283537.00	43.00
	50.56-60.55	618350.00	460609.00	34.00
	Total	500810.00	495564.00	291.00
Uniformity	0- 10.55	0.69	0.21	104.00
	10.56- 20.55	0.58	0.26	6.00
	20.56- 30.55	0.74	0.20	45.00
	30.56- 40.55	0.70	0.21	59.00
	40.56- 50.55	0.59	0.20	43.00

	50.56-60.55	0.68	0.25	34.00
	Total	0.68	0.22	291.00
Variance	0- 10.55	511.23	2027.30	104.00
	10.56- 20.55	154.33	137.37	6.00
	20.56- 30.55	52.73	61.26	45.00
	30.56- 40.55	88.18	184.78	59.00
	40.56- 50.55	269.07	601.45	43.00
	50.56-60.55	148.92	236.28	34.00
	Total	269.08	1250.25	291.00
a. region = ANT.CC				

Multivariate Tests[c,d]

Effect		Value	F	Hypothesis df	Error df	Sig.
Intercept	Pillai's Trace	1.00	3519.00	16.00	264.00	0.00
time_days	Pillai's Trace	0.07	1.177[a]	16.00	264.00	0.29
dosegr	Pillai's Trace	0.56	2.11	80.00	1340.00	<0.001**
dosegr * time_days	Pillai's Trace	0.25	0.86	80.00	1340.00	0.80
a. Exact statistic						
b. The statistic is an upper bound on F that yields a lower bound on the significance level.						
c. region = ANT.CC						
d. Design: Intercept + time_days + dosegr + dosegr * time_days						

Note : * indicates p value is significant at 0.05 means P <0.05
**** indicates p value is significant at 0.05 means P <0.01**

In this table : Effect of dose on TA features is significant. P value of test statistic pillai's trace is <0.001

there is no significant effect of time on TA features as p value of test statistic pillai's trace is 0.287 > 005 and also interaction effect of dose and time is not significant as p value of test statistic pillai's trace is 0.796.

There was a statistically significant differences in TA feature based on a dose level in groups, F (80, 1340) = 2.108, p < .0005; Pillai trace = 0.559,

We can see from this table that dose level has a statistically significant effect on TA features like, contrast Correlation, Entropy, Total Energy, and Uniformity.

Tests of Between-Subjects Effects[r]						
Source	Dependent Variable	Type III Sum of Squares	df	Mean Square	F	Sig.
Corrected Model	@10Percentile	55874.708[a]	11	5079.519	1.693	.074
	@90Percentile	77846.268[b]	11	7076.933	2.356	.009
	Contrast	28.629[c]	11	2.603	2.985	.001
	correlation	4.205[d]	11	.382	1.564	.109
	Energy	8.527E11[e]	11	7.752E10	2.287	.011
	Entropy	5.946[f]	11	.541	2.287	.011
	Kurtosis	7.185[g]	11	.653	.894	.547
	maximum	82825.389[h]	11	7529.581	2.377	.008
	Mean	64207.682[i]	11	5837.062	2.089	.021
	MeanAbsoluteDeviation	1279.154[j]	11	116.287	.693	.745
	Median	63914.139[k]	11	5810.376	2.103	.020
	Minimum	53339.401[l]	11	4849.036	1.634	.089
	Range	11032.358[m]	11	1002.942	1.070	.386
	Skewness	5.596[n]	11	.509	1.215	.276
	TotalEnergy	1.174E13[o]	11	1.067E12	5.006	.000
	Uniformity	.895[p]	11	.081	1.807	.053
	Variance	1.159E7[q]	11	1053263.405	.665	.771
Intercept	@10Percentile	1420227.518	1	1420227.518	473.433	.000
	@90Percentile	1818438.501	1	1818438.501	605.359	.000
	Contrast	18.952	1	18.952	21.736	.000
	correlation	1.757	1	1.757	7.189	.008
	Energy	4.021E12	1	4.021E12	118.641	.000
	Entropy	32.821	1	32.821	138.897	.000
	Kurtosis	296.031	1	296.031	405.207	.000
	maximum	1904447.350	1	1904447.350	601.300	.000
	Mean	1607031.151	1	1607031.151	575.012	.000
	MeanAbsoluteDeviation	3746.248	1	3746.248	22.321	.000
	Median	1599907.153	1	1599907.153	578.947	.000
	Minimum	1346295.213	1	1346295.213	453.792	.000
	Range	48275.795	1	48275.795	51.484	.000
	Skewness	.002	1	.002	.004	.952
	TotalEnergy	1.923E13	1	1.923E13	90.220	.000
	Uniformity	21.572	1	21.572	479.321	.000
	Variance	2271497.903	1	2271497.903	1.435	.232
time_days	@10Percentile	6602.737	1	6602.737	2.201	.139
	@90Percentile	7810.946	1	7810.946	2.600	.108
	Contrast	.097	1	.097	.112	.738

	correlation	.004	1	.004	.018	.893
	Energy	8.602E10	1	8.602E10	2.538	.112
	Entropy	.140	1	.140	.594	.441
	Kurtosis	.065	1	.065	.089	.765
	maximum	6748.551	1	6748.551	2.131	.145
	Mean	7207.996	1	7207.996	2.579	.109
	MeanAbsoluteDeviation	8.484	1	8.484	.051	.822
	Median	7914.841	1	7914.841	2.864	.092
	Minimum	5537.748	1	5537.748	1.867	.173
	Range	59.807	1	59.807	.064	.801
	Skewness	1.854	1	1.854	4.427	.036
	TotalEnergy	7.690E11	1	7.690E11	3.607	.059
	Uniformity	.021	1	.021	.459	.499
	Variance	5572.733	1	5572.733	.004	.953
dosegr	@10Percentile	12284.135	5	2456.827	.819	.537
	@90Percentile	15465.284	5	3093.057	1.030	.400
	Contrast	5.997	5	1.199	1.375	**.044***
	correlation	2.867	5	.573	2.346	**.042***
	Energy	2.013E11	5	4.026E10	1.188	.315
	Entropy	3.275	5	.655	2.772	**.018***
	Kurtosis	3.186	5	.637	.872	.500
	maximum	13236.272	5	2647.254	.836	.525
	Mean	12987.486	5	2597.497	.929	.462
	MeanAbsoluteDeviation	511.037	5	102.207	.609	.693
	Median	13230.403	5	2646.081	.958	.444
	Minimum	11678.816	5	2335.763	.787	.560
	Range	2989.707	5	597.941	.638	.671
	Skewness	1.467	5	.293	.701	.623
	TotalEnergy	7.361E12	5	1.472E12	6.906	**.000****
	Uniformity	.523	5	.105	2.326	**.043***
	Variance	6406658.102	5	1281331.620	.809	.544
dosegr * time_days	@10Percentile	2321.003	5	464.201	.155	.978
	@90Percentile	3408.207	5	681.641	.227	.951
	Contrast	3.321	5	.664	.762	.578
	correlation	.998	5	.200	.816	.539
	Energy	3.594E10	5	7.189E9	.212	.957
	Entropy	.625	5	.125	.529	.755
	Kurtosis	2.107	5	.421	.577	.718
	maximum	4446.344	5	889.269	.281	.923
	Mean	2681.876	5	536.375	.192	.965

	MeanAbsoluteDeviation	105.702	5	21.140	.126	.986
	Median	2472.996	5	494.599	.179	.970
	Minimum	2442.834	5	488.567	.165	.975
	Range	549.206	5	109.841	.117	.989
	Skewness	2.219	5	.444	1.060	.383
	TotalEnergy	1.058E12	5	2.116E11	.992	.423
	Uniformity	.156	5	.031	.694	.628
	Variance	606457.619	5	121291.524	.077	.996
Error	@10Percentile	836957.145	279	2999.846		
	@90Percentile	838088.039	279	3003.900		
	Contrast	243.272	279	.872		
	correlation	68.197	279	.244		
	Energy	9.457E12	279	3.389E10		
	Entropy	65.927	279	.236		
	Kurtosis	203.828	279	.731		
	maximum	883653.641	279	3167.217		
	Mean	779742.526	279	2794.776		
	MeanAbsoluteDeviation	46825.502	279	167.833		
	Median	771010.793	279	2763.480		
	Minimum	827727.568	279	2966.765		
	Range	261615.440	279	937.690		
	Skewness	116.808	279	.419		
	TotalEnergy	5.948E13	279	2.132E11		
	Uniformity	12.557	279	.045		
	Variance	4.417E8	279	1583227.945		
Total	@10Percentile	7662932.049	291			
	@90Percentile	9728549.444	291			
	Contrast	346.999	291			
	correlation	84.858	291			
	Energy	2.722E13	291			
	Entropy	220.476	291			
	Kurtosis	1776.362	291			
	maximum	1.024E7	291			
	Mean	8574530.867	291			
	MeanAbsoluteDeviation	69066.593	291			
	Median	8502257.236	291			
	Minimum	7376685.904	291			
	Range	519004.961	291			
	Skewness	127.423	291			
	TotalEnergy	1.442E14	291			

	Uniformity	149.616	291			
	Variance	4.744E8	291			
Corrected Total	@10Percentile	892831.853	290			
	@90Percentile	915934.307	290			
	Contrast	271.901	290			
	correlation	72.403	290			
	Energy	1.031E13	290			
	Entropy	71.872	290			
	Kurtosis	211.012	290			
	maximum	966479.030	290			
	Mean	843950.209	290			
	MeanAbsoluteDeviation	48104.656	290			
	Median	834924.932	290			
	Minimum	881066.969	290			
	Range	272647.799	290			
	Skewness	122.404	290			
	TotalEnergy	7.122E13	290			
	Uniformity	13.451	290			
	Variance	4.533E8	290			
a. R Squared = .063 (Adjusted R Squared = .026)						
b. R Squared = .085 (Adjusted R Squared = .049)						
c. R Squared = .105 (Adjusted R Squared = .070)						
d. R Squared = .058 (Adjusted R Squared = .021)						
e. R Squared = .083 (Adjusted R Squared = .047)						
f. R Squared = .083 (Adjusted R Squared = .047)						
g. R Squared = .034 (Adjusted R Squared = -.004)						
h. R Squared = .086 (Adjusted R Squared = .050)						
i. R Squared = .076 (Adjusted R Squared = .040)						
j. R Squared = .027 (Adjusted R Squared = -.012)						
k. R Squared = .077 (Adjusted R Squared = .040)						
l. R Squared = .061 (Adjusted R Squared = .023)						
m. R Squared = .040 (Adjusted R Squared = .003)						
n. R Squared = .046 (Adjusted R Squared = .008)						
o. R Squared = .165 (Adjusted R Squared = .132)						
p. R Squared = .067 (Adjusted R Squared = .030)						
q. R Squared = .026 (Adjusted R Squared = -.013)						
r. region = ANT.CC						

Note : * indicates p value is significant at 0.05 means P <0.05

** indicates p value is significant at 0.05 means P <0.01

2.Region = L.CER

Between-Subjects Factors[a]			
		Value Label	N
dose (Binned)	1	0- 10.55	127
	2	10.56- 20.55	13
	3	20.56- 30.55	31
	6	50.56-60.55	121

Descriptive Statistics				
	dose (Binned)	Mean	Std. Deviation	N
@10Percentile	0- 10.55	203.94	61.27	127.00
	10.56- 20.55	192.72	53.37	13.00
	20.56- 30.55	189.27	53.89	31.00
	50.56-60.55	186.60	50.88	121.00
	Total	194.70	56.37	292.00
@90Percentile	0- 10.55	222.07	66.81	127.00
	10.56- 20.55	207.09	58.25	13.00
	20.56- 30.55	204.82	56.82	31.00
	50.56-60.55	205.29	54.84	121.00
	Total	212.62	60.95	292.00
Contrast	0- 10.55	0.30	0.18	127.00
	10.56- 20.55	0.19	0.17	13.00
	20.56- 30.55	0.27	0.20	31.00
	50.56-60.55	0.32	0.22	121.00
	Total	0.30	0.20	292.00
correlation	0- 10.55	0.19	0.33	127.00
	10.56- 20.55	0.39	0.46	13.00
	20.56- 30.55	0.19	0.38	31.00
	50.56-60.55	0.19	0.35	121.00
	Total	0.20	0.35	292.00
Energy	0- 10.55	1099000.00	719947.00	127.00
	10.56- 20.55	985080.00	553223.00	13.00
	20.56- 30.55	785470.00	566626.00	31.00
	50.56-60.55	899540.00	678355.00	121.00
	Total	977990.00	687611.00	292.00
Entropy	0- 10.55	0.74	0.39	127.00

	10.56- 20.55	0.50	0.40	13.00
	20.56- 30.55	0.62	0.40	31.00
	50.56-60.55	0.75	0.42	121.00
	Total	0.72	0.41	292.00
Kurtosis	0- 10.55	2.60	0.73	127.00
	10.56- 20.55	2.52	0.58	13.00
	20.56- 30.55	2.70	0.65	31.00
	50.56-60.55	2.70	0.86	121.00
	Total	2.65	0.77	292.00
maximum	0- 10.55	226.88	68.24	127.00
	10.56- 20.55	210.58	58.69	13.00
	20.56- 30.55	209.77	57.14	31.00
	50.56-60.55	210.75	56.24	121.00
	Total	217.66	62.17	292.00
Mean	0- 10.55	212.99	63.78	127.00
	10.56- 20.55	199.59	55.64	13.00
	20.56- 30.55	197.15	55.25	31.00
	50.56-60.55	195.84	52.77	121.00
	Total	203.60	58.49	292.00
MeanAbsoluteDeviation	0- 10.55	6.11	2.92	127.00
	10.56- 20.55	4.73	1.97	13.00
	20.56- 30.55	5.11	1.93	31.00
	50.56-60.55	6.26	2.69	121.00
	Total	6.00	2.72	292.00
Median	0- 10.55	213.12	63.95	127.00
	10.56- 20.55	199.42	56.09	13.00
	20.56- 30.55	197.08	55.28	31.00
	50.56-60.55	195.75	52.67	121.00
	Total	203.61	58.57	292.00
Minimum	0- 10.55	198.59	60.03	127.00
	10.56- 20.55	188.90	51.37	13.00
	20.56- 30.55	185.51	53.01	31.00
	50.56-60.55	181.54	50.12	121.00
	Total	189.71	55.31	292.00
Range	0- 10.55	28.29	12.44	127.00
	10.56- 20.55	21.68	8.77	13.00
	20.56- 30.55	24.26	9.02	31.00
	50.56-60.55	29.21	12.03	121.00
	Total	27.95	11.93	292.00
Skewness	0- 10.55	-0.04	0.50	127.00
	10.56- 20.55	0.14	0.49	13.00
	20.56- 30.55	0.11	0.48	31.00
	50.56-60.55	0.08	0.55	121.00

	Total	0.03	0.52	292.00
TotalEnergy	0- 10.55	1506900.00	1917550.00	127.00
	10.56- 20.55	1676200.00	1387570.00	13.00
	20.56- 30.55	2201700.00	1206270.00	31.00
	50.56-60.55	2472600.00	1653870.00	121.00
	Total	1988400.00	1776880.00	292.00
Uniformity	0- 10.55	0.67	0.18	127.00
	10.56- 20.55	0.77	0.19	13.00
	20.56- 30.55	0.72	0.19	31.00
	50.56-60.55	0.67	0.19	121.00
	Total	0.68	0.19	292.00
Variance	0- 10.55	67.11	74.56	127.00
	10.56- 20.55	37.34	31.02	13.00
	20.56- 30.55	46.65	42.16	31.00
	50.56-60.55	69.57	62.56	121.00
	Total	64.63	65.76	292.00
a. region = L.CER				

Multivariate Tests[c,d]

Effect		Value	F	Hypothesis df	Error df	Sig.
Intercept	Pillai's Trace	0.998	6.828E3[a]	16	269	0
time_days	Pillai's Trace	0.098	1.834[a]	16	269	0.027
dosegr	Pillai's Trace	0.331	2.103	48	813	<0.001 **
dosegr * time_days	Pillai's Trace	0.177	1.064	48	813	0.36
a. Exact statistic						
b. The statistic is an upper bound on F that yields a lower bound on the significance level.						
c. region = L.CER						
d. Design: Intercept + time_days + dosegr + dosegr * time_days						

Note : * indicates p value is significant at 0.05 means P <0.05

**** indicates p value is significant at 0.05 means P <0.01**

There was a statistically significant difference in TA features based on time in days, F (16, 269) = 1.834, p < 0.05, Pillai's Trace = **0.098**

And dose levels , F (48, 813) = 2.103, p < 0.05 Pillai Trace = 0.33

Tests of Between-Subjects Effects[r]						
Source	Dependent Variable	Type III Sum of Squares	df	Mean Square	F	Sig.
Corrected Model	@10Percentile	46388.146[a]	7	6626.88	2.14	0.039
	@90Percentile	57982.556[b]	7	8283.22	2.30	0.027
	Contrast	.524[c]	7	0.08	1.83	0.081
	correlation	1.619[d]	7	0.23	1.91	0.068
	Energy	7.470E12[e]	7	1067000000000.00	2.33	0.025
	Entropy	1.909[f]	7	0.27	1.66	0.118
	Kurtosis	2.635[g]	7	0.38	0.63	0.735
	maximum	59152.899[h]	7	8450.41	2.25	0.03
	Mean	51894.599[i]	7	7413.51	2.23	0.032
	MeanAbsoluteDeviation	159.939[j]	7	22.85	3.25	0.002
	Median	52160.569[k]	7	7451.51	2.24	0.031
	Minimum	44007.524[l]	7	6286.79	2.11	0.043
	Range	3131.790[m]	7	447.40	3.32	0.002
	Skewness	2.823[n]	7	0.40	1.50	0.167
	TotalEnergy	9.485E13[o]	7	13550000000000.00	4.67	0
	Uniformity	.322[p]	7	0.05	1.31	0.243
	Variance	74767.690[q]	7	10681.10	2.56	0.014
Intercept	@10Percentile	2183295.70	1	2183295.70	705.97	0
	@90Percentile	2606173.03	1	2606173.03	723.56	0
	Contrast	4.43	1	4.43	108.33	0
	correlation	2.20	1	2.20	18.20	0
	Energy	56510000000000.00	1	56510000000000.00	123.35	0
	Entropy	24.38	1	24.38	148.78	0
	Kurtosis	362.82	1	362.82	602.79	0
	maximum	2728552.66	1	2728552.66	727.28	0
	Mean	2386949.67	1	2386949.67	718.47	0
	MeanAbsoluteDeviation	1975.29	1	1975.29	281.34	0
	Median	2380555.46	1	2380555.46	714.67	0

	Minimum	2091811.28	1	2091811.28	702.14	0
	Range	42239.94	1	42239.94	313.62	0
	Skewness	1.40	1	1.40	5.19	0.023
	TotalEnergy	276300000000000.00	1	2763000000000000.00	95.24	0
	Uniformity	27.12	1	27.12	774.45	0
	Variance	229418.32	1	229418.32	55.04	0
time_days	@10Percentile	5627.22	1	5627.22	1.82	0.178
	@90Percentile	8790.23	1	8790.23	2.44	0.119
	Contrast	0.03	1	0.03	0.77	0.381
	correlation	0.18	1	0.18	1.48	0.224
	Energy	562900000000.00	1	562900000000.00	1.23	0.269
	Entropy	0.05	1	0.05	0.28	0.597
	Kurtosis	0.11	1	0.11	0.19	0.665
	maximum	9568.35	1	9568.35	2.55	0.111
	Mean	7040.93	1	7040.93	2.12	0.147
	MeanAbsoluteDeviation	23.22	1	23.22	3.31	0.07
	Median	6670.29	1	6670.29	2.00	0.158
	Minimum	5956.66	1	5956.66	2.00	0.158
	Range	425.95	1	425.95	3.16	0.076
	Skewness	0.74	1	0.74	2.76	0.098
	TotalEnergy	7832000000000.00	1	7832000000000.00	2.70	0.101
	Uniformity	0.00	1	0.00	0.02	0.896
	Variance	9363.34	1	9363.34	2.25	0.135
dosegr	@10Percentile	660.76	3	220.25	0.07	0.975
	@90Percentile	1327.38	3	442.46	0.12	0.947
	Contrast	0.24	3	0.08	1.99	0.115
	correlation	0.72	3	0.24	1.98	0.117
	Energy	668900000000.00	3	223000000000.00	0.49	0.692
	Entropy	0.72	3	0.24	1.47	0.223
	Kurtosis	0.19	3	0.06	0.10	0.959
	maximum	1667.49	3	555.83	0.15	0.931
	Mean	901.28	3	300.43	0.09	0.965
	MeanAbsoluteDeviation	49.85	3	16.62	2.37	0.071
	Median	1000.09	3	333.36	0.10	0.96
	Minimum	394.60	3	131.54	0.04	0.988
	Range	1044.42	3	348.14	2.59	0.053
	Skewness	1.42	3	0.47	1.76	0.155

	TotalEnergy	70530000000000.00	3	23510000000000.00	8.10	**<0.001****
	Uniformity	0.14	3	0.05	1.33	0.266
	Variance	25396.43	3	8465.48	2.03	0.11
dosegr * time_days	@10Percentile	10851.14	3	3617.05	1.17	0.322
	@90Percentile	15114.40	3	5038.13	1.40	0.243
	Contrast	0.23	3	0.08	1.86	0.137
	correlation	1.11	3	0.37	3.06	0.028
	Energy	1880000000000.00	3	626500000000.00	1.37	0.253
	Entropy	0.67	3	0.22	1.35	0.258
	Kurtosis	0.52	3	0.17	0.29	0.835
	maximum	15702.96	3	5234.32	1.40	0.244
	Mean	12865.30	3	4288.44	1.29	0.278
	MeanAbsoluteDeviation	57.99	3	19.33	2.75	**0.043***
	Median	13042.60	3	4347.53	1.31	0.273
	Minimum	9866.65	3	3288.88	1.10	0.348
	Range	1009.84	3	336.61	2.50	0.06
	Skewness	1.37	3	0.46	1.70	0.168
	TotalEnergy	17200000000000.00	3	5735000000000.00	1.98	0.118
	Uniformity	0.13	3	0.04	1.21	0.305
	Variance	25224.46	3	8408.16	2.02	0.112
Error	@10Percentile	878307.94	284	3092.63		
	@90Percentile	1022928.64	284	3601.86		
	Contrast	11.61	284	0.04		
	correlation	34.38	284	0.12		
	Energy	130100000000000.00	284	458200000000.00		
	Entropy	46.54	284	0.16		
	Kurtosis	170.94	284	0.60		
	maximum	1065496.65	284	3751.75		
	Mean	943522.08	284	3322.26		
	MeanAbsoluteDeviation	1993.96	284	7.02		
	Median	946000.73	284	3330.99		

	Minimum	846087.02	284	2979.18		
	Range	38250.04	284	134.68		
	Skewness	76.30	284	0.27		
	TotalEnergy	823900000000000.00	284	2901000000000.00		
	Uniformity	9.94	284	0.04		
	Variance	1183757.88	284	4168.16		
Total	@10Percentile	11990000.00	292			
	@90Percentile	14280000.00	292			
	Contrast	38.25	292			
	correlation	47.68	292			
	Energy	416900000000000.00	292			
	Entropy	200.22	292			
	Kurtosis	2221.05	292			
	maximum	14960000.00	292			
	Mean	13100000.00	292			
	MeanAbsoluteDeviation	12675.55	292			
	Median	13100000.00	292			
	Minimum	11400000.00	292			
	Range	269478.44	292			
	Skewness	79.43	292			
	TotalEnergy	2073000000000000.00	292			
	Uniformity	146.15	292			
	Variance	2478241.12	292			
Corrected Total	@10Percentile	924696.09	291			

	@90Percentile	1080911.20	291			
	Contrast	12.13	291			
	correlation	36.00	291			
	Energy	137600000000000.00	291			
	Entropy	48.45	291			
	Kurtosis	173.58	291			
	maximum	1124649.55	291			
	Mean	995416.68	291			
	MeanAbsoluteDeviation	2153.90	291			
	Median	998161.30	291			
	Minimum	890094.54	291			
	Range	41381.83	291			
	Skewness	79.12	291			
	TotalEnergy	918800000000000.00	291			
	Uniformity	10.27	291			
	Variance	1258525.57	291			
a. R Squared = .050 (Adjusted R Squared = .027)						
b. R Squared = .054 (Adjusted R Squared = .030)						
c. R Squared = .043 (Adjusted R Squared = .020)						
d. R Squared = .045 (Adjusted R Squared = .021)						
e. R Squared = .054 (Adjusted R Squared = .031)						
f. R Squared = .039 (Adjusted R Squared = .016)						
g. R Squared = .015 (Adjusted R Squared = -.009)						
h. R Squared = .053 (Adjusted R Squared = .029)						
i. R Squared = .052 (Adjusted R Squared = .029)						

j. R Squared = .074 (Adjusted R Squared = .051)					
k. R Squared = .052 (Adjusted R Squared = .029)					
l. R Squared = .049 (Adjusted R Squared = .026)					
m. R Squared = .076 (Adjusted R Squared = .053)					
n. R Squared = .036 (Adjusted R Squared = .012)					
o. R Squared = .103 (Adjusted R Squared = .081)					
p. R Squared = .031 (Adjusted R Squared = .008)					
q. R Squared = .059 (Adjusted R Squared = .036)					
r. region = L.CER					

Note : * indicates p value is significant at 0.05 means P <0.05
**** indicates p value is significant at 0.05 means P <0.01**

Conclusion: from this table that dose level has a statistically significant effect on Total Energy TA feature

3.**Region = L.CS**

Between-Subjects Factors[a]			
		Value Label	N
dose (Binned)	1	0- 10.55	135
	2	10.56- 20.55	20
	3	20.56- 30.55	54
	4	30.56- 40.55	57
	5	40.56- 50.55	13
	6	50.56-60.55	13

Descriptive Statistics[a]				
	dose (Binned)	Mean	Std. Deviation	N
@10Percentile	0- 10.55	207.87	72.73	135.00
	10.56- 20.55	206.96	35.06	20.00
	20.56- 30.55	183.22	53.53	54.00
	30.56- 40.55	177.79	52.79	57.00
	40.56- 50.55	193.95	55.30	13.00
	50.56-60.55	203.34	53.19	13.00
	Total	196.56	63.15	292.00
@90Percentile	0- 10.55	223.20	76.54	135.00
	10.56- 20.55	225.27	36.05	20.00
	20.56- 30.55	198.41	55.27	54.00
	30.56- 40.55	195.09	56.72	57.00
	40.56- 50.55	216.81	56.25	13.00
	50.56-60.55	218.09	51.27	13.00
	Total	212.76	66.03	292.00
Contrast	0- 10.55	0.27	0.21	135.00
	10.56- 20.55	0.32	0.17	20.00
	20.56- 30.55	0.30	0.21	54.00
	30.56- 40.55	0.28	0.26	57.00
	40.56- 50.55	0.39	0.25	13.00
	50.56-60.55	0.22	0.15	13.00
	Total	0.28	0.22	292.00
correlation	0- 10.55	0.20	0.36	135.00
	10.56- 20.55	0.11	0.26	20.00
	20.56- 30.55	0.20	0.39	54.00
	30.56- 40.55	0.27	0.39	57.00

	40.56- 50.55	0.18	0.34	13.00
	50.56-60.55	0.16	0.39	13.00
	Total	0.20	0.36	292.00
Energy	0- 10.55	1212500.00	907193.00	135.00
	10.56- 20.55	964280.00	346862.00	20.00
	20.56- 30.55	703180.00	494248.00	54.00
	30.56- 40.55	768160.00	657710.00	57.00
	40.56- 50.55	842850.00	498479.00	13.00
	50.56-60.55	1234900.00	446153.00	13.00
	Total	999100.00	764525.00	292.00
Entropy	0- 10.55	0.65	0.39	135.00
	10.56- 20.55	0.76	0.31	20.00
	20.56- 30.55	0.67	0.40	54.00
	30.56- 40.55	0.65	0.43	57.00
	40.56- 50.55	0.83	0.42	13.00
	50.56-60.55	0.55	0.31	13.00
	Total	0.67	0.39	292.00
Kurtosis	0- 10.55	2.75	0.73	135.00
	10.56- 20.55	2.65	0.78	20.00
	20.56- 30.55	2.76	1.17	54.00
	30.56- 40.55	2.79	1.37	57.00
	40.56- 50.55	2.90	1.30	13.00
	50.56-60.55	2.58	0.52	13.00
	Total	2.75	0.99	292.00
maximum	0- 10.55	228.10	78.07	135.00
	10.56- 20.55	230.35	36.73	20.00
	20.56- 30.55	203.52	55.63	54.00
	30.56- 40.55	206.27	70.59	57.00
	40.56- 50.55	225.86	60.58	13.00
	50.56-60.55	223.12	51.06	13.00
	Total	219.13	69.30	292.00
Mean	0- 10.55	215.39	74.51	135.00
	10.56- 20.55	216.60	35.31	20.00
	20.56- 30.55	190.63	54.55	54.00
	30.56- 40.55	186.42	54.59	57.00

	40.56- 50.55	204.62	55.20	13.00
	50.56-60.55	210.94	52.14	13.00
	Total	204.56	64.48	292.00
MeanAbsoluteDeviation	0- 10.55	5.08	2.48	135.00
	10.56- 20.55	6.05	2.20	20.00
	20.56- 30.55	5.14	2.18	54.00
	30.56- 40.55	6.61	6.35	57.00
	40.56- 50.55	7.87	3.68	13.00
	50.56-60.55	4.87	1.23	13.00
	Total	5.57	3.61	292.00
Median	0- 10.55	215.34	74.65	135.00
	10.56- 20.55	217.08	35.71	20.00
	20.56- 30.55	190.14	55.10	54.00
	30.56- 40.55	185.26	54.26	57.00
	40.56- 50.55	203.24	54.90	13.00
	50.56-60.55	210.72	52.11	13.00
	Total	204.18	64.68	292.00
Minimum	0- 10.55	203.02	70.42	135.00
	10.56- 20.55	201.19	34.97	20.00
	20.56- 30.55	180.17	53.22	54.00
	30.56- 40.55	174.17	51.71	57.00
	40.56- 50.55	189.53	54.37	13.00
	50.56-60.55	198.96	53.21	13.00
	Total	192.26	61.53	292.00
Range	0- 10.55	25.08	12.34	135.00
	10.56- 20.55	29.16	12.44	20.00
	20.56- 30.55	23.35	9.29	54.00
	30.56- 40.55	32.10	42.54	57.00
	40.56- 50.55	36.33	16.52	13.00
	50.56-60.55	24.16	6.53	13.00
	Total	26.87	21.70	292.00
Skewness	0- 10.55	0.07	0.47	135.00
	10.56- 20.55	-0.19	0.43	20.00
	20.56- 30.55	0.28	0.56	54.00
	30.56- 40.55	0.26	0.68	57.00
	40.56- 50.55	0.42	0.62	13.00

	50.56-60.55	0.05	0.34	13.00
	Total	0.14	0.55	292.00
TotalEnergy	0- 10.55	1615000.00	2246720.00	135.00
	10.56- 20.55	1724200.00	1296370.00	20.00
	20.56- 30.55	2450200.00	1909240.00	54.00
	30.56- 40.55	2232200.00	1438810.00	57.00
	40.56- 50.55	3772300.00	2390100.00	13.00
	50.56-60.55	2436500.00	1288730.00	13.00
	Total	2030000.00	2017560.00	292.00
Uniformity	0- 10.55	0.72	0.18	135.00
	10.56- 20.55	0.66	0.15	20.00
	20.56- 30.55	0.70	0.19	54.00
	30.56- 40.55	0.71	0.19	57.00
	40.56- 50.55	0.65	0.19	13.00
	50.56-60.55	0.77	0.15	13.00
	Total	0.71	0.18	292.00
Variance	0- 10.55	49.55	60.59	135.00
	10.56- 20.55	63.88	55.06	20.00
	20.56- 30.55	46.90	43.10	54.00
	30.56- 40.55	193.66	937.67	57.00
	40.56- 50.55	115.10	109.30	13.00
	50.56-60.55	37.25	17.47	13.00
	Total	80.54	418.62	292.00
a. region = L.CS				

Multivariate Tests[c,d]

Effect		Value	F	Hypothesis df	Error df	Sig.
Intercept	Pillai's Trace	1.00	5.227E3[a]	16.00	265.00	<0.001**
time_days	Pillai's Trace	0.06	1.141[a]	16.00	265.00	0.32
dosegr	Pillai's Trace	0.52	1.94	80.00	1345.00	<0.001**
dosegr * time_days	Pillai's Trace	0.22	0.79	80.00	1345.00	0.92
a. Exact statistic						

b. The statistic is an upper bound on F that yields a lower bound on the significance level.					
c. region = L.CS					
d. Design: Intercept + time_days + dosegr + dosegr * time_days					

Note : * indicates p value is significant at 0.05 means P <0.05
**** indicates p value is significant at 0.05 means P <0.01**

There was a statistically significant difference in TA features based on dose levels, F (80, 1345) = 1.94, p < 0.05
Pillai Trace = 0.52

Tests of Between-Subjects Effects[r]						
Source	Dependent Variable	Type III Sum of Squares	df	Mean Square	F	Sig.
Corrected Model	@10Percentile	100021.424[a]	11	9092.86	2.40	0.007
	@90Percentile	103175.644[b]	11	9379.60	2.25	0.012
	Contrast	.525[c]	11	0.05	1.00	0.45
	correlation	1.863[d]	11	0.17	1.29	0.228
	Energy	2.004E13[e]	11	1822000000000.00	3.40	0
	Entropy	1.384[f]	11	0.13	0.80	0.636
	Kurtosis	3.407[g]	11	0.31	0.31	0.984
	maximum	95686.868[h]	11	8698.81	1.87	0.043
	Mean	102310.989[i]	11	9301.00	2.35	0.009
	MeanAbsoluteDeviation	231.935[j]	11	21.09	1.66	0.083
	Median	106700.339[k]	11	9700.03	2.45	0.006
	Minimum	91155.157[l]	11	8286.83	2.30	0.011
	Range	5471.471[m]	11	497.41	1.06	0.395
	Skewness	6.335[n]	11	0.58	2.00	0.028
	TotalEnergy	1.241E14[o]	11	11280000000000.00	2.98	0.001
	Uniformity	.328[p]	11	0.03	0.89	0.546
	Variance	1.005E6[q]	11	91376.32	0.51	0.895

Intercept	@10Percentile	2687599.00	1	2687599.00	709.52	0
	@90Percentile	3166648.21	1	3166648.21	760.78	0
	Contrast	5.78	1	5.78	120.65	0
	correlation	1.24	1	1.24	9.42	0.002
	Energy	73480000000000.00	1	73480000000000.00	137.12	0
	Entropy	31.17	1	31.17	199.19	0
	Kurtosis	475.50	1	475.50	473.06	0
	maximum	3368036.25	1	3368036.25	724.37	0
	Mean	2925207.13	1	2925207.13	739.50	0
	MeanAbsoluteDeviation	2288.13	1	2288.13	180.01	0
	Median	2917380.68	1	2917380.68	735.56	0
	Minimum	2559830.65	1	2559830.65	709.37	0
	Range	55353.84	1	55353.84	117.81	0
	Skewness	0.95	1	0.95	3.30	0.071
	TotalEnergy	507500000000000.00	1	507500000000000.00	134.00	0
	Uniformity	28.89	1	28.89	866.39	0
	Variance	443445.52	1	443445.52	2.48	0.116
time_days	@10Percentile	25407.32	1	25407.32	6.71	**0.01***
	@90Percentile	27718.77	1	27718.77	6.66	**0.01***
	Contrast	0.02	1	0.02	0.39	0.534
	correlation	0.21	1	0.21	1.57	0.211
	Energy	2344000000000.00	1	2344000000000.00	4.37	**0.037***
	Entropy	0.11	1	0.11	0.70	0.402
	Kurtosis	0.52	1	0.52	0.52	0.471
	maximum	29335.02	1	29335.02	6.31	**0.013***
	Mean	27169.47	1	27169.47	6.87	**0.009****
	MeanAbsoluteDeviation	4.37	1	4.37	0.34	0.558

	Median	27777.31	1	27777.31	7.00	**0.009****
	Minimum	23105.62	1	23105.62	6.40	**0.012***
	Range	371.31	1	371.31	0.79	0.375
	Skewness	0.05	1	0.05	0.18	0.671
	TotalEnergy	29770000000000.00	1	29770000000000.00	7.86	**0.005****
	Uniformity	0.01	1	0.01	0.30	0.583
	Variance	133.27	1	133.27	0.00	0.978
dosegr	@10Percentile	25548.62	5	5109.72	1.35	0.244
	@90Percentile	28368.25	5	5673.65	1.36	0.238
	Contrast	0.32	5	0.06	1.33	0.251
	correlation	0.81	5	0.16	1.23	0.294
	Energy	6187000000000.00	5	1237000000000.00	2.31	**0.044***
	Entropy	0.74	5	0.15	0.94	0.456
	Kurtosis	2.31	5	0.46	0.46	0.807
	maximum	28161.67	5	5632.34	1.21	0.304
	Mean	26786.61	5	5357.32	1.35	0.242
	MeanAbsoluteDeviation	39.48	5	7.90	0.62	0.684
	Median	27692.94	5	5538.59	1.40	0.226
	Minimum	21961.14	5	4392.23	1.22	0.301
	Range	1243.89	5	248.78	0.53	0.754
	Skewness	1.92	5	0.38	1.34	0.249
	TotalEnergy	77880000000000.00	5	15580000000000.00	4.11	**0.001****
	Uniformity	0.19	5	0.04	1.14	0.341
	Variance	238635.97	5	47727.19	0.27	0.931
dosegr * time_days	@10Percentile	17200.91	5	3440.18	0.91	0.476
	@90Percentile	15466.41	5	3093.28	0.74	0.592
	Contrast	0.18	5	0.04	0.76	0.579
	correlation	1.39	5	0.28	2.11	0.064
	Energy	1249000000000.00	5	249900000000.00	0.47	0.801
	Entropy	0.35	5	0.07	0.44	0.82
	Kurtosis	2.24	5	0.45	0.45	0.816
	maximum	16298.85	5	3259.77	0.70	0.623
	Mean	16668.48	5	3333.70	0.84	0.52
	Mean Absolute Deviation	15.79	5	3.16	0.25	0.94

	Median	17091.95	5	3418.39	0.86	0.507
	Minimum	16784.61	5	3356.92	0.93	0.462
	Range	327.64	5	65.53	0.14	0.983
	Skewness	0.38	5	0.08	0.27	0.931
	TotalEnergy	235200000000000.00	5	4704000000000.00	1.24	0.29
	Uniformity	0.13	5	0.03	0.80	0.552
	Variance	34620.70	5	6924.14	0.04	0.999
Error	@10Percentile	1060621.18	280	3787.93		
	@90Percentile	1165462.90	280	4162.37		
	Contrast	13.41	280	0.05		
	correlation	36.70	280	0.13		
	Energy	1500000000000000.00	280	535900000000.00		
	Entropy	43.81	280	0.16		
	Kurtosis	281.44	280	1.01		
	maximum	1301899.27	280	4649.64		
	Mean	1107583.07	280	3955.65		
	MeanAbsoluteDeviation	3559.16	280	12.71		
	Median	1110543.92	280	3966.23		
	Minimum	1010412.83	280	3608.62		
	Range	131563.58	280	469.87		
	Skewness	80.53	280	0.29		
	TotalEnergy	10600000000000000.00	280	3787000000000.00		
	Uniformity	9.34	280	0.03		
	Variance	49990000.00	280	178541.79		
Total	@10Percentile	12440000.00	292			
	@90Percentile	14490000.00	292			

	Contrast	37.21	292			
	correlation	50.82	292			
	Energy	461600000000000.00	292			
	Entropy	174.41	292			
	Kurtosis	2497.92	292			
	maximum	15420000.00	292			
	Mean	13430000.00	292			
	MeanAbsoluteDeviation	12852.99	292			
	Median	13390000.00	292			
	Minimum	11890000.00	292			
	Range	347893.55	292			
	Skewness	92.73	292			
	TotalEnergy	2388000000000000.00	292			
	Uniformity	156.38	292			
	Variance	52890000.00	292			
Corrected Total	@10Percentile	1160642.60	291			
	@90Percentile	1268638.54	291			
	Contrast	13.93	291			
	correlation	38.56	291			
	Energy	170100000000000.00	291			
	Entropy	45.20	291			
	Kurtosis	284.85	291			
	maximum	1397586.14	291			
	Mean	1209894.06	291			

	MeanAbsoluteDeviation	3791.09	291			
	Median	1217244.25	291			
	Minimum	1101567.98	291			
	Range	137035.06	291			
	Skewness	86.87	291			
	TotalEnergy	1185000000000000.00	291			
	Uniformity	9.67	291			
	Variance	51000000.00	291			
a. R Squared = .086 (Adjusted R Squared = .050)						
b. R Squared = .081 (Adjusted R Squared = .045)						
c. R Squared = .038 (Adjusted R Squared = .000)						
d. R Squared = .048 (Adjusted R Squared = .011)						
e. R Squared = .118 (Adjusted R Squared = .083)						
f. R Squared = .031 (Adjusted R Squared = -.007)						
g. R Squared = .012 (Adjusted R Squared = -.027)						
h. R Squared = .068 (Adjusted R Squared = .032)						
i. R Squared = .085 (Adjusted R Squared = .049)						
j. R Squared = .061 (Adjusted R Squared = .024)						
k. R Squared = .088 (Adjusted R Squared = .052)						
l. R Squared = .083 (Adjusted R Squared = .047)						
m. R Squared = .040 (Adjusted R Squared = .002)						
n. R Squared = .073 (Adjusted R Squared = .037)						
o. R Squared = .105 (Adjusted R Squared = .070)						
p. R Squared = .034 (Adjusted R Squared = -.004)						
q. R Squared = .020 (Adjusted R Squared = -.019)						
r. region = L.CS						

Note : * indicates p value is significant at 0.05 means P <0.05

**** indicates p value is significant at 0.05 means P <0.01**

Conclusion: from this table that dose level has a statistically significant effect on Energy and Total energy TA feature

Conclusion: from this table that Time in days has a statistically significant effect on @10percentile, @90percentile , Energy , Maximum, Mean, Median , Minimum, Total Energy

Estimated Marginal Means

4.Region = L.THALAMUS

Between-Subjects Factors[a]			
		Value Label	N
dose (Binned)	1	0- 10.55	88
	2	10.56- 20.55	25
	3	20.56- 30.55	21
	4	30.56- 40.55	39
	5	40.56- 50.55	39
	6	50.56-60.55	80
a. region = L.THALAMUS			

Descriptive Statistics[a]				
	dose (Binned)	**Mean**	**Std. Deviation**	**N**
@10Percentile	0- 10.55	228.24	68.19	88
	10.56- 20.55	206.36	82.99	25
	20.56- 30.55	179.37	45.24	21
	30.56- 40.55	212.64	52.84	39
	40.56- 50.55	183.78	54.69	39
	50.56-60.55	208.29	52.34	80
	Total	209.37	62.14	292
@90Percentile	0- 10.55	255.70	74.56	88
	10.56- 20.55	230.62	95.44	25
	20.56- 30.55	198.63	54.73	21
	30.56- 40.55	236.88	55.37	39
	40.56- 50.55	205.74	58.88	39
	50.56-60.55	233.18	57.30	80
	Total	234.09	68.60	292
Contrast	0- 10.55	0.41	0.23	88
	10.56- 20.55	0.44	0.37	25
	20.56- 30.55	0.29	0.25	21
	30.56- 40.55	0.36	0.25	39
	40.56- 50.55	0.31	0.19	39
	50.56-60.55	0.39	0.27	80
	Total	0.38	0.26	292
correlation	0- 10.55	0.21	0.25	88
	10.56- 20.55	0.15	0.17	25
	20.56- 30.55	0.38	0.39	21
	30.56- 40.55	0.20	0.26	39
	40.56- 50.55	0.22	0.26	39
	50.56-60.55	0.18	0.24	80
	Total	0.21	0.26	292
Energy	0- 10.55	1448400.00	816298.00	88
	10.56- 20.55	1398100.00	1336250.00	25

	20.56- 30.55	784250.00	542679.00	21
	30.56- 40.55	1086500.00	623705.00	39
	40.56- 50.55	862810.00	678337.00	39
	50.56-60.55	1042100.00	708720.00	80
	Total	1158500.00	818873.00	292
Entropy	0- 10.55	1.03	0.40	88
	10.56- 20.55	0.99	0.36	25
	20.56- 30.55	0.71	0.52	21
	30.56- 40.55	0.94	0.41	39
	40.56- 50.55	0.81	0.39	39
	50.56-60.55	0.95	0.39	80
	Total	0.94	0.41	292
Kurtosis	0- 10.55	2.82	2.08	88
	10.56- 20.55	2.80	0.78	25
	20.56- 30.55	2.88	0.97	21
	30.56- 40.55	2.59	0.86	39
	40.56- 50.55	2.55	0.71	39
	50.56-60.55	2.41	0.62	80
	Total	2.64	1.31	292
maximum	0- 10.55	265.62	80.01	88
	10.56- 20.55	239.20	99.62	25
	20.56- 30.55	203.89	58.93	21
	30.56- 40.55	242.70	57.94	39
	40.56- 50.55	210.85	59.82	39
	50.56-60.55	239.31	59.03	80
	Total	241.33	72.31	292
Mean	0- 10.55	242.34	71.66	88
	10.56- 20.55	217.87	87.95	25
	20.56- 30.55	188.68	49.38	21
	30.56- 40.55	224.56	53.78	39
	40.56- 50.55	194.60	56.61	39
	50.56-60.55	220.76	54.78	80
	Total	221.72	65.27	292
MeanAbsoluteDeviation	0- 10.55	9.32	4.54	88
	10.56- 20.55	8.08	4.48	25
	20.56- 30.55	6.46	3.75	21
	30.56- 40.55	8.03	4.37	39
	40.56- 50.55	7.30	2.71	39
	50.56-60.55	8.36	2.86	80
	Total	8.30	3.90	292
Median	0- 10.55	242.55	72.43	88
	10.56- 20.55	217.44	87.07	25
	20.56- 30.55	188.72	48.70	21
	30.56- 40.55	224.53	54.06	39

	40.56- 50.55	194.96	56.71	39
	50.56-60.55	220.71	54.47	80
	Total	221.78	65.36	292
Minimum	0- 10.55	220.57	65.25	88
	10.56- 20.55	199.71	82.30	25
	20.56- 30.55	172.93	42.54	21
	30.56- 40.55	206.31	52.77	39
	40.56- 50.55	177.66	54.43	39
	50.56-60.55	201.93	51.89	80
	Total	202.62	60.70	292
Range	0- 10.55	45.05	31.07	88
	10.56- 20.55	39.49	20.36	25
	20.56- 30.55	30.96	18.99	21
	30.56- 40.55	36.38	19.20	39
	40.56- 50.55	33.19	13.05	39
	50.56-60.55	37.39	13.73	80
	Total	38.72	22.16	292
Skewness	0- 10.55	0.02	0.66	88
	10.56- 20.55	0.19	0.49	25
	20.56- 30.55	-0.07	0.66	21
	30.56- 40.55	0.00	0.51	39
	40.56- 50.55	-0.05	0.52	39
	50.56-60.55	-0.02	0.40	80
	Total	0.01	0.55	292
TotalEnergy	0- 10.55	1479000.00	1051770.00	88
	10.56- 20.55	2678700.00	3864500.00	25
	20.56- 30.55	1440500.00	1035730.00	21
	30.56- 40.55	2905600.00	1643740.00	39
	40.56- 50.55	1912500.00	1337970.00	39
	50.56-60.55	3506900.00	2006590.00	80
	Total	2382900.00	2011980.00	292
Uniformity	0- 10.55	0.57	0.16	88
	10.56- 20.55	0.57	0.14	25
	20.56- 30.55	0.69	0.22	21
	30.56- 40.55	0.59	0.17	39
	40.56- 50.55	0.65	0.17	39
	50.56-60.55	0.59	0.16	80
	Total	0.60	0.17	292
Variance	0- 10.55	175.56	288.61	88
	10.56- 20.55	131.32	193.37	25
	20.56- 30.55	84.33	119.02	21
	30.56- 40.55	123.22	176.29	39
	40.56- 50.55	90.89	66.68	39
	50.56-60.55	114.45	82.25	80

	Total	130.17	191.03	292
a. region = L.THALAMUS				

Multivariate Tests[c,d]						
Effect		Value	F	Hypothesis df	Error df	Sig.
Intercept	Pillai's Trace	0.996	4.515E3[a]	16.00	265.00	0.00
time_days	Pillai's Trace	0.063	1.108[a]	16.00	265.00	0.35
Dosegr	**Pillai's Trace**	**0.635**	**2.45**	**80.00**	**1345.00**	**<0.001****
dosegr * time_days	Pillai's Trace	0.268	0.95	80.00	1345.00	0.60
a. Exact statistic						
b. The statistic is an upper bound on F that yields a lower bound on the significance level.						
c. region = L.THALAMUS						
d. Design: Intercept + time_days + dosegr + dosegr * time_days						

Note : * indicates p value is significant at 0.05 means P <0.05
**** indicates p value is significant at 0.05 means P <0.01**

There was a statistically significant difference in TA features based on dose levels, F (80, 1345) = 2.45
p < 0.001 Pillai Trace = 0.635

Tests of Between-Subjects Effects[r]						
Source	Dependent Variable	Type III Sum of Squares	df	Mean Square	F	Sig.
Corrected Model	@10Percentile	123439.698[a]	11	11221.79	3.14	0.001
	@90Percentile	153713.373[b]	11	13973.94	3.22	0
	Contrast	.746[c]	11	0.07	1.02	0.427
	correlation	1.055[d]	11	0.10	1.47	0.144
	Energy	2.293E13[e]	11	2085000000000.00	3.39	0
	Entropy	2.810[f]	11	0.26	1.55	0.114
	Kurtosis	13.163[g]	11	1.20	0.69	0.745

	maximum	176786.261[h]	11	16071.48	3.35	0
	Mean	140237.521[i]	11	12748.87	3.25	0
	MeanAbsoluteDeviation	287.770[j]	11	26.16	1.77	0.058
	Median	139736.124[k]	11	12703.28	3.22	0
	Minimum	118413.460[l]	11	10764.86	3.16	0
	Range	8106.984[m]	11	737.00	1.53	0.12
	Skewness	1.905[n]	11	0.17	0.57	0.851
	TotalEnergy	2.663E14[o]	11	24210000000000.00	7.43	0
	Uniformity	.405[p]	11	0.04	1.31	0.216
	Variance	416667.215[q]	11	37878.84	1.04	0.411
Intercept	@10Percentile	4198506.88	1	4198506.88	1175.00	<0.05
	@90Percentile	5240345.83	1	5240345.83	1207.00	<0.05
	Contrast	14.14	1	14.14	213.09	<0.05
	correlation	3.45	1	3.45	52.69	<0.05
	Energy	135300000000000.00	1	1353000000000000.00	220.04	<0.05
	Entropy	80.67	1	80.67	488.55	<0.05
	Kurtosis	673.58	1	673.58	389.98	<0.05
	maximum	5571500.76	1	5571500.76	1160.00	<0.05
	Mean	4698175.02	1	4698175.02	1196.00	<0.05
	MeanAbsoluteDeviation	6547.31	1	6547.31	443.98	<0.05
	Median	4705894.73	1	4705894.73	1194.00	<0.05
	Minimum	3922902.38	1	3922902.38	1152.00	<0.05
	Range	144225.90	1	144225.90	299.68	<0.05
	Skewness	0.03	1	0.03	0.10	0.751
	TotalEnergy	628600000000000.00	1	6286000000000000.00	193.04	<0.05
	Uniformity	34.40	1	34.40	1226.00	<0.05
	Variance	1645290.65	1	1645290.65	45.16	<0.05

time_days	@10Percentile	13060.41	1	13060.41	3.66	0.057
	@90Percentile	17054.17	1	17054.17	3.93	0.048
	Contrast	0.09	1	0.09	1.35	0.247
	correlation	0.15	1	0.15	2.25	0.135
	Energy	1626000000000.00	1	1626000000000.00	2.64	0.105
	Entropy	0.11	1	0.11	0.68	0.41
	Kurtosis	0.03	1	0.03	0.02	0.888
	maximum	19111.04	1	19111.04	3.98	0.047
	Mean	14949.38	1	14949.38	3.81	0.052
	MeanAbsoluteDeviation	37.44	1	37.44	2.54	0.112
	Median	15500.30	1	15500.30	3.93	0.048
	Minimum	11618.72	1	11618.72	3.41	0.066
	Range	927.36	1	927.36	1.93	0.166
	Skewness	0.00	1	0.00	0.00	0.961
	TotalEnergy	12360000000000.00	1	12360000000000.00	3.80	0.052
	Uniformity	0.00	1	0.00	0.06	0.815
	Variance	33480.47	1	33480.47	0.92	0.339
dosegr	@10Percentile	60780.31	5	12156.06	3.40	**0.005****
	@90Percentile	73617.12	5	14723.42	3.39	**0.005****
	Contrast	0.39	5	0.08	1.18	0.322
	correlation	0.33	5	0.07	1.01	0.414
	Energy	12050000000000.00	5	2410000000000.00	3.92	**0.002****
	Entropy	1.16	5	0.23	1.41	0.221
	Kurtosis	11.03	5	2.21	1.28	0.274
	maximum	86596.45	5	17319.29	3.61	**0.004****
	Mean	68583.93	5	13716.79	3.49	**0.004****
	MeanAbsoluteDeviation	107.17	5	21.44	1.45	0.205
	Median	67430.32	5	13486.07	3.42	**0.005****
	Minimum	58865.81	5	11773.16	3.46	**0.005****
	Range	3412.22	5	682.44	1.42	0.218
	Skewness	0.79	5	0.16	0.52	0.762
	TotalEnergy	164400000000000.00	5	32880000000000.00	10.10	**<0.001****
	Uniformity	0.16	5	0.03	1.17	0.324
	Variance	210719.63	5	42143.93	1.16	0.331
dosegr * time_days	@10Percentile	18933.36	5	3786.67	1.06	0.383
	@90Percentile	19217.82	5	3843.56	0.89	0.491
	Contrast	0.04	5	0.01	0.13	0.985
	correlation	0.17	5	0.03	0.51	0.771

	Energy	2698000000000.00	5	539600000000.00	0.88	0.497
	Entropy	0.09	5	0.02	0.11	0.991
	Kurtosis	3.50	5	0.70	0.41	0.845
	maximum	20312.63	5	4062.53	0.85	0.518
	Mean	19119.45	5	3823.89	0.97	0.434
	MeanAbsoluteDeviation	33.14	5	6.63	0.45	0.814
	Median	18218.60	5	3643.72	0.93	0.465
	Minimum	20082.27	5	4016.45	1.18	0.32
	Range	635.25	5	127.05	0.26	0.932
	Skewness	0.77	5	0.15	0.51	0.771
	Total Energy	25080000000000.00	5	5016000000000.00	1.54	0.177
	Uniformity	0.03	5	0.01	0.21	0.957
	Variance	54724.85	5	10944.97	0.30	0.912
Error	@10Percentile	1000099.03	280	3571.78		
	@90Percentile	1215691.43	280	4341.76		
	Contrast	18.58	280	0.07		
	correlation	18.32	280	0.07		
	Energy	172200000000000.00	280	615000000000.00		
	Entropy	46.23	280	0.17		
	Kurtosis	483.62	280	1.73		
	maximum	1344752.44	280	4802.69		
	Mean	1099463.56	280	3926.66		
	MeanAbsoluteDeviation	4129.13	280	14.75		
	Median	1103504.51	280	3941.09		
	Minimum	953837.88	280	3406.56		
	Range	134756.24	280	481.27		
	Skewness	84.71	280	0.30		
	Total Energy	911700000000000.00	280	3256000000000.00		
	Uniformity	7.85	280	0.03		
	Variance	10200000.00	280	36436.72		
Total	@10Percentile	13920000.00	292			
	@90Percentile	17370000.00	292			
	Contrast	61.10	292			
	correlation	32.36	292			
	Energy	587000000000000.00	292			
	Entropy	306.66	292			
	Kurtosis	2534.86	292			

	maximum	18530000.00	292			
	Mean	15590000.00	292			
	MeanAbsoluteDeviation	24546.95	292			
	Median	15610000.00	292			
	Minimum	13060000.00	292			
	Range	580591.91	292			
	Skewness	86.62	292			
	Total Energy	2836000000000000.00	292			
	Uniformity	113.01	292			
	Variance	15570000.00	292			
Corrected Total	@10Percentile	1123538.73	291			
	@90Percentile	1369404.80	291			
	Contrast	19.33	291			
	correlation	19.38	291			
	Energy	1951000000000000.00	291			
	Entropy	49.04	291			
	Kurtosis	496.79	291			
	maximum	1521538.70	291			
	Mean	1239701.08	291			
	MeanAbsoluteDeviation	4416.90	291			
	Median	1243240.63	291			
	Minimum	1072251.34	291			
	Range	142863.22	291			
	Skewness	86.61	291			
	TotalEnergy	1178000000000000.00	291			
	Uniformity	8.26	291			
	Variance	10620000.00	291			
a. R Squared = .110 (Adjusted R Squared = .075)						
b. R Squared = .112 (Adjusted R Squared = .077)						
c. R Squared = .039 (Adjusted R Squared = .001)						
d. R Squared = .054 (Adjusted R Squared = .017)						
e. R Squared = .118 (Adjusted R Squared = .083)						
f. R Squared = .057 (Adjusted R Squared = .020)						
g. R Squared = .026 (Adjusted R Squared = -.012)						

h. R Squared = .116 (Adjusted R Squared = .081)					
i. R Squared = .113 (Adjusted R Squared = .078)					
j. R Squared = .065 (Adjusted R Squared = .028)					
k. R Squared = .112 (Adjusted R Squared = .078)					
l. R Squared = .110 (Adjusted R Squared = .075)					
m. R Squared = .057 (Adjusted R Squared = .020)					
n. R Squared = .022 (Adjusted R Squared = -.016)					
o. R Squared = .226 (Adjusted R Squared = .196)					
p. R Squared = .049 (Adjusted R Squared = .012)					
q. R Squared = .039 (Adjusted R Squared = .001)					
r. region = L.THALAMUS					

Note : * indicates p value is significant at 0.05 means P <0.05
**** indicates p value is significant at 0.05 means P <0.01**

Conclusion: from this table that dose level has a statistically significant effect on @10percentile , @90percentile ,Energy ,Maximum , Mean , Median , Minimum and Total energy TA feature

Conclusion: from this table it has seen that Time in days has a statistically significant effect on @90percentile , Maximum, Median..

5.Region = MED

Between-Subjects Factors[a]			
		Value Label	N
dose (Binned)	1	0- 10.55	118
	2	10.56- 20.55	27
	3	20.56- 30.55	19
	4	30.56- 40.55	21
	5	40.56- 50.55	6
	6	50.56-60.55	101
a. region = MED			

Descriptive Statistics[a]				
	dose (Binned)	Mean	Std. Deviation	N
@10Percentile	0- 10.55	223.33	64.73	118
	10.56- 20.55	212.26	107.14	27
	20.56- 30.55	191.69	48.32	19
	30.56- 40.55	222.16	62.53	21
	40.56- 50.55	201.71	56.71	6
	50.56-60.55	227.30	67.24	101
	Total	221.09	69.42	292
@90Percentile	0- 10.55	255.59	76.21	118
	10.56- 20.55	236.66	118.43	27
	20.56- 30.55	215.22	55.01	19
	30.56- 40.55	251.20	68.85	21
	40.56- 50.55	229.45	65.06	6
	50.56-60.55	258.68	72.99	101
	Total	251.43	78.40	292
Contrast	0- 10.55	0.67	0.61	118
	10.56- 20.55	0.55	0.49	27
	20.56- 30.55	0.46	0.30	19
	30.56- 40.55	0.61	0.49	21
	40.56- 50.55	0.48	0.28	6
	50.56-60.55	0.64	0.52	101
	Total	0.63	0.54	292
Correlation	0- 10.55	0.11	0.17	118
	10.56- 20.55	0.07	0.21	27
	20.56- 30.55	-0.02	0.11	19
	30.56- 40.55	0.14	0.28	21
	40.56- 50.55	0.07	0.11	6
	50.56-60.55	0.12	0.19	101
	Total	0.10	0.19	292

Energy	0- 10.55	1376300.00	809389.00	118
	10.56- 20.55	1420600.00	1669650.00	27
	20.56- 30.55	760220.00	422844.00	19
	30.56- 40.55	1091500.00	668216.00	21
	40.56- 50.55	1098300.00	598717.00	6
	50.56-60.55	1424100.00	1088700.00	101
	Total	1330700.00	999397.00	292
Entropy	0- 10.55	1.18	0.45	118
	10.56- 20.55	1.03	0.40	27
	20.56- 30.55	0.92	0.35	19
	30.56- 40.55	1.13	0.52	21
	40.56- 50.55	1.01	0.41	6
	50.56-60.55	1.17	0.41	101
	Total	1.14	0.44	292
Kurtosis	0- 10.55	2.88	1.02	118
	10.56- 20.55	2.93	0.88	27
	20.56- 30.55	2.99	1.29	19
	30.56- 40.55	2.67	0.86	21
	40.56- 50.55	3.08	1.53	6
	50.56-60.55	2.92	1.72	101
	Total	2.90	1.31	292
Maximum	0- 10.55	266.98	79.46	118
	10.56- 20.55	245.89	127.31	27
	20.56- 30.55	224.94	54.88	19
	30.56- 40.55	260.34	74.67	21
	40.56- 50.55	240.59	64.51	6
	50.56-60.55	270.48	79.97	101
	Total	262.49	83.57	292
Mean	0- 10.55	238.97	69.62	118
	10.56- 20.55	224.11	112.59	27
	20.56- 30.55	203.55	50.98	19
	30.56- 40.55	236.15	65.84	21
	40.56- 50.55	216.16	60.56	6
	50.56-60.55	242.54	69.89	101
	Total	235.86	73.42	292
MeanAbsoluteDeviation	0- 10.55	10.67	5.70	118
	10.56- 20.55	8.38	5.30	27
	20.56- 30.55	8.17	2.43	19
	30.56- 40.55	9.76	4.59	21
	40.56- 50.55	9.02	2.92	6
	50.56-60.55	10.56	5.17	101
	Total	10.16	5.24	292
Median	0- 10.55	238.35	69.16	118
	10.56- 20.55	223.90	111.31	27

	20.56- 30.55	203.26	50.76	19
	30.56- 40.55	235.65	65.95	21
	40.56- 50.55	216.20	61.31	6
	50.56-60.55	241.46	69.97	101
	Total	235.16	73.07	292
Minimum	0- 10.55	214.77	62.95	118
	10.56- 20.55	204.76	106.39	27
	20.56- 30.55	184.30	47.57	19
	30.56- 40.55	215.72	60.61	21
	40.56- 50.55	194.10	54.66	6
	50.56-60.55	219.12	67.08	101
	Total	213.01	68.39	292
Range	0- 10.55	52.21	26.16	118
	10.56- 20.55	41.13	23.89	27
	20.56- 30.55	40.64	14.92	19
	30.56- 40.55	44.61	21.05	21
	40.56- 50.55	46.49	16.47	6
	50.56-60.55	51.36	27.77	101
	Total	49.48	25.65	292
Skewness	0- 10.55	0.16	0.58	118
	10.56- 20.55	0.02	0.65	27
	20.56- 30.55	0.12	0.52	19
	30.56- 40.55	0.23	0.52	21
	40.56- 50.55	0.18	0.54	6
	50.56-60.55	0.21	0.67	101
	Total	0.16	0.61	292
TotalEnergy	0- 10.55	1622400.00	1181690.00	118
	10.56- 20.55	3465100.00	6156190.00	27
	20.56- 30.55	2752500.00	1850570.00	19
	30.56- 40.55	4265300.00	2343280.00	21
	40.56- 50.55	5237100.00	2854910.00	6
	50.56-60.55	3394800.00	2239140.00	101
	Total	2743700.00	2720350.00	292
Uniformity	0- 10.55	0.52	0.16	118
	10.56- 20.55	0.57	0.14	27
	20.56- 30.55	0.61	0.16	19
	30.56- 40.55	0.53	0.19	21
	40.56- 50.55	0.60	0.17	6
	50.56-60.55	0.52	0.16	101
	Total	0.53	0.16	292
Variance	0- 10.55	224.18	277.00	118
	10.56- 20.55	145.26	225.51	27
	20.56- 30.55	115.89	76.06	19
	30.56- 40.55	175.08	164.55	21

	40.56- 50.55	142.74	102.11	6
	50.56-60.55	217.88	275.36	101
	Total	202.45	255.04	292
a. region = MED				

Multivariate Tests[c,d]						
Effect		Value	F	Hypothesis df	Error df	Sig.
Intercept	Pillai's Trace	0.99	2193.00	16.00	265.00	<0.001**
time_days	Pillai's Trace	0.12	2.23	16.00	265.00	0.005**
Dosegr	Pillai's Trace	0.50	1.88	80.00	1345.00	<0.001**
dosegr * time_days	Pillai's Trace	0.34	1.24	80.00	1345.00	0.081
a. Exact statistic						
b. The statistic is an upper bound on F that yields a lower bound on the significance level.						
c. region = MED						
d. Design: Intercept + time_days + dosegr + dosegr * time_days						

Note : * indicates p value is significant at 0.05 means P <0.05
**** indicates p value is significant at 0.05 means P <0.01**

There was a statistically significant difference in TA features based on Time in days F (16,265) = 2.231, p < 0.05 Pillai Trace = 0.12

There was a statistically significant difference in TA features based on dose levels , F (80, 1345) = 1.88, p < 0.05 Pillai Trace = 0.50

Tests of Between-Subjects Effects[r]						
Source	**Dependent Variable**	**Type III Sum of Squares**	**df**	**Mean Square**	**F**	**Sig.**
Corrected Model	@10Percentile	133594.62	11	12144.97	2.68	0.003
	@90Percentile	181174.377[b]	11	16470.40	2.87	0.001
	Contrast	3.825[c]	11	0.35	1.21	0.279
	correlation	.481[d]	11	0.04	1.23	0.268
	Energy	2.703E13[e]	11	2457000000000.00	2.61	0.004
	Entropy	4.839[f]	11	0.44	2.44	0.006

	Kurtosis	12.469[g]	11	1.13	0.65	0.781
	maximum	219587.451[h]	11	19962.50	3.08	0.001
	Mean	156387.589[i]	11	14217.05	2.82	0.002
	Mean Absolute Deviation	510.444[j]	11	46.40	1.74	0.065
	Median	154701.032[k]	11	14063.73	2.82	0.002
	Minimum	123378.578[l]	11	11216.23	2.54	0.005
	Range	16098.651[m]	11	1463.51	2.34	0.009
	Skewness	1.944[n]	11	0.18	0.47	0.923
	TotalEnergy	4.039E14[o]	11	36720000000000.00	5.88	0
	Uniformity	.670[p]	11	0.06	2.54	0.004
	Variance	964895.168[q]	11	87717.74	1.37	0.188
Intercept	@10Percentile	2644455.24	1	2644455.24	583.55	0
	@90Percentile	3402716.39	1	3402716.39	592.77	0
	Contrast	22.28	1	22.28	77.63	0
	correlation	0.36	1	0.36	10.17	0.002
	Energy	99150000000000.00	1	99150000000000.00	105.31	0
	Entropy	70.25	1	70.25	389.36	0
	Kurtosis	459.85	1	459.85	265.30	0
	maximum	3732554.98	1	3732554.98	576.54	0
	Mean	3009538.65	1	3009538.65	596.75	0
	Mean Absolute Deviation	5215.27	1	5215.27	195.25	0
	Median	2995441.10	1	2995441.10	599.56	0
	Minimum	2454222.98	1	2454222.98	555.27	0
	Range	133507.04	1	133507.04	213.23	0
	Skewness	1.75	1	1.75	4.63	0.032
	TotalEnergy	9067000000000000.00	1	9067000000000000.00	145.11	0
	Uniformity	12.24	1	12.24	511.22	0

	Variance	2182178.51	1	2182178.51	34.02	0
time_days	@10Percentile	39482.94	1	39482.94	8.71	0.003**
	@90Percentile	53172.47	1	53172.47	9.26	0.003**
	Contrast	1.01	1	1.01	3.51	0.062
	correlation	0.00	1	0.00	0.05	0.818
	Energy	4809000000000.00	1	4809000000000.00	5.11	0.025*
	Entropy	1.53	1	1.53	8.50	0.004**
	Kurtosis	2.76	1	2.76	1.59	0.208
	maximum	62492.26	1	62492.26	9.65	0.002**
	Mean	46507.11	1	46507.11	9.22	0.003**
	Mean Absolute Deviation	81.75	1	81.75	3.06	0.081
	Median	46039.08	1	46039.08	9.22	0.003**
	Minimum	35912.97	1	35912.97	8.13	0.005**
	Range	3657.51	1	3657.51	5.84	0.016**
	Skewness	0.11	1	0.11	0.28	0.598
	TotalEnergy	67410000000000.00	1	67410000000000.00	10.79	0.001**
	Uniformity	0.23	1	0.23	9.45	0.002**
	Variance	149096.66	1	149096.66	2.32	0.129
dosegr	@10Percentile	50009.17	5	10001.83	2.21	0.054
	@90Percentile	65540.58	5	13108.12	2.28	0.047
	Contrast	0.89	5	0.18	0.62	0.686
	correlation	0.18	5	0.04	1.03	0.403
	Energy	9054000000000.00	5	1811000000000.00	1.92	0.091
	Entropy	1.19	5	0.24	1.32	0.257
	Kurtosis	5.10	5	1.02	0.59	0.709
	maximum	79594.16	5	15918.83	2.46	0.033*
	Mean	57634.57	5	11526.91	2.29	0.046*
	MeanAbsolute Deviation	210.09	5	42.02	1.57	0.168
	Median	57061.46	5	11412.29	2.28	0.047*
	Minimum	47291.25	5	9458.25	2.14	0.061
	Range	5400.06	5	1080.01	1.73	0.129
	Skewness	0.49	5	0.10	0.26	0.934

	TotalEnergy	272600000000000.00	5	54530000000000.00	8.73	<0.001**
	Uniformity	0.13	5	0.03	1.08	0.37
	Variance	354392.58	5	70878.52	1.11	0.358
dosegr * time_days	@10Percentile	62566.43	5	12513.29	2.76	0.019
	@90Percentile	76185.68	5	15237.14	2.65	0.023*
	Contrast	1.37	5	0.28	0.96	0.445
	correlation	0.10	5	0.02	0.56	0.732
	Energy	10070000000000.00	5	2014000000000.00	2.14	0.061
	Entropy	1.45	5	0.29	1.61	0.158
	Kurtosis	7.26	5	1.45	0.84	0.524
	maximum	91648.93	5	18329.79	2.83	0.016*
	Mean	70440.84	5	14088.17	2.79	0.018*
	MeanAbsolute Deviation	96.28	5	19.26	0.72	0.608
	Median	71817.80	5	14363.56	2.88	0.015*
	Minimum	57667.06	5	11533.41	2.61	0.025*
	Range	4252.06	5	850.41	1.36	0.24
	Skewness	0.25	5	0.05	0.13	0.985
	TotalEnergy	72600000000000.00	5	14520000000000.00	2.32	0.043*
	Uniformity	0.24	5	0.05	2.01	0.077
	Variance	170408.14	5	34081.63	0.53	0.753
Error	@10Percentile	1268857.81	280	4531.64		
	@90Percentile	1607312.33	280	5740.40		
	Contrast	80.35	280	0.29		
	correlation	9.97	280	0.04		
	Energy	263600000000000.00	280	941500000000.00		
	Entropy	50.52	280	0.18		
	Kurtosis	485.33	280	1.73		
	maximum	1812723.04	280	6474.01		
	Mean	1412094.71	280	5043.20		

	MeanAbsolute Deviation	7479.20	280	26.71		
	Median	1398903.62	280	4996.08		
	Minimum	1237571.53	280	4419.90		
	Range	175309.59	280	626.11		
	Skewness	106.05	280	0.38		
	TotalEnergy	1750000000000000.00	280	6249000000000.00		
	Uniformity	6.70	280	0.02		
	Variance	17960000.00	280	64152.41		
Total	@10Percentile	15680000.00	292			
	@90Percentile	20250000.00	292			
	Contrast	199.75	292			
	correlation	13.63	292			
	Energy	8077000000000000.00	292			
	Entropy	432.90	292			
	Kurtosis	2950.47	292			
	maximum	22150000.00	292			
	Mean	17810000.00	292			
	MeanAbsoluteDeviation	38117.77	292			
	Median	17700000.00	292			
	Minimum	14610000.00	292			
	Range	906190.93	292			
	Skewness	115.90	292			
	TotalEnergy	4352000000000000.00	292			
	Uniformity	90.64	292			

	Variance	30900000.00	292			
Corrected Total	@10Percentile	1402452.44	291			
	@90Percentile	1788486.71	291			
	Contrast	84.17	291			
	correlation	10.45	291			
	Energy	290600000000000.00	291			
	Entropy	55.35	291			
	Kurtosis	497.80	291			
	maximum	2032310.49	291			
	Mean	1568482.30	291			
	MeanAbsoluteDeviation	7989.65	291			
	Median	1553604.65	291			
	Minimum	1360950.11	291			
	Range	191408.24	291			
	Skewness	107.99	291			
	TotalEnergy	2153000000000000.00	291			
	Uniformity	7.37	291			
	Variance	18930000.00	291			
a. R Squared = .095 (Adjusted R Squared = .060)						
b. R Squared = .101 (Adjusted R Squared = .066)						
c. R Squared = .045 (Adjusted R Squared = .008)						
d. R Squared = .046 (Adjusted R Squared = .009)						
e. R Squared = .093 (Adjusted R Squared = .057)						
f. R Squared = .087 (Adjusted R Squared = .052)						
g. R Squared = .025 (Adjusted R Squared = -.013)						

h. R Squared = .108 (Adjusted R Squared = .073)					
i. R Squared = .100 (Adjusted R Squared = .064)					
j. R Squared = .064 (Adjusted R Squared = .027)					
k. R Squared = .100 (Adjusted R Squared = .064)					
l. R Squared = .091 (Adjusted R Squared = .055)					
m. R Squared = .084 (Adjusted R Squared = .048)					
n. R Squared = .018 (Adjusted R Squared = -.021)					
o. R Squared = .188 (Adjusted R Squared = .156)					
p. R Squared = .091 (Adjusted R Squared = .055)					
q. R Squared = .051 (Adjusted R Squared = .014)					
r. region = MED					

Note : * indicates p value is significant at 0.05 means P <0.05
**** indicates p value is significant at 0.05 means P <0.01**

Conclusion: from this table that Time in days has a statistically significant effect on @10percentile ,@90percentile , Energy , Entropy, Maximum, Mean, Median,Minimum,Range,Total Energy , Uniformity,

Conclusion: from this table that dose level has a statistically significant effect on @90percentile ,Maximum , Mean , Median , and Total energy TA feature

Conclusion: from this table that interaction effect of dose level and time in days has a statistically significant effect on @10percentile ,@90percentile ,Maximum , Mean , Median , Minimum and Total energy TA feature

6.Region = PONS

Between-Subjects Factors[a]			
		Value Label	N
dose (Binned)	1	0- 10.55	42
	2	10.56- 20.55	23
	3	20.56- 30.55	16
	4	30.56- 40.55	48
	5	40.56- 50.55	30
	6	50.56-60.55	133
a. region = PONS			

Descriptive Statistics[a]				
	dose (Binned)	Mean	Std. Deviation	N
@10Percentile	0- 10.55	192.11	45.67	42
	10.56- 20.55	192.99	53.45	23
	20.56- 30.55	189.95	53.16	16
	30.56- 40.55	178.04	50.87	48
	40.56- 50.55	187.61	79.93	30
	50.56-60.55	183.93	50.73	133
	Total	185.56	53.85	292
@90Percentile	0- 10.55	218.07	53.20	42
	10.56- 20.55	215.11	58.84	23
	20.56- 30.55	211.81	59.43	16
	30.56- 40.55	198.75	52.92	48
	40.56- 50.55	214.19	87.59	30
	50.56-60.55	208.42	55.39	133
	Total	209.52	59.04	292
Contrast	0- 10.55	0.50	0.27	42
	10.56- 20.55	0.48	0.20	23
	20.56- 30.55	0.43	0.28	16
	30.56- 40.55	0.37	0.22	48
	40.56- 50.55	0.50	0.28	30
	50.56-60.55	0.47	0.25	133
	Total	0.46	0.25	292
correlation	0- 10.55	0.09	0.22	42
	10.56- 20.55	-0.06	0.11	23
	20.56- 30.55	0.08	0.17	16
	30.56- 40.55	0.14	0.31	48
	40.56- 50.55	0.04	0.20	30
	50.56-60.55	0.08	0.20	133
	Total	0.08	0.22	292

Energy	0- 10.55	1118500.00	530117.00	42
	10.56- 20.55	768690.00	431310.00	23
	20.56- 30.55	983510.00	537414.00	16
	30.56- 40.55	906200.00	717298.00	48
	40.56- 50.55	891080.00	860209.00	30
	50.56-60.55	879870.00	625378.00	133
	Total	916600.00	641368.00	292
Entropy	0- 10.55	1.04	0.33	42
	10.56- 20.55	0.92	0.29	23
	20.56- 30.55	0.92	0.37	16
	30.56- 40.55	0.87	0.33	48
	40.56- 50.55	1.01	0.43	30
	50.56-60.55	1.00	0.34	133
	Total	0.98	0.35	292
Kurtosis	0- 10.55	2.66	0.64	42
	10.56- 20.55	2.83	1.20	23
	20.56- 30.55	2.79	0.67	16
	30.56- 40.55	2.72	0.72	48
	40.56- 50.55	2.67	0.86	30
	50.56-60.55	2.66	0.68	133
	Total	2.69	0.75	292
maximum	0- 10.55	227.27	56.22	42
	10.56- 20.55	220.50	58.19	23
	20.56- 30.55	218.39	60.22	16
	30.56- 40.55	205.75	55.25	48
	40.56- 50.55	222.55	90.03	30
	50.56-60.55	215.95	57.16	133
	Total	217.07	60.93	292
Mean	0- 10.55	205.15	49.18	42
	10.56- 20.55	203.50	55.76	23
	20.56- 30.55	200.99	56.57	16
	30.56- 40.55	188.40	51.75	48
	40.56- 50.55	200.27	84.11	30
	50.56-60.55	196.15	52.97	133
	Total	197.44	56.38	292
MeanAbsoluteDeviation	0- 10.55	8.54	2.92	42
	10.56- 20.55	7.48	2.84	23
	20.56- 30.55	7.29	2.32	16

	30.56- 40.55	6.99	1.90	48
	40.56- 50.55	8.90	4.61	30
	50.56-60.55	8.23	3.09	133
	Total	8.03	3.08	292
Median	0- 10.55	205.05	48.74	42
	10.56- 20.55	202.76	55.68	23
	20.56- 30.55	200.83	56.74	16
	30.56- 40.55	188.65	51.66	48
	40.56- 50.55	199.19	84.97	30
	50.56-60.55	196.12	53.00	133
	Total	197.27	56.43	292
Minimum	0- 10.55	185.07	45.94	42
	10.56- 20.55	185.95	50.86	23
	20.56- 30.55	183.23	54.47	16
	30.56- 40.55	171.93	49.92	48
	40.56- 50.55	181.71	76.61	30
	50.56-60.55	177.11	49.53	133
	Total	178.91	52.60	292
Range	0- 10.55	42.20	14.39	42
	10.56- 20.55	34.55	10.99	23
	20.56- 30.55	35.16	11.32	16
	30.56- 40.55	33.82	9.92	48
	40.56- 50.55	40.84	21.74	30
	50.56-60.55	38.83	14.41	133
	Total	38.16	14.49	292
Skewness	0- 10.55	0.06	0.46	42
	10.56- 20.55	0.14	0.60	23
	20.56- 30.55	0.03	0.54	16
	30.56- 40.55	0.02	0.48	48
	40.56- 50.55	0.30	0.52	30
	50.56-60.55	0.06	0.51	133
	Total	0.08	0.51	292
TotalEnergy	0- 10.55	915240.00	461899.00	42
	10.56- 20.55	1823700.00	1267620.00	23
	20.56- 30.55	1376000.00	820532.00	16
	30.56- 40.55	1627400.00	1314300.00	48
	40.56- 50.55	2074800.00	3032830.00	30
	50.56-60.55	2301400.00	1516270.00	133

	Total	1879600.00	1633680.00	292
Uniformity	0- 10.55	0.55	0.13	42
	10.56- 20.55	0.60	0.14	23
	20.56- 30.55	0.61	0.16	16
	30.56- 40.55	0.62	0.15	48
	40.56- 50.55	0.57	0.17	30
	50.56-60.55	0.57	0.14	133
	Total	0.58	0.14	292
Variance	0- 10.55	125.97	89.17	42
	10.56- 20.55	94.02	64.21	23
	20.56- 30.55	90.40	52.43	16
	30.56- 40.55	79.43	41.47	48
	40.56- 50.55	150.04	157.89	30
	50.56-60.55	116.80	86.75	133
	Total	112.15	90.35	292
a. region = PONS				

Multivariate Tests[c,d]

Effect		Value	F	Hypothesis df	Error df	Sig.
Intercept	Pillai's Trace	0.996	4.559E3[a]	16	265.00	<0.001**
time_days	Pillai's Trace	0.051	.895[a]	16	265.00	0.58
dosegr	Pillai's Trace	0.414	1.518	80	1345.00	<0.001**
dosegr * time_days	Pillai's Trace	0.327	1.176	80	1345.00	0.14
a. Exact statistic						
b. The statistic is an upper bound on F that yields a lower bound on the significance level.						
c. region = PONS						
d. Design: Intercept + time_days + dosegr + dosegr * time_days						

Note : * indicates p value is significant at 0.05 means P <0.05

**** indicates p value is significant at 0.05 means P <0.01**

"There was a statistically significant difference in TA features based on dose levels , F (80, 1345) = 1.518, p < 0.05 Pillai Trace = 0.414

"

Tests of Between-Subjects Effects[r]						
Source	Dependent Variable	Type III Sum of Squares	df	Mean Square	F	Sig.
Corrected Model	@10Percentile	64539.332[a]	11	5867.21	2.11	0.02
	@90Percentile	87141.537[b]	11	7921.96	2.39	0.008
	Contrast	1.537[c]	11	0.14	2.29	0.011
	correlation	.724[d]	11	0.07	1.37	0.187
	Energy	9.227E12[e]	11	838800000000.00	2.13	0.019
	Entropy	3.516[f]	11	0.32	2.85	0.001
	Kurtosis	1.398[g]	11	0.13	0.22	0.996
	maximum	93847.005[h]	11	8531.55	2.42	0.007
	Mean	74640.862[i]	11	6785.53	2.23	0.013
	MeanAbsoluteDeviation	309.265[j]	11	28.12	3.21	0
	Median	73937.916[k]	11	6721.63	2.21	0.014
	Minimum	56836.764[l]	11	5166.98	1.93	0.035
	Range	6920.489[m]	11	629.14	3.25	0
	Skewness	2.481[n]	11	0.23	0.86	0.584
	TotalEnergy	1.080E14[o]	11	9815000000000.00	4.11	0
	Uniformity	.530[p]	11	0.05	2.46	0.006
	Variance	252956.915[q]	11	22996.08	3.03	0.001
Intercept	@10Percentile	3000888.70	1	3000888.70	1078.00	0
	@90Percentile	3804973.11	1	3804973.11	1149.00	0
	Contrast	16.68	1	16.68	273.75	0
	correlation	0.23	1	0.23	4.68	0.031
	Energy	75060000000000.00	1	75060000000000.00	190.24	0
	Entropy	76.64	1	76.64	683.16	0
	Kurtosis	605.36	1	605.36	1052.00	0

	maximum	4063241.13	1	4063241.13	1153.00	0
	Mean	3379797.12	1	3379797.12	1113.00	0
	MeanAbsoluteDeviation	5247.20	1	5247.20	598.76	0
	Median	3361679.82	1	3361679.82	1104.00	0
	Minimum	2783877.09	1	2783877.09	1042.00	0
	Range	120584.52	1	120584.52	622.98	0
	Skewness	0.77	1	0.77	2.90	0.089
	TotalEnergy	2598000000000000.00	1	2598000000000000.00	108.80	0
	Uniformity	27.96	1	27.96	1425.00	0
	Variance	980624.91	1	980624.91	129.35	0
time_days	@10Percentile	2596.36	1	2596.36	0.93	0.335
	@90Percentile	3251.31	1	3251.31	0.98	0.323
	Contrast	0.00	1	0.00	0.05	0.827
	correlation	0.03	1	0.03	0.56	0.455
	Energy	189600000000.00	1	189600000000.00	0.48	0.489
	Entropy	0.01	1	0.01	0.09	0.771
	Kurtosis	0.02	1	0.02	0.03	0.865
	maximum	2994.01	1	2994.01	0.85	0.357
	Mean	2715.40	1	2715.40	0.89	0.345
	MeanAbsoluteDeviation	1.14	1	1.14	0.13	0.719
	Median	2447.28	1	2447.28	0.80	0.371
	Minimum	2113.67	1	2113.67	0.79	0.375
	Range	76.44	1	76.44	0.40	0.53
	Skewness	0.01	1	0.01	0.02	0.882
	TotalEnergy	1057000000000.00	1	1057000000000.00	0.44	0.506
	Uniformity	0.00	1	0.00	0.08	0.772
	Variance	15.88	1	15.88	0.00	0.964
dosegr	@10Percentile	15340.08	5	3068.02	1.10	0.359
	@90Percentile	23564.70	5	4712.94	1.42	0.216

	Contrast	0.79	5	0.16	2.59	0.026*
	correlation	0.44	5	0.09	1.82	0.109
	Energy	1487000000000.00	5	297500000000.00	0.75	0.584
	Entropy	1.84	5	0.37	3.28	0.007**
	Kurtosis	0.64	5	0.13	0.22	0.953
	maximum	25071.50	5	5014.30	1.42	0.216
	Mean	18865.78	5	3773.16	1.24	0.289
	MeanAbsoluteDeviation	165.67	5	33.13	3.78	0.002**
	Median	19002.03	5	3800.41	1.25	0.287
	Minimum	13938.97	5	2787.79	1.04	0.393
	Range	3296.87	5	659.37	3.41	0.005**
	Skewness	0.88	5	0.18	0.66	0.651
	TotalEnergy	73090000000000.00	5	14620000000000.00	6.12	<0.001**
	Uniformity	0.27	5	0.05	2.77	0.019*
	Variance	129350.85	5	25870.17	3.41	0.005**
dosegr * time_days	@10Percentile	32763.80	5	6552.76	2.35	0.041*
	@90Percentile	42133.93	5	8426.79	2.54	0.028*
	Contrast	0.81	5	0.16	2.64	0.024*
	correlation	0.07	5	0.01	0.30	0.912
	Energy	4140000000000.00	5	828000000000.00	2.10	0.066
	Entropy	1.61	5	0.32	2.87	0.015*
	Kurtosis	0.58	5	0.12	0.20	0.961
	maximum	45251.20	5	9050.24	2.57	0.027*
	Mean	37304.41	5	7460.88	2.46	0.034*
	MeanAbsoluteDeviation	115.93	5	23.19	2.65	0.023*
	Median	37820.24	5	7564.05	2.48	0.032*
	Minimum	30019.82	5	6003.97	2.25	0.05
	Range	2362.58	5	472.52	2.44	0.035*
	Skewness	0.63	5	0.13	0.48	0.79
	TotalEnergy	18640000000000.00	5	3728000000000.00	1.56	0.171
	Uniformity	0.24	5	0.05	2.42	0.036*
	Variance	87247.77	5	17449.55	2.30	0.045*
Error	@10Percentile	779440.46	280	2783.72		

	@90Percentile	927374.33	280	3312.05		
	Contrast	17.07	280	0.06		
	correlation	13.46	280	0.05		
	Energy	1105000000000000.00	280	394600000000.00		
	Entropy	31.41	280	0.11		
	Kurtosis	161.10	280	0.58		
	maximum	986336.58	280	3522.63		
	Mean	850319.59	280	3036.86		
	MeanAbsoluteDeviation	2453.76	280	8.76		
	Median	852868.77	280	3045.96		
	Minimum	748341.71	280	2672.65		
	Range	54196.75	280	193.56		
	Skewness	73.80	280	0.26		
	TotalEnergy	668700000000000.00	280	2388000000000.00		
	Uniformity	5.49	280	0.02		
	Variance	2122719.86	280	7581.14		
Total	@10Percentile	10900000.00	292			
	@90Percentile	13830000.00	292			
	Contrast	80.46	292			
	correlation	15.97	292			
	Energy	365000000000000.00	292			
	Entropy	313.23	292			
	Kurtosis	2278.56	292			
	maximum	14840000.00	292			

	Mean	12310000.00	292			
	MeanAbsoluteDeviation	21591.59	292			
	Median	12290000.00	292			
	Minimum	10150000.00	292			
	Range	486309.34	292			
	Skewness	78.27	292			
	TotalEnergy	180800000000000.00	292			
	Uniformity	104.14	292			
	Variance	6048229.84	292			
Corrected Total	@10Percentile	843979.79	291			
	@90Percentile	1014515.86	291			
	Contrast	18.60	291			
	correlation	14.18	291			
	Energy	119700000000000.00	291			
	Entropy	34.93	291			
	Kurtosis	162.50	291			
	maximum	1080183.58	291			
	Mean	924960.45	291			
	MeanAbsoluteDeviation	2763.02	291			
	Median	926806.69	291			
	Minimum	805178.47	291			
	Range	61117.24	291			
	Skewness	76.28	291			
	TotalEnergy	776600000000000.00	291			

	Uniformity	6.02	291			
	Variance	2375676.77	291			
a. R Squared = .076 (Adjusted R Squared = .040)						
b. R Squared = .086 (Adjusted R Squared = .050)						
c. R Squared = .083 (Adjusted R Squared = .047)						
d. R Squared = .051 (Adjusted R Squared = .014)						
e. R Squared = .077 (Adjusted R Squared = .041)						
f. R Squared = .101 (Adjusted R Squared = .065)						
g. R Squared = .009 (Adjusted R Squared = -.030)						
h. R Squared = .087 (Adjusted R Squared = .051)						
i. R Squared = .081 (Adjusted R Squared = .045)						
j. R Squared = .112 (Adjusted R Squared = .077)						
k. R Squared = .080 (Adjusted R Squared = .044)						
l. R Squared = .071 (Adjusted R Squared = .034)						
m. R Squared = .113 (Adjusted R Squared = .078)						
n. R Squared = .033 (Adjusted R Squared = -.005)						
o. R Squared = .139 (Adjusted R Squared = .105)						
p. R Squared = .088 (Adjusted R Squared = .052)						
q. R Squared = .106 (Adjusted R Squared = .071)						
r. region = PONS						

Note : * indicates p value is significant at 0.05 means P <0.05
**** indicates p value is significant at 0.05 means P <0.01**

Conclusion: from this table that dose level has a statistically significant effect on Contrast , Entropy, Mean absolute deviation , range , total energy ,Uniformity , varience.

Conclusion: from this table that interaction effect of dose (level and time in days) has a statistically significant effect on @10percentile , @90percentile ,Contrast , Entropy, maximum,Mean ,Mean absolute deviation , Median ,range ,Uniformity , variance.

After getting significant results in Tests of Between-Subjects Effects[r] we compare variation between all possible pairs of dose groups (independent variables) in this table we found significant variation between these pairs given above.

7.Region = POST.CC

Between-Subjects Factors[a]			
		Value Label	N
dose (Binned)	1	0- 10.55	115
	2	10.56- 20.55	16
	3	20.56- 30.55	35
	4	30.56- 40.55	45
	5	40.56- 50.55	22
	6	50.56-60.55	58
a. region = POST.CC			

Descriptive Statistics[a]				
	dose (Binned)	Mean	Std. Deviation	N
@10Percentile	0- 10.55	162.66	69.31	115
	10.56- 20.55	170.57	65.98	16
	20.56- 30.55	152.41	38.21	35
	30.56- 40.55	147.17	41.49	45
	40.56- 50.55	166.79	58.34	22
	50.56-60.55	158.04	40.59	58
	Total	158.86	56.22	291
@90Percentile	0- 10.55	192.81	60.64	115
	10.56- 20.55	188.87	77.63	16
	20.56- 30.55	165.61	40.04	35
	30.56- 40.55	169.36	44.74	45
	40.56- 50.55	184.44	62.94	22
	50.56-60.55	173.23	43.54	58
	Total	181.16	55.04	291
Contrast	0- 10.55	0.44	0.58	115
	10.56- 20.55	0.54	0.72	16
	20.56- 30.55	0.31	0.27	35
	30.56- 40.55	0.72	0.86	45
	40.56- 50.55	0.47	0.40	22
	50.56-60.55	0.30	0.27	58
	Total	0.45	0.57	291
correlation	0- 10.55	0.26	0.51	115
	10.56- 20.55	0.13	0.53	16
	20.56- 30.55	0.26	0.56	35
	30.56- 40.55	0.12	0.50	45
	40.56- 50.55	0.01	0.43	22
	50.56-60.55	0.28	0.53	58
	Total	0.22	0.51	291

Energy	0- 10.55	329810.00	239379.00	115
	10.56- 20.55	290150.00	250891.00	16
	20.56- 30.55	201050.00	127874.00	35
	30.56- 40.55	189910.00	101729.00	45
	40.56- 50.55	282740.00	196370.00	22
	50.56-60.55	196040.00	106848.00	58
	Total	260290.00	195772.00	291
Entropy	0- 10.55	0.76	0.53	115
	10.56- 20.55	0.67	0.52	16
	20.56- 30.55	0.53	0.43	35
	30.56- 40.55	0.82	0.57	45
	40.56- 50.55	0.75	0.43	22
	50.56-60.55	0.59	0.46	58
	Total	0.70	0.51	291
Kurtosis	0- 10.55	2.40	1.06	115
	10.56- 20.55	2.54	0.84	16
	20.56- 30.55	2.48	0.87	35
	30.56- 40.55	2.34	0.67	45
	40.56- 50.55	2.41	0.73	22
	50.56-60.55	2.10	0.52	58
	Total	2.35	0.86	291
maximum	0- 10.55	197.67	62.17	115
	10.56- 20.55	194.29	84.33	16
	20.56- 30.55	169.23	41.37	35
	30.56- 40.55	174.54	48.87	45
	40.56- 50.55	187.74	63.56	22
	50.56-60.55	175.75	44.33	58
	Total	185.37	57.11	291
Mean	0- 10.55	177.63	60.47	115
	10.56- 20.55	179.21	70.47	16
	20.56- 30.55	158.88	39.13	35
	30.56- 40.55	158.23	41.46	45
	40.56- 50.55	175.23	60.53	22
	50.56-60.55	165.51	41.70	58
	Total	169.86	53.03	291
MeanAbsoluteDeviation	0- 10.55	12.35	22.12	115
	10.56- 20.55	6.92	6.51	16
	20.56- 30.55	5.09	2.56	35

	30.56- 40.55	8.26	6.49	45
	40.56- 50.55	6.65	4.05	22
	50.56-60.55	5.75	3.13	58
	Total	8.80	14.63	291
Median	0- 10.55	181.89	58.08	115
	10.56- 20.55	177.94	68.17	16
	20.56- 30.55	158.40	39.26	35
	30.56- 40.55	158.33	40.09	45
	40.56- 50.55	175.34	61.50	22
	50.56-60.55	165.28	41.57	58
	Total	171.40	52.02	291
Minimum	0- 10.55	159.31	68.50	115
	10.56- 20.55	168.34	66.73	16
	20.56- 30.55	149.62	37.95	35
	30.56- 40.55	142.64	43.63	45
	40.56- 50.55	162.35	56.01	22
	50.56-60.55	155.53	40.48	58
	Total	155.54	55.95	291
Range	0- 10.55	38.37	48.34	115
	10.56- 20.55	25.95	23.56	16
	20.56- 30.55	19.61	10.91	35
	30.56- 40.55	31.90	27.87	45
	40.56- 50.55	25.40	14.28	22
	50.56-60.55	20.23	11.33	58
	Total	29.83	34.38	291
Skewness	0- 10.55	0.10	0.68	115
	10.56- 20.55	0.16	0.78	16
	20.56- 30.55	0.08	0.80	35
	30.56- 40.55	0.06	0.65	45
	40.56- 50.55	0.11	0.65	22
	50.56-60.55	0.10	0.57	58
	Total	0.10	0.67	291
TotalEnergy	0- 10.55	486580.00	729537.00	115
	10.56- 20.55	285160.00	233369.00	16
	20.56- 30.55	413530.00	304515.00	35
	30.56- 40.55	671940.00	392559.00	45
	40.56- 50.55	853480.00	838702.00	22
	50.56-60.55	623470.00	367400.00	58

	Total	550410.00	584674.00	291
Uniformity	0- 10.55	0.67	0.22	115
	10.56- 20.55	0.71	0.22	16
	20.56- 30.55	0.76	0.20	35
	30.56- 40.55	0.65	0.23	45
	40.56- 50.55	0.67	0.19	22
	50.56-60.55	0.73	0.21	58
	Total	0.69	0.22	291
Variance	0- 10.55	673.45	2357.30	115
	10.56- 20.55	128.15	266.92	16
	20.56- 30.55	49.07	60.24	35
	30.56- 40.55	173.36	275.20	45
	40.56- 50.55	83.53	98.86	22
	50.56-60.55	59.34	75.72	58
	Total	324.04	1511.11	291
a. region = POST.CC				

Multivariate Tests[c,d]

Effect		Value	F	Hypothesis df	Error df	Sig.
Intercept	Pillai's Trace	0.998	6.751E3[a]	16	264	<0.001**
time_days	Pillai's Trace	0.077	1.382[a]	16	264	0.15
dosegr	Pillai's Trace	0.436	1.599	80	1340.00	<0.001**
dosegr * time_days	Pillai's Trace	0.251	0.884	80	1.34E+03	0.756
a. Exact statistic						
b. The statistic is an upper bound on F that yields a lower bound on the significance level.						
c. region = POST.CC						
d. Design: Intercept + time_days + dosegr + dosegr * time_days						

Note : * indicates p value is significant at 0.05 means P <0.05
**** indicates p value is significant at 0.05 means P <0.01**

There was a statistically significant difference in TA features based on dose levels, F (80, 1340) = 1.599, p < 0.05 Pillai Trace = 0.436

Conclusion: from this table that dose level has a statistically significant effect on @90percentile, Energy, Maximum, Mean, Median, total energy.

Tests of Between-Subjects Effects[r]						
Source	Dependent Variable	Type III Sum of Squares	df	Mean Square	F	Sig.
Corrected Model	@10Percentile	57510.685[a]	11	5228.24	1.70	0.073
	@90Percentile	90992.686[b]	11	8272.06	2.93	0.001
	Contrast	7.571[c]	11	0.69	2.21	0.014
	correlation	3.781[d]	11	0.34	1.31	0.216
	Energy	1.643E12[e]	11	149400000000.00	4.40	0
	Entropy	4.541[f]	11	0.41	1.63	0.09
	Kurtosis	7.155[g]	11	0.65	0.87	0.57
	maximum	99280.998[h]	11	9025.55	2.97	0.001
	Mean	69719.399[i]	11	6338.13	2.37	0.008
	MeanAbsoluteDeviation	2976.242[j]	11	270.57	1.28	0.236
	Median	76356.238[k]	11	6941.48	2.73	0.002
	Minimum	54981.317[l]	11	4998.30	1.64	0.089
	Range	21857.791[m]	11	1987.07	1.73	0.067
	Skewness	2.563[n]	11	0.23	0.51	0.895
	TotalEnergy	7.427E12[o]	11	675200000000.00	2.05	0.024
	Uniformity	.767[p]	11	0.07	1.50	0.132
	Variance	2.498E7[q]	11	2270540.92	0.99	0.452
Intercept	@10Percentile	2561330.04	1	2561330.04	831.85	0
	@90Percentile	3249041.85	1	3249041.85	1151.00	0
	Contrast	25.32	1	25.32	81.37	0
	correlation	1.85	1	1.85	7.06	0.008
	Energy	7258000000000.00	1	7258000000000.00	213.78	0
	Entropy	49.86	1	49.86	196.80	0
	Kurtosis	524.30	1	524.30	701.25	0
	maximum	3422248.09	1	3422248.09	1128.00	0

	Mean	2884849.89	1	2884849.89	1079.00	0
	MeanAbsoluteDeviation	6178.31	1	6178.31	29.19	0
	Median	2890417.81	1	2890417.81	1138.00	0
	Minimum	2447829.12	1	2447829.12	800.86	0
	Range	81440.57	1	81440.57	70.79	0
	Skewness	1.77	1	1.77	3.89	0.05
	TotalEnergy	37120000000000.00	1	371200000000000.00	112.94	0
	Uniformity	38.44	1	38.44	824.82	0
	Variance	3601079.22	1	3601079.22	1.58	0.21
time_days	@10Percentile	26005.87	1	26005.87	8.45	0.004**
	@90Percentile	36779.91	1	36779.91	13.03	<0.001**
	Contrast	0.99	1	0.99	3.18	0.076
	correlation	0.09	1	0.09	0.35	0.554
	Energy	287300000000.00	1	287300000000.00	8.46	0.004**
	Entropy	0.75	1	0.75	2.94	0.087
	Kurtosis	1.34	1	1.34	1.80	0.181
	maximum	41851.27	1	41851.27	13.79	<0.001**
	Mean	30641.39	1	30641.39	11.46	0.001**
	MeanAbsoluteDeviation	158.36	1	158.36	0.75	0.388
	Median	29451.43	1	29451.43	11.60	0.001**
	Minimum	23930.31	1	23930.31	7.83	0.005**
	Range	2488.17	1	2488.17	2.16	0.143
	Skewness	0.29	1	0.29	0.63	0.43
	TotalEnergy	1502000000000.00	1	1502000000000.00	4.57	0.033*
	Uniformity	0.13	1	0.13	2.68	0.103
	Variance	26184.75	1	26184.75	0.01	0.915
dosegr	@10Percentile	30671.47	5	6134.30	1.99	0.08
	@90Percentile	44480.51	5	8896.10	3.15	0.009**
	Contrast	1.98	5	0.40	1.28	0.275
	correlation	1.37	5	0.27	1.05	0.391

	Energy	837800000000.00	5	167600000000.00	4.94	<0.001**
	Entropy	1.37	5	0.28	1.08	0.369
	Kurtosis	3.21	5	0.64	0.86	0.51
	maximum	46244.98	5	9249.00	3.05	0.011*
	Mean	36309.64	5	7261.93	2.72	0.02*
	MeanAbsoluteDeviation	609.58	5	121.92	0.58	0.718
	Median	38800.29	5	7760.06	3.06	0.011*
	Minimum	30222.37	5	6044.47	1.98	0.082
	Range	5085.68	5	1017.14	0.88	0.492
	Skewness	1.43	5	0.29	0.63	0.678
	TotalEnergy	4291000000000.00	5	858200000000.00	2.61	0.025*
	Uniformity	0.25	5	0.05	1.08	0.371
	Variance	6148236.32	5	1229647.26	0.54	0.747
dosegr * time_days	@10Percentile	21296.70	5	4259.34	1.38	0.231
	@90Percentile	28609.45	5	5721.89	2.03	0.075
	Contrast	1.20	5	0.24	0.77	0.57
	correlation	1.13	5	0.23	0.86	0.507
	Energy	289500000000.00	5	57890000000.00	1.71	0.133
	Entropy	0.47	5	0.09	0.37	0.871
	Kurtosis	1.23	5	0.25	0.33	0.895
	maximum	31625.96	5	6325.19	2.08	0.068
	Mean	24639.17	5	4927.83	1.84	0.104
	MeanAbsoluteDeviation	321.21	5	64.24	0.30	0.911
	Median	24634.89	5	4926.98	1.94	0.088
	Minimum	20054.81	5	4010.96	1.31	0.259
	Range	2938.70	5	587.74	0.51	0.768
	Skewness	2.40	5	0.48	1.05	0.386
	TotalEnergy	856900000000.00	5	171400000000.00	0.52	0.76
	Uniformity	0.11	5	0.02	0.47	0.796
	Variance	1101098.53	5	220219.71	0.10	0.993
Error	@10Percentile	859058.81	279	3079.06		
	@90Percentile	787562.70	279	2822.81		

	Contrast	86.81	279	0.31		
	correlation	73.03	279	0.26		
	Energy	9472000000000.00	279	33950000000.00		
	Entropy	70.68	279	0.25		
	Kurtosis	208.60	279	0.75		
	maximum	846664.91	279	3034.64		
	Mean	745780.74	279	2673.05		
	MeanAbsoluteDeviation	59057.57	279	211.68		
	Median	708476.28	279	2539.34		
	Minimum	852764.11	279	3056.50		
	Range	320970.43	279	1150.43		
	Skewness	127.12	279	0.46		
	TotalEnergy	91710000000000.00	279	328700000000.00		
	Uniformity	13.00	279	0.05		
	Variance	637200000.00	279	2283953.38		
Total	@10Percentile	8260247.02	291			
	@90Percentile	10430000.00	291			
	Contrast	152.47	291			
	correlation	90.45	291			
	Energy	30830000000000.00	291			
	Entropy	218.97	291			
	Kurtosis	1822.59	291			
	maximum	10950000.00	291			
	Mean	9212007.24	291			

	MeanAbsoluteDeviation	84562.90	291			
	Median	9333837.19	291			
	Minimum	7947718.95	291			
	Range	601781.33	291			
	Skewness	132.50	291			
	TotalEnergy	1873000000000000.00	291			
	Uniformity	153.00	291			
	Variance	692800000.00	291			
Corrected Total	@10Percentile	916569.49	290			
	@90Percentile	878555.39	290			
	Contrast	94.38	290			
	correlation	76.81	290			
	Energy	111100000000000.00	290			
	Entropy	75.22	290			
	Kurtosis	215.75	290			
	maximum	945945.91	290			
	Mean	815500.14	290			
	MeanAbsoluteDeviation	62033.81	290			
	Median	784832.52	290			
	Minimum	907745.43	290			
	Range	342828.23	290			
	Skewness	129.68	290			
	TotalEnergy	991300000000000.00	290			
	Uniformity	13.77	290			

	Variance	662200000.00	290			
a. R Squared = .063 (Adjusted R Squared = .026)						
b. R Squared = .104 (Adjusted R Squared = .068)						
c. R Squared = .080 (Adjusted R Squared = .044)						
d. R Squared = .049 (Adjusted R Squared = .012)						
e. R Squared = .148 (Adjusted R Squared = .114)						
f. R Squared = .060 (Adjusted R Squared = .023)						
g. R Squared = .033 (Adjusted R Squared = -.005)						
h. R Squared = .105 (Adjusted R Squared = .070)						
i. R Squared = .085 (Adjusted R Squared = .049)						
j. R Squared = .048 (Adjusted R Squared = .010)						
k. R Squared = .097 (Adjusted R Squared = .062)						
l. R Squared = .061 (Adjusted R Squared = .024)						
m. R Squared = .064 (Adjusted R Squared = .027)						
n. R Squared = .020 (Adjusted R Squared = -.019)						
o. R Squared = .075 (Adjusted R Squared = .038)						
p. R Squared = .056 (Adjusted R Squared = .018)						
q. R Squared = .038 (Adjusted R Squared = .000)						
r. region = POST.CC						

Note : * indicates p value is significant at 0.05 means P <0.05

**** indicates p value is significant at 0.05 means P <0.01**

8.Region = PTV

Between-Subjects Factors[a]			
		Value Label	N
dose (Binned)	4	30.56- 40.55	4
	5	40.56- 50.55	13
	6	50.56-60.55	253
a. region = PTV			

Descriptive Statistics[a]				
	dose (Binned)	Mean	Std. Deviation	N
@10Percentile	30.56- 40.55	149.52	22.85	4
	40.56- 50.55	184.75	103.49	13
	50.56-60.55	203.16	65.95	253
	Total	201.48	67.93	270
@90Percentile	30.56- 40.55	168.83	14.89	4
	40.56- 50.55	208.59	118.31	13
	50.56-60.55	247.34	84.05	253
	Total	244.31	86.02	270
Contrast	30.56- 40.55	0.21	0.20	4
	40.56- 50.55	0.64	0.92	13
	50.56-60.55	1.08	2.05	253
	Total	1.05	2.00	270
correlation	30.56- 40.55	0.42	0.43	4
	40.56- 50.55	0.13	0.40	13
	50.56-60.55	0.30	0.27	253
	Total	0.29	0.28	270
Energy	30.56- 40.55	673800.00	135205.00	4
	40.56- 50.55	786750.00	1223020.00	13
	50.56-60.55	1262100.00	1067330.00	253
	Total	1230500.00	1072010.00	270
Entropy	30.56- 40.55	0.66	0.54	4
	40.56- 50.55	0.90	0.60	13
	50.56-60.55	1.33	0.63	253
	Total	1.30	0.64	270
Kurtosis	30.56- 40.55	2.36	0.44	4
	40.56- 50.55	2.91	0.84	13
	50.56-60.55	3.27	2.53	253
	Total	3.24	2.46	270
maximum	30.56- 40.55	173.40	13.90	4
	40.56- 50.55	216.51	121.06	13
	50.56-60.55	268.11	98.41	253
	Total	264.22	99.87	270

Mean	30.56- 40.55	160.12	16.85	4
	40.56- 50.55	196.28	110.13	13
	50.56-60.55	223.36	72.19	253
	Total	221.12	74.27	270
MeanAbsoluteDeviation	30.56- 40.55	6.21	2.70	4
	40.56- 50.55	8.66	5.95	13
	50.56-60.55	15.60	13.70	253
	Total	15.12	13.45	270
Median	30.56- 40.55	160.53	15.73	4
	40.56- 50.55	195.99	110.39	13
	50.56-60.55	220.02	71.84	253
	Total	217.98	73.88	270
Minimum	30.56- 40.55	144.96	26.43	4
	40.56- 50.55	175.82	97.34	13
	50.56-60.55	194.68	63.57	253
	Total	193.03	65.33	270
Range	30.56- 40.55	28.43	13.63	4
	40.56- 50.55	40.69	26.67	13
	50.56-60.55	73.43	61.65	253
	Total	71.19	60.59	270
Skewness	30.56- 40.55	-0.12	0.46	4
	40.56- 50.55	-0.01	0.61	13
	50.56-60.55	0.44	0.86	253
	Total	0.41	0.85	270
TotalEnergy	30.56- 40.55	2342200.00	469992.00	4
	40.56- 50.55	3705900.00	4917920.00	13
	50.56-60.55	2479500.00	2194230.00	253
	Total	2536500.00	2379380.00	270
Uniformity	30.56- 40.55	0.72	0.24	4
	40.56- 50.55	0.62	0.22	13
	50.56-60.55	0.49	0.20	253
	Total	0.50	0.21	270
Variance	30.56- 40.55	65.53	62.52	4
	40.56- 50.55	156.95	249.12	13
	50.56-60.55	643.99	1474.46	253
	Total	611.97	1433.48	270
a. region = PTV				

Multivariate Tests[c,d]						
Effect		Value	F	Hypothesis df	Error df	Sig.
Intercept	Pillai's Trace	0.97	5.370E2[a]	16.00	249.00	<0.001**
time_days	Pillai's Trace	0.06	.907[a]	16.00	249.00	0.56
dosegr	Pillai's Trace	0.12	1.01	32.00	500.00	0.46
dosegr * time_days	Pillai's Trace	0.09	0.69	32.00	500.00	0.90
a. Exact statistic						
b. The statistic is an upper bound on F that yields a lower bound on the significance level.						
c. region = PTV						
d. Design: Intercept + time_days + dosegr + dosegr * time_days						

Note : * indicates p value is significant at 0.05 means P <0.05
**** indicates p value is significant at 0.05 means P <0.01**

There was a no statistically significant effect on TA features

Tests of Between-Subjects Effects[r]						
Source	Dependent Variable	Type III Sum of Squares	df	Mean Square	F	Sig.
Corrected Model	@10Percentile	40333.225[a]	5	8066.65	1.77	0.12
	@90Percentile	71284.547[b]	5	14256.91	1.96	0.09
	Contrast	5.469[c]	5	1.09	0.27	0.93
	correlation	.772[d]	5	0.15	2.02	0.08
	Energy	1.031E13[e]	5	2061000000000.00	1.82	0.11
	Entropy	5.045[f]	5	1.01	2.53	0.03
	Kurtosis	7.756[g]	5	1.55	0.25	0.94
	maximum	102525.527[h]	5	20505.11	2.10	0.07
	Mean	55698.817[i]	5	11139.76	2.06	0.07
	MeanAbsolute Deviation	999.981[j]	5	200.00	1.11	0.36
	Median	54707.231[k]	5	10941.45	2.04	0.07
	Minimum	37702.828[l]	5	7540.57	1.79	0.12
	Range	22599.049[m]	5	4519.81	1.24	0.29
	Skewness	4.505[n]	5	0.90	1.25	0.28

	TotalEnergy	4.710E13[o]	5	942000000000.00	1.69	0.14
	Uniformity	.569[p]	5	0.11	2.74	0.02
	Variance	4.154E6[q]	5	830875.46	0.40	0.85
Intercept	@10Percentile	434621.51	1	434621.51	95.53	0.00
	@90Percentile	605179.70	1	605179.70	83.24	0.00
	Contrast	6.28	1	6.28	1.56	0.21
	correlation	0.45	1	0.45	5.92	0.02
	Energy	120700000000000.00	1	12070000000000.00	10.66	0.00
	Entropy	16.98	1	16.98	42.56	0.00
	Kurtosis	107.64	1	107.64	17.51	0.00
	maximum	669545.44	1	669545.44	68.49	0.00
	Mean	517545.86	1	517545.86	95.67	0.00
	MeanAbsolute Deviation	1720.80	1	1720.80	9.53	0.00
	Median	513956.51	1	513956.51	96.00	0.00
	Minimum	391106.09	1	391106.09	93.00	0.00
	Range	37199.92	1	37199.92	10.18	0.00
	Skewness	0.06	1	0.06	0.09	0.77
	TotalEnergy	115000000000000.00	1	11500000000000000.00	20.58	0.00
	Uniformity	4.26	1	4.26	102.41	0.00
	Variance	1255230.51	1	1255230.51	0.60	0.44
time_days	@10Percentile	267.96	1	267.96	0.06	0.81
	@90Percentile	0.57	1	0.57	0.00	0.99
	Contrast	0.06	1	0.06	0.02	0.90
	correlation	0.29	1	0.29	3.79	0.05
	Energy	1346000000.00	1	1346000000.00	0.00	0.97
	Entropy	0.74	1	0.74	1.86	0.17
	Kurtosis	0.02	1	0.02	0.00	0.95
	maximum	2.14	1	2.14	0.00	0.99
	Mean	29.16	1	29.16	0.01	0.94
	MeanAbsolute Deviation	27.34	1	27.34	0.15	0.70
	Median	11.15	1	11.15	0.00	0.96
	Minimum	600.37	1	600.37	0.14	0.71
	Range	530.90	1	530.90	0.15	0.70
	Skewness	0.68	1	0.68	0.95	0.33
	TotalEnergy	1116000000.00	1	1116000000.00	0.00	0.99
	Uniformity	0.12	1	0.12	2.87	0.09
	Variance	6817.02	1	6817.02	0.00	0.95
Dosegr	@10Percentile	18142.52	2	9071.26	1.99	0.14
	@90Percentile	34277.79	2	17138.89	2.36	0.10

	Contrast	2.08	2	1.04	0.26	0.77
	correlation	0.40	2	0.20	2.63	0.07
	Energy	3882000000000.00	2	1941000000000.00	1.72	0.18
	Entropy	1.33	2	0.67	1.67	0.19
	Kurtosis	4.97	2	2.48	0.40	0.67
	maximum	52051.90	2	26025.95	2.66	0.07
	Mean	24184.00	2	12092.00	2.24	0.11
	MeanAbsolute Deviation	378.60	2	189.30	1.05	0.35
	Median	21825.70	2	10912.85	2.04	0.13
	Minimum	18429.92	2	9214.96	2.19	0.11
	Range	8983.93	2	4491.97	1.23	0.29
	Skewness	3.74	2	1.87	2.60	0.08
	TotalEnergy	4285000000000.00	2	2143000000000.00	0.38	0.68
	Uniformity	0.11	2	0.06	1.36	0.26
	Variance	1807814.31	2	903907.16	0.44	0.65
dosegr * time_days	@10Percentile	3562.35	2	1781.17	0.39	0.68
	@90Percentile	2826.99	2	1413.49	0.19	0.82
	Contrast	0.13	2	0.06	0.02	0.98
	correlation	0.35	2	0.18	2.30	0.10
	Energy	529000000000.00	2	264500000000.00	0.23	0.79
	Entropy	0.75	2	0.38	0.94	0.39
	Kurtosis	1.40	2	0.70	0.11	0.89
	maximum	3906.66	2	1953.33	0.20	0.82
	Mean	3326.97	2	1663.49	0.31	0.74
	MeanAbsolute Deviation	14.18	2	7.09	0.04	0.96
	Median	3473.58	2	1736.79	0.32	0.72
	Minimum	4567.52	2	2283.76	0.54	0.58
	Range	297.33	2	148.67	0.04	0.96
	Skewness	0.81	2	0.41	0.56	0.57
	TotalEnergy	2377000000000.00	2	1189000000000.00	0.21	0.81
	Uniformity	0.14	2	0.07	1.69	0.19
	Variance	8937.57	2	4468.78	0.00	1.00
Error	@10Percentile	1201121.94	264	4549.70		
	@90Percentile	1919307.46	264	7270.10		
	Contrast	1065.42	264	4.04		
	correlation	20.18	264	0.08		
	Energy	298800000000000.00	264	1132000000000.00		
	Entropy	105.32	264	0.40		

	Kurtosis	1622.64	264	6.15		
	maximum	2580687.57	264	9775.33		
	Mean	1428118.16	264	5409.54		
	MeanAbsolute Deviation	47660.04	264	180.53		
	Median	1413447.31	264	5353.97		
	Minimum	1110280.81	264	4205.61		
	Range	965064.90	264	3655.55		
	Skewness	189.70	264	0.72		
	TotalEnergy	1476000000000000.00	264	5590000000000.00		
	Uniformity	10.97	264	0.04		
	Variance	548600000.00	264	2078047.97		
Total	@10Percentile	12200000.00	270			
	@90Percentile	18110000.00	270			
	Contrast	1366.76	270			
	correlation	43.57	270			
	Energy	71790000000000.00	270			
	Entropy	568.33	270			
	Kurtosis	4466.63	270			
	maximum	21530000.00	270			
	Mean	14690000.00	270			
	MeanAbsolute Deviation	110421.42	270			
	Median	14300000.00	270			
	Minimum	11210000.00	270			
	Range	2355923.86	270			
	Skewness	239.12	270			
	TotalEnergy	32600000000000000.00	270			
	Uniformity	78.84	270			
	Variance	653900000.00	270			
Corrected Total	@10Percentile	1241455.17	269			
	@90Percentile	1990592.00	269			
	Contrast	1070.89	269			
	correlation	20.96	269			
	Energy	30910000000000.00	269			
	Entropy	110.36	269			
	Kurtosis	1630.39	269			
	maximum	2683213.10	269			
	Mean	1483816.97	269			

	MeanAbsolute Deviation	48660.02	269			
	Median	1468154.54	269			
	Minimum	1147983.64	269			
	Range	987663.95	269			
	Skewness	194.20	269			
	TotalEnergy	1523000000000000.00	269			
	Uniformity	11.54	269			
	Variance	552800000.00	269			
a. R Squared = .032 (Adjusted R Squared = .014)						
b. R Squared = .036 (Adjusted R Squared = .018)						
c. R Squared = .005 (Adjusted R Squared = -.014)						
d. R Squared = .037 (Adjusted R Squared = .019)						
e. R Squared = .033 (Adjusted R Squared = .015)						
f. R Squared = .046 (Adjusted R Squared = .028)						
g. R Squared = .005 (Adjusted R Squared = -.014)						
h. R Squared = .038 (Adjusted R Squared = .020)						
i. R Squared = .038 (Adjusted R Squared = .019)						
j. R Squared = .021 (Adjusted R Squared = .002)						
k. R Squared = .037 (Adjusted R Squared = .019)						
l. R Squared = .033 (Adjusted R Squared = .015)						
m. R Squared = .023 (Adjusted R Squared = .004)						
n. R Squared = .023 (Adjusted R Squared = .005)						
o. R Squared = .031 (Adjusted R Squared = .013)						
p. R Squared = .049 (Adjusted R Squared = .031)						
q. R Squared = .008 (Adjusted R Squared = -.011)						
r. region = PTV						

Note : * indicates p value is significant at 0.05 means P <0.05
**** indicates p value is significant at 0.05 means P <0.01**

9.Region = R.CER

Between-Subjects Factors[a]			
		Value Label	N
dose (Binned)	1	0- 10.55	132
	2	10.56- 20.55	14
	3	20.56- 30.55	24
	5	40.56- 50.55	17
	6	50.56-60.55	105
a. region = R.CER			

Descriptive Statistics[a]				
	dose (Binned)	Mean	Std. Deviation	N
@10Percentile	0- 10.55	204.69	60.97	132
	10.56- 20.55	200.19	45.90	14
	20.56- 30.55	189.60	57.98	24
	40.56- 50.55	194.58	55.16	17
	50.56-60.55	188.02	53.35	105
	Total	196.65	57.27	292
@90Percentile	0- 10.55	221.66	65.29	132
	10.56- 20.55	215.33	49.48	14
	20.56- 30.55	205.68	61.44	24
	40.56- 50.55	212.40	62.61	17
	50.56-60.55	206.80	58.68	105
	Total	214.16	61.84	292
Contrast	0- 10.55	0.30	0.20	132
	10.56- 20.55	0.22	0.26	14
	20.56- 30.55	0.30	0.20	24
	40.56- 50.55	0.32	0.22	17
	50.56-60.55	0.32	0.21	105

	Total	0.30	0.21	292
correlation	0- 10.55	0.16	0.33	132
	10.56-20.55	0.26	0.43	14
	20.56-30.55	0.21	0.39	24
	40.56-50.55	0.17	0.34	17
	50.56-60.55	0.14	0.30	105
	Total	0.16	0.33	292
Energy	0- 10.55	1095500.00	702524.00	132
	10.56-20.55	1075900.00	661117.00	14
	20.56-30.55	829790.00	621347.00	24
	40.56-50.55	672250.00	367334.00	17
	50.56-60.55	943730.00	757221.00	105
	Total	993520.00	706215.00	292
Entropy	0- 10.55	0.71	0.38	132
	10.56-20.55	0.53	0.45	14
	20.56-30.55	0.68	0.40	24
	40.56-50.55	0.73	0.40	17
	50.56-60.55	0.75	0.39	105
	Total	0.71	0.39	292
Kurtosis	0- 10.55	2.77	0.69	132
	10.56-20.55	2.77	0.62	14
	20.56-30.55	2.60	0.57	24
	40.56-50.55	2.83	0.92	17
	50.56-60.55	2.59	0.79	105
	Total	2.69	0.73	292
maximum	0- 10.55	226.93	67.27	132
	10.56-20.55	220.35	51.98	14
	20.56-30.55	210.31	62.84	24

	40.56-50.55	216.47	63.39	17
	50.56-60.55	211.97	60.26	105
	Total	219.26	63.57	292
Mean	0- 10.55	213.16	63.05	132
	10.56-20.55	207.87	47.54	14
	20.56-30.55	197.45	59.40	24
	40.56-50.55	203.34	58.52	17
	50.56-60.55	197.26	55.83	105
	Total	205.33	59.40	292
MeanAbsoluteDeviation	0- 10.55	5.63	2.37	132
	10.56-20.55	5.05	1.99	14
	20.56-30.55	5.38	2.37	24
	40.56-50.55	6.02	2.62	17
	50.56-60.55	6.24	3.17	105
	Total	5.82	2.69	292
Median	0- 10.55	213.08	63.03	132
	10.56-20.55	208.03	47.51	14
	20.56-30.55	197.19	58.99	24
	40.56-50.55	203.43	58.61	17
	50.56-60.55	197.20	55.83	105
	Total	205.26	59.37	292
Minimum	0- 10.55	199.36	60.02	132
	10.56-20.55	194.51	45.21	14
	20.56-30.55	186.10	58.18	24
	40.56-50.55	188.51	53.76	17
	50.56-60.55	183.22	52.43	105
	Total	191.60	56.37	292
Range	0- 10.55	27.57	11.79	132
	10.56-20.55	25.85	12.11	14

	20.56-30.55	24.21	9.08	24
	40.56-50.55	27.95	12.12	17
	50.56-60.55	28.75	13.52	105
	Total	27.66	12.27	292
Skewness	0- 10.55	-0.02	0.48	132
	10.56-20.55	-0.13	0.37	14
	20.56-30.55	0.09	0.51	24
	40.56-50.55	-0.12	0.66	17
	50.56-60.55	0.08	0.43	105
	Total	0.02	0.48	292
TotalEnergy	0- 10.55	1541300.00	2095590.00	132
	10.56-20.55	1974100.00	1467470.00	14
	20.56-30.55	2108700.00	1358910.00	24
	40.56-50.55	2366300.00	1469070.00	17
	50.56-60.55	2636100.00	1776540.00	105
	Total	2050400.00	1927030.00	292
Uniformity	0- 10.55	0.69	0.18	132
	10.56-20.55	0.78	0.20	14
	20.56-30.55	0.69	0.19	24
	40.56-50.55	0.67	0.18	17
	50.56-60.55	0.68	0.18	105
	Total	0.69	0.18	292
Variance	0- 10.55	57.49	60.62	132
	10.56-20.55	45.92	41.56	14
	20.56-30.55	50.48	48.43	24
	40.56-50.55	66.26	55.37	17
	50.56-60.55	71.36	72.68	105
	Total	61.86	63.55	292

a. region = R.CER				

Multivariate Tests[c,d]						
Effect		Value	F	Hypothesis df	Error df	Sig.
Intercept	Pillai's Trace	1.00	6.454E3[a]	16.00	267.00	<0.001**
time_days	Pillai's Trace	0.10	1.870[a]	16.00	267.00	0.023*
Dosegr	Pillai's Trace	0.35	1.64	64.00	1080.00	0.002**
dosegr * time_days	Pillai's Trace	0.27	1.21	64.00	1080.00	0.13
a. Exact statistic						
b. The statistic is an upper bound on F that yields a lower bound on the significance level.						
c. region = R.CER						
d. Design: Intercept + time_days + dosegr + dosegr * time_days						

Note : * indicates p value is significant at 0.05 means P <0.05
**** indicates p value is significant at 0.05 means P <0.01**

There was a statistically significant difference in TA features based on time in days F (16, 267) = 1.87, p < 0.05 Pillai Trace = 0.1

There was a statistically significant difference in TA features based on dose levels F (64, 1080) = 1.64, p < 0.05 Pillai Trace = 0.35

Tests of Between-Subjects Effects[r]						
Source	Dependent Variable	Type III Sum of Squares	df	Mean Square	F	Sig.
Corrected Model	@10Percentile	36707.397[a]	9	4078.60	1.25	0.26
	@90Percentile	37896.386[b]	9	4210.71	1.11	0.36
	Contrast	.358[c]	9	0.04	0.92	0.51
	correlation	.578[d]	9	0.06	0.58	0.81
	Energy	7.013E12[e]	9	779200000000.00	1.59	0.12
	Entropy	1.394[f]	9	0.16	1.02	0.43
	Kurtosis	9.009[g]	9	1.00	1.93	0.05
	maximum	41693.915[h]	9	4632.66	1.15	0.33
	Mean	36888.537[i]	9	4098.73	1.17	0.32

	MeanAbsoluteDeviation	76.966[j]	9	8.55	1.19	0.30
	Median	36255.183[k]	9	4028.35	1.15	0.33
	Minimum	33219.242[l]	9	3691.03	1.17	0.32
	Range	2207.601[m]	9	245.29	1.66	0.10
	Skewness	4.505[n]	9	0.50	2.28	0.02
	TotalEnergy	9.748E13[o]	9	10830000000000.00	3.11	0.00
	Uniformity	.267[p]	9	0.03	0.92	0.51
	Variance	41394.464[q]	9	4599.39	1.14	0.33
Intercept	@10Percentile	2454226.84	1	2454226.84	754.26	0.00
	@90Percentile	2917899.08	1	2917899.08	765.55	0.00
	Contrast	6.41	1	6.41	148.73	0.00
	correlation	1.30	1	1.30	11.85	0.00
	Energy	58440000000000.00	1	58440000000000.00	119.32	0.00
	Entropy	33.45	1	33.45	219.17	0.00
	Kurtosis	401.70	1	401.70	772.43	0.00
	maximum	3068652.58	1	3068652.58	762.85	0.00
	Mean	2675186.91	1	2675186.91	762.05	0.00
	MeanAbsoluteDeviation	2263.22	1	2263.22	314.52	0.00
	Median	2671174.63	1	2671174.63	761.43	0.00
	Minimum	2323615.00	1	2323615.00	735.00	0.00
	Range	51718.11	1	51718.11	350.42	0.00
	Skewness	0.67	1	0.67	3.07	0.08
	TotalEnergy	362500000000000.00	1	362500000000000.00	103.98	0.00
	Uniformity	26.65	1	26.65	823.62	0.00
	Variance	281206.57	1	281206.57	69.94	0.00

time_days	@10Percentile	7616.91	1	7616.91	2.34	0.13
	@90Percentile	10495.35	1	10495.35	2.75	0.10
	Contrast	0.17	1	0.17	3.85	0.05
	correlation	0.16	1	0.16	1.50	0.22
	Energy	496200000000.00	1	496200000000.00	1.01	0.32
	Entropy	0.56	1	0.56	3.65	0.06
	Kurtosis	1.18	1	1.18	2.28	0.13
	maximum	12310.53	1	12310.53	3.06	0.08
	Mean	8701.55	1	8701.55	2.48	0.12
	MeanAbsoluteDeviation	29.80	1	29.80	4.14	0.043 *
	Median	8459.96	1	8459.96	2.41	0.12
	Minimum	6985.61	1	6985.61	2.21	0.14
	Range	749.27	1	749.27	5.08	0.025 *
	Skewness	1.80	1	1.80	8.21	0.004 **
	TotalEnergy	12580000000000.00	1	12580000000000.00	3.61	0.06
	Uniformity	0.09	1	0.09	2.79	0.10
	Variance	11908.49	1	11908.49	2.96	0.09
dosegr	@10Percentile	1389.01	4	347.25	0.11	0.98
	@90Percentile	1074.53	4	268.63	0.07	0.99
	Contrast	0.01	4	0.00	0.08	0.99
	correlation	0.02	4	0.01	0.05	1.00
	Energy	1342000000000.00	4	335500000000.00	0.69	0.60
	Entropy	0.18	4	0.05	0.29	0.88
	Kurtosis	4.34	4	1.09	2.09	0.08
	maximum	1286.25	4	321.56	0.08	0.99
	Mean	1235.39	4	308.85	0.09	0.99
	MeanAbsoluteDeviation	9.75	4	2.44	0.34	0.85
	Median	1232.17	4	308.04	0.09	0.99
	Minimum	1405.79	4	351.45	0.11	0.98
	Range	461.01	4	115.25	0.78	0.54
	Skewness	1.10	4	0.28	1.26	0.29
	TotalEnergy	64880000000000.00	4	16220000000000.00	4.65	0.001 **
	Uniformity	0.06	4	0.02	0.48	0.75

	Variance	4585.32	4	1146.33	0.29	0.89
dosegr * time_days	@10Percentile	4491.93	4	1122.98	0.35	0.85
	@90Percentile	4416.62	4	1104.16	0.29	0.89
	Contrast	0.08	4	0.02	0.46	0.76
	correlation	0.34	4	0.09	0.78	0.54
	Energy	1153000000000.00	4	288200000000.00	0.59	0.67
	Entropy	0.21	4	0.05	0.34	0.85
	Kurtosis	6.50	4	1.63	3.13	0.015 *
	maximum	4348.44	4	1087.11	0.27	0.90
	Mean	4362.62	4	1090.66	0.31	0.87
	MeanAbsoluteDeviation	5.36	4	1.34	0.19	0.95
	Median	4177.59	4	1044.40	0.30	0.88
	Minimum	4584.96	4	1146.24	0.36	0.84
	Range	368.79	4	92.20	0.63	0.65
	Skewness	2.49	4	0.62	2.83	0.03
	TotalEnergy	11030000000000.00	4	2758000000000.00	0.79	0.53
	Uniformity	0.06	4	0.01	0.44	0.78
	Variance	3188.05	4	797.01	0.20	0.94
Error	@10Percentile	917576.81	282	3253.82		
	@90Percentile	1074849.27	282	3811.52		
	Contrast	12.16	282	0.04		
	correlation	31.02	282	0.11		
	Energy	138100000000000.00	282	489800000000.00		
	Entropy	43.04	282	0.15		
	Kurtosis	146.66	282	0.52		
	maximum	1134380.35	282	4022.63		
	Mean	989968.77	282	3510.53		
	MeanAbsoluteDeviation	2029.21	282	7.20		
	Median	989290.21	282	3508.12		

	Minimum	891511.15	282	3161.39		
	Range	41620.47	282	147.59		
	Skewness	61.98	282	0.22		
	TotalEnergy	983100000000000.00	282	3486000000000.00		
	Uniformity	9.12	282	0.03		
	Variance	1133831.39	282	4020.68		
Total	@10Percentile	12250000.00	292			
	@90Percentile	14510000.00	292			
	Contrast	39.29	292			
	correlation	39.31	292			
	Energy	433400000000000.00	292			
	Entropy	193.60	292			
	Kurtosis	2271.08	292			
	maximum	15210000.00	292			
	Mean	13340000.00	292			
	MeanAbsoluteDeviation	11998.00	292			
	Median	13330000.00	292			
	Minimum	11640000.00	292			
	Range	267211.64	292			
	Skewness	66.56	292			
	TotalEnergy	2308000000000000.00	292			
	Uniformity	148.02	292			
	Variance	2292524.88	292			
Corrected Total	@10Percentile	954284.21	291			

	@90Percentile	1112745.66	291			
	Contrast	12.52	291			
	correlation	31.60	291			
	Energy	145100000000000.00	291			
	Entropy	44.43	291			
	Kurtosis	155.66	291			
	maximum	1176074.26	291			
	Mean	1026857.31	291			
	MeanAbsoluteDeviation	2106.17	291			
	Median	1025545.39	291			
	Minimum	924730.39	291			
	Range	43828.07	291			
	Skewness	66.49	291			
	TotalEnergy	1081000000000000.00	291			
	Uniformity	9.39	291			
	Variance	1175225.86	291			
a. R Squared = .038 (Adjusted R Squared = .008)						
b. R Squared = .034 (Adjusted R Squared = .003)						
c. R Squared = .029 (Adjusted R Squared = -.002)						
d. R Squared = .018 (Adjusted R Squared = -.013)						
e. R Squared = .048 (Adjusted R Squared = .018)						
f. R Squared = .031 (Adjusted R Squared = .000)						
g. R Squared = .058 (Adjusted R Squared = .028)						
h. R Squared = .035 (Adjusted R Squared = .005)						
i. R Squared = .036 (Adjusted R Squared = .005)						

j. R Squared = .037 (Adjusted R Squared = .006)					
k. R Squared = .035 (Adjusted R Squared = .005)					
l. R Squared = .036 (Adjusted R Squared = .005)					
m. R Squared = .050 (Adjusted R Squared = .020)					
n. R Squared = .068 (Adjusted R Squared = .038)					
o. R Squared = .090 (Adjusted R Squared = .061)					
p. R Squared = .028 (Adjusted R Squared = -.003)					
q. R Squared = .035 (Adjusted R Squared = .004)					
r. region = R.CER					

Note : * indicates p value is significant at 0.05 means P <0.05

**** indicates p value is significant at 0.05 means P <0.01**

Conclusion: from this table that time in days has a statistically significant effect on Mean absolute deviation, Range , skewness.

Conclusion: from this table that time in days has a statistically significant effect on Total Energy

After getting significant results in Tests of Between-Subjects Effects[r] we compare variation between all possible pairs of dose groups (independent variables) in this table we found significant variation between these pairs given above.

**** indicates p value is significant at 0.05 means P <0.01**

10.Region = R.CS

Between-Subjects Factors[a]			
		Value Label	N
dose (Binned)	1	0- 10.55	146
	2	10.56- 20.55	30
	3	20.56- 30.55	40
	4	30.56- 40.55	48
	5	40.56- 50.55	6
	6	50.56-60.55	22
a. region = R.CS			

Descriptive Statistics[a]				
	dose (Binned)	Mean	Std. Deviation	N
@10Percentile	0- 10.55	207.36	70.96	146
	10.56- 20.55	194.28	43.56	30
	20.56- 30.55	181.59	52.11	40
	30.56- 40.55	177.49	49.91	48
	40.56- 50.55	188.60	57.11	6
	50.56-60.55	200.87	56.01	22
	Total	196.70	62.45	292
@90Percentile	0- 10.55	223.40	75.97	146
	10.56- 20.55	214.55	48.41	30
	20.56- 30.55	196.39	52.70	40
	30.56- 40.55	193.81	51.49	48
	40.56- 50.55	205.23	55.58	6
	50.56-60.55	221.74	62.72	22
	Total	213.43	66.38	292
Contrast	0- 10.55	0.26	0.23	146
	10.56- 20.55	0.37	0.25	30
	20.56- 30.55	0.26	0.23	40
	30.56- 40.55	0.30	0.24	48
	40.56- 50.55	0.26	0.18	6
	50.56-60.55	0.31	0.15	22
	Total	0.28	0.23	292
correlation	0- 10.55	0.17	0.33	146
	10.56- 20.55	0.13	0.31	30
	20.56- 30.55	0.26	0.45	40
	30.56- 40.55	0.31	0.41	48
	40.56- 50.55	0.37	0.38	6
	50.56-60.55	0.20	0.30	22

	Total	0.21	0.36	292
Energy	0- 10.55	1145700.00	865206.00	146
	10.56- 20.55	1077500.00	536851.00	30
	20.56- 30.55	698840.00	528893.00	40
	30.56- 40.55	781590.00	672958.00	48
	40.56- 50.55	913310.00	526153.00	6
	50.56-60.55	931950.00	443631.00	22
	Total	996770.00	750617.00	292
Entropy	0- 10.55	0.65	0.38	146
	10.56- 20.55	0.82	0.47	30
	20.56- 30.55	0.58	0.42	40
	30.56- 40.55	0.68	0.45	48
	40.56- 50.55	0.72	0.43	6
	50.56-60.55	0.78	0.35	22
	Total	0.67	0.41	292
Kurtosis	0- 10.55	2.86	1.04	146
	10.56- 20.55	2.74	0.49	30
	20.56- 30.55	2.46	0.62	40
	30.56- 40.55	2.50	0.75	48
	40.56- 50.55	2.66	0.74	6
	50.56-60.55	3.21	2.00	22
	Total	2.76	1.02	292
maximum	0- 10.55	228.94	77.82	146
	10.56- 20.55	221.38	50.63	30
	20.56- 30.55	200.09	52.81	40
	30.56- 40.55	198.23	53.16	48
	40.56- 50.55	210.99	58.44	6
	50.56-60.55	229.34	61.57	22
	Total	218.83	67.94	292
Mean	0- 10.55	215.34	73.40	146
	10.56- 20.55	203.94	45.08	30
	20.56- 30.55	188.87	52.33	40
	30.56- 40.55	185.59	50.65	48
	40.56- 50.55	196.90	56.83	6
	50.56-60.55	211.31	59.28	22
	Total	204.97	64.29	292
MeanAbsoluteDeviation	0- 10.55	5.38	2.79	146
	10.56- 20.55	6.61	4.41	30
	20.56- 30.55	4.93	1.79	40
	30.56- 40.55	5.49	2.63	48
	40.56- 50.55	5.68	2.01	6

	50.56-60.55	6.99	2.55	22
	Total	5.59	2.87	292
Median	0- 10.55	215.27	73.32	146
	10.56- 20.55	203.17	44.89	30
	20.56- 30.55	188.57	52.53	40
	30.56- 40.55	185.50	50.90	48
	40.56- 50.55	197.39	56.53	6
	50.56-60.55	211.15	60.02	22
	Total	204.80	64.34	292
Minimum	0- 10.55	202.69	69.93	146
	10.56- 20.55	188.37	42.76	30
	20.56- 30.55	178.02	50.75	40
	30.56- 40.55	173.77	49.09	48
	40.56- 50.55	182.57	56.83	6
	50.56-60.55	195.97	54.84	22
	Total	192.17	61.40	292
Range	0- 10.55	26.25	12.48	146
	10.56- 20.55	33.00	22.57	30
	20.56- 30.55	22.08	8.54	40
	30.56- 40.55	24.46	11.38	48
	40.56- 50.55	28.42	9.99	6
	50.56-60.55	33.37	11.84	22
	Total	26.66	13.50	292
Skewness	0- 10.55	0.10	0.51	146
	10.56- 20.55	0.12	0.48	30
	20.56- 30.55	0.09	0.44	40
	30.56- 40.55	0.05	0.52	48
	40.56- 50.55	-0.02	0.28	6
	50.56-60.55	0.30	0.93	22
	Total	0.10	0.54	292
TotalEnergy	0- 10.55	1812100.00	2301870.00	146
	10.56- 20.55	1142000.00	635562.00	30
	20.56- 30.55	2682700.00	2119890.00	40
	30.56- 40.55	2109200.00	1218290.00	48
	40.56- 50.55	4355000.00	2508890.00	6
	50.56-60.55	3168100.00	1814030.00	22
	Total	2065700.00	2059340.00	292
Uniformity	0- 10.55	0.71	0.18	146
	10.56- 20.55	0.66	0.19	30
	20.56- 30.55	0.74	0.20	40
	30.56- 40.55	0.69	0.20	48

	40.56- 50.55	0.68	0.20	6
	50.56-60.55	0.65	0.16	22
	Total	0.70	0.19	292
Variance	0- 10.55	54.99	79.13	146
	10.56- 20.55	96.82	135.62	30
	20.56- 30.55	40.71	31.22	40
	30.56- 40.55	54.35	53.01	48
	40.56- 50.55	54.29	38.80	6
	50.56-60.55	87.19	61.82	22
	Total	59.64	78.13	292
a. region = R.CS				

Multivariate Tests[c,d]

Effect		Value	F	Hypothesis df	Error df	Sig.
Intercept	Pillai's Trace	0.998	7.200E3[a]	16	265	0
time_days	Pillai's Trace	0.094	1.723[a]	16	265	0.043*
dosegr	Pillai's Trace	0.558	2.114	80	1345.00	<0.001**
dosegr * time_days	Pillai's Trace	0.276	0.982	80	1345.00	0.525
a. Exact statistic						
b. The statistic is an upper bound on F that yields a lower bound on the significance level.						
c. region = R.CS						
d. Design: Intercept + time_days + dosegr + dosegr * time_days						

Note : * indicates p value is significant at 0.05 means P <0.05
**** indicates p value is significant at 0.05 means P <0.01**

There was a statistically significant difference in TA features based on time in days F (16, 265) = 1.723, p < 0.05 Pillai Trace = 0.094

There was a statistically significant difference in TA features based on dose levels F (80, 1345) = 2.114, p < 0.05 Pillai Trace = 0.558

Tests of Between-Subjects Effects[r]

Source	Dependent Variable	Type III Sum of Squares	df	Mean Square	F	Sig.
Corrected Model	@10Percentile	93621.363[a]	11	8511.03	2.29	0.01
	@90Percentile	105669.652[b]	11	9606.33	2.29	0.01

	Contrast	.693[c]	11	0.06	1.23	0.27
	correlation	2.129[d]	11	0.19	1.51	0.13
	Energy	1.468E13[e]	11	1335000000000.00	2.50	0.01
	Entropy	3.305[f]	11	0.30	1.87	0.04
	Kurtosis	15.480[g]	11	1.41	1.37	0.19
	maximum	117147.426[h]	11	10649.77	2.43	0.01
	Mean	99529.134[i]	11	9048.10	2.30	0.01
	MeanAbsoluteDeviation	224.248[j]	11	20.39	2.63	0.00
	Median	99734.562[k]	11	9066.78	2.30	0.01
	Minimum	87033.257[l]	11	7912.11	2.19	0.02
	Range	5960.962[m]	11	541.91	3.22	0.00
	Skewness	1.397[n]	11	0.13	0.43	0.94
	TotalEnergy	1.513E14[o]	11	13760000000000.00	3.56	0.00
	Uniformity	.544[p]	11	0.05	1.42	0.16
	Variance	126899.831[q]	11	11536.35	1.96	0.03
Intercept	@10Percentile	2135012.22	1	2135012.22	574.19	0.00
	@90Percentile	2536684.71	1	2536684.71	603.63	0.00
	Contrast	5.10	1	5.10	99.71	0.00
	correlation	2.02	1	2.02	15.71	0.00
	Energy	57210000000000.00	1	5721000000000.00	107.31	0.00
	Entropy	31.76	1	31.76	197.88	0.00
	Kurtosis	409.45	1	409.45	397.87	0.00
	maximum	2686986.51	1	2686986.51	613.71	0.00
	Mean	2331045.81	1	2331045.81	591.59	0.00
	MeanAbsoluteDeviation	1996.93	1	1996.93	257.91	0.00
	Median	2327308.61	1	2327308.61	589.82	0.00

	Minimum	2022061.78	1	2022061.78	560.64	0.00
	Range	47180.54	1	47180.54	280.69	0.00
	Skewness	1.01	1	1.01	3.40	0.07
	TotalEnergy	4836000000000000.00	1	4836000000000000.00	125.06	0.00
	Uniformity	21.37	1	21.37	613.74	0.00
	Variance	251193.92	1	251193.92	42.64	0.00
time_days	@10Percentile	16327.48	1	16327.48	4.39	0.037*
	@90Percentile	18592.14	1	18592.14	4.42	0.036*
	Contrast	0.05	1	0.05	0.91	0.34
	correlation	0.11	1	0.11	0.89	0.35
	Energy	1653000000000.00	1	1653000000000.00	3.10	0.08
	Entropy	0.63	1	0.63	3.91	0.049*
	Kurtosis	0.92	1	0.92	0.90	0.34
	maximum	20942.55	1	20942.55	4.78	0.03*
	Mean	17673.78	1	17673.78	4.49	0.035*
	MeanAbsoluteDeviation	15.14	1	15.14	1.96	0.16
	Median	17619.94	1	17619.94	4.47	0.035*
	Minimum	14690.48	1	14690.48	4.07	0.045*
	Range	552.77	1	552.77	3.29	0.07
	Skewness	0.11	1	0.11	0.37	0.54
	TotalEnergy	261000000000000.00	1	261000000000000.00	6.75	0.01*
	Uniformity	0.15	1	0.15	4.18	0.042*
	Variance	2747.47	1	2747.47	0.47	0.50
dosegr	@10Percentile	38158.87	5	7631.77	2.05	0.07
	@90Percentile	39325.45	5	7865.09	1.87	0.10
	Contrast	0.09	5	0.02	0.36	0.88
	correlation	0.64	5	0.13	1.00	0.42

	Energy	5537000000000.00	5	1107000000000.00	2.08	0.07
	Entropy	0.33	5	0.07	0.41	0.84
	Kurtosis	4.43	5	0.89	0.86	0.51
	maximum	42309.18	5	8461.84	1.93	0.09
	Mean	38772.86	5	7754.57	1.97	0.08
	MeanAbsoluteDeviation	44.71	5	8.94	1.16	0.33
	Median	39354.51	5	7870.90	2.00	0.08
	Minimum	36358.76	5	7271.75	2.02	0.08
	Range	1149.10	5	229.82	1.37	0.24
	Skewness	0.84	5	0.17	0.57	0.73
	TotalEnergy	87010000000000.00	5	17400000000000.00	4.50	0.001**
	Uniformity	0.06	5	0.01	0.33	0.90
	Variance	20654.82	5	4130.96	0.70	0.62
dosegr * time_days	@10Percentile	20991.25	5	4198.25	1.13	0.35
	@90Percentile	23391.25	5	4678.25	1.11	0.35
	Contrast	0.16	5	0.03	0.62	0.68
	correlation	0.74	5	0.15	1.15	0.33
	Energy	1979000000000.00	5	395900000000.00	0.74	0.59
	Entropy	0.76	5	0.15	0.95	0.45
	Kurtosis	2.60	5	0.52	0.51	0.77
	maximum	25199.13	5	5039.83	1.15	0.33
	Mean	21896.24	5	4379.25	1.11	0.35
	MeanAbsoluteDeviation	72.42	5	14.48	1.87	0.10
	Median	21721.49	5	4344.30	1.10	0.36
	Minimum	19644.80	5	3928.96	1.09	0.37
	Range	1138.53	5	227.71	1.36	0.24
	Skewness	0.23	5	0.05	0.16	0.98
	TotalEnergy	24460000000000.00	5	4891000000000.00	1.27	0.28
	Uniformity	0.13	5	0.03	0.73	0.60
	Variance	33278.09	5	6655.62	1.13	0.35
Error	@10Percentile	1041123.68	280	3718.30		
	@90Percentile	1176667.68	280	4202.39		

	Contrast	14.33	280	0.05		
	correlation	35.98	280	0.13		
	Energy	1493000000000000.00	280	533100000000.00		
	Entropy	44.94	280	0.16		
	Kurtosis	288.15	280	1.03		
	maximum	1225908.47	280	4378.25		
	Mean	1103291.59	280	3940.33		
	MeanAbsoluteDeviation	2167.95	280	7.74		
	Median	1104828.00	280	3945.81		
	Minimum	1009884.57	280	3606.73		
	Range	47064.02	280	168.09		
	Skewness	83.19	280	0.30		
	TotalEnergy	1083000000000000.00	280	3867000000000.00		
	Uniformity	9.75	280	0.04		
	Variance	1649370.92	280	5890.61		
Total	@10Percentile	12430000.00	292			
	@90Percentile	14580000.00	292			
	Contrast	38.30	292			
	correlation	50.48	292			
	Energy	4541000000000000.00	292			
	Entropy	180.81	292			
	Kurtosis	2523.77	292			
	maximum	15330000.00	292			
	Mean	13470000.00	292			

	MeanAbsoluteDeviation	11520.66	292			
	Median	13450000.00	292			
	Minimum	11880000.00	292			
	Range	260559.42	292			
	Skewness	87.69	292			
	TotalEnergy	2480000000000000.00	292			
	Uniformity	154.75	292			
	Variance	2814797.96	292			
Corrected Total	@10Percentile	1134745.04	291			
	@90Percentile	1282337.33	291			
	Contrast	15.03	291			
	correlation	38.11	291			
	Energy	164000000000000.00	291			
	Entropy	48.25	291			
	Kurtosis	303.63	291			
	maximum	1343055.89	291			
	Mean	1202820.72	291			
	MeanAbsoluteDeviation	2392.20	291			
	Median	1204562.56	291			
	Minimum	1096917.83	291			
	Range	53024.98	291			
	Skewness	84.58	291			
	TotalEnergy	123400000000000.00	291			
	Uniformity	10.29	291			

	Variance	1776270.75	291			
a. R Squared = .083 (Adjusted R Squared = .046)						
b. R Squared = .082 (Adjusted R Squared = .046)						
c. R Squared = .046 (Adjusted R Squared = .009)						
d. R Squared = .056 (Adjusted R Squared = .019)						
e. R Squared = .090 (Adjusted R Squared = .054)						
f. R Squared = .069 (Adjusted R Squared = .032)						
g. R Squared = .051 (Adjusted R Squared = .014)						
h. R Squared = .087 (Adjusted R Squared = .051)						
i. R Squared = .083 (Adjusted R Squared = .047)						
j. R Squared = .094 (Adjusted R Squared = .058)						
k. R Squared = .083 (Adjusted R Squared = .047)						
l. R Squared = .079 (Adjusted R Squared = .043)						
m. R Squared = .112 (Adjusted R Squared = .078)						
n. R Squared = .017 (Adjusted R Squared = -.022)						
o. R Squared = .123 (Adjusted R Squared = .088)						
p. R Squared = .053 (Adjusted R Squared = .016)						
q. R Squared = .071 (Adjusted R Squared = .035)						
r. region = R.CS						

Note : * indicates p value is significant at 0.05 means P <0.05
**** indicates p value is significant at 0.05 means P <0.01**

Conclusion: from this table that time in days has a statistically significant effect on @10percentile , @90percentile , Entropy, maximum,Mean , Median ,minimum,Total energy and Uniformity

Conclusion: from this table that dose level has a statistically significant effect on Total energy.

11.Region = R.THALAMUS

Between-Subjects Factors[a]			
		Value Label	N
dose (Binned)	1	0- 10.55	85
	2	10.56- 20.55	35
	3	20.56- 30.55	14
	4	30.56- 40.55	33
	5	40.56- 50.55	40
	6	50.56-60.55	85
a. region = R.THALAMUS			

Descriptive Statistics[a]				
	dose (Binned)	Mean	Std. Deviation	N
@10Percentile	0- 10.55	235.26	69.22	85.00
	10.56- 20.55	205.86	79.86	35.00
	20.56- 30.55	174.77	43.21	14.00
	30.56- 40.55	222.52	61.37	33.00
	40.56- 50.55	186.26	39.59	40.00
	50.56-60.55	209.79	58.88	85.00
	Total	213.27	64.57	292.00
@90Percentile	0- 10.55	263.10	74.59	85.00
	10.56- 20.55	234.31	92.46	35.00
	20.56- 30.55	193.37	48.23	14.00
	30.56- 40.55	245.82	66.08	33.00
	40.56- 50.55	209.54	43.38	40.00
	50.56-60.55	236.24	65.41	85.00
	Total	239.20	71.24	292.00
Contrast	0- 10.55	0.40	0.22	85.00
	10.56- 20.55	0.46	0.75	35.00
	20.56- 30.55	0.31	0.14	14.00
	30.56- 40.55	0.38	0.19	33.00
	40.56- 50.55	0.35	0.20	40.00
	50.56-60.55	0.39	0.23	85.00
	Total	0.39	0.33	292.00
correlation	0- 10.55	0.25	0.23	85.00
	10.56- 20.55	0.29	0.23	35.00
	20.56- 30.55	0.28	0.34	14.00
	30.56- 40.55	0.16	0.24	33.00
	40.56- 50.55	0.18	0.27	40.00
	50.56-60.55	0.25	0.24	85.00
	Total	0.24	0.25	292.00
Energy	0- 10.55	1477600.00	811623.00	85.00

	10.56- 20.55	1483400.00	1362530.00	35.00
	20.56- 30.55	708040.00	535447.00	14.00
	30.56- 40.55	1176100.00	759920.00	33.00
	40.56- 50.55	931850.00	686036.00	40.00
	50.56-60.55	1064700.00	747383.00	85.00
	Total	1212400.00	875584.00	292.00
Entropy	0- 10.55	1.05	0.38	85.00
	10.56- 20.55	1.02	0.45	35.00
	20.56- 30.55	0.80	0.37	14.00
	30.56- 40.55	0.95	0.34	33.00
	40.56- 50.55	0.87	0.39	40.00
	50.56-60.55	0.99	0.43	85.00
	Total	0.98	0.40	292.00
Kurtosis	0- 10.55	2.70	0.82	85.00
	10.56- 20.55	2.57	0.70	35.00
	20.56- 30.55	2.54	0.63	14.00
	30.56- 40.55	2.75	1.59	33.00
	40.56- 50.55	2.46	0.62	40.00
	50.56-60.55	2.48	0.65	85.00
	Total	2.59	0.86	292.00
maximum	0- 10.55	272.04	76.91	85.00
	10.56- 20.55	243.19	99.79	35.00
	20.56- 30.55	199.03	49.98	14.00
	30.56- 40.55	253.18	70.36	33.00
	40.56- 50.55	215.62	43.55	40.00
	50.56-60.55	242.93	67.70	85.00
	Total	246.74	74.46	292.00
Mean	0- 10.55	248.86	71.46	85.00
	10.56- 20.55	220.08	85.71	35.00
	20.56- 30.55	183.62	45.38	14.00
	30.56- 40.55	233.69	63.23	33.00
	40.56- 50.55	198.26	41.45	40.00
	50.56-60.55	223.06	62.04	85.00
	Total	226.13	67.55	292.00
MeanAbsoluteDeviation	0- 10.55	9.21	3.83	85.00
	10.56- 20.55	9.73	5.84	35.00
	20.56- 30.55	6.32	2.61	14.00
	30.56- 40.55	8.07	2.79	33.00
	40.56- 50.55	7.55	2.68	40.00
	50.56-60.55	8.87	3.77	85.00
	Total	8.68	3.89	292.00
Median	0- 10.55	248.30	71.56	85.00
	10.56- 20.55	219.97	84.18	35.00

	20.56- 30.55	182.69	44.28	14.00
	30.56- 40.55	233.75	62.91	33.00
	40.56- 50.55	198.51	41.55	40.00
	50.56-60.55	222.86	61.69	85.00
	Total	225.89	67.17	292.00
Minimum	0- 10.55	228.09	66.56	85.00
	10.56- 20.55	199.16	80.52	35.00
	20.56- 30.55	170.39	41.56	14.00
	30.56- 40.55	215.09	61.11	33.00
	40.56- 50.55	181.34	39.48	40.00
	50.56-60.55	203.24	57.89	85.00
	Total	206.75	63.28	292.00
Range	0- 10.55	43.94	18.19	85.00
	10.56- 20.55	44.02	24.47	35.00
	20.56- 30.55	28.64	11.68	14.00
	30.56- 40.55	38.10	14.41	33.00
	40.56- 50.55	34.28	12.94	40.00
	50.56-60.55	39.68	16.66	85.00
	Total	39.99	17.74	292.00
Skewness	0- 10.55	0.21	0.47	85.00
	10.56- 20.55	0.03	0.52	35.00
	20.56- 30.55	0.25	0.50	14.00
	30.56- 40.55	0.07	0.57	33.00
	40.56- 50.55	-0.01	0.41	40.00
	50.56-60.55	0.03	0.50	85.00
	Total	0.09	0.49	292.00
TotalEnergy	0- 10.55	1554000.00	1059420.00	85.00
	10.56- 20.55	2361700.00	3584470.00	35.00
	20.56- 30.55	1730100.00	1185880.00	14.00
	30.56- 40.55	3537500.00	1815690.00	33.00
	40.56- 50.55	2028500.00	1064170.00	40.00
	50.56-60.55	3429100.00	2270410.00	85.00
	Total	2494200.00	2141790.00	292.00
Uniformity	0- 10.55	0.56	0.15	85.00
	10.56- 20.55	0.58	0.18	35.00
	20.56- 30.55	0.63	0.17	14.00
	30.56- 40.55	0.58	0.15	33.00
	40.56- 50.55	0.63	0.17	40.00
	50.56-60.55	0.57	0.17	85.00
	Total	0.58	0.16	292.00
Variance	0- 10.55	149.95	141.78	85.00
	10.56- 20.55	182.25	284.04	35.00
	20.56- 30.55	67.71	46.60	14.00

	30.56- 40.55	109.20	83.13	33.00
	40.56- 50.55	95.96	74.41	40.00
	50.56-60.55	134.33	119.16	85.00
	Total	133.33	147.51	292.00
a. region = R.THALAMUS				

Multivariate Tests[c,d]						
Effect		Value	F	Hypothesis df	Error df	Sig.
Intercept	Pillai's Trace	0.997	5.137E3[a]	16	265	0
time_days	Pillai's Trace	0.061	1.076[a]	16	265	0.378
dosegr	Pillai's Trace	0.62	2.38	80	1345	<0.001 **
dosegr * time_days	Pillai's Trace	0.22	0.77	80	1345	1
a. Exact statistic						
b. The statistic is an upper bound on F that yields a lower bound on the significance level.						
c. region = R.THALAMUS						
d. Design: Intercept + time_days + dosegr + dosegr * time_days						

Tests of Between-Subjects Effects[r]						
Source	Dependent Variable	Type III Sum of Squares	df	Mean Square	F	Sig.
Corrected Model	@10Percentile	129062.561[a]	11	11732.96	3.03	0.001
	@90Percentile	158251.727[b]	11	14386.52	3.05	0.001
	Contrast	1.085[c]	11	0.10	0.93	0.516
	correlation	1.079[d]	11	0.10	1.66	0.082
	Energy	2.240E13[e]	11	2036000000000.00	2.84	0.002
	Entropy	3.738[f]	11	0.34	2.17	0.016
	Kurtosis	5.823[g]	11	0.53	0.71	0.726
	maximum	174276.887[h]	11	15843.35	3.08	0.001
	Mean	141025.511[i]	11	12820.50	3.03	0.001
	MeanAbsoluteDeviation	343.964[j]	11	31.27	2.16	0.017
	Median	138553.758[k]	11	12595.80	3.00	0.001
	Minimum	116614.678[l]	11	10601.33	2.83	0.002

	Range	8174.315[m]	11	743.12	2.50	0.005
	Skewness	3.463[n]	11	0.32	1.30	0.223
	TotalEnergy	2.338E14[o]	11	212500000000000.00	5.41	0.000
	Uniformity	.508[p]	11	0.05	1.76	0.061
	Variance	438634.838[q]	11	39875.89	1.89	0.040
Intercept	@10Percentile	3786330.88	1	3786330.88	977.77	0.000
	@90Percentile	4804337.49	1	4804337.49	1020.00	0.000
	Contrast	15.85	1	15.85	148.75	0.000
	correlation	4.07	1	4.07	69.01	0.000
	Energy	1286000000000000.00	1	1286000000000000.00	179.48	0.000
	Entropy	93.48	1	93.48	596.07	0.000
	Kurtosis	551.89	1	551.89	743.50	0.000
	maximum	5125705.06	1	5125705.06	997.33	0.000
	Mean	4269994.93	1	4269994.93	1007.00	0.000
	MeanAbsoluteDeviation	6863.97	1	6863.97	472.94	0.000
	Median	4254989.17	1	4254989.17	1014.00	0.000
	Minimum	3554945.26	1	3554945.26	949.18	0.000
	Range	143296.89	1	143296.89	481.27	0.000
	Skewness	1.80	1	1.80	7.43	0.007
	TotalEnergy	6142000000000000.00	1	6142000000000000.00	156.18	0.000
	Uniformity	24.59	1	24.59	936.03	0.000
	Variance	1853510.89	1	1853510.89	88.06	0.000
time_days	@10Percentile	9512.78	1	9512.78	2.46	0.118
	@90Percentile	16039.86	1	16039.86	3.41	0.066
	Contrast	0.49	1	0.49	4.59	0.033*
	correlation	0.01	1	0.01	0.18	0.674
	Energy	1662000000000.00	1	1662000000000.00	2.32	0.129
	Entropy	1.95	1	1.95	12.46	<0.001**
	Kurtosis	0.00	1	0.00	0.00	0.967

	maximum	18117.38	1	18117.38	3.53	0.061
	Mean	12238.68	1	12238.68	2.89	0.090
	MeanAbsoluteDeviation	99.44	1	99.44	6.85	0.009**
	Median	11867.20	1	11867.20	2.83	0.094
	Minimum	8499.80	1	8499.80	2.27	0.133
	Range	1798.31	1	1798.31	6.04	0.015*
	Skewness	0.33	1	0.33	1.35	0.247
	TotalEnergy	12470000000000.00	1	12470000000000.00	3.17	0.076
	Uniformity	0.30	1	0.30	11.40	0.001**
	Variance	107351.36	1	107351.36	5.10	0.025*
dosegr	@10Percentile	53452.11	5	10690.42	2.76	0.019*
	@90Percentile	61851.32	5	12370.26	2.63	0.024*
	Contrast	0.12	5	0.02	0.22	0.955
	correlation	0.41	5	0.08	1.37	0.235
	Energy	10050000000000.00	5	2009000000000.00	2.80	0.017*
	Entropy	0.34	5	0.07	0.43	0.829
	Kurtosis	0.62	5	0.12	0.17	0.975
	maximum	66131.82	5	13226.37	2.57	0.027*
	Mean	56811.94	5	11362.39	2.68	0.022*
	MeanAbsoluteDeviation	98.13	5	19.63	1.35	0.243
	Median	55213.48	5	11042.70	2.63	0.024*
	Minimum	48514.15	5	9702.83	2.59	0.026*
	Range	2747.78	5	549.56	1.85	0.104
	Skewness	0.52	5	0.11	0.43	0.825
	TotalEnergy	124900000000000.00	5	24980000000000.00	6.35	<0.001**
	Uniformity	0.03	5	0.01	0.22	0.953
	Variance	162057.70	5	32411.54	1.54	0.177
dosegr * time_days	@10Percentile	13156.82	5	2631.37	0.68	0.639
	@90Percentile	13327.97	5	2665.59	0.57	0.726
	Contrast	0.09	5	0.02	0.17	0.975
	correlation	0.58	5	0.12	1.97	0.084
	Energy	1546000000000.00	5	309200000000.00	0.43	0.827
	Entropy	0.21	5	0.04	0.27	0.931
	Kurtosis	2.00	5	0.40	0.54	0.746
	maximum	13702.93	5	2740.59	0.53	0.751
	Mean	13318.96	5	2663.79	0.63	0.678

	MeanAbsoluteDeviation	4.56	5	0.91	0.06	0.997
	Median	12924.57	5	2584.92	0.62	0.688
	Minimum	11498.12	5	2299.62	0.61	0.689
	Range	433.32	5	86.66	0.29	0.918
	Skewness	0.91	5	0.18	0.75	0.585
	TotalEnergy	8981000000000.00	5	1796000000000.00	0.46	0.808
	Uniformity	0.05	5	0.01	0.39	0.854
	Variance	16090.87	5	3218.17	0.15	0.979
Error	@10Percentile	1084275.28	280	3872.41		
	@90Percentile	1318784.92	280	4709.95		
	Contrast	29.84	280	0.11		
	correlation	16.53	280	0.06		
	Energy	2007000000000000.00	280	7168000000000.00		
	Entropy	43.91	280	0.16		
	Kurtosis	207.84	280	0.74		
	maximum	1439041.16	280	5139.43		
	Mean	1186864.63	280	4238.80		
	MeanAbsoluteDeviation	4063.78	280	14.51		
	Median	1174564.03	280	4194.87		
	Minimum	1048675.97	280	3745.27		
	Range	83369.36	280	297.75		
	Skewness	67.74	280	0.24		
	TotalEnergy	1101000000000000.00	280	3932000000000.00		
	Uniformity	7.36	280	0.03		
	Variance	5893615.80	280	21048.63		
Total	@10Percentile	14490000.00	292			
	@90Percentile	18180000.00	292			
	Contrast	75.18	292			
	correlation	34.12	292			
	Energy	6523000000000000.00	292			
	Entropy	329.14	292			

	Kurtosis	2165.21	292			
	maximum	19390000.00	292			
	Mean	16260000.00	292			
	MeanAbsoluteDeviation	26396.66	292			
	Median	16210000.00	292			
	Minimum	13650000.00	292			
	Range	558607.80	292			
	Skewness	73.69	292			
	TotalEnergy	3152000000000000.00	292			
	Uniformity	106.41	292			
	Variance	11520000.00	292			
Corrected Total	@10Percentile	1213337.84	291			
	@90Percentile	1477036.65	291			
	Contrast	30.92	291			
	correlation	17.61	291			
	Energy	223100000000000.00	291			
	Entropy	47.65	291			
	Kurtosis	213.66	291			
	maximum	1613318.05	291			
	Mean	1327890.15	291			
	MeanAbsoluteDeviation	4407.74	291			
	Median	1313117.79	291			
	Minimum	1165290.64	291			
	Range	91543.68	291			
	Skewness	71.21	291			
	TotalEnergy	1335000000000000.00	291			
	Uniformity	7.86	291			
	Variance	6332250.64	291			

a. R Squared = .106 (Adjusted R Squared = .071)					
b. R Squared = .107 (Adjusted R Squared = .072)					
c. R Squared = .035 (Adjusted R Squared = -.003)					
d. R Squared = .061 (Adjusted R Squared = .024)					
e. R Squared = .100 (Adjusted R Squared = .065)					
f. R Squared = .078 (Adjusted R Squared = .042)					
g. R Squared = .027 (Adjusted R Squared = -.011)					
h. R Squared = .108 (Adjusted R Squared = .073)					
i. R Squared = .106 (Adjusted R Squared = .071)					
j. R Squared = .078 (Adjusted R Squared = .042)					
k. R Squared = .106 (Adjusted R Squared = .070)					
l. R Squared = .100 (Adjusted R Squared = .065)					
m. R Squared = .089 (Adjusted R Squared = .054)					
n. R Squared = .049 (Adjusted R Squared = .011)					
o. R Squared = .175 (Adjusted R Squared = .143)					
p. R Squared = .065 (Adjusted R Squared = .028)					
q. R Squared = .069 (Adjusted R Squared = .033)					
r. region = R.THALAMUS					

Note : * indicates p value is significant at 0.05 means P <0.05
**** indicates p value is significant at 0.05 means P <0.01**

There was a statistically significant difference in TA features based on dose level F (80, 1345) = 2.38, p < 0.05 Pillai Trace = 0.62

Note : * indicates p value is significant at 0.05 means P <0.05
**** indicates p value is significant at 0.05 means P <0.01**

Conclusion: from this table that time in days has a statistically significant effect on contrast ,Entropy, Mean absolute deviation, Range ,Uniformity and variance.

Conclusion: from this table that dose level has a statistically significant effect on @10percentile ,@90percentile, Energy, Maximum, Mean, Median, Minimum, Total energy

APPENDIX 3: STATISTICAL GRAPHS SHOWING COMPARISON OF TEXTURAL FEATURES BETWEEN PHOTON AND PROTON THERAPY

This appendix contains the hypothesis test summary of Mann Whitney U test between proton and photon therapy at different dose levels.

DOSE_GROUP = A-DOSE

Hypothesis Test Summary

	Null Hypothesis	Test	Sig.[a,b]	Decision
1	The distribution of @10Percentile is the same across categories of Typeoftherapy.	Independent-Samples Mann-Whitney U Test	.015	Reject the null hypothesis.
2	The distribution of @90Percentile is the same across categories of Typeoftherapy.	Independent-Samples Mann-Whitney U Test	.002	Reject the null hypothesis.
3	The distribution of Contrast is the same across categories of Typeoftherapy.	Independent-Samples Mann-Whitney U Test	.028	Reject the null hypothesis.
4	The distribution of Energy is the same across categories of Typeoftherapy.	Independent-Samples Mann-Whitney U Test	.020	Reject the null hypothesis.
5	The distribution of Entropy is the same across categories of Typeoftherapy.	Independent-Samples Mann-Whitney U Test	.007	Reject the null hypothesis.
6	The distribution of Kurtosis is the same across categories of Typeoftherapy.	Independent-Samples Mann-Whitney U Test	.481	Retain the null hypothesis.
7	The distribution of Maximum is the same across categories of Typeoftherapy.	Independent-Samples Mann-Whitney U Test	<.001	Reject the null hypothesis.
8	The distribution of Mean is the same across categories of Typeoftherapy.	Independent-Samples Mann-Whitney U Test	.008	Reject the null hypothesis.
9	The distribution of MeanAbsoluteDeviation is the same across categories of Typeoftherapy.	Independent-Samples Mann-Whitney U Test	<.001	Reject the null hypothesis.
10	The distribution of Median is the same across categories of Typeoftherapy.	Independent-Samples Mann-Whitney U Test	.006	Reject the null hypothesis.
11	The distribution of Minimum is the same across categories of Typeoftherapy.	Independent-Samples Mann-Whitney U Test	.019	Reject the null hypothesis.
12	The distribution of Range is the same across categories of Typeoftherapy.	Independent-Samples Mann-Whitney U Test	<.001	Reject the null hypothesis.
13	The distribution of Skewness is the same across categories of Typeoftherapy.	Independent-Samples Mann-Whitney U Test	.050	Retain the null hypothesis.
14	The distribution of TotalEnergy is the same across categories of Typeoftherapy.	Independent-Samples Mann-Whitney U Test	.000	Reject the null hypothesis.
15	The distribution of Uniformity is the same across categories of Typeoftherapy.	Independent-Samples Mann-Whitney U Test	.040	Reject the null hypothesis.
16	The distribution of Variance is the same across categories of Typeoftherapy.	Independent-Samples Mann-Whitney U Test	<.001	Reject the null hypothesis.

a. The significance level is .050.

b. Asymptotic significance is displayed.

DOSE_GROUP = B-DOSE

Hypothesis Test Summary

	Null Hypothesis	Test	Sig.[a,b]	Decision
1	The distribution of @10Percentile is the same across categories of Typeoftherapy.	Independent-Samples Mann-Whitney U Test	.267	Retain the null hypothesis.
2	The distribution of @90Percentile is the same across categories of Typeoftherapy.	Independent-Samples Mann-Whitney U Test	.220	Retain the null hypothesis.
3	The distribution of Contrast is the same across categories of Typeoftherapy.	Independent-Samples Mann-Whitney U Test	.741	Retain the null hypothesis.
4	The distribution of Energy is the same across categories of Typeoftherapy.	Independent-Samples Mann-Whitney U Test	.232	Retain the null hypothesis.
5	The distribution of Entropy is the same across categories of Typeoftherapy.	Independent-Samples Mann-Whitney U Test	.271	Retain the null hypothesis.
6	The distribution of Kurtosis is the same across categories of Typeoftherapy.	Independent-Samples Mann-Whitney U Test	.239	Retain the null hypothesis.
7	The distribution of Maximum is the same across categories of Typeoftherapy.	Independent-Samples Mann-Whitney U Test	.187	Retain the null hypothesis.
8	The distribution of Mean is the same across categories of Typeoftherapy.	Independent-Samples Mann-Whitney U Test	.244	Retain the null hypothesis.
9	The distribution of MeanAbsoluteDeviation is the same across categories of Typeoftherapy.	Independent-Samples Mann-Whitney U Test	.095	Retain the null hypothesis.
10	The distribution of Median is the same across categories of Typeoftherapy.	Independent-Samples Mann-Whitney U Test	.229	Retain the null hypothesis.
11	The distribution of Minimum is the same across categories of Typeoftherapy.	Independent-Samples Mann-Whitney U Test	.295	Retain the null hypothesis.
12	The distribution of Range is the same across categories of Typeoftherapy.	Independent-Samples Mann-Whitney U Test	.164	Retain the null hypothesis.
13	The distribution of Skewness is the same across categories of Typeoftherapy.	Independent-Samples Mann-Whitney U Test	.560	Retain the null hypothesis.
14	The distribution of TotalEnergy is the same across categories of Typeoftherapy.	Independent-Samples Mann-Whitney U Test	.000	Reject the null hypothesis.
15	The distribution of Uniformity is the same across categories of Typeoftherapy.	Independent-Samples Mann-Whitney U Test	.250	Retain the null hypothesis.
16	The distribution of Variance is the same across categories of Typeoftherapy.	Independent-Samples Mann-Whitney U Test	.122	Retain the null hypothesis.

a. The significance level is .050.

b. Asymptotic significance is displayed.

DOSE_GROUP = C-DOSE

Hypothesis Test Summary

	Null Hypothesis	Test	Sig.[a,b]	Decision
1	The distribution of @10Percentile is the same across categories of Typeoftherapy.	Independent-Samples Mann-Whitney U Test	.003	Reject the null hypothesis.
2	The distribution of @90Percentile is the same across categories of Typeoftherapy.	Independent-Samples Mann-Whitney U Test	.002	Reject the null hypothesis.
3	The distribution of Contrast is the same across categories of Typeoftherapy.	Independent-Samples Mann-Whitney U Test	<.001	Reject the null hypothesis.
4	The distribution of Energy is the same across categories of Typeoftherapy.	Independent-Samples Mann-Whitney U Test	.020	Reject the null hypothesis.
5	The distribution of Entropy is the same across categories of Typeoftherapy.	Independent-Samples Mann-Whitney U Test	.019	Reject the null hypothesis.
6	The distribution of Kurtosis is the same across categories of Typeoftherapy.	Independent-Samples Mann-Whitney U Test	.171	Retain the null hypothesis.
7	The distribution of Maximum is the same across categories of Typeoftherapy.	Independent-Samples Mann-Whitney U Test	.002	Reject the null hypothesis.
8	The distribution of Mean is the same across categories of Typeoftherapy.	Independent-Samples Mann-Whitney U Test	.003	Reject the null hypothesis.
9	The distribution of MeanAbsoluteDeviation is the same across categories of Typeoftherapy.	Independent-Samples Mann-Whitney U Test	.013	Reject the null hypothesis.
10	The distribution of Median is the same across categories of Typeoftherapy.	Independent-Samples Mann-Whitney U Test	.003	Reject the null hypothesis.
11	The distribution of Minimum is the same across categories of Typeoftherapy.	Independent-Samples Mann-Whitney U Test	.004	Reject the null hypothesis.
12	The distribution of Range is the same across categories of Typeoftherapy.	Independent-Samples Mann-Whitney U Test	.004	Reject the null hypothesis.
13	The distribution of Skewness is the same across categories of Typeoftherapy.	Independent-Samples Mann-Whitney U Test	.532	Retain the null hypothesis.
14	The distribution of TotalEnergy is the same across categories of Typeoftherapy.	Independent-Samples Mann-Whitney U Test	<.001	Reject the null hypothesis.
15	The distribution of Uniformity is the same across categories of Typeoftherapy.	Independent-Samples Mann-Whitney U Test	.043	Reject the null hypothesis.
16	The distribution of Variance is the same across categories of Typeoftherapy.	Independent-Samples Mann-Whitney U Test	.006	Reject the null hypothesis.

a. The significance level is .050.

b. Asymptotic significance is displayed.

DOSE_GROUP = D-DOSE

Hypothesis Test Summary

	Null Hypothesis	Test	Sig.[a,b]	Decision
1	The distribution of @10Percentile is the same across categories of Typeoftherapy.	Independent-Samples Mann-Whitney U Test	.268	Retain the null hypothesis.
2	The distribution of @90Percentile is the same across categories of Typeoftherapy.	Independent-Samples Mann-Whitney U Test	.315	Retain the null hypothesis.
3	The distribution of Contrast is the same across categories of Typeoftherapy.	Independent-Samples Mann-Whitney U Test	.832	Retain the null hypothesis.
4	The distribution of Energy is the same across categories of Typeoftherapy.	Independent-Samples Mann-Whitney U Test	.012	Reject the null hypothesis.
5	The distribution of Entropy is the same across categories of Typeoftherapy.	Independent-Samples Mann-Whitney U Test	.793	Retain the null hypothesis.
6	The distribution of Kurtosis is the same across categories of Typeoftherapy.	Independent-Samples Mann-Whitney U Test	.595	Retain the null hypothesis.
7	The distribution of Maximum is the same across categories of Typeoftherapy.	Independent-Samples Mann-Whitney U Test	.324	Retain the null hypothesis.
8	The distribution of Mean is the same across categories of Typeoftherapy.	Independent-Samples Mann-Whitney U Test	.274	Retain the null hypothesis.
9	The distribution of MeanAbsoluteDeviation is the same across categories of Typeoftherapy.	Independent-Samples Mann-Whitney U Test	.849	Retain the null hypothesis.
10	The distribution of Median is the same across categories of Typeoftherapy.	Independent-Samples Mann-Whitney U Test	.251	Retain the null hypothesis.
11	The distribution of Minimum is the same across categories of Typeoftherapy.	Independent-Samples Mann-Whitney U Test	.297	Retain the null hypothesis.
12	The distribution of Range is the same across categories of Typeoftherapy.	Independent-Samples Mann-Whitney U Test	.414	Retain the null hypothesis.
13	The distribution of Skewness is the same across categories of Typeoftherapy.	Independent-Samples Mann-Whitney U Test	.038	Reject the null hypothesis.
14	The distribution of TotalEnergy is the same across categories of Typeoftherapy.	Independent-Samples Mann-Whitney U Test	<.001	Reject the null hypothesis.
15	The distribution of Uniformity is the same across categories of Typeoftherapy.	Independent-Samples Mann-Whitney U Test	.832	Retain the null hypothesis.
16	The distribution of Variance is the same across categories of Typeoftherapy.	Independent-Samples Mann-Whitney U Test	.755	Retain the null hypothesis.

a. The significance level is .050.

b. Asymptotic significance is displayed.

DOSE_GROUP = E-DOSE

Hypothesis Test Summary

	Null Hypothesis	Test	Sig.[a,b]	Decision
1	The distribution of @10Percentile is the same across categories of Typeoftherapy.	Independent-Samples Mann-Whitney U Test	.805	Retain the null hypothesis.
2	The distribution of @90Percentile is the same across categories of Typeoftherapy.	Independent-Samples Mann-Whitney U Test	.877	Retain the null hypothesis.
3	The distribution of Contrast is the same across categories of Typeoftherapy.	Independent-Samples Mann-Whitney U Test	.630	Retain the null hypothesis.
4	The distribution of Energy is the same across categories of Typeoftherapy.	Independent-Samples Mann-Whitney U Test	.983	Retain the null hypothesis.
5	The distribution of Entropy is the same across categories of Typeoftherapy.	Independent-Samples Mann-Whitney U Test	.734	Retain the null hypothesis.
6	The distribution of Kurtosis is the same across categories of Typeoftherapy.	Independent-Samples Mann-Whitney U Test	.997	Retain the null hypothesis.
7	The distribution of Maximum is the same across categories of Typeoftherapy.	Independent-Samples Mann-Whitney U Test	.917	Retain the null hypothesis.
8	The distribution of Mean is the same across categories of Typeoftherapy.	Independent-Samples Mann-Whitney U Test	.805	Retain the null hypothesis.
9	The distribution of MeanAbsoluteDeviation is the same across categories of Typeoftherapy.	Independent-Samples Mann-Whitney U Test	.910	Retain the null hypothesis.
10	The distribution of Median is the same across categories of Typeoftherapy.	Independent-Samples Mann-Whitney U Test	.731	Retain the null hypothesis.
11	The distribution of Minimum is the same across categories of Typeoftherapy.	Independent-Samples Mann-Whitney U Test	.907	Retain the null hypothesis.
12	The distribution of Range is the same across categories of Typeoftherapy.	Independent-Samples Mann-Whitney U Test	.569	Retain the null hypothesis.
13	The distribution of Skewness is the same across categories of Typeoftherapy.	Independent-Samples Mann-Whitney U Test	.183	Retain the null hypothesis.
14	The distribution of TotalEnergy is the same across categories of Typeoftherapy.	Independent-Samples Mann-Whitney U Test	<.001	Reject the null hypothesis.
15	The distribution of Uniformity is the same across categories of Typeoftherapy.	Independent-Samples Mann-Whitney U Test	.733	Retain the null hypothesis.
16	The distribution of Variance is the same across categories of Typeoftherapy.	Independent-Samples Mann-Whitney U Test	.779	Retain the null hypothesis.

a. The significance level is .050.

b. Asymptotic significance is displayed.

..

APPENDIX 4: DATABASE SHOWING DEMOGRAPHIC DETAILS

This appendix contains the demographic, clinical and radiotherapy details of all the patients included in this study.

11	10	9	6	5	4	3	2	1	SR NO
BMS284	BMS111	BMS154	BMS251	BMS7	BMS153	BMS96	BMS205	BMS327	**CODE**
F	M	M	F	F	F	M	M	M	Sex
Cerebellar	Supratentorial midline	Cerebellar	Supratentorial midline	Supratentorial midline	Cerebellar	Hemispheric cerebral	Brainstem	Cerebellar	**Location**
Yes	Yes	No	No	No	Yes	No	No	No	**Metastasi**
Medulloblastoma	Germ Cell Tumours	Rare Embryonal Tumours	Meningioma	Low Grade Glioma	Medulloblastoma	Low Grade Glioma	Low Grade Glioma	Ependymoma	**Diagnostic Group**
MEDULLOBLASTOMA	METASTATIC GERMINOMA	ATYPICAL TERATOID RHYBDOID	MENINGIOMA	OPG (LGG)	MEDULLOBLASTOMA	OLIGODENDROGLIOMA	PILOCYTIC ASTRO	Ependymoma	**Diagnosis**
PHT	PHT	PHT	PR	PR	PHT	PR	PR	PR	**TYPE OF**
Yes	No	Yes	No	Yes	Yes	No	No	No	**CHEMO**
No	No	No	No	No	No	Yes	Yes	No	**Biopsy**
NTR(Near total)	NA	GTR(Complete)	Subtotal Resection	NA	GTR(Complete)	GTR(Complete)	Subtotal Resection	GTR(Complete)	**SURGERY type**
54	40	54	50	54	56	54	54	54	**R DOSE**
30	25	30	28	30	31	30	30	30	**FRACTIO**

22	21	20	19	18	17	16	15	14	13	12
BMS314	BMS315	BMS293	BMS89	BMS280	BMS231	BMS158	BMS44	BMS250	BMS239	BMS67
M	F	M	F	F	F	M	F	M	F	M
Brainstem	Supratentorial midline	Hemispheric cerebral	Cerebellar	Supratentorial midline	Supratentorial midline	Hemispheric cerebral	Supratentorial midline	Supratentorial midline	Supratentorial midline	Supratentorial midline
No	Yes	No	No	No	No	No	No	Yes	No	No
Low Grade Glioma	Medulloblastoma	High Grade Glioma	Ependymoma	Tumours of the Sellar region (pi	Tumours of the Sellar region (pi	Ependymoma	Low Grade Glioma	Germ Cell Tumours	Low Grade Glioma	Tumours of the Sellar region (pi
PILOCYTIC ASTROCYTOMA	MEDULLOBLASTOMA	ANAPLASTIC ASTROCYTOMA	EPENDYMOMA	CRANIOPHARYNGIOMA	CRANIOPHARYNGIOMA	EPENDYMOMA	PILOCYTIC ASTROCYTOMA	METASTATIC NGGCT	LGG	CRANIOPHARYNGIOMA
PR	PHT	PHT	PHT	PR	PR	PR	PHT	PHT	PR	PHT
No	Yes	Yes	No	No	No	No	No	Yes	Yes	No
Yes	No	No	No	No	No	No	No	Yes	No	Yes
NTR(Near total)	Subtotal Resection	Subtotal Resection	GTR(Complete)	Subtotal Resection	Subtotal Resection	GTR(Complete)	Subtotal Resection	NA	Subtotal Resection	NTR(Near total)
50	56	54	59	54	54	59	54	54	54	54
28	31	30	33	30	30	33	30	35	30	30

33	32	31	30	29	28	27	26	25	24	23
BMS78	BMS119	BMS73	BMS229	BMS94	BMS235	BMS137	BMS53	BMS135	BMS76	BMS334
M	F	M	M	F	M	M	F	F	F	F
Supratentorial midline	Supratentorial midline	Hemispheric cerebral	Supratentorial midline	Supratentorial midline	Cerebellar	Supratentorial midline	Supratentorial midline	Hemispheric cerebral	Cerebellar	Supratentorial midline
No	No	No	No	No	No	No	No	No	No	No
Germ Cell Tumours	Low Grade Glioma	Ependymoma	Germ Cell Tumours	Rare Embryonal Tumours	Ependymoma	Tumours of the Sellar region (pi	Tumours of the Sellar region (pi	High Grade Glioma	Medulloblastoma	Tumours of the Sellar region (pi
GERMINOMA	OPG (LGG)	EPENDYMOMA	GERMINOMA	PINEOBLASTOMA	EPENDYMOMA	CRANIOPHARYNGIOMA	CRANIOPHARYNGIOMA	HGG OF THALAMUS	MEDULLOBLASTOMA	CRANIOPHARYNGIOMA
PHT	PR	PHT	PHT	PHT	PR	PR	PHT	PHT	PHT	PR
No	No	No	Yes	Yes	No	No	No	Yes	Yes	No
No	No	No	Yes	Yes	No	Yes	Yes	Yes	No	No
NA	Subtotal Resection	GTR(Complete)	NA	GTR(Complete)	GTR(Complete)	Subtotal Resection	GTR(Complete)	NTR(Near total)	GTR(Complete)	Subtotal Resection
40	50	59	40	55	59	54	54	54	60	54
25	28	33	25	33	33	30	30	30	44	30

44	**43**	**42**	**41**	**40**	**39**	**38**	**37**	**36**	**35**	**34**
BMS123	BMS292	BMS59	BMS294	BMS253	BMS90	BMS172	BMS148	BMS266	BMS182	BMS188
F	M	F	M	M	F	M	F	M	F	F
Brainstem	Cerebellar	Brainstem	Cerebellar	Cerebellar	Cerebellar	Supratentorial midline	Hemispheric cerebral	Cerebellar	Supratentorial midline	Hemispheric cerebral
No	No	No	Yes	No	No	No	No	Yes	No	No
Low Grade Glioma	Medulloblastoma	Ependymoma	Medulloblastoma	Medulloblastoma	Medulloblastoma	Tumours of the Sellar region (pi	High Grade Glioma	Medulloblastoma	Tumours of the Sellar region (pi	Ependymoma
LGG	MEDULLOBLASTOMA	EPENDYMOMA	MEDULLOBLASTOMA	MEDULLOBLASTOMA	MEDULLOBLASTOMA	CRANIOPHARYNGIOMA	HGG	MEDULLOBLASTOMA	CRANIOPHARYNGIOMA	EPENDYMOMA
PHT	PHT	PHT	PHT	PHT	PHT	PR	PHT	PHT	PR	PR
No	Yes	No	Yes	Yes	Yes	No	Yes	Yes	No	No
Yes	No	No	Yes	No	No	No	No	No	No	No
NA	GTR(Complete)	GTR(Complete)	GTR(Complete)	GTR(Complete)	GTR(Complete)	Subtotal Resection	Subtotal Resection	Subtotal Resection	GTR(Complete)	GTR(Complete)
54	56	59	56	54	56	54	54	56	54	59
30	31	33	31	30	31	30	30	31	30	33

51	50	49	48	47	46	45
BMS168	BMS160	BMS263	BMS121	BMS325	BMS255	BMS277
F	F	F	M	F	F	M
Cerebellar	Supratentorial midline	Cerebellar	Cerebellar	Cerebellar	Cerebellar	Cerebellar
No	No	Yes	No	No	Yes	No
Medulloblastoma	Low Grade Glioma	Medulloblastoma	Medulloblastoma	Ependymoma	Ependymoma	Tumours of the Sellar region (pi
MEDULLOBLASTOMA	OPTIC PATHWAY GLIOMA	MEDULLOBLASTOMA	MEDULLOBLASTOMA	EPENDYMOMA	EPENDYMOMA	CRANIOPHARYNGIOMA
PHT	PHT	PHT	PHT	PR	PR	PR
Yes	No	Yes	Yes	Yes	No	No
No	Yes	No	No	No	No	No
GTR(Complete)	NTR(Near total)	GTR(Complete)	GTR(Complete)	GTR(Complete)	GTR(Complete)	Subtotal Resection
54	50	56	54	54	54	54
30	28	31	30	30	30	30

Appendix 5 Intra-class Correlation Coefficient

ICC Interpretation

There are no standard values for acceptable reliability using ICC. A low ICC could not only reflect the low degree of rater or measurement agreement but also relate to the lack of variability among the sampled subjects, the small number of subjects, and the small number of raters being tested.[2, 20] As a rule of thumb, researchers should try to obtain at least 30 heterogeneous samples and involve at least 3 raters whenever possible when conducting a reliability study. Under such conditions, we suggest that ICC values less than 0.5 are indicative of poor reliability, values between 0.5 and 0.75 indicate moderate reliability, values between 0.75 and 0.9 indicate good reliability, and values greater than 0.90 indicate excellent reliability.[2]

How to Report ICC

There is currently a lack of standard for reporting ICC in the clinical research community. Given that different forms of ICC involve distinct assumptions in their calculation and will lead to different interpretations, it is imperative for researchers to report detailed information about their ICC estimates. We suggest that the best practice of reporting ICC should include the following items: software information, "Model," "Type," and "Definition" selections. In addition, both ICC estimates and their 95% confidence intervals should be reported. For instance, the ICC information could be reported as such:

ICC estimates and their 95% confident intervals were calculated using SPSS statistical package version 23 (SPSS Inc, Chicago, IL) based on a mean-rating (k = 3), absolute-agreement, 2-way mixed-effects model.

Values less than 0.5 are indicative of poor reliability, values between 0.5 and 0.75 indicate moderate reliability, values between 0.75 and 0.9 indicate good reliability, and values greater than 0.90 indicate excellent reliability.

For instance, according to the above guideline, if the 95% confident interval of an ICC estimate is 0.83-0.94, the level of reliability can be regarded as "good' to "excellent." It is because, in this case, the true ICC value supposes to land on any point between 0.83 and 0.94. However, let us say that the 95% confident interval of an ICC estimate is 0.92-0.99; the level of reliability should be regarded as "excellent" because even in the worst case scenario, the true ICC is still greater than 0.9.

1. **Parameter -- 10Percentile**

Case Processing Summary			
		N	%
Cases	Valid	11.00	100.00
	Excluded[a]	0.00	0.00
	Total	11.00	100.00
a. Listwise deletion based on all variables in the procedure.			

Reliability Statistics	
Cronbach's Alpha	N of Items
0.98	7.00

Item Statistics			
	Mean	Std. Deviation	N
10Percentile D1	298.27	40.46	11.00
10Percentile D2	302.06	38.76	11.00
10Percentile D3	296.35	33.95	11.00
10Percentile D4	298.32	38.97	11.00
10Percentile D5	295.72	38.52	11.00
10Percentile D6	288.50	35.48	11.00
10Percentile D7	294.04	46.43	11.00

Scale Statistics			
Mean	Variance	Std. Deviation	N of Items
2073.30	67010.00	258.86	7.00

Intraclass Correlation Coefficient

	Intraclass Correlation[a]	95% Confidence Interval		F Test with True Value 0			
		Lower Bound	Upper Bound	Value	df1	df2	Sig
Single Measures	.876[b]	0.75	0.96	50.57	10.00	60.00	0.00
Average Measures	.980[c]	0.96	0.99	50.57	10.00	60.00	0.00
Two-way mixed effects model where people effects are random and measures effects are fixed.							
a. Type A intraclass correlation coefficients using an absolute agreement definition.							
b. The estimator is the same, whether the interaction effect is present or not.							
c. This estimate is computed assuming the interaction effect is absent, because it is not estimable otherwise.							

ICC average measures =0.980 indicates excellent reliability.

2. **Parameter -- 90Percentile**

Case Processing Summary			
		N	%
Cases	Valid	11.00	100.00
	Excluded[a]	0.00	0.00
	Total	11.00	100.00
a. Listwise deletion based on all variables in the procedure.			

Reliability Statistics	
Cronbach's Alpha	N of Items
0.97	7.00

Item Statistics			
	Mean	Std. Deviation	N
90Percentile D1	341.41	66.13	11.00
90Percentile D2	341.34	47.77	11.00
90Percentile D3	335.64	41.13	11.00
90Percentile D4	334.41	46.97	11.00
90Percentile D5	333.08	39.59	11.00
90Percentile D6	327.44	45.80	11.00
90Percentile D7	333.88	46.27	11.00

Scale Statistics			
Mean	Variance	Std. Deviation	N of Items
2347.20	99080.00	314.77	7.00

Intraclass Correlation Coefficient							
	Intraclass Correlation[a]	95% Confidence Interval		F Test with True Value 0			
		Lower Bound	Upper Bound	Value	df1	df2	Sig
Single Measures	.846[b]	0.70	0.95	38.51	10.00	60.00	0.00
Average Measures	.975[c]	0.94	0.99	38.51	10.00	60.00	0.00
Two-way mixed effects model where people effects are random and measures effects are fixed.							
a. Type A intraclass correlation coefficients using an absolute agreement definition.							
b. The estimator is the same, whether the interaction effect is present or not.							
c. This estimate is computed assuming the interaction effect is absent, because it is not estimable otherwise.							

Case Processing Summary			
		N	%
Cases	Valid	11.00	100.00
	Excluded[a]	0.00	0.00
	Total	11.00	100.00

ICC average measures =0.975 indicates excellent reliability.

3. Energy

Reliability Statistics	
Cronbach's Alpha	N of Items
0.83	7.00

Item Statistics			
	Mean	Std. Deviation	N
Energy D1	7683500.00	4176710.00	11.00
Energy D2	2028700.00	814206.00	11.00
Energy D3	1964000.00	773757.00	11.00
Energy D4	1985900.00	802188.00	11.00
Energy D5	1963200.00	762024.00	11.00
Energy D6	2041900.00	878232.00	11.00
Energy D7	1944400.00	843342.00	11.00

Scale Statistics			
Mean	Variance	Std. Deviation	N of Items
19612000.00	75200000000000.00	8671680.00	7.00

Intraclass Correlation Coefficient							
	Intraclass Correlation[a]	95% Confidence Interval		F Test with True Value 0			
		Lower Bound	Upper Bound	Value	df1	df2	Sig
Single Measures	.170[b]	0.04	0.45	6.04	10.00	60.00	0.00
Average Measures	.589[c]	0.22	0.85	6.04	10.00	60.00	0.00
Two-way mixed effects model where people effects are random and measures effects are fixed.							
a. Type A intraclass correlation coefficients using an absolute agreement definition.							
b. The estimator is the same, whether the interaction effect is present or not.							
c. This estimate is computed assuming the interaction effect is absent, because it is not estimable otherwise.							

ICC average measures =0.589 indicates moderate reliability.

4. **Parameter -- Entropy**

Case Processing Summary			
		N	%
Cases	Valid	11.00	100.00
	Excluded[a]	0.00	0.00
	Total	11.00	100.00
a. Listwise deletion based on all variables in the procedure.			

Reliability Statistics	
Cronbach's Alpha	N of Items
0.92	7.00

Item Statistics			
	Mean	Std. Deviation	N
Entropy D1	1.43	0.62	11.00
Entropy D2	1.37	0.41	11.00
Entropy D3	1.39	0.44	11.00
Entropy D4	1.17	0.36	11.00
Entropy D5	1.36	0.40	11.00
Entropy D6	1.32	0.41	11.00
Entropy D7	1.37	0.46	11.00

Scale Statistics			
Mean	Variance	Std. Deviation	N of Items
9.41	6.68	2.58	7.00

Intraclass Correlation Coefficient							
	Intraclass Correlation[a]	95% Confidence Interval		F Test with True Value 0			
		Lower Bound	Upper Bound	Value	df1	df2	Sig
Single Measures	.625[b]	0.40	0.85	12.68	10.00	60.00	0.00
Average Measures	.921[c]	0.82	0.98	12.68	10.00	60.00	0.00
Two-way mixed effects model where people effects are random and measures effects are fixed.							
a. Type A intraclass correlation coefficients using an absolute agreement definition.							
b. The estimator is the same, whether the interaction effect is present or not.							
c. This estimate is computed assuming the interaction effect is absent, because it is not estimable otherwise.							

ICC average measures =0.921 indicates excellent reliability.

5. Kurtosis

Case Processing Summary			
		N	%
Cases	Valid	11.00	100.00
	Excluded[a]	0.00	0.00
	Total	11.00	100.00
a. Listwise deletion based on all variables in the procedure.			

Reliability Statistics	
Cronbach's Alpha	N of Items
0.62	7.00

Item Statistics			
	Mean	Std. Deviation	N
Kurtosis D1	2.61	0.55	11.00
Kurtosis D2	2.55	0.49	11.00
Kurtosis D3	2.57	0.62	11.00
Kurtosis D4	2.48	0.47	11.00
Kurtosis D5	2.52	0.60	11.00
Kurtosis D6	2.60	0.77	11.00
Kurtosis D7	2.79	0.69	11.00

Scale Statistics			
Mean	Variance	Std. Deviation	N of Items
18.12	5.46	2.34	7.00

Intraclass Correlation Coefficient

	Intraclass Correlation[a]	95% Confidence Interval		F Test with True Value 0			
		Lower Bound	Upper Bound	Value	df1	df2	Sig
Single Measures	.196[b]	0.02	0.53	2.61	10.00	60.00	0.01
Average Measures	.631[c]	0.14	0.89	2.61	10.00	60.00	0.01

Two-way mixed effects model where people effects are random and measures effects are fixed.

a. Type A intraclass correlation coefficients using an absolute agreement definition.

b. The estimator is the same, whether the interaction effect is present or not.

c. This estimate is computed assuming the interaction effect is absent, because it is not estimable otherwise.

ICC average measures =0.631 indicates moderate reliability

6. Maximum

Case Processing Summary			
		N	%
Cases	Valid	11.00	100.00
	Excluded[a]	0.00	0.00
	Total	11.00	100.00
a. Listwise deletion based on all variables in the procedure.			

Reliability Statistics	
Cronbach's Alpha	N of Items
0.97	7.00

Item Statistics			
	Mean	Std. Deviation	N
Maximum D1	356.37	76.55	11.00
Maximum D2	351.85	54.72	11.00
Maximum D3	344.35	47.10	11.00
Maximum D4	342.07	47.91	11.00
Maximum D5	343.64	45.87	11.00
Maximum D6	335.64	47.02	11.00
Maximum D7	347.49	58.17	11.00

Scale Statistics			
Mean	Variance	Std. Deviation	N of Items
2421.40	125600.00	354.33	7.00

Intraclass Correlation Coefficient

	Intraclass Correlation[a]	95% Confidence Interval		F Test with True Value 0			
		Lower Bound	Upper Bound	Value	df1	df2	Sig
Single Measures	.827[b]	0.67	0.94	34.37	10.00	60.00	0.00
Average Measures	.971[c]	0.94	0.99	34.37	10.00	60.00	0.00
Two-way mixed effects model where people effects are random and measures effects are fixed.							
a. Type A intraclass correlation coefficients using an absolute agreement definition.							
b. The estimator is the same, whether the interaction effect is present or not.							
c. This estimate is computed assuming the interaction effect is absent, because it is not estimable otherwise.							

ICC average measures =0.971 indicates excellent reliability.

7. Mean Absolute Deviation

Case Processing Summary			
		N	%
Cases	Valid	11.00	100.00
	Excluded[a]	0.00	0.00
	Total	11.00	100.00

Reliability Statistics	
Cronbach's Alpha	N of Items
0.92	7.00

Item Statistics			
	Mean	Std. Deviation	N
MeanAbsoluteDeviation D1	13.70	10.67	11.00
MeanAbsoluteDeviation D2	13.54	6.12	11.00
MeanAbsoluteDeviation D3	12.90	5.71	11.00
MeanAbsoluteDeviation D4	12.13	5.51	11.00
MeanAbsoluteDeviation D5	12.54	5.47	11.00
MeanAbsoluteDeviation D6	12.65	5.03	11.00
MeanAbsoluteDeviation D7	14.10	6.47	11.00

Scale Statistics

Mean	Variance	Std. Deviation	N of Items
91.56	1498.00	38.71	7.00

Intraclass Correlation Coefficient							
	Intraclass Correlation[a]	95% Confidence Interval		F Test with True Value 0			
		Lower Bound	Upper Bound	Value	df1	df2	Sig
Single Measures	.649[b]	0.42	0.86	13.19	10.00	60.00	0.00
Average Measures	.928[c]	0.84	0.98	13.19	10.00	60.00	0.00
Two-way mixed effects model where people effects are random and measures effects are fixed.							
a. Type A intraclass correlation coefficients using an absolute agreement definition.							
b. The estimator is the same, whether the interaction effect is present or not.							
c. This estimate is computed assuming the interaction effect is absent, because it is not estimable otherwise.							

ICC average measures =0.928 indicates excellent reliability.

8. Mean

Case Processing Summary			
		N	%
Cases	Valid	11.00	100.00
	Excluded[a]	0.00	0.00
	Total	11.00	100.00
a. Listwise deletion based on all variables in the procedure.			

Reliability Statistics	
Cronbach's Alpha	N of Items
0.98	7.00

Item Statistics			
	Mean	Std. Deviation	N
Mean D1	319.44	51.94	11.00
Mean D2	320.76	41.51	11.00
Mean D3	314.96	37.79	11.00
Mean D4	316.07	41.25	11.00
Mean D5	314.91	37.43	11.00
Mean D6	306.49	36.90	11.00
Mean D7	312.04	44.90	11.00

Scale Statistics			
Mean	Variance	Std. Deviation	N of Items
2204.70	77430.00	278.27	7.00

Intraclass Correlation Coefficient			
	Intraclass Correlation[a]	95% Confidence Interval	F Test with True Value 0

		Lower Bound	Upper Bound	Value	df1	df2	Sig
Single Measures	.878[b]	0.76	0.96	52.41	10.00	60.00	0.00
Average Measures	.981[c]	0.96	0.99	52.41	10.00	60.00	0.00
Two-way mixed effects model where people effects are random and measures effects are fixed.							
a. Type A intraclass correlation coefficients using an absolute agreement definition.							
b. The estimator is the same, whether the interaction effect is present or not.							
c. This estimate is computed assuming the interaction effect is absent, because it is not estimable otherwise.							

ICC average measures =0.981 indicates excellent reliability.

9. Median

Case Processing Summary			
		N	%
Cases	Valid	11.00	100.00
	Excluded[a]	0.00	0.00
	Total	11.00	100.00

Reliability Statistics	
Cronbach's Alpha	N of Items
0.98	7.00

Item Statistics			
	Mean	Std. Deviation	N
Median D1	318.63	51.40	11.00
Median D2	318.86	38.56	11.00
Median D3	314.31	37.47	11.00
Median D4	316.19	40.47	11.00
Median D5	315.22	36.35	11.00
Median D6	305.71	35.34	11.00
Median D7	310.52	43.88	11.00

Scale Statistics

Mean	Variance	Std. Deviation	N of Items
2199.40	73220.00	270.59	7.00

Intraclass Correlation Coefficient							
	Intraclass Correlation[a]	95% Confidence Interval		F Test with True Value 0			
		Lower Bound	Upper Bound	Value	df1	df2	Sig

Single Measures	.877[b]	0.76	0.96	52.07	10.00	60.00	0.00
Average Measures	.980[c]	0.96	0.99	52.07	10.00	60.00	0.00

Two-way mixed effects model where people effects are random and measures effects are fixed.

a. Type A intraclass correlation coefficients using an absolute agreement definition.

b. The estimator is the same, whether the interaction effect is present or not.

c. This estimate is computed assuming the interaction effect is absent, because it is not estimable otherwise.

ICC average measures =0.980 indicates excellent reliability.

10. Minimum

Case Processing Summary			
		N	%
Cases	Valid	11.00	100.00
	Excluded[a]	0.00	0.00
	Total	11.00	100.00
a. Listwise deletion based on all variables in the procedure.			

Reliability Statistics	
Cronbach's Alpha	N of Items
0.98	7.00

Item Statistics			
	Mean	Std. Deviation	N
Minimum D1	285.08	38.94	11.00
Minimum D2	290.26	38.15	11.00
Minimum D3	285.50	35.92	11.00
Minimum D4	290.48	37.52	11.00
Minimum D5	287.89	38.30	11.00
Minimum D6	277.68	35.62	11.00
Minimum D7	279.25	41.45	11.00

Mean	Variance	Std. Deviation	N of Items
1996.10	62900.00	250.79	7.00

Intraclass Correlation Coefficient							
	Intraclass Correlation[a]	95% Confidence Interval		F Test with True Value 0			
		Lower Bound	Upper Bound	Value	df1	df2	Sig

Single Measures	.864[b]	0.73	0.95	47.36	10.00	60.00	0.00
Average Measures	.978[c]	0.95	0.99	47.36	10.00	60.00	0.00
Two-way mixed effects model where people effects are random and measures effects are fixed.							
a. Type A intraclass correlation coefficients using an absolute agreement definition.							
b. The estimator is the same, whether the interaction effect is present or not.							
c. This estimate is computed assuming the interaction effect is absent, because it is not estimable otherwise.							

ICC average measures =0.978 indicates excellent reliability.

11. Range

Case Processing Summary			
		N	%
Cases	Valid	11.00	100.00
	Excluded[a]	0.00	0.00
	Total	11.00	100.00
a. Listwise deletion based on all variables in the procedure.			

Reliability Statistics	
Cronbach's Alpha	N of Items
0.92	7.00

Item Statistics			
	Mean	Std. Deviation	N
Range D1	71.29	49.39	11.00
Range D2	61.59	25.18	11.00
Range D3	58.85	27.42	11.00
Range D4	51.59	19.73	11.00
Range D5	55.75	22.68	11.00
Range D6	57.96	22.19	11.00
Range D7	68.24	34.81	11.00

Scale Statistics			
Mean	Variance	Std. Deviation	N of Items
425.27	30330.00	174.15	7.00

Intraclass Correlation Coefficient			
	Intraclass Correlation[a]	95% Confidence Interval	F Test with True Value 0

		Lower Bound	Upper Bound	Value	df1	df2	Sig
Single Measures	.608[b]	0.38	0.84	12.38	10.00	60.00	0.00
Average Measures	.916[c]	0.81	0.97	12.38	10.00	60.00	0.00
Two-way mixed effects model where people effects are random and measures effects are fixed.							
a. Type A intraclass correlation coefficients using an absolute agreement definition.							
b. The estimator is the same, whether the interaction effect is present or not.							
c. This estimate is computed assuming the interaction effect is absent, because it is not estimable otherwise.							

ICC average measures =0.916 indicates excellent reliability

12. Total Energy

Case Processing Summary			
		N	%
Cases	Valid	11.00	100.00
	Excluded[a]	0.00	0.00
	Total	11.00	100.00
a. Listwise deletion based on all variables in the procedure.			

Reliability Statistics	
Cronbach's Alpha	N of Items
0.83	7.00

Item Statistics			
	Mean	Std. Deviation	N
TotalEnergy D1	7327500.00	3983220.00	11.00
TotalEnergy D2	1934700.00	776487.00	11.00
TotalEnergy D3	1873000.00	737912.00	11.00
TotalEnergy D4	1893900.00	765026.00	11.00
TotalEnergy D5	1872300.00	726722.00	11.00
TotalEnergy D6	1947300.00	837547.00	11.00
TotalEnergy D7	1854300.00	804273.00	11.00

Scale Statistics			
Mean	Variance	Std. Deviation	N of Items
18703000.00	68390000000000.00	8269950.00	7.00

Intraclass Correlation Coefficient							
	Intraclass Correlation[a]	95% Confidence Interval		F Test with True Value 0			
		Lower Bound	Upper Bound	Value	df1	df2	Sig
Single Measures	.170[b]	0.04	0.45	6.04	10.00	60.00	0.00
Average Measures	.589[c]	0.22	0.85	6.04	10.00	60.00	0.00
Two-way mixed effects model where people effects are random and measures effects are fixed.							
a. Type A intraclass correlation coefficients using an absolute agreement definition.							
b. The estimator is the same, whether the interaction effect is present or not.							
c. This estimate is computed assuming the interaction effect is absent, because it is not estimable otherwise.							

ICC average measures =0.589 indicates moderate reliability

13. uniformity

Case Processing Summary			
		N	%
Cases	Valid	11.00	100.00
	Excludeda	0.00	0.00
	Total	11.00	100.00
a. Listwise deletion based on all variables in the procedure.			

Reliability Statistics	
Cronbach's Alpha	N of Items
0.91	7.00

Item Statistics			
	Mean	Std. Deviation	N
Uniformity D1	0.44	0.13	11.00
Uniformity D2	0.47	0.13	11.00
Uniformity D3	0.44	0.12	11.00
Uniformity D4	0.49	0.10	11.00
Uniformity D5	0.44	0.11	11.00
Uniformity D6	0.47	0.14	11.00
Uniformity D7	0.47	0.15	11.00

Scale Statistics			
Mean	Variance	Std. Deviation	N of Items
3.22	0.50	0.71	7.00

Intraclass Correlation Coefficient

	Intraclass Correlation[a]	95% Confidence Interval		F Test with True Value 0			
		Lower Bound	Upper Bound	Value	df1	df2	Sig
Single Measures	.605[b]	0.37	0.84	11.39	10.00	60.00	0.00
Average Measures	.915[c]	0.81	0.97	11.39	10.00	60.00	0.00

Two-way mixed effects model where people effects are random and measures effects are fixed.

a. Type A intraclass correlation coefficients using an absolute agreement definition.

b. The estimator is the same, whether the interaction effect is present or not.

c. This estimate is computed assuming the interaction effect is absent, because it is not estimable otherwise.

ICC average measures =0.915 indicates excellent reliability

14. Variancee

Case Processing Summary			
		N	%
Cases	Valid	11.00	100.00
	Excluded[a]	0.00	0.00
	Total	11.00	100.00
a. Listwise deletion based on all variables in the procedure.			

Reliability Statistics	
Cronbach's Alpha	N of Items
0.89	7.00

Item Statistics			
	Mean	Std. Deviation	N
Variance D1	421.78	806.76	11.00
Variance D2	312.55	289.39	11.00
Variance D3	298.49	289.50	11.00
Variance D4	243.58	241.82	11.00
Variance D5	267.41	219.51	11.00
Variance D6	281.01	232.92	11.00
Variance D7	366.01	349.36	11.00

Scale Statistics			
Mean	Variance	Std. Deviation	N of Items
2190.80	4700000.00	2167.91	7.00

Intraclass Correlation Coefficient			
	Intraclass Correlation[a]	95% Confidence Interval	F Test with True Value 0

		Lower Bound	Upper Bound	Value	df1	df2	Sig
Single Measures	.554[b]	0.32	0.81	9.37	10.00	60.00	0.00
Average Measures	.897[c]	0.77	0.97	9.37	10.00	60.00	0.00

Two-way mixed effects model where people effects are random and measures effects are fixed.

a. Type A intraclass correlation coefficients using an absolute agreement definition.

b. The estimator is the same, whether the interaction effect is present or not.

c. This estimate is computed assuming the interaction effect is absent, because it is not estimable otherwise.

ICC average measures =0.897 indicates good reliability

15. Sum squres

		N	%
Cases	Valid	11.00	100.00
	Excluded[a]	0.00	0.00
	Total	11.00	100.00

a. Listwise deletion based on all variables in the procedure.

Reliability Statistics	
Cronbach's Alpha	N of Items
0.89	7.00

Item Statistics			
	Mean	Std. Deviation	N
SumSquares D1	0.73	1.22	11.00
SumSquares D2	0.52	0.43	11.00
SumSquares D3	0.53	0.43	11.00
SumSquares D4	0.42	0.35	11.00
SumSquares D5	0.48	0.30	11.00
SumSquares D6	0.49	0.38	11.00
SumSquares D7	0.57	0.47	11.00

Scale Statistics			
Mean	Variance	Std. Deviation	N of Items
3.75	10.18	3.19	7.00

Intraclass Correlation Coefficient							
	Intraclass Correlation[a]	95% Confidence Interval		F Test with True Value 0			
		Lower Bound	Upper Bound	Value	df1	df2	Sig
Single Measures	.534[b]	0.30	0.80	8.78	10.00	60.00	0.00

Average Measures	.889[c]	0.75	0.97	8.78	10.00	60.00	0.00
Two-way mixed effects model where people effects are random and measures effects are fixed.							
a. Type A intraclass correlation coefficients using an absolute agreement definition.							
b. The estimator is the same, whether the interaction effect is present or not.							
c. This estimate is computed assuming the interaction effect is absent, because it is not estimable otherwise.							

ICC average measures =0.889 indicates good reliability

Bibliography

1. Chu, C., et al., *Stem-Cell Therapy as a Potential Strategy for Radiation-Induced Brain Injury.* Stem Cell Rev Rep, 2020. **16**(4): p. 639-649.
2. Pek-Lan Khong, D.L.W.K., Godfrey C. F. Chan, Jonathan S. T. Sham, Fu-Luk Chan, and Gaik-Cheng Ooi, *Diffusion-Tensor Imaging for the Detection and Quantification of Treatment-Induced White Matter Injury in Children with Medulloblastoma- A Pilot Study. American Journal of Neuroradiology 24, 734–740..pdf.* Am J Neuroradiol, 2003. **24**: p. 734–740.
3. UK, C.R. *Chidrens Cancer Statistics UK*. 2021 Dec 2021]; Available from: https://www.cancerresearchuk.org/health-professional/cancer-statistics/childrens-cancers/incidence#heading-Three.
4. Macedoni-Luksic, M., Jereb, B., Todorovski, L., *Long-term sequelae in children treated for brain tumors: impairments, disability, and handicap.* Pediatr Hematol Oncol, 2003. **20**: p. 89–101.
5. Patay, Z., *New Concepts in the Imaging of Pediatric Brain Tumors: The Revival of Age-old Real Estate Principles.* Current Radiology Reports, 2016. **4**(6).
6. Korshunov, A., et al., *Adult and pediatric medulloblastomas are genetically distinct and require different algorithms for molecular risk stratification.* J Clin Oncol, 2010. **28**(18): p. 3054-60.
7. Wen, P.Y. and R.J. Packer, *The 2021 WHO Classification of Tumors of the Central Nervous System: clinical implications.* Neuro Oncol, 2021. **23**(8): p. 1215-1217.
8. Ajithkumar, T., et al., *Prevention of radiotherapy-induced neurocognitive dysfunction in survivors of paediatric brain tumours: the potential role of modern imaging and radiotherapy techniques.* The Lancet Oncology, 2017. **18**(2): p. e91-e100.
9. Kortmann, R.D., et al., *Current and future strategies in radiotherapy of childhood low-grade glioma of the brain. Part II: Treatment-related late toxicity.* Strahlenther Onkol, 2003. **179**(9): p. 585-97.
10. Armstrong, G.T., et al., *Region-specific radiotherapy and neuropsychological outcomes in adult survivors of childhood CNS malignancies.* Neuro Oncol, 2010. **12**(11): p. 1173-86.
11. Passos, J., et al., *Late Cerebrovascular Complications After Radiotherapy for Childhood Primary Central Nervous System Tumors.* Pediatr Neurol, 2015. **53**(3): p. 211-5.
12. Elizabeth M. Wells, N.J.U., Kristy Seidel, Wendy Leisenring, Charles A. Sklar, Gregory T. Armstrong, Lisa Diller, Allison King, Kevin R. Krull, Joseph P. Neglia, and K.W. Marilyn Stovall, Kevin C. Oeffinger, Leslie L. Robison, and Roger J. Packer, *Longitudinal assessment of late-onset neurologic conditions in survivors of childhood central nervous system tumors: a Childhood Cancer Survivor Study report.* Neuro- Oncology, 2018. **20**(1): p. 132-142.
13. Ullrich, N.J. and L. Embry, *Neurocognitive dysfunction in survivors of childhood brain tumors.* Semin Pediatr Neurol, 2012. **19**(1): p. 35-42.
14. Subramanian S, A.T., *Childhood Brain Tumors*. Updated 2021 Aug 12, In: StatPearls
15. Sharma, N.S.a.D., *An Overview of Pediatric CNS Malignancies*, in *Current Cancer Treatment*. IntechOpen.
16. Commissioning, S.f.P.H.S.o.b.o.N.E.S., *NHS England Evidence review- The safety of proton beam therapy for childhood tumours.pdf*. 2018. p. 52.
17. Fangusaro, J., *Pediatric high grade glioma: a review and update on tumor clinical characteristics and biology.* Front Oncol, 2012. **2**: p. 105.
18. Robert A Zimmerman, L.T.B. *Pediatric Brain Tumors*. [cited 2022; Available from: https://radiologykey.com/pediatric-brain-tumors-3/.
19. Rossi, A., et al., *Medulloblastoma: from molecular pathology to therapy.* Clin Cancer Res, 2008. **14**(4): p. 971-6.
20. Goncalves, F.G., A.N. Viaene, and A. Vossough, *Advanced Magnetic Resonance Imaging in Pediatric Glioblastomas.* Front Neurol, 2021. **12**: p. 733323.
21. Abubakar, D.S. and H.C. Traunecker, *Current perspectives on childhood brain tumours: a review.* Paediatrics and Child Health, 2014. **24**(4): p. 155-160.
22. Das, K.K., et al., *Pediatric glioblastoma: clinico-radiological profile and factors affecting the outcome.* Childs Nerv Syst, 2012. **28**(12): p. 2055-62.
23. Klasner, A., *Brain Tumour*, in *Pediatric Emergency Medicine*, S.G.R. Jill M. Baren, John A. Brennan, Lance Brown,, Editor. 2008, W.B. Saunders. p. 385-387.
24. Guerreiro Stucklin, A.S., et al., *Review of molecular classification and treatment implications of pediatric brain tumors.* Curr Opin Pediatr, 2018. **30**(1): p. 3-9.
25. Koob, M. and N. Girard, *Cerebral tumors: specific features in children.* Diagn Interv Imaging, 2014. **95**(10): p. 965-83.
26. Louis, D.N., et al., *The 2021 WHO Classification of Tumors of the Central Nervous System: a summary.* Neuro Oncol, 2021. **23**(8): p. 1231-1251.
27. Baroni LV, S.L., Heled A, et al, *Ultra high-risk PFA ependymoma is characterized by loss of chromosome 6q*. Neuro Oncol, 2021. **23**: p. 1360-1370.

28. Thorbinson, C. and J.P. Kilday, *Childhood Malignant Brain Tumors: Balancing the Bench and Bedside.* Cancers (Basel), 2021. **13**(23).
29. Maher El Doussouki, A.G.O.C., *Molecular genetics of medulloblastoma in children- diagnostic, therapeutic and prognostic implications.pdf.* FutureNeurol, 2019. **14**(1): p. 1748-6971.
30. Juraschka, K. and M.D. Taylor, *Medulloblastoma in the age of molecular subgroups: a review.* J Neurosurg Pediatr, 2019. **24**(4): p. 353-363.
31. Borja, M.J., et al., *Conventional and advanced MRI features of pediatric intracranial tumors: supratentorial tumors.* AJR Am J Roentgenol, 2013. **200**(5): p. W483-503.
32. Cha, S., *Update on Brain Tumor Imaging- From Anatomy to Physiology.pdf.* Am J Neuroradiol. **27**: p. 475-87.
33. Kamil Zeleňák, C.r.V.a.P.c.e.H., *Radiology Imaging Techniques of Brain Tumours, Clinical Management and Evolving Novel Therapeutic Strategies for Patients with Brain Tumors*, T. Lichtor, Editor. 2013, IntechOpen,.
34. Michael A. Jacobs, T.S.I., Ronald Ouwerkerk., *MR Imaging: Brief Overview and Emerging Applications.* RSNA, 2007. **27**.
35. Currie, S., et al., *Understanding MRI: basic MR physics for physicians.* Postgrad Med J, 2013. **89**(1050): p. 209-23.
36. Berger, A., *How does it work : Magnetic resonance imaging.* BMJ : British Medical Journal, 2002. **324**: p. 35.
37. Preston, D.C. *Magnetic Resonance Imaging (MRI) of the Brain and Spine: Basics*. 2016; Available from: https://case.edu/med/neurology/NR/MRI%20Basics.htm.
38. Kamson, D. and C. Tsien, *Chapter 54 - Novel Magnetic Resonance Imaging and Positron Emission Tomography in the RT Planning and Assessment of Response of Malignant Gliomas*, in *Molecular Imaging (Second Edition)*, B.D. Ross and S.S. Gambhir, Editors. 2021, Academic Press. p. 1031-1048.
39. Jahng, G.H., et al., *Perfusion magnetic resonance imaging: a comprehensive update on principles and techniques.* Korean J Radiol, 2014. **15**(5): p. 554-77.
40. Mullen, K.M. and R.Y. Huang, *An Update on the Approach to the Imaging of Brain Tumors.* Curr Neurol Neurosci Rep, 2017. **17**(7): p. 53.
41. Villanueva-Meyer, J.E., M.C. Mabray, and S. Cha, *Current Clinical Brain Tumor Imaging.* Neurosurgery, 2017. **81**(3): p. 397-415.
42. Zhang, Y., et al., *Brain structural abnormalities in survivors of pediatric posterior fossa brain tumors: a voxel-based morphometry study using free-form deformation.* Neuroimage, 2008. **42**(1): p. 218-29.
43. Zhou, Z. and Z.R. Lu, *Gadolinium-based contrast agents for magnetic resonance cancer imaging.* Wiley Interdiscip Rev Nanomed Nanobiotechnol, 2013. **5**(1): p. 1-18.
44. Grist, J.T., et al., *Distinguishing between paediatric brain tumour types using multi-parametric magnetic resonance imaging and machine learning: A multi-site study.* Neuroimage Clin, 2020. **25**: p. 102172.
45. Anwar Padhani , K.M., *Multiparametric Imaging of Tumor Response to Therapy.* RSNA, 2010. **256**(2).
46. Ritu Shah, S.V., Rojymon Jacob, , et al., *Radiation Necrosis in the Brain- Imaging Features and Differentiation from Tumor Recurrence.* RSNA, 2012. **32**: p. 1343–1359.
47. Nilsson, M., et al., *Imaging brain tumour microstructure.* Neuroimage, 2018. **182**: p. 232-250.
48. Resende, L.L. and C. Alves, *Imaging of brain tumors in children: the basics-a narrative review.* Transl Pediatr, 2021. **10**(4): p. 1138-1168.
49. Sawlani, V., et al., *Multiparametric MRI: practical approach and pictorial review of a useful tool in the evaluation of brain tumours and tumour-like lesions.* Insights Imaging, 2020. **11**(1): p. 84.
50. Peyrl, A., et al., *Chapter 34 - Brain tumors – other treatment modalities*, in *Handbook of Clinical Neurology*, G.G. Kovacs and I. Alafuzoff, Editors. 2018, Elsevier. p. 547-560.
51. Roth, J., S. Constantini, and J.V. Rosenfeld, *Management of brain tumors in the pediatric patient*, in *Brain Tumors*. 2012. p. 329-346.
52. Chintagumpala, M. and A. Gajjar, *Brain tumors.* Pediatr Clin North Am, 2015. **62**(1): p. 167-78.
53. Grant, R., *Overview: Brain tumour diagnosis and management/Royal College of Physicians guidelines.* J Neurol Neurosurg Psychiatry, 2004. **75 Suppl 2**: p. ii18-23.
54. Obaid S., C.P., Mercier C., Crevier L, *Neurosurgery. In: Scheinemann K., Bouffet E. (eds) Pediatric Neuro-oncology.* 2015, Springer, NY.
55. Taggart D., G.R., Banerjee A, *Late Effects of Treatment and Palliative Care.*, in *Pediatric CNS Tumors*, B.A. Gupta N., Haas-Kogan D., Editor. 2010, Pediatric Oncology. Springer, Berlin, Heidelberg.
56. Murphy, E.S., et al., *Radiosurgery for Pediatric Brain Tumors.* Pediatr Blood Cancer, 2016. **63**(3): p. 398-405.
57. Ryan Lingo P., C.A.F., Klimo P, *Principles of Pediatric Neurosurgery. In: Gajjar A., Reaman G., Racadio J., Smith F. (eds) Brain Tumors in Children*. 2018.
58. Goodden, J., et al., *The role of surgery in optic pathway/hypothalamic gliomas in children.* J Neurosurg Pediatr, 2014. **13**(1): p. 1-12.
59. Charpentier, A.-M., et al., *Radiotherapy*, in *Pediatric Neuro-oncology*, K. Scheinemann and E. Bouffet, Editors. 2015, Springer New York: New York, NY. p. 195-205.
60. McBride S.M., H.-K.D.A., *Advances in Radiation Therapy.*, in *Pediatric CNS Tumors.*, B.A. Gupta N., Haas-Kogan

D., Editor. 2010, Springer: Berlin, Heidelberg.
61. Ordóñez-Rubiano E.G., H.R.S., Rivera-Osorio L., Johnson J.M, *Imaging of Pediatric Central Nervous System Tumors*, in *Radiation Oncology for Pediatric CNS Tumors*, P.A. Mahajan A., Editor. 2018, Springer.
62. Jordan, B.F. and P. Sonveaux, *Targeting tumor perfusion and oxygenation to improve the outcome of anticancer therapy.* Front Pharmacol, 2012. **3**: p. 94.
63. Daniels, T.B. and N.N. Laack, *Conformal Radiation Therapy for Pediatric CNS Tumors*, in *Radiation Oncology for Pediatric CNS Tumors*, A. Mahajan and A. Paulino, Editors. 2018, Springer International Publishing: Cham. p. 431-439.
64. Mohan, R. and D. Grosshans, *Proton therapy - Present and future.* Adv Drug Deliv Rev, 2017. **109**: p. 26-44.
65. Abreu, C.E., et al., *Stereotactic body radiotherapy in lung cancer: an update.* J Bras Pneumol, 2015. **41**(4): p. 376-87.
66. Mailhot Vega, R., et al., *Cost effectiveness of proton versus photon radiation therapy with respect to the risk of growth hormone deficiency in children.* Cancer, 2015. **121**(10): p. 1694-702.
67. Leroy, R., et al., *Proton Therapy in Children: A Systematic Review of Clinical Effectiveness in 15 Pediatric Cancers.* Int J Radiat Oncol Biol Phys, 2016. **95**(1): p. 267-78.
68. Mizumoto, M., et al., *Proton Beam Therapy for Pediatric Brain Tumor.* Neurol Med Chir (Tokyo), 2017. **57**(7): p. 343-355.
69. Yock, T.I., et al., *Long-term toxic effects of proton radiotherapy for paediatric medulloblastoma: a phase 2 single-arm study.* The Lancet Oncology, 2016. **17**(3): p. 287-298.
70. Radiotherapy, N.E.S.S.C.R.G.f., *Clinical Commissioning Policy Proposition- Proton Beam Therapy for Children, Teenagers and Young Adults in the treatment of malignant and non-malignant tumours*. 2020, NHS England Reference: 200808P.
71. Mohan, R., A. Mahajan, and B.D. Minsky, *New strategies in radiation therapy: exploiting the full potential of protons.* Clin Cancer Res, 2013. **19**(23): p. 6338-43.
72. Jones, B., *Proton radiobiology and its clinical implications.* Ecancermedicalscience, 2017. **11**: p. 777.
73. Mitin, T. and A.L. Zietman, *Promise and pitfalls of heavy-particle therapy.* J Clin Oncol, 2014. **32**(26): p. 2855-63.
74. Bishop, A.J., et al., *Proton beam therapy versus conformal photon radiation therapy for childhood craniopharyngioma: multi-institutional analysis of outcomes, cyst dynamics, and toxicity.* Int J Radiat Oncol Biol Phys, 2014. **90**(2): p. 354-61.
75. Vanderwaeren, L., et al., *Clinical Progress in Proton Radiotherapy: Biological Unknowns.* Cancers (Basel), 2021. **13**(4).
76. Kralik, S.F., et al., *Radiation Necrosis in Pediatric Patients with Brain Tumors Treated with Proton Radiotherapy.* AJNR Am J Neuroradiol, 2015. **36**(8): p. 1572-8.
77. Joseph K. Salama, a.C.G., et al., *Counterpoints: Is Proton Beam Therapy Better Than Standard Radiation Therapy? – Hematology & Oncology.* Clinical Advances in Hematology & Oncology, 2014. **12**(12).
78. charity, T.b.t., *chemotherapy-for-brain-tumours.* 2018.
79. Lee, J.J., Donna L., *Chemotherapy*, in *Pediatric Neuro-oncology*, K.B. Scheinemann, Eric, Editor. 2015, Springer New York: New York, NY. p. 207-215.
80. Guerrini-Rousseau, L., et al., *Role of neoadjuvant chemotherapy in metastatic medulloblastoma: a comparative study in 92 children.* Neuro Oncol, 2020. **22**(11): p. 1686-1695.
81. Gottardo, N.G. and A. Gajjar, *Chemotherapy for malignant brain tumors of childhood.* J Child Neurol, 2008. **23**(10): p. 1149-59.
82. Svolos, P., et al., *Measurable Supratentorial White Matter Volume Changes in Patients with Diffuse Intrinsic Pontine Glioma Treated with an Anti-Vascular Endothelial Growth Factor Agent, Steroids, and Radiation.* AJNR Am J Neuroradiol, 2017. **38**(6): p. 1235-1241.
83. Wen, U.N.C.P.Y., *Use of the Response Assessment in Neuro-Oncology (RANO) criteria in clinical trials and clinical practice.pdf.* CNS Oncol, 2019. **8**(1).
84. Erker, C., et al., *Response assessment in paediatric high-grade glioma: recommendations from the Response Assessment in Pediatric Neuro-Oncology (RAPNO) working group.* The Lancet Oncology, 2020. **21**(6): p. e317-e329.
85. Tamrazi, B., et al., *Current concepts and challenges in the radiologic assessment of brain tumors in children: part 2.* Pediatr Radiol, 2018. **48**(13): p. 1844-1860.
86. Nelson, M.B., et al., *Structural brain alterations in children an average of 5 years after surgery and chemotherapy for brain tumors.* J Neurooncol, 2014. **119**(2): p. 317-26.
87. Turgut, M., *Cerebellar Mutism.* Journal of Neurosurgery: Pediatrics, 2008. **1**(3): p. 262-262.
88. Patay, Z., *Postoperative posterior fossa syndrome: unraveling the etiology and underlying pathophysiology by using magnetic resonance imaging.* Childs Nerv Syst, 2015. **31**(10): p. 1853-8.
89. Sergeant, A., et al., *Analysis of surgical and MRI factors associated with cerebellar mutism.* J Neurooncol, 2017. **133**(3): p. 539-552.

90. Avula, S., et al., *Diffusion abnormalities on intraoperative magnetic resonance imaging as an early predictor for the risk of posterior fossa syndrome.* Neuro Oncol, 2015. **17**(4): p. 614-22.
91. Gragert, M.N., T.N. Antonini, and L.S. Kahalley, *Neuropsychological Late Effects of Radiotherapy for Pediatric Brain Tumors*, in *Radiation Oncology for Pediatric CNS Tumors*, A. Mahajan and A. Paulino, Editors. 2018, Springer International Publishing: Cham. p. 507-535.
92. Greene-Schloesser, D., et al., *Radiation-induced brain injury: A review.* Front Oncol, 2012. **2**: p. 73.
93. Khong, P.L., et al., *White matter anisotropy in post-treatment childhood cancer survivors: preliminary evidence of association with neurocognitive function.* J Clin Oncol, 2006. **24**(6): p. 884-90.
94. Chawla, S., et al., *Radiation injury to the normal brain measured by 3D-echo-planar spectroscopic imaging and diffusion tensor imaging: initial experience.* J Neuroimaging, 2015. **25**(1): p. 97-104.
95. Petr J, P.I., Hofheinz F, Mutsaerts HJMM, Asllani I, van Osch MJP, Seidlitz A, Krukowski P, Gommlich A, Beuthien-Baumann B, Jentsch C, Maus J, Troost EGC, Baumann M, Krause M, van den Hoff J., *Photon vs. proton radiochemotherapy: Effects on brain tissue volume and perfusion.* Radiother Oncol, 2018. **128**(1): p. 121-127.
96. Ralph Salloum, K.B., Melissa Gerstle, Helen Spoudeas, Susan R. Rose, *Late Effects of Treatment for Childhood Brain and Spinal Tumors*, in *Brain and Spinal Tumors of Childhood*, G.P. David A. Walker, Roger E. Taylor, Ian F. Pollack, Editor. 2020, CRC Press: New York.
97. Balentova, S. and M. Adamkov, *Molecular, Cellular and Functional Effects of Radiation-Induced Brain Injury: A Review.* Int J Mol Sci, 2015. **16**(11): p. 27796-815.
98. Matsos, A., et al., *Chemotherapy-induced cognitive impairments: White matter pathologies.* Cancer Treatment Reviews, 2017. **61**: p. 6-14.
99. QIBA, R. *The Quantitative Imaging Biomarkers Alliance (QIBA)*. in *RSNA*. 2007.
100. Avanzo, M., J. Stancanello, and I. El Naqa, *Beyond imaging: The promise of radiomics.* Phys Med, 2017. **38**: p. 122-139.
101. Mills, A.F., et al., *Principles of Quantitative MR Imaging with Illustrated Review of Applicable Modular Pulse Diagrams.* Radiographics, 2017. **37**(7): p. 2083-2105.
102. Bhavya Shah, M.S.W.A., MD • Jonathan Scalera, MD Hernan Jara, PhD • Jorge A. Soto, MD, *Quantitative MR Imaging- Physical Principles and Sequence Design in Abdominal Imaging.pdf.* RSNA, 2021. **31**: p. 867-880.
103. Mukherjee, P., et al., *Diffusion tensor MR imaging and fiber tractography: theoretic underpinnings.* AJNR Am J Neuroradiol, 2008. **29**(4): p. 632-41.
104. Strimbu, K.T., Jorge A, *What are biomarkers?,.* Current Opinion in HIV and AIDS, 2010. **5**(6): p. 463-466.
105. McCullough, B.J. and J.W. Henson, *Issues in Response Assessment of Brain Tumor Chemotherapy*, in *Handbook of Brain Tumor Chemotherapy, Molecular Therapeutics, and Immunotherapy*. 2018. p. 715-727.
106. Lambin, P., et al., *Radiomics: extracting more information from medical images using advanced feature analysis.* Eur J Cancer, 2012. **48**(4): p. 441-6.
107. Kumar, V., et al., *Radiomics: the process and the challenges.* Magn Reson Imaging, 2012. **30**(9): p. 1234-48.
108. Ismail, M., et al., *Shape Features of the Lesion Habitat to Differentiate Brain Tumor Progression from Pseudoprogression on Routine Multiparametric MRI: A Multisite Study.* AJNR Am J Neuroradiol, 2018. **39**(12): p. 2187-2193.
109. Rizzo, S., et al., *Radiomics: the facts and the challenges of image analysis.* Eur Radiol Exp, 2018. **2**(1): p. 36.
110. Shi, L., et al., *Radiomics for Response and Outcome Assessment for Non-Small Cell Lung Cancer.* Technol Cancer Res Treat, 2018. **17**: p. 1533033818782788.
111. Wu, J., et al., *Radiomics and radiogenomics for precision radiotherapy.* J Radiat Res, 2018. **59**(suppl_1): p. i25-i31.
112. Fave, X., et al., *Delta-radiomics features for the prediction of patient outcomes in non-small cell lung cancer.* Sci Rep, 2017. **7**(1): p. 588.
113. Adrien Depeursinge, J.F., Omar S. Al-Kadi, *Chapter 1 - Fundamentals of Texture Processing for Biomedical Image Analysis: A General Definition and Problem Formulation*, in *Biomedical Texture Analysis*, O.S.A.-K. Adrien Depeursinge, J.Ross Mitchell, Editor. 2017. p. 1-27.
114. de Oliveira, M.S., et al., *MR imaging texture analysis of the corpus callosum and thalamus in amnestic mild cognitive impairment and mild Alzheimer disease.* AJNR Am J Neuroradiol, 2011. **32**(1): p. 60-6.
115. Ranjbar, S. and J. Ross Mitchell, *An Introduction to Radiomics: An Evolving Cornerstone of Precision Medicine*, in *Biomedical Texture Analysis*. 2017. p. 223-245.
116. Suoranta, S., et al., *3D texture analysis reveals imperceptible MRI textural alterations in the thalamus and putamen in progressive myoclonic epilepsy type 1, EPM1.* PLoS One, 2013. **8**(7): p. e69905.
117. Ditmer, A., et al., *Diagnostic accuracy of MRI texture analysis for grading gliomas.* J Neurooncol, 2018. **140**(3): p. 583-589.
118. Zhao, S., et al., *Radiomics signature extracted from diffusion-weighted magnetic resonance imaging predicts outcomes in osteosarcoma.* J Bone Oncol, 2019. **19**: p. 100263.
119. Yip, S.S. and H.J. Aerts, *Applications and limitations of radiomics.* Phys Med Biol, 2016. **61**(13): p. R150-66.
120. van Griethuysen, J.J.M., et al., *Computational Radiomics System to Decode the Radiographic Phenotype.* Cancer

Res, 2017. **77**(21): p. e104-e107.
121. *<Kairuddin_2017_IOP_Conf._Ser.%3A_Mater._Sci._Eng._226_012136.pdf>.*
122. Cai, W.L. and G.B. Hong, *Quantitative image analysis for evaluation of tumor response in clinical oncology.* Chronic Dis Transl Med, 2018. **4**(1): p. 18-28.
123. Wirth, M.A., *Texture analysis.* University of Guelph
Computing and Information Science
Image Processing Group, 2004.
124. Albregtsen, F., *INF 4300 – Digital Image Analysis.* 07.09.2011.
125. Arrigoni, F., et al., *Conventional MRI.* Handb Clin Neurol, 2018. **154**: p. 219-234.
126. Yoo, D.H., et al., *MR Imaging Evaluation of Intracerebral Hemorrhages and T2 Hyperintense White Matter Lesions Appearing after Radiation Therapy in Adult Patients with Primary Brain Tumors.* PLoS One, 2015. **10**(8): p. e0136795.
127. Zwanenburg, A., et al., *The Image Biomarker Standardization Initiative: Standardized Quantitative Radiomics for High-Throughput Image-based Phenotyping.* Radiology, 2020. **295**(2): p. 328-338.
128. Park, J.E., et al., *Reproducibility and Generalizability in Radiomics Modeling: Possible Strategies in Radiologic and Statistical Perspectives.* Korean J Radiol, 2019. **20**(7): p. 1124-1137.
129. Moradmand, H., S.M.R. Aghamiri, and R. Ghaderi, *Impact of image preprocessing methods on reproducibility of radiomic features in multimodal magnetic resonance imaging in glioblastoma.* J Appl Clin Med Phys, 2020. **21**(1): p. 179-190.
130. Crum, W.R., T. Hartkens, and D.L. Hill, *Non-rigid image registration: theory and practice.* Br J Radiol, 2004. **77 Spec No 2**: p. S140-53.
131. Köser, K., *Affine Registration*, in *Computer Vision: A Reference Guide*, K. Ikeuchi, Editor. 2014, Springer US: Boston, MA. p. 22-25.
132. Du, G.E.J., *Medical Image Registration Using B-Spline Transform.* International Journal of Simulation: Systems, Science & Technology, 2016.
133. Semple, B.D., et al., *Brain development in rodents and humans: Identifying benchmarks of maturation and vulnerability to injury across species.* Prog Neurobiol, 2013. **106-107**: p. 1-16.
134. NAMIC-Wiki-contributors. *Projects:RegistrationLibrary:RegLib C37*. 10 July 2017; Available from: https://www.na-mic.org/w/index.php?title=Projects:RegistrationLibrary:RegLib_C37&oldid=97765.
135. Boyes, R.G., et al., *Intensity non-uniformity correction using N3 on 3-T scanners with multichannel phased array coils.* NeuroImage, 2008. **39**(4): p. 1752-1762.
136. Tustison, N.J., et al., *N4ITK: improved N3 bias correction.* IEEE Trans Med Imaging, 2010. **29**(6): p. 1310-20.
137. Fouladi, M., et al., *White matter lesions detected by magnetic resonance imaging after radiotherapy and high-dose chemotherapy in children with medulloblastoma or primitive neuroectodermal tumor.* J Clin Oncol, 2004. **22**(22): p. 4551-60.
138. Sabin, N.D., et al., *Imaging changes in very young children with brain tumors treated with proton therapy and chemotherapy.* AJNR Am J Neuroradiol, 2013. **34**(2): p. 446-50.
139. Bronk, J.K., et al., *Analysis of pseudoprogression after proton or photon therapy of 99 patients with low grade and anaplastic glioma.* Clin Transl Radiat Oncol, 2018. **9**: p. 30-34.
140. Tsang, D.S., et al., *Pseudoprogression in pediatric low-grade glioma after irradiation.* J Neurooncol, 2017. **135**(2): p. 371-379.
141. Nioche, C., et al., *LIFEx: A Freeware for Radiomic Feature Calculation in Multimodality Imaging to Accelerate Advances in the Characterization of Tumor Heterogeneity.* Cancer Research, 2018. **78**(16): p. 4786-4789.
142. Szychot, E., et al., *Estimating brain volume loss after radiation therapy in children treated for posterior fossa tumors (Corpus callosum and whole brain volume changes following radiotherapy in children).* Advances in Clinical and Experimental Medicine, 2020. **29**(3): p. 331-337.
143. Lawrence, Y.R., et al., *Radiation dose-volume effects in the brain.* Int J Radiat Oncol Biol Phys, 2010. **76**(3 Suppl): p. S20-7.
144. Per Hall, H.-O.A., Dimitrios Trichopoulos, Nancy L Pedersen, Pagona Lagiou, Anders Ekbom, Martin Ingvar, Marie Lundell, Fredrik Granath, *<Effect of low doses of ionising radiation in infancy on cognitive function in adulthood-Swedish population based cohort study .pdf>*. BMJ : British Medical Journal, 2004. **328**.
145. Elida Vázquez, M.I.D., MD • Angel Sánchez-Montañez, MD Ignasi Barber, MD • José Sánchez-Toledo, MD • Goya Enríquez, MD, *Side Effects of Oncologic Therapies in the Pediatric Central Nervous System Update on Neuroimaging Findings.* RSNA, 2011. **31**: p. 1123-1139.
146. Connor, M., et al., *Regional susceptibility to dose-dependent white matter damage after brain radiotherapy.* Radiotherapy and Oncology, 2017. **123**(2): p. 209-217.
147. Toussaint, L., et al., *Radiation doses to brain substructures associated with cognition in radiotherapy of pediatric brain tumors.* Acta Oncol, 2019. **58**(10): p. 1457-1462.
148. Merchant, T.E.e.a., *Modeling radiation dosimetry to predict cognitive outcomes in pediatric patients with CNS*

embryonal tumors including medulloblastoma. International Journal of Radiation Oncology, Biology, Physics, 2005. **65**(1): p. 220-221.
149. Dietrich, U., et al., *White matter disease in children treated for malignant brain tumors.* Childs Nerv Syst, 2001. **17**(12): p. 731-8.
150. Jacob, J., et al., *Cognitive impairment and morphological changes after radiation therapy in brain tumors: A review.* Radiotherapy and Oncology, 2018. **128**(2): p. 221-228.
151. Sundgren, P.C. and Y. Cao, *Brain irradiation: effects on normal brain parenchyma and radiation injury.* Neuroimaging Clin N Am, 2009. **19**(4): p. 657-68.
152. Bianchini, L., et al., *A multicenter study on radiomic features from T2 -weighted images of a customized MR pelvic phantom setting the basis for robust radiomic models in clinics.* Magn Reson Med, 2021. **85**(3): p. 1713-1726.
153. Yun, J., et al., *Radiomic features and multilayer perceptron network classifier: a robust MRI classification strategy for distinguishing glioblastoma from primary central nervous system lymphoma.* Sci Rep, 2019. **9**(1): p. 5746.
154. Bologna, M., V. Corino, and L. Mainardi, *Technical Note: Virtual phantom analyses for preprocessing evaluation and detection of a robust feature set for MRI-radiomics of the brain.* Medical physics, 2019. **46**(11): p. 5116-5123.
155. Jensen, L.J., et al., *Stability of Radiomic Features across Different Region of Interest Sizes-A CT and MR Phantom Study.* Tomography, 2021. **7**(2): p. 238-252.
156. Cunliffe, A., et al., *Lung texture in serial thoracic computed tomography scans: correlation of radiomics-based features with radiation therapy dose and radiation pneumonitis development.* Int J Radiat Oncol Biol Phys, 2015. **91**(5): p. 1048-56.
157. Nardone, V., et al., *Texture analysis as a predictor of radiation-induced xerostomia in head and neck patients undergoing IMRT.* La radiologia medica, 2018. **123**(6): p. 415-423.
158. Scalco, E., et al., *Texture analysis for the assessment of structural changes in parotid glands induced by radiotherapy.* Radiotherapy and Oncology, 2013. **109**(3): p. 384-387.
159. Seibert, T.M., et al., *Cerebral Cortex Regions Selectively Vulnerable to Radiation Dose-Dependent Atrophy.* International Journal of Radiation Oncology, Biology, Physics, 2017. **97**(5): p. 910-918.
160. Merchant, T.E., *Clinical Controversies: Proton Therapy for Pediatric Tumors.* Seminars in Radiation Oncology, 2013. **23**(2): p. 97-108.
161. Main, C., et al., *The effectiveness and safety of proton beam radiation therapy in children with malignant central nervous system (CNS) tumours: protocol for a systematic review.* Syst Rev, 2016. **5**(1): p. 124.
162. Byskov, C.S., et al., *Treatment plan comparison of proton vs photon radiotherapy for lower-grade gliomas.* Phys Imaging Radiat Oncol, 2021. **20**: p. 98-104.
163. Chaki, J. and N. Dey, *Statistical Texture Features*, in *Texture Feature Extraction Techniques for Image Recognition*. 2020, Springer Singapore: Singapore. p. 7-23.
164. Viselner, G., et al., *Brain MR findings in patients treated with particle therapy for skull base tumors.* Insights Imaging, 2019. **10**(1): p. 94.
165. Song, J., et al., *Radiation-induced brain injury in patients with meningioma treated with proton or photon therapy.* J Neurooncol, 2021. **153**(1): p. 169-180.
166. Valdes Hernandez, M.D.C., et al., *Application of Texture Analysis to Study Small Vessel Disease and Blood-Brain Barrier Integrity.* Front Neurol, 2017. **8**: p. 327.
167. Wang, X., et al., *Investigation of MRI-based radiomics model in differentiation between sinonasal primary lymphomas and squamous cell carcinomas.* Jpn J Radiol, 2021. **39**(8): p. 755-762.
168. Luhr, A., et al., *"Radiobiology of Proton Therapy": Results of an international expert workshop.* Radiother Oncol, 2018. **128**(1): p. 56-67.
169. Fossati, P., U. Ricardi, and R. Orecchia, *Pediatric medulloblastoma: toxicity of current treatment and potential role of protontherapy.* Cancer Treat Rev, 2009. **35**(1): p. 79-96.
170. Khatua, S., et al., *Childhood Medulloblastoma: Current Therapies, Emerging Molecular Landscape and Newer Therapeutic Insights.* Curr Neuropharmacol, 2018. **16**(7): p. 1045-1058.
171. Witzmann, K., F. Raschke, and E.G.C. Troost, *MR Image Changes of Normal-Appearing Brain Tissue after Radiotherapy.* Cancers (Basel), 2021. **13**(7).
172. Albano, D., et al., *Imaging side effects and complications of chemotherapy and radiation therapy: a pictorial review from head to toe.* Insights Imaging, 2021. **12**(1): p. 76.
173. Gudrunardottir, T., et al., *Treatment developments and the unfolding of the quality of life discussion in childhood medulloblastoma: a review.* Childs Nerv Syst, 2014. **30**(6): p. 979-90.
174. Packer, R.J. and G. Vezina, *Management of and prognosis with medulloblastoma: therapy at a crossroads.* Arch Neurol, 2008. **65**(11): p. 1419-24.
175. Hall, M.D., et al., *Risk of Radiation Vasculopathy and Stroke in Pediatric Patients Treated With Proton Therapy for Brain and Skull Base Tumors.* Int J Radiat Oncol Biol Phys, 2018. **101**(4): p. 854-859.
176. Chen, T.H., *Childhood Posterior Reversible Encephalopathy Syndrome: Clinicoradiological Characteristics, Managements, and Outcome.* Front Pediatr, 2020. **8**: p. 585.

177. L Levisohn , A.C.-G., J D Schmahmann, *Neuropsychological consequences of cerebellar tumour resection in children- cerebellar cognitive affective syndrome in a paediatric population.pdf.* Brain Imaging Behav, 2000. **123**: p. 1041-50.
178. Spiteri, M., et al., *Fully-Automated Identification of Imaging Biomarkers for Post-Operative Cerebellar Mutism Syndrome Using Longitudinal Paediatric MRI.* Neuroinformatics, 2020. **18**(1): p. 151-162.
179. Patay, Z., et al., *MR Imaging Characteristics of Wingless-Type-Subgroup Pediatric Medulloblastoma.* AJNR Am J Neuroradiol, 2015. **36**(12): p. 2386-93.
180. Kovalchuk, A. and B. Kolb, *Low dose radiation effects on the brain - from mechanisms and behavioral outcomes to mitigation strategies.* Cell Cycle, 2017. **16**(13): p. 1266-1270.
181. Larroza, A., et al., *Support vector machine classification of brain metastasis and radiation necrosis based on texture analysis in MRI.* J Magn Reson Imaging, 2015. **42**(5): p. 1362-8.